Author:
Cox, Matthew Vernon

Title:
Evaluation of EEG-based depth of anaesthesia monitoring

Evaluation of EEG-Based Depth of Anaesthesia Monitoring

by

Matthew Cox

Faculty of Medicine and Dentistry

University of BRISTOL

2008

This thesis is submitted to the Faculty of Medicine and Dentistry, University of Bristol, in fulfillment of the requirements for the degree of Doctor of Philosophy. This thesis is entirely my own work, and except where otherwise stated, describes my own research.

M.V.Cox, University of Bristol

Matthew Vernon Cox
University of Bristol

Doctor of Philosophy
2008

Evaluation of EEG Based Depth of Anaesthesia Monitoring

Abstract

The use of the electroencephalograph (EEG) as a means of monitoring the action of anaesthetic agents on the brain is supported by the observation that the signal characteristics change during agent delivery. In 2001 a University of Bristol team patented a novel data reduction method of the EEG for characterising categorical changes in consciousness. After pre-whitening the EEG signal with Gaussian white noise a parametric spectral estimation technique was applied. Two frequency domain indices were then proposed: the relative power found between 8Hz to 12Hz and 0.5Hz to 32Hz termed the 'alpha index', and the relative power between 0.5Hz to 4Hz and 0.5Hz to 32Hz termed the 'delta index'.

The research and development of a precision EEG monitoring device designed to embody the novel algorithm is described in this thesis. The efficacy of the technique was evaluated using simulated and real EEG data recorded during Propofol anaesthesia

The simulated data showed improvements could be made to the patented method. Real EEG data collected whilst patients were wakeful and data from patients unresponsive to noxious stimuli were cleaned of obvious artifacts and analysed using the proposed algorithm. A Bayesian diagnostic test showed the alpha index had 65% sensitivity and selectivity to patient state. The delta index showed 72% sensitivity and selectivity.

Taking a pragmatic approach, the literature is reviewed in this thesis to evaluate the use of EEG in depth of anaesthesia monitoring. Pertinent aspects of the sciences are profiled to identify physiological links to the characteristics of the EEG signal. Methods of data reduction are also reviewed to identify useful features and possible sources of error.

In conclusion it is shown that the proposed indices do not provide a robust measure of depth of anaesthesia. An approach for further research is proposed based on the review work.

Acknowledgements

The resolute determination of Professors Mark Griffiths and Alan Preece to commercialise the innovation underpinning this study must be acknowledged, as must the help and support of the Department of Trade Industry representative, Dr David Britton.

The invaluable advice and encouragement of Dr Mark Tooley throughout the course of this work, but especially in the latter stages during which other commitments were circumnavigated to ensure that continual support was provided, leaves me with a substantial debt of gratitude.

The constant love and encouragement of my parents, Ruth and Keith, has been fundamental to all that I have achieved. To them both I offer my eternal thanks.

Many of the personal sacrifices made in completing this work were shared with understanding and grace that no one could ask of another, and so I save my final thanks to the endlessly wonderful Jan.

Matthew Cox, May 2008

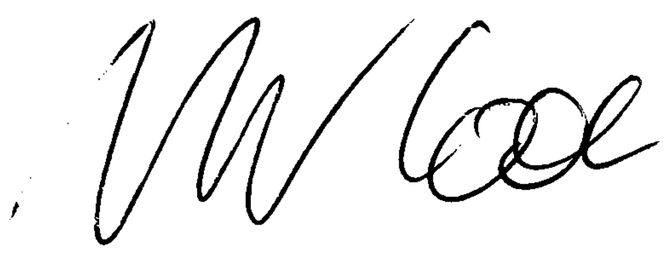

List of Figures

List of Tables

Chapter 1

Introduction

The word 'Anaesthesia' is derived from the Greek word 'anaisthesia' meaning 'lack of sensation'; 'an'- meaning 'without' and 'aisthesis' meaning 'feeling'. Although use of the word can be traced back to as early as the 1st Century AD, it is frequently reported to have been first used in its modern clinical sense by physician-poet Oliver Wendell Holmes, on November 21st 1846. In a letter to dental-physician William Thomas Green Morton of the Massachusetts General Hospital in Boston, Holmes outlines a suitable nomenclature appropriate to Morton's use of diethyl ether (often referred to as ether) to render a surgical patient without feeling during a public demonstration. It is thought that the discovery of ether's solvent properties may predate this by some 600 years and awareness of its analgesic properties can be traced back to the 16th Century (Leake, 1925).

The motivation for establishing a method that could be used to assert a state of anaesthesia was the elimination of pain in patients undergoing surgery (Duncum, 1994). Morton's work showed that diethyl ether meets this requirement and thus the term anaesthesia became embedded in common language. However, work published shortly after Morton's demonstration shows recognition amongst physicians that the action of ether includes a range of supplemental features to that of pain suppression. English physician John Snow noted that ether also reversibly combines effects of paralysis and amnesia whilst not harming the patient when responsibly administered (Snow, 1847). Each of these features is of importance and thus, since Holmes' descriptor remains in popular use, ether is referred to as a single agent general anaesthetic where the term is used to describe an agent that has all of these properties. Locally acting anaesthetics are not treated in this work.

The use of ether has been phased out due to its explosive flammable volatility. Modern alternatives constitute an array of substances that can be administered to affect one, or combinations of, the required components of ether anaesthesia to a degree suited to the needs of the particular patient. This leaves the term anaesthesia with no direct meaning in the pharmacological sense and so debate of what components constitute anaesthesia has

developed. Where Snow and others have sited reversible analgesia, unconsciousness and immobility as essential components, others argue for example that since pain is conscious awareness of noxious stimulation, if anaesthesia includes unconsciousness then there is no requirement for analgesia (Antogini, 2002; Heinke, 2002). Others suggest that amnesia and immobility are sufficient (Eger, 1974; Hug, 1990).

Although safer agents have superceded ether and other early anaesthetic agents, modern alternatives do not constitute a risk-free ideal. A wide variety of agent side effects have been noted the severity of which determines their Lethal Dose index (LD_{50}): the dose required to cause a fatality in 50% of the population. Monitoring and management of the cardiovascular and respiratory systems is required for all patients undergoing anaesthesia as both systems are subject to instabilities that are not possible to fully predetermine. In addition, anaesthetics may cause hyperkalemia, malignant hyperthermia, convulsions, anaphylaxis, and laryngospasm all of which may directly or indirectly cause death.

Numerous factors complicate statistical analyses relating the use of anaesthesia to patient mortality (Duberman and Bendixen, 1986) especially with any historical context (Jones, 2001). Lunn and Mushin (1982) reported that of the 0.6% of patients that died in the UK within 6 days of a surgical procedure, 0.01% could be attributed directly to anaesthesia, although no distinction is made as to whether these were preventable. This translates to approximately 1 in 20,000. Fleischer (2000) reported that 1 death in 200,000 could be directly attributed to anaesthesia. These analyses appear to show a significant improvement in safety over the last 20 years, but it is also possible that the difference represents the complexity of profiling inharmonious data. In either case the figures suggest death as a result of a modern anaesthetic procedure is relatively unlikely.

Incidence of awareness without pain is estimated to occur in 0.2% to 0.4% of all anaesthetic procedures (Jones, 1994). Incidence of awareness with pain is thought to be much lower; Jones offers a figure of 0.01%. Although this figure is comparable to the incidence of patient mortality, the risk of such an incidence is distributed unevenly over the range of surgical interventions. For example, procedures that require a neuromuscular blockade carry a higher risk of awareness during surgery as such drugs ablate many indications useful in assessing depth of anaesthesia. Since most anaesthetic agents tend to excite the cardiovascular system, surgical treatment of trauma or cardiac pathologies will also carry a greater risk of awareness as the anaesthetist will try to maintain anaesthesia with minimal dosing. Similarly, when performing procedures on prepartum patients there is an additional motivation to ensure only low levels of toxic agent reach the foetus. Figure 1.1 presents the positive attributes of anaesthesia along with the negative side effects.

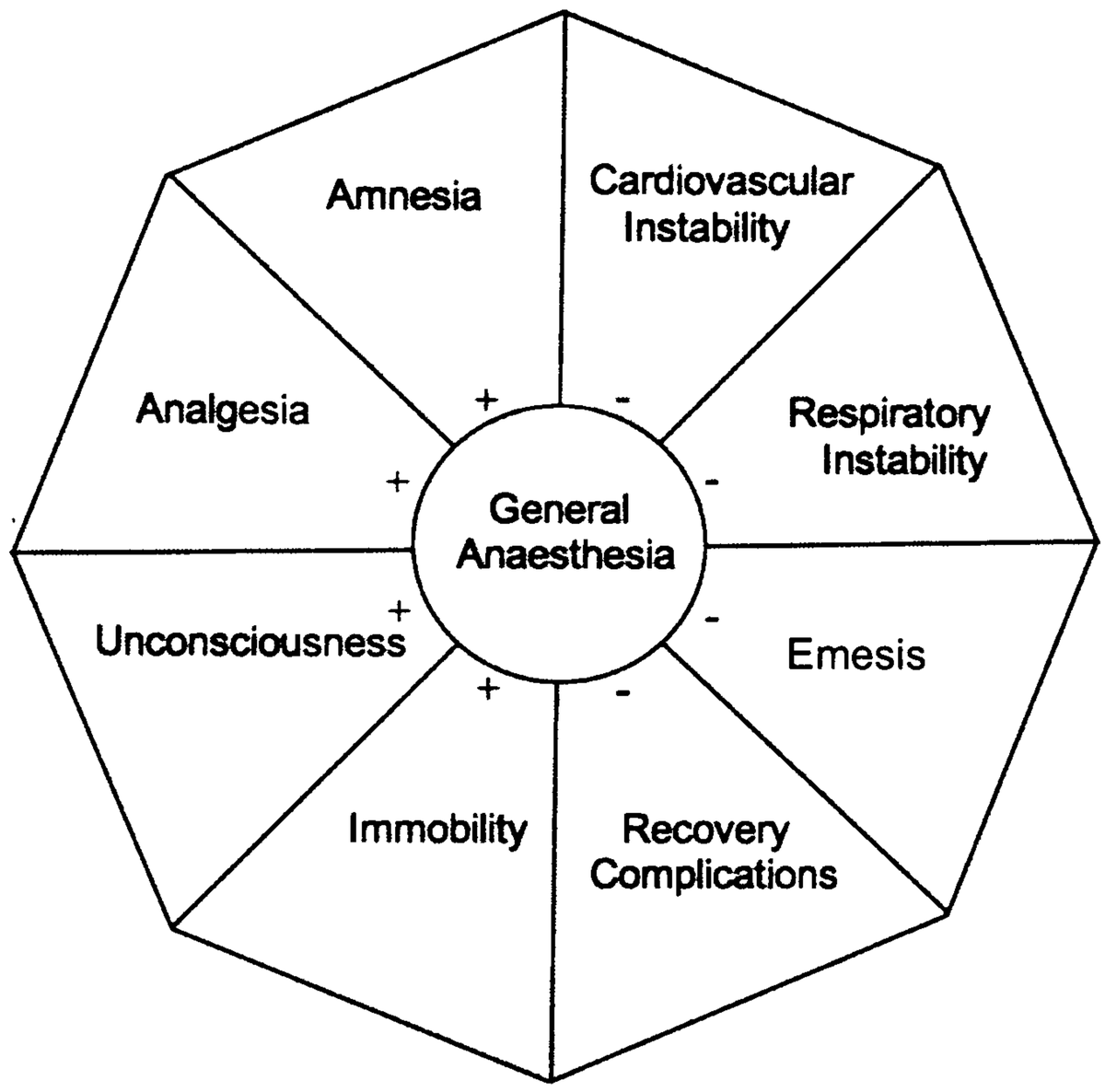

Figure 1.1: Positive and Negative Components of Anaesthesia.
Adapted from: Urban and Bleckwenn, 2002.

This figure suggests that the morbid ramifications of overexposure predicate maintenance of anaesthesia with the lowest doses needed to meet procedural requirements. It is very important that the patient is adequately anaesthetised because the consequences of patients becoming aware during surgery can be very severe and therefore constitutes the primary motivation for identifying a metric for monitoring the depth of anaesthesia.

The patient on whom Morton performed his first public presentation of ether later reported that he had experienced pain during the operation (Bigelow, 1846). This was followed by other reports that together established the concept of intraoperative awareness as a complication of anaesthesia.

John Snow (1847) was of the first to use the term 'depth of anaesthesia'. White (1987) summarises the concept as a continuum resulting from the opposing effects of the anaesthetic agents and surgical noxious stimuli. However, modern agents can be selected to vary the strength of the required features of anaesthesia as appropriate to a particular patient. It might therefore be argued that there is no single variable of anaesthetic depth and instead

multiple continua must be considered. The term depth of anaesthesia has an intuitive meaning and so is firmly entrenched in language. Its use is therefore unlikely to cease but many in the field choose to avoid the expression instead using a more correct term such as 'adequacy of anaesthesia'.

Clark and Rosner (1973) noted that all anaesthetic agents in use at the time affect changes in the EEG signal, and subsequently considerable efforts have since been exerted in pursuit of a parameter of the EEG that can be used as a metric on which anaesthetic agent delivery can be graduated. Many research methods simply apply data reduction techniques to EEG data recorded during anaesthetic delivery in attempts to, somewhat serendipitously, identify a common characteristic. This approach requires several assumptions to be made.

The first is that a depth of anaesthesia correlate is at all available in the EEG signal. Whilst Clark and Rosner (1973) observe that the EEG signal varies during all techniques of anaesthesia, it is possible that the signal variations noted are not representative of the neuropharmacological processes of anaesthesia but rather are the derivation of the neurophysiological side-effects of particular anaesthetic procedures. If EEG only indirectly measures depth of anaesthesia there is a greatly increased possibility of physiological or pharmacological circumstances that may affect similar or distorted measurements. Ideally the physiological basis of the characteristic would be identified such that the limitations of the measurement can be clearly defined. With such a complex signal, meeting this requirement may not be possible.

Incumbent on any serendipitous design methodology would be assurance that all anaesthetic techniques over the range of patient physiologies yield the same parameter characteristic. In addition the approach also assumes that any characteristic identified holds a direct relationship with a feature of anaesthesia fundamental to the motivations for monitoring the depth of anaesthesia. For example, can it be assumed that an EEG parameter shown to correlate well with the termination and return of auditory perception during anaesthesia will also represent transitions in sensory pain perception?

1.1 Aims of Thesis

The aim of this thesis is to present an extensive review to evaluate the use of EEG in depth of anaesthesia monitoring. Secondly, a novel index of the EEG called the alpha index is

evaluated to determine if the alpha index could be a useful measure in awareness and depth of anaesthesia monitoring.

The novel index is described in a patent held by the University of Bristol (see appendix A). The principle assumption of the patent is that the activity of frequency components between 8 and 12 Hz characterise the state of conscious sedation. It is suggested that an increase in alpha bandwidth activity will be observed during the onset of anaesthetic agent delivery whilst the subject is not yet unconscious and will subsequently decrease as anaesthetic agent titration ablates consciousness. Upon termination of agent administration the subject will return to a state of sedation during which alpha bandwidth activity will again increase before dropping away again through arousal. Emergence of sub-alpha bandwidth activity is discussed in the patent as a feature that provides distinction between deepening anaesthesia and arousal. Griffiths and the Bristol team behind the project (Griffiths et al., 1991) suggest that the relationship between alpha bandwidth and delta bandwidth relative amplitude might be used to monitor depth of anaesthesia. Griffiths et al. present the association of relative spectral variation during an anaesthetic procedure with graphs showing the composite of snapshots from 8 patient recordings at 4 distinct stages of the procedure. This is given in figure 1.2. The top left graph shows the composite of data recorded at some point before anaesthetic delivery with the patients' eyes closed. The bottom left graph presents a composite of data recorded during light anaesthesia. The top right graph shows the composite of data recorded during deepening anaesthesia and the bottom right graph presents data from some point during the recovery.

On this basis Griffiths proposes that these features of relative spectral power may be used to detect, and therefore prevent, unwanted arousal during surgery. It is also suggested that the technique may form the basis of a closed-loop anaesthesia delivery system.

The patent body describes the emergence of alpha bandwidth activity as poorly represented by earlier methods. This claim is elucidated with discussion of poor sensitivity to emerging EEG sub-bandwidth power characteristics caused by noisy data and the spectral leakage observed in the application of the Fast Fourier Transform algorithm.

As an improvement, an autocorrelation-based Yule Walker method was proposed for spectral transformation to which a relative power distribution analysis is applied and visually presented. It was suggested that the addition of Gaussian noise to the signal can agreeably contribute to the analysis by attenuating or eradicating rogue results and further highlight low amplitude band power trends. The disruption to the spectral resolution caused by noise was described in the patent as being minimal and not of practical importance.

The addition of noise forms the novel succession to earlier methods and is thus the basis of the intellectual property.

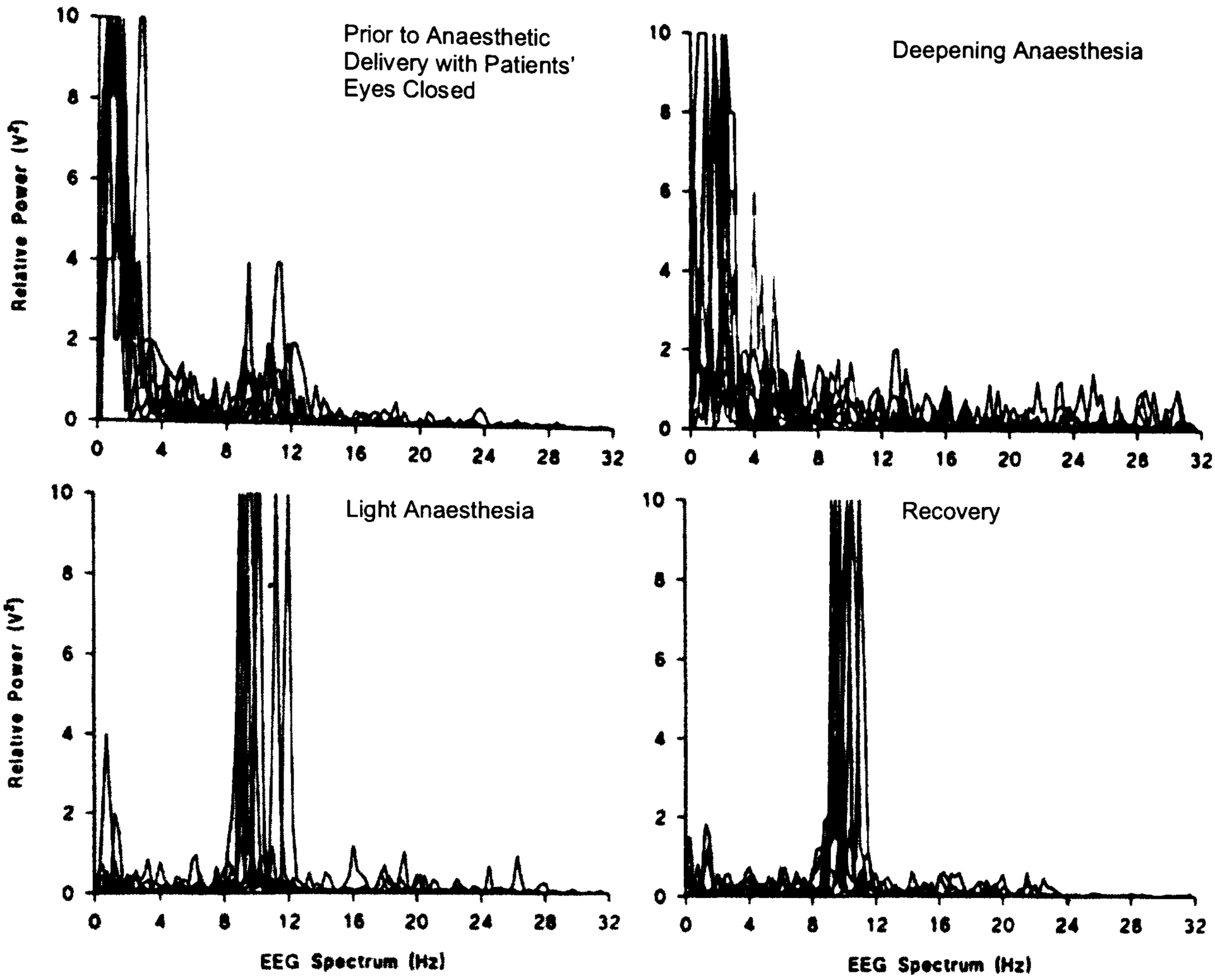

Figure 1.2: Spectral characteristics during anaesthetic agent delivery.
Adapted from: Griffiths et al., 1991. Reproduced with permission.

As part of this thesis the method described in the patent was developed into a production prototype EEG monitor using a department of Trade and Industry (DTI) initiative termed the 'Teaching Company Scheme' (now called 'Knowledge Transfer Partnership'). Under the scheme the field knowledge and intellectual property held by the University was brought together with the commercial experience and resources of an industrial partner. This DTI project formed the basis of this thesis, and as part of the work, an advanced EEG monitor device was developed to embody the patented mathematics. The performance of the patented mathematics is analysed using synthetic and real EEG data.

Other aims of the thesis are to offer improvements to the patented technique, and identify a course for future work.

Chapter 2

Consciousness and Intraoperative Awareness

Depression of the central nervous system such that intra-operative noxious stimuli are not recalled is cited as the principle motivation driving Morton's 19th Century Etherization work (Bigelow, 1846). Whilst many have associated this requirement with the concept of unconsciousness, modern clinical definitions distance themselves from the term (Eger et al., 2003). Use of the term 'awareness' is more common in the literature of anaesthesia than the term consciousness but, since no clear distinction exists between their definitions, it might be assumed that this is for emotive reasons. Used to describe a symptom of consciousness, the term 'intraoperative awareness' might not convey so strongly a failure on the part of an anaesthetist as the term 'return of consciousness' might imply. The severe distress caused in some incidences of awareness has lead to litigation proceedings in which such semantics are important.

From the Latin 'conscius' meaning 'share knowledge with', a typical modern definition of the word 'conscious' is 'aware of and responding to one's surroundings'. Other definitions include 'awareness of one's own existence, sensation and thoughts'. Many of these descriptors have continuums of meaning. Medical definitions use words such as 'alert' or 'awake' where the word alert is defined in its common sense as 'heightened watchfulness', or 'preparation for action' and the word aware is described in terms of cognitive functions such as 'knowledge', 'understanding' and 'realisation'. These too have continuums of meaning and thus do not present clear endpoints for monitoring, a problem exacerbated when patients with cognitive abnormalities are considered.

Although recent studies are beginning to readdress the problem of what constitutes consciousness from the perspective of the anaesthetist (Mashour, 2004; Pinault, 2004; Steriade, 2004), in general, modern studies tend focus on the components of consciousness identified as contributors to the phenomenon of intraoperative awareness.

Vickers (1987) suggests that efforts to define consciousness are futile, and it may be of more use to consider a definition of unconsciousness and to define consciousness as 'non-unconsciousness'. In his discussion Vickers offers the following definition of unconsciousness:

> *'No evidence, either at the time or later, of perception registration or retention of mental images corresponding accurately to real events'*

Whilst this definition is not directly of use to the problem of real-time depth of anaesthesia monitoring, perception and memory are of central importance in many studies of intraoperative awareness.

Psychologists divide the mechanisms of memory in a number of ways: temporally (as in short or long term memory), content (semantic or episodic memory), and by the mode of encoding (implicit or explicit memory). Of most pertinence to the present study is the distinction between implicit and explicit memory. In terms of experience, implicit memory is that which may be recalled without effort, whilst explicit memories require effort for retrieval. The relevance of implicit and explicit memory to depth of anaesthesia assessment was first presented by Levinson (1965). In Levinson's experiment alarming comments were directed towards ten patients during anaesthetic procedures. One month later recall of the dialog was not possible until it was encouraged using hypnosis, suggesting distinct memory encoding, storage or retrieval mechanisms exist.

Griffith and Jones (Griffith and Jones, 1990) published a classification of intraoperative awareness based on a literature review. In it they identify 4 stages:

1. Conscious perception with implicit memory;
2. Conscious perception without implicit memory;
3. Subconscious perception with explicit memory;
4. No perception and no memory.

Stage 1 of the classification could be applied to the pre-anaesthetised patient and thus only offers a stage of discernable distinction at the termination of anaesthesia. Stage 2 describes the state of consciousness when patients are able to respond to commands whilst sedated but cannot recall dialog postoperatively (Russell, 1986). Stage 3 is considered to be the start of adequate anaesthesia in most cases. As demonstrated by Levinson (1965), Stage 3 has been shown to exist in distinction to stage 4 by the success or failure of postoperative recall whilst under hypnosis (Russell and Wang, 1997). It is not possible to confirm that the state of

'no perception' described in stage 4 actually exists, as without memory there is no means by which perception can be confirmed. However, having no memory of intra-operative events is not uncommon and so perception without memory may be clinically irrelevant. If perception does exist without memory, then the anaesthetic agents that promote amnesia will be the source of significant under-reporting of incidence of awareness (Russell, 1993).

Jones (1994) went on to produce a further report on the incidence of awareness as related specifically to pain that is cited often in related studies (for example Schwender et al., 1997; Andrade and Deeprose, 2007; Düzel et al., 1997). In this paper Jones refers to the following stages of anaesthesia:

1. Conscious awareness with pain;
2. Conscious awareness without pain;
3. Unconscious awareness;
4. No Awareness.

This subsequent study from Jones (Jones, 1994) seems primarily to have been presented to acknowledge that postoperative awareness of pain can be a function of adequacy of analgesia, whether that be locally acting or as a component of a general anaesthetic. Jones cites Artusio's demonstration that he could maintain a conversation with a patient during cardiac surgery using a combination of local anaesthesia and a light general anaesthetic (Artusio, 1955). Postoperative recall of dialog was reported as being absent in most of Artusio's patients. Modern studies confirm this finding (Renna et al., 2000; Russell and Wang, 2001; Andrade et al., 2001). It is also of note that Artusio's study indicates that functionality in the speech processing temporal-parietal region of the brain can persist during adequate anaesthesia.

Although both schemes presented above have been used as the basis for statistical analysis there is no standardized approach to the classification of incidence of intraoperative awareness, nor are there requirements to make such assessment routine during surgery. It is likely therefore, that reporting of awareness is low.

Without definitions based on clinical endpoints for the terms awareness and anaesthesia, various physicians beginning with Dr John Snow (1847) published commentaries of the clinical signs and effects observed during ether anaesthesia. By identifying commonality in the incremental changes observed over increasing agent concentration, graduations or stages of anaesthesia, could be identified along side the associated characteristics. In his work entitled "Inhalation Anesthesia—A Fundamental Guide" Arthur Guedel (1937) presented

one such classification scheme that enjoyed many years of acceptance. Guedel identifies four stages of anaesthesia:

1. Analgesia: patient experiences sedation, amnesia and analgesia;
2. Delirium: patient shows inhibited movement akin to a dream state;
3. Surgical Anaesthesia: patient shows changes in respiratory characteristics, skeletal muscle relaxation and ocular changes;
4. Respiratory Paralysis: patient undergoes cardiovascular and respiratory collapse.

The success of Guedel's scheme, which is still presented in the education of anaesthetists today, relates to the descriptors selected providing a characterisation to all of the anaesthetic agents in popular use at the time: chloroform, diethyl ether and cyclopropane. Subsequently, Guedel's classification was widely adopted as a metric for standard anaesthetic practice.

In the years following Morton's ether demonstration, commercial interests spawned an industry of anaesthetic substance development. Numerous improved agents were developed, promoted, patronized and, with vary degrees of success, commercialized. Advances were made with agents that widened the gap between the concentration of agent required to reach anaesthesia and their lethal dose (LD_{50}), as well as improving the quality and speed of recovery.

Single agent anaesthetics are still used today, but there is a large range of substances of varied molecular structure that aim to meet subsets of the components of ether anaesthesia, enabling the anaesthetic practitioner to vary concentrations, and thus effects, as appropriate to a particular patient's needs. Introduced in the 1940's, the first component agent to be employed was the muscle relaxant curare. The laryngeal muscular reflex causes complication to the insertion of an endo-tracheal tube, an airway adjunct used to deliver mechanical ventilation. The introduction of curare enabled the concentration of anaesthetic agent used to be reduced as suspension of the laryngeal reflex could be achieved separately. Such advances diminished the scope of the classification scheme developed by Guedel as the use of different agents presents differing observable characteristics. The introduction of new agents led to manipulations of the classification schemes but the introduction of intravenous anaesthetic agents that display much faster onsets for example, finally invalidated the work of Guedel and others.

It was not until the 1980s that a truly incremental classification scheme was presented. Taking a pragmatic view of the effects of anaesthesia Prys-Roberts (1987) mapped the observable somatic and autonomic reflexes ablated by anaesthesia to a continuum of agent

concentration without reference to consciousness. Figure 2.1 summarises the scheme developed by Prys-Roberts which when read from left to right presents somatic and autonomic reflexes in the order that they are ablated with increasing dose of anaesthetic agent.

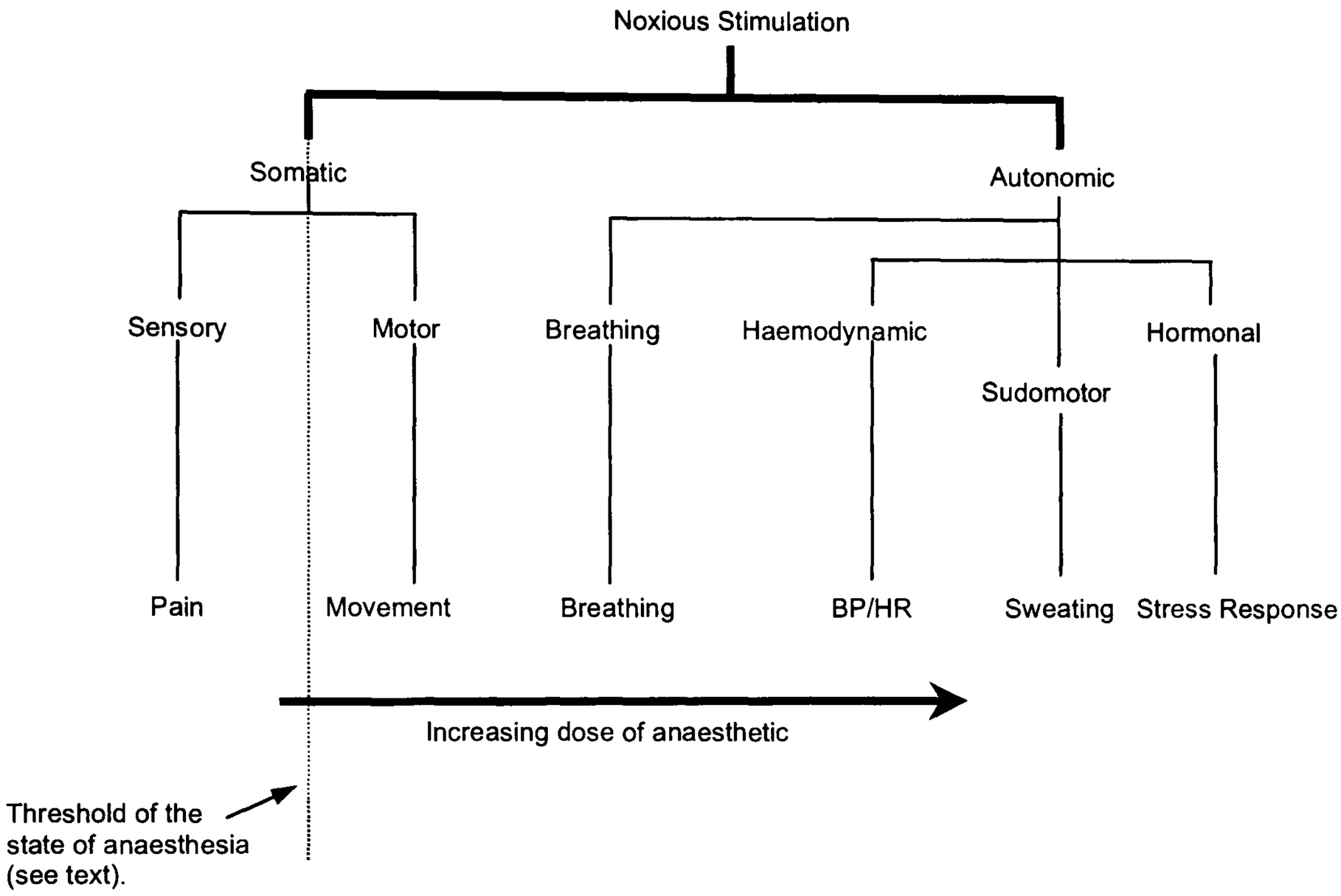

Figure 2.1: Responses to Noxious Stimulation. Adapted from: Prys-Roberts, 1987.

Prys-Roberts suggests that the state of anaesthesia has been reached when the perception of pain (shown to the left of the figure) has been lost along with the ability to recall events. Prys-Roberts notes that the concentration of anaesthetic agent required to ablate somatic motor responses to noxious stimuli is sufficient to ensure unconsciousness and, therefore, perception of pain. This observation places the threshold of the state of anaesthesia between ablation of pain and movement (dotted vertical line in the figure). Prys-Roberts' scheme presents the state of anaesthesia as an "all or nothing" phenomenon again suggesting that the term 'depth of anaesthesia' is not appropriate.

Whilst the figure shows that fluctuations in respiratory rate and tidal volumes as a response to noxious stimuli are ablated with higher doses of agent than are required to ensure loss of

perception of pain and recall, Prys-Roberts also notes that surgical noxious stimuli cause a shift to the left in observed responses presented in the figure. Such responses can thus be used to provide an indication of the possible return of pain perception and recall.

Chapter 3

Non-EEG Based Methods of Anaesthetic Depth Assessment

Various non-EEG based techniques have been developed that contribute useful feedback to assessment of depth of anaesthesia. Those that have found more popular use are presented here along with discussion of their advantages and limitations.

3.1 Agent Delivery Measures

With knowledge of the potency of an agent, measurement of the physiological uptake should, albeit somewhat indirectly, give an indication of depth of anaesthesia. Anaesthetic agents vary in their potency; for inhaled agents this can be characterised by a Minimum Alveolar Concentration (MAC) value. The MAC, first described by Eger and colleagues (1965), is the agent concentration at equilibrium in the lungs, required to prevent a reflex response to a skin incision in 50% of patients. The 50% statistic is used as it is the median point of the concentration-response probability distribution across all patients. The reference to a 'minimum' measurement in the term MAC relates to the practicalities of anaesthesia delivery. An agent with a low MAC is thus a potent agent because only a small amount is required to produce anaesthesia, whilst a high MAC indicates that a greater quantity of agent will be required. The MAC of most agents is fundamentally determined by their fat solubility: the more fat soluble the higher the potency, a relationship identified and credited to both Meyer (1899) and Overton (1901). As well as easing the passage of such agents through the tightly packed endothelial cells of the blood-brain barrier, Meyer and Overton postulated that this relationship indicates that agent potency is determined by how readily molecules of agent dissolve in neuronal lipid cell membranes.

Using one of the various breeds of gas analyser it is possible to monitor the end-tidal concentration of inhaled anaesthetic agent and, with the agent's MAC value in mind, ensure that an appropriate concentration of agent is being delivered.

Of course the MAC parameter has no relevance to intravenous anaesthesia. An equivalent assay-based measure of multiple agent concentrations in the blood for example, could not currently form a practical solution for routine monitoring during surgery, but a loosely analogous measure to the MAC, called the Minimum Infusion Rate (MIR), has been proposed (Forrest et al., 1994). The concentration of each agent required to abolish reflex responses to skin incision in 50% of the population is again used as the measure of agent potency. With this knowledge the rate at which each agent should be titrated to maintain the required dose can be calculated.

The main problem with the MIR approach is that it provides no account of agent pharmacokinetics with respect to the physiology of the particular patient. An increment in sophistication to the MIR is the Target Controlled Infusion (TCI) system that is based on desired plasma concentration. Various agent attributes that are available in pharmacology literature are first required. Typical examples are given in table 3.1.

Agent Attribute	Description
Potency	Often described by their lethal dose index (LD_{50})
Bioavailability	The proportion of an administered dose that reaches the plasma unchanged.
Drug Clearance	A measurement of the rate at which the agent is eliminated from the plasma.
Drug Distribution	A relative measure of how the concentration of the agent varies between the plasma and various tissues.
Protein Binding	Describes the reduction in efficacy of the agent as a result of the agent binding to blood plasma proteins.
Degree of ionisation	The ratio between the number of ionized agent molecules and the number of agent molecules dissolved in water.

Table 3.1. Pharmacological agent attributes used in Target-Controlled Infusion systems.

Together with patient age, height, and body weight it is possible to calculate the infusion rate that is required to maintain a chosen effector-site or plasma concentration of the agent. A range of Target-Controlled Infusion (TCI) systems have now been developed that control of automatic agent delivery via a mechanical syringe driver. The benefit of delivering

intravenous agents with precisely calculated dosing has been noted in several studies (for example Ecoffey et al., 2001; Vivand and Léone, 2001). In the absence of a metric by which TCI efficacy can be ascertained, the US Food Drug and Administration (FDA) have not yet authorised the use of TCI systems in the US, however acceptance of TCI systems has been rapidly proliferating elsewhere and the FDA are expected to follow.

Whilst the TCI incorporates appreciation of some basic patient physiological parameters, neither TCI nor MIR can be considered to be a practical analogy to the MAC as there is no method of routinely assessing plasma drug concentrations in real-time. The efficacy of agent administration techniques with TCI systems might therefore be affected by anatomical and physiological variability between patients.

Whilst many studies acknowledge that the MAC and TCI measures enable much greater control of agent delivery (for example Ruhberg and colleagues, 2007), in a large study Sebel et al. (2004) note that use of inhaled agent end-tidal concentration monitoring alone will not eradicate the incidence of intra-operative awareness.

3.2 Clinical Signs

Examples of the clinical signs that can be routinely monitored during surgery include blood pressure, heart rate, sweating, tearing, pupil reactivity, and muscle reflexes. In one system presented by Evans and Davies (1984) systolic blood pressure, heart rate, sweating and tearing are each given a score from 0 to 2 that are then added to give a number of maximum 8 indicating the patient is insufficiently anaesthetised. The strategy of assessing depth of anaesthesia by combining several simple assessments is advantageous as taken individually clinical signs can show variation for reasons unrelated to the quantity of anaesthetic agents being administered; for example the use of prescription hypertension drugs such as beta-adrenergic blockers precludes use of blood pressure as a sole measure, similarly opioid use will override pupil reactivity, and noxious stimulation will affect autonomic responses independently of the concentration of anaesthetic agent (Cullen et al., 1972). Interpatient variability of clinical signs should also be considered, as should the sensitivity of autonomic responses during an anaesthetic procedure that will deteriorate over time (Cullen et al., 1972).

Whilst clinical signs are of use to the anaesthetist, consideration of the real-time context of the patient and procedure must be maintained, as they do not constitute a stable means of depth of anaesthesia monitoring.

3.3 Isolated Forearm Technique

The principle underpinning the isolated forearm technique is that if a region of the body can be isolated from the distribution of muscle relaxant, the patient will, if inadequately anaesthetised, be able to control movement in that region in response to verbal command. This is often conducted by applying a tourniquet to an arm prior to muscle relaxant administration at a pressure somewhere above the peripheral artery systolic pressure. Although accepted as a useful measure and having been used extensively has a benchmark for assessing other techniques, may not be without limitations. To prevent ischemia the tourniquet has to be periodically released. Whilst this can be timed prior to administration of further muscle relaxant, Russell and colleagues (Russell et al., 1979) report of patients hearing the verbal commands but being unable to move their arm indicating that the muscle relaxant had reached a functional concentration in the arm. However, in a personal communication, Russell revised the conclusions drawn in this study, stating that lack of attention to the instructions appears to be the cause of failure to respond rather than the rise in concentration of the neuromuscular blockade (Russell, 2008).

Whilst there are comparatively few motor neurones in the central nervous system, they each receive many thousands of synaptic contacts. Since they evidently constitute an integrated pathway to many others, it might be assumed that motor neuron activity will persist as an indication of consciousness during increasing anaesthesia longer than many others. However, Russell's latter theory has implications on the efficacy of what is sometimes discussed as a gold standard approach to which other methods of monitoring depth of anaesthesia are tested. In addition, as the technique detects the presence of awareness rather than providing prior indication of its return, the isolated forearm technique cannot be viewed as a complete solution to the problem of depth of anaesthesia monitoring.

3.4 Spontaneous surface electromyography

Use of spontaneous surface electromyography (SEMG) as a means of monitoring depth of anaesthesia has been used with some degree of success (for example Niemi-Murola and Paloheimo, 2005). There are a number of sites around the body that provide spontaneous muscle activity as a function of depth of anaesthesia. Muscles of the face, oesophagus and abdominal wall have each been used in such commercially available monitors as the 'FACE' monitor from Patient Comfort, Inc., (California, USA). The frontalis muscles of the face have been shown to lose tone as a direct indication of unconsciousness, and despite being highly subjective, there is evidence that awakening is preceded by a significant rise in the activity of these muscle groups (Herrogots et al., 1989).

Spontaneous lower oesophageal contractions (SLOC) occur during periods of stress. Provoked lower oesophageal contractions (PLOC) are the result of a reflex that naturally occurs in response to the presence of a bolus of food but can be artificially recreated with the use of a balloon catheter. Both SLOC and PLOC can be measured with a pressure transducer and have been shown to provide a good correlation with known consciousness and unconsciousness. However the efficacy of the oesophageal technique does not extend to good resolution at the transition between consciousness and unconsciousness (Isaac and Roden, 1990).

The desirability to maintain paralysis through surgery and the relatively low toxicity of neuromuscular blockades, can equate to high doses of blockade being administered. Whilst in the case of the frontalis muscles the action of muscle relaxants have been shown to be less effective (Dutton et al., 1998), their use does impact on the reliability of SEMG techniques. Rampil suggests that good anaesthetic practice should include only minimally administered neuromuscular blockade (Rampil, 2003) but if they are used at all, SEMG techniques may only indicate adequacy of neuromuscular blockade rather than anaesthesia.

3.5 Heart rate variability

Mean heart rate is a straightforward parameter to monitor during surgery and is a vital indicator of cardiovascular stability. However, beat-to-beat heart rate variability can be used to present more information relating to depth of anaesthesia (Pomfrett et al., 1991).

It has been established that the first site of action of anaesthetic agents is the brainstem, with subsequent action propagated across the brain via efferent projections from the mid-brain. It is also known that afferent messaging from cardiovascular and respiratory stretch receptors such as those of the baroreceptors and chest walls, converge at, and are subsequently mediated by, the solitary nucleus of the brainstem medulla. Spectral analysis of the electrocardiogram (ECG) over epochs of 60 seconds shows three components of beat-to-beat variability (Sakuma et al., 1989) described in figure 3.1. Variation in the peak seen below 0.05Hz is attributed to the sleep cycle and will thus vary during the course of a 24 hour period. The peak observed between 0.05Hz and 0.15Hz varies in association to the baroreceptor reflex, whilst the movement in the peak seen between 0.15Hz and 0.4Hz present variations observed with changes in frequency of respiration.

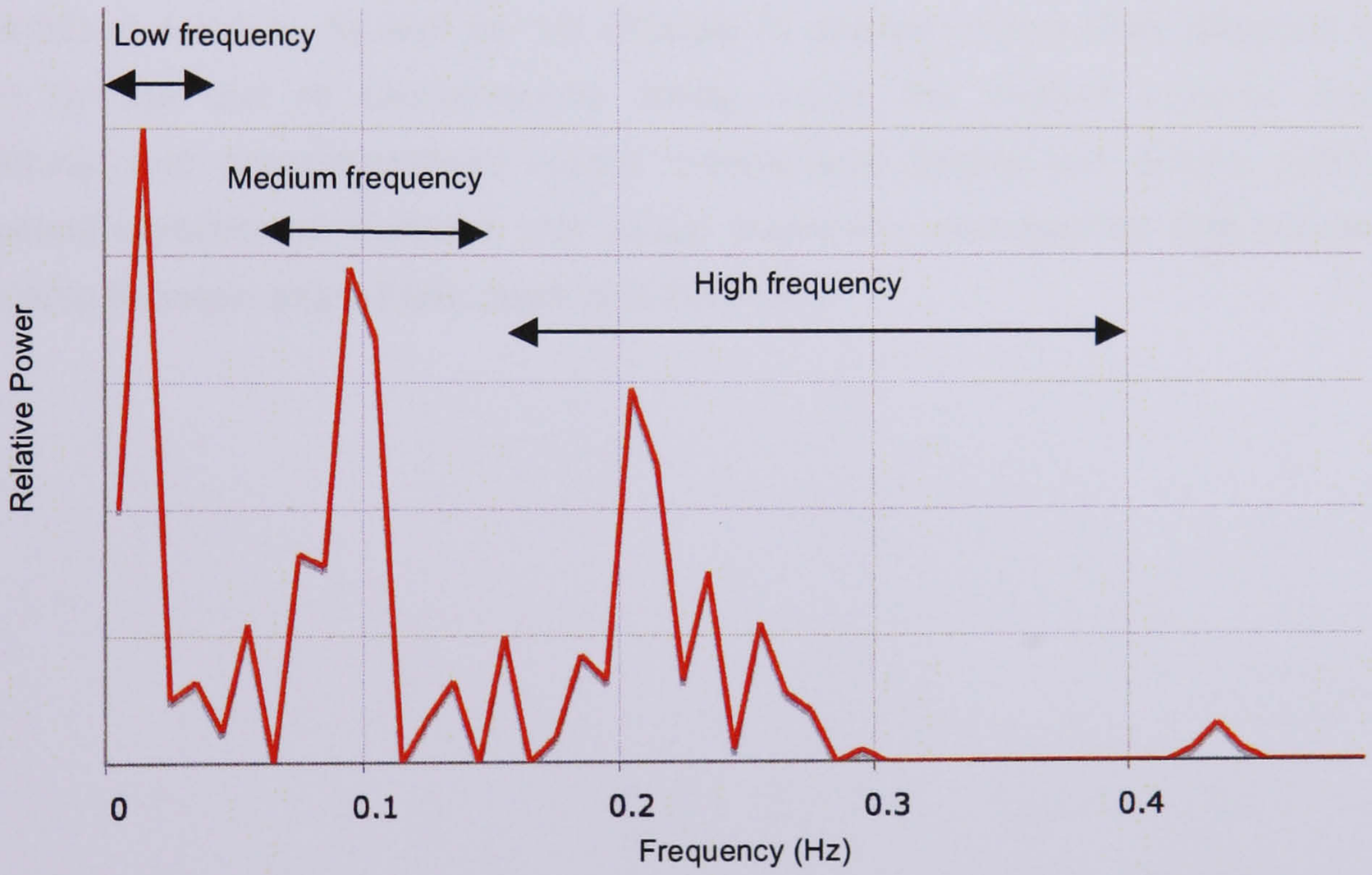

Figure 3.1: Frequency domain power distribution of heart rate variability.

The high frequency component shows the complementary sympathetic and parasympathetic elements of autonomic control of the heart rate: sympathetic control increasing during inspiration and parasympathetic control increasing during expiration. The variation in the duration of the high frequency component, termed 'respiratory sinus arrhythmia' (RSA), is in the order of 20% of the mean heart rate and can be clearly seen with a monitor phase-locked to the high amplitude 'R-Wave' component of the ECG signal. The relatively long epochs

required to assess the RSA diminishes the issue of artefact as the mean noise component tends towards zero over long periods.

It is thought that the derivation of RSA response directly relates to the functionality of the medulla. At the onset of anaesthesia the medulla relinquishes control of cardiac rhythm and thus the relationship between the respiratory cycle and cardiac rhythm is lost. Subsequently the RSA variation drops, but with lightening anaesthesia the relationship recovers and the RSA increases (Donchin et al., 1985). This has been shown to be the case regardless of whether intravenous or inhaled anaesthetic agents are used.

In congruence with observation that anaesthetic depth is reduced in response to surgical stimulation, the RSA response increases and more so during light anaesthesia than would be observed during lightening anaesthesia alone (Pomfrett et al., 1993). This is a useful feature of the metric with respect to the application; however, the technique has not been adopted as a generalised solution. As well as the difficulty in predetermining RSA response variation caused by the use of cardiovascular acting drugs, the method requires integrity of sympathetic and parasympathetic control mechanisms (Healy and Cohen, 1995). The widespread condition of diabetes can cause autonomic neuropathies that will break the relationship between anaesthetic depth and the RSA.

Chapter 4

EEG - Physiological Principles

To establish whether EEG can be used to monitor depth of anaesthesia several fundamental questions need to be answered. Of primary importance is to establish what information EEG presents not only so that the relationship between the signal and its derivation might be defined, but also so that the limitations of the signal's interpretation are known. Before discussion of EEG methods of depth of anaesthesia assessment, an appreciation of the current understanding of the underlying electro-physiology of the signal is required.

Where as the endocrine system provides the body with a chemical communication system with the release and metabolism of hormones, the nervous system forms an electrical communication network by conducting and transferring action potentials often over considerable distances. There are a number of subdivisions of the nervous system determined by their locality and function, but by far the largest is the Central Nervous System comprising of the brain and the spinal chord.

Along with the entire nervous system, the brain is comprised of variants of two cellular elements: 'glial' cells and 'neurons'. Glia (from the Greek for 'glue') were considered only to provide structural support to the profuse yet less abundant neurons as glia do not propagate communication 'action potentials' and lack the polarity of their neuronal counterparts. The range of functions now attributed to the glia include: neuronal structural support, regulation of blood flow around the brain, distribution of nutrients and oxygen to neurons, insulation between other cellular elements, phagocytosis and damage repair. More recently glia have been shown to act as a sink and source of ions in the transmission of electrical activity between neurons, and may further directly contribute to the EEG by effectively amplifying action potentials (Speckmann and Elger, 1999).

The neuron constitutes the functional unit of the nervous communication network. Several structurally distinct types of neuronal cell have been identified. Table 4.1 presents those found in the central nervous system.

Cell Type	Location	Function
Basket cells	Cerebellum, the hippocampus, and the cortex	Transmit 'inhibitory' signals within the brain
Betz cells	Primary motor cortex	Afferent motor control
Granule cells	Cerebellum, cortex, hippocampus, and olfactory bulb.	Diverse functionality
Medium spiny neurons	Corpus striatum	Controlling movements of the body, limbs and eyes.
Mossy fibers	Spinal cord and brainstem	Excite granule cells with afferent signaling from spinal cord
Purkinje cells	Cerebellum	Output signals from the cerebellar cortex
Pyramidal cells	Hippocampus and cortex.	Major transmitter of signals within the brain, hence termed 'interneuron'
Renshaw cell	Multiple regions of the brainstem and the cortex	Mediate motor control
Stellate cell	Cerebellar cortex	Interneuron

Table 4.1: Types of neuron cell found in the central nervous system.

There are two general mechanisms by which a neuron will receive a signal; electrical synapsing and chemical synapsing. Chemical synapses are considered to be more plentiful in the brain than their electrical counterparts but this may be because electrical synapses are more difficult to identify (Bennett, 2004).

4.1 Chemical Synpasing

Provided certain extracellular conditions are met, notably a sufficient concentration of calcium ions, an action potential in a presynaptic neuron initiates chemical neurotransmitter release at its synaptic membrane. Figure 4.1 presents a schematic of the synaptic junction. Neurotransmitter molecules in the synaptic cleft bind with substance specific receptors on the postsynaptic membrane. If the receptor is of the ligand-gated channel type, the localised region of the membrane's permeability to Cl-, Na+ and K+ ions is altered. If the ions are not in equilibrium across the postsynaptic membrane there is a subsequent ion flow that affects a

change in the post-synaptic membrane potential. The change in potential causes an electronic flow towards the neuron axon. If sufficient flow is present, as would be caused by simultaneous stimulation at several synaptic junctions of the same cell, a voltage threshold is reached and an action potential will be generated propagating transmission along the cell axon. The membrane stimulation is brought to an end by enzyme-facilitated neurotransmitter breakdown and reuptake by the pre-synaptic cell. Although active mechanisms contribute, the dissipation of the somatic potential is largely passive, occurring over relatively long periods of between milliseconds to seconds. Figure 4.2 presents the changes in post-synaptic membrane potential observed during action potential stimulation. As can be seen in the figure, at rest the polarisation of the membrane gives rise to a potential of around -65mV. The neurotransmitter receptors determine which ions gates are opened. A subsequent flow of positive ions is termed 'excitory' as it causes depolarization of the negatively charged membrane, whilst negatively charged ion flow is termed 'inhibitory' as it hyperpolarises the membrane. It is the balance between excitory post-synaptic potentials (EPSPs) and inhibitory post-synaptic potentials (IPSPs) that determines whether the voltage threshold of action potential propagation is reached. If the threshold is breached, the membrane potential briefly rises to +60mV before falling with an overshoot to a passive decrease in potential back to the resting voltage of -65mV.

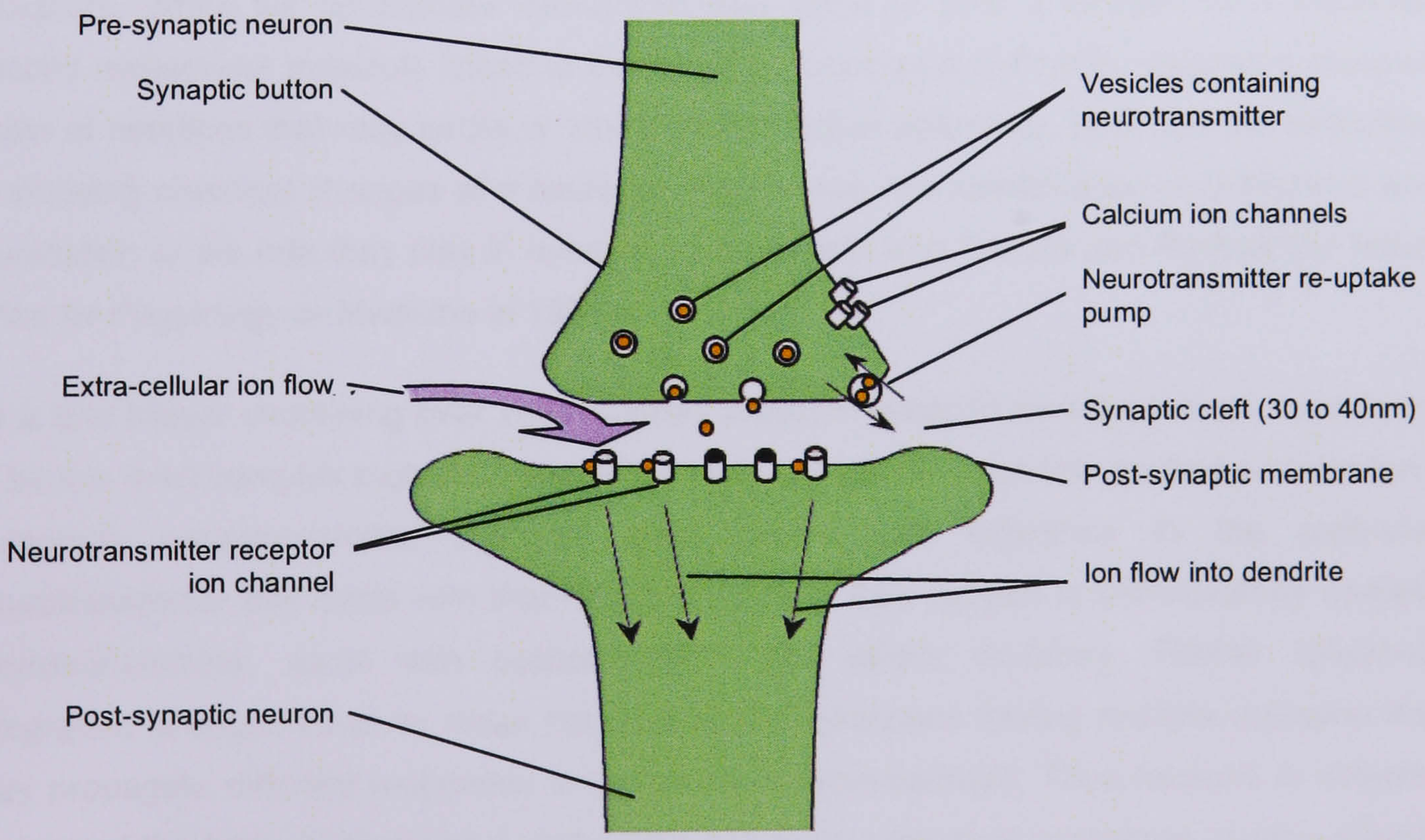

Figure 4.1: Schematic diagram of neuron synapse.

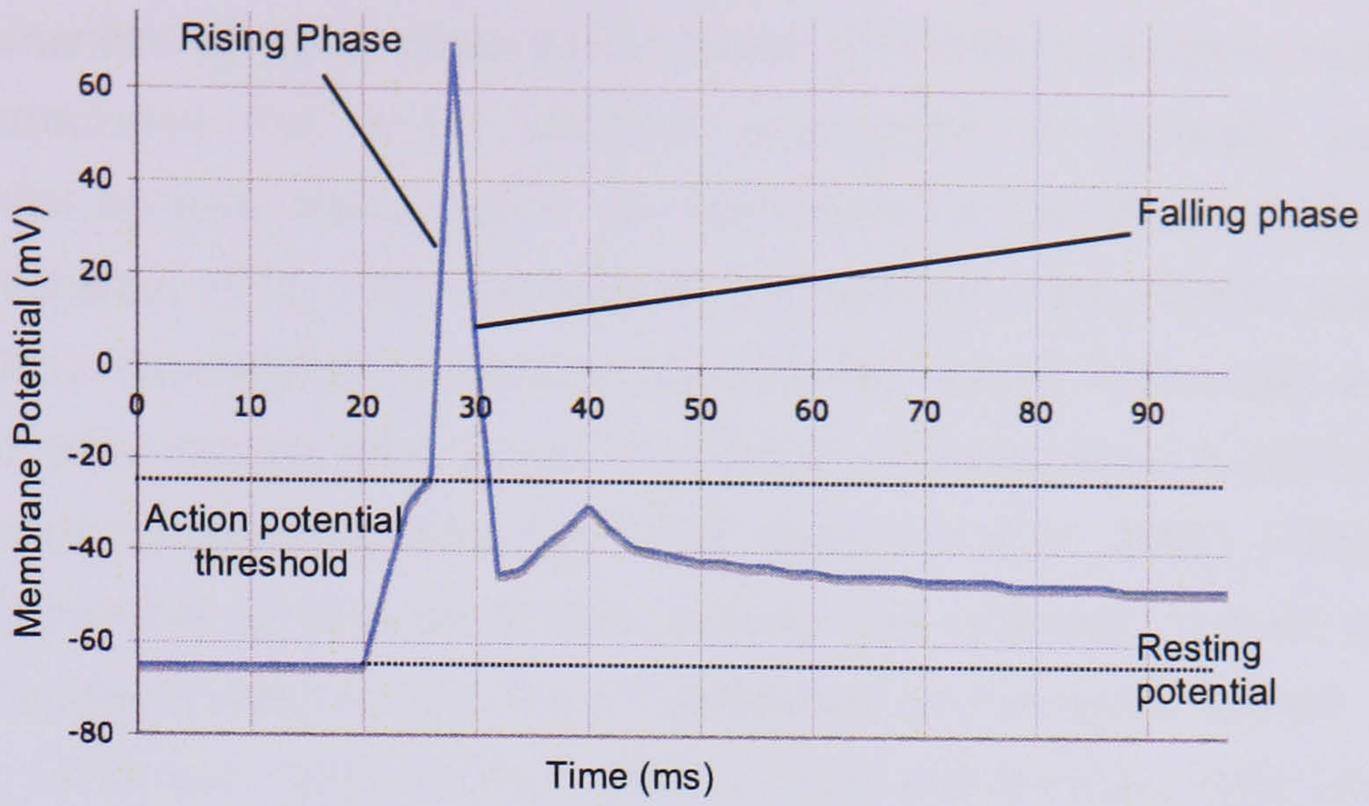

Figure 4.2: Changes in post-synaptic membrane potential during action potential propagation.

Although it is the receptor that asserts which ion gates are opened, neurotransmitters are also commonly termed excitory or inhibitory. Prolonged exposure of the postsynaptic membrane to neurotransmitter can produce desensitisation leading to lack of response.

An alternative chemical neurotransmission process is provided by 'second messenger-linked' receptors. When the appropriate neurotransmitter binds to such a receptor an intracellular second messenger molecule linked to the receptor, such as a G-Protein, initiates a complex chain of reactions that may excite or inhibit further action potentials. Such are the difficulties in studying chemical changes at a neuronal level in vivo, the identification of G-Proteins and elucidation of the role they play in synaptic transmission won Gilman and Rodbell the Nobel Prize for Physiology or Medicine in 1994.

As a lipid bilayer containing over 1000 different proteins, synaptic membranes are considered to be the most complex molecular structure in cell biology. The densely packed proteins form numerous neurotransmitter receptor sites named with reference to the particular neurotransmitter that binds with them. Each neuron is thus subject to interaction by multiple neurotransmitters, some with excitory effect and others inhibitory. Further functional integration is engendered by many neurotransmitter receptors having multiple subtypes that may propagate different responses to the same neurotransmitter. Thus neurons in different regions of the brain exposed to a particular neurotransmitter may propagate varying effects. Conversely, each neuron may synthesize, and thus release, only one or two different neurotransmitters upon action potential excitation. This gives rise to distinct neural transmission pathways that, through knowledge of localisation, can be linked to specific functionality.

The cellular mechanism by which anaesthetics assert their effects remains unclear. Various studies have concluded that action potential propagation is generally unaffected by anaesthesia, whilst synaptic transmission has been shown to be inhibited (Somjen, 1963; Weakly, 1969; Richards, 1972; 1973; Richards and Strupinkski, 1986). Urban and colleagues (Urban et al., 1991), showed that synaptic sodium channel activity is generally unaffected by anaesthesia and other groups have shown that levels of intracellular neurotransmitter are generally unaffected (Crossland and Merrick, 1954; Potashner et al., 1980). Evidence for both pre-synaptic suppression of neurotransmitter release and inhibition of their post-synaptic reception by anaesthetic agents has been established in numerous animal and human studies over the 1970s and 1980s (Collins, 1980; Kendall and Minchin, 1982; Minchin, 1981, Potashner et al., 1980). As such, and in the absence of a complete understanding of the mechanisms responsible for affecting global changes in consciousness, the science of anaesthetic neuropsychopharmacology organises itself with respect to the chemical neurotransmitter pathways affected by each agent.

There are a great many known neurotransmitter substances and many more that remain unknown, however there is a small subset that are considered to be the principle protagonists of desired pharmacological outcomes, the remainder are thought to elicit modulatory effects to the functionality of the principle subset. Table 4.2 gives an overview of the major neurotransmitters, their functionality that is directly pertinent to the present study, and the principles centres of their pathway innervation

Neurotransmitter	Functionality Associated with Consciousness	Principle Subcortical Centres of Pathway Innervation
Glutamate	1. Memory 2. Cognitive processing	1. Hippocampus (Hudspith, 1997) 2. Lateral Septum (Puma and Bizot, 1999) 3. Nucleus Accumbens (Sou et al., 2006) 4. Dentate Gyrus (Richards and White, 1975) 5. Coritcthalamic and Thalamicoritcal pathways (Pinault, 2004)
Gamma-aminobutyric acid (GABA)	1. Memory 2. Anxiolysis 3. Muscle relaxant 4. Sedation	1. Cerebellum (Bonin and Orser, 2008) 2. Hippocampus (Bonin and Orser, 2008) 3. Thalamocortical Relay neurons (Bonin and Orser, 2008) 4. Neocortex (Bonin and Orser, 2008) 5. Dentate Gyrus (Bonin and Orser, 2008) 6. Thalamic Reticular Nuclei (Pinault, 2004)
Acetylcholine	1. Neuromuscular junctions 2. Cognitive processing & Learning 3. Arousal	1. Basil Forebrain (Steriade, 2004) 2. Coritcthalamic and Thalamicortical pathways (Steriade, 2004) 3. Pedunculopontine Tegmental Nucleus (Kodama and Honda 1999) 4. Laterodorsal Tegmental Nucleus (Imon et al., 1996) 5. Hippocampus (Kikuchi et al., 1998)
Seratonin	1. Sensory function 2. Perception 3. Cognition 4. Sleep	1. Raphe Nucleus (Mukaida et al., 2007) 2. Hippocampus (Whittington and Virág, 2006)
Glycine	1. Sensory function 2. Motor control	1. Hippocampus (Betz, 1991) 2. Thalamus (Betz, 1991) 3. Cerebellum (Betz, 1991)
Adrenalin	1. Arousal	1. Locus Coeruleus (Hirota and Kushikata, 2001) 2. Medulla (Berecek and Brody, 1982)
Dopamine	1. Sleep 2. Attention 3. Learning	1. Substantia Nigra (Robinson et al., 2004)
Histamine	1. Nocicpetion 2. Sleep	1. Tuberomamillary Nucleus (Haas and Panula, 2003)
Orexin	1. Wakenfulness	1. Hypothalamus (Kelz et al., 2008)

Table 4.2: Major neurotransmitters of the central nervous system.

4.2 Electrical Synpasing

Camillo Golgi first proposed electrical synpasing as a mechanism of communication in the early 1900s (Grant, 2007). At the time there was much debate as to whether neurotransmission was a function of a chemically mediated system or the result of direct electrical synapsing. The importance of both lines of research was recognised in 1906 when the Nobel Prize in Physiology or Medicine was awarded jointly to Golgi and Santiago Ramón y Cajal, a strong advocate of the chemical transmission theory. Without the sophisticated techniques needed to study them, theories relating electrical synpasing to neurophysiological

phenomenon declined in number and subsequently electrical synpasing neurons have not been well profiled (Connors and Long, 2004). Most neurophysiology texts do not provide treatment beyond their anatomy and basic mode of operation, often stating that the advantages of the faster transmissions speeds possible through direct interfacing are of more benefit to cold-blooded animals, inferring by their lack of further treatment that this is where they are only to be found. Over the last ten years improved analysis techniques have revealed that electrical synapses are to be found throughout the central nervous system (Bennett, 2004).

Figure 4.3 shows the form of an electrical synapse junction. Electrical synapses exist where neurons are physically linked with intra-membrane polypeptide gap junctions that form conduits from one neuron to the next through which water and small water soluble molecules may pass. Thus current flow is direct, allowing high-speed transmission.

In addition to an excitory threshold needing to be reached, a low-pass filtering effect requires an amount of current potential synchrony to exist such that an action potential is generated in the postsynaptic neuron (Bennett, 2000). Increased concentrations of both intracellular calcium and hydrogen ions have been shown to close gap junction conduits. Although electrical synpasing has been thought to be more prolific in reflex communication where the speed of synaptic transmission may assist functionality, recent studies suggest they may play a significant role in the propagation of rhythmical activity of the brain (Blethyn et al., 2007).

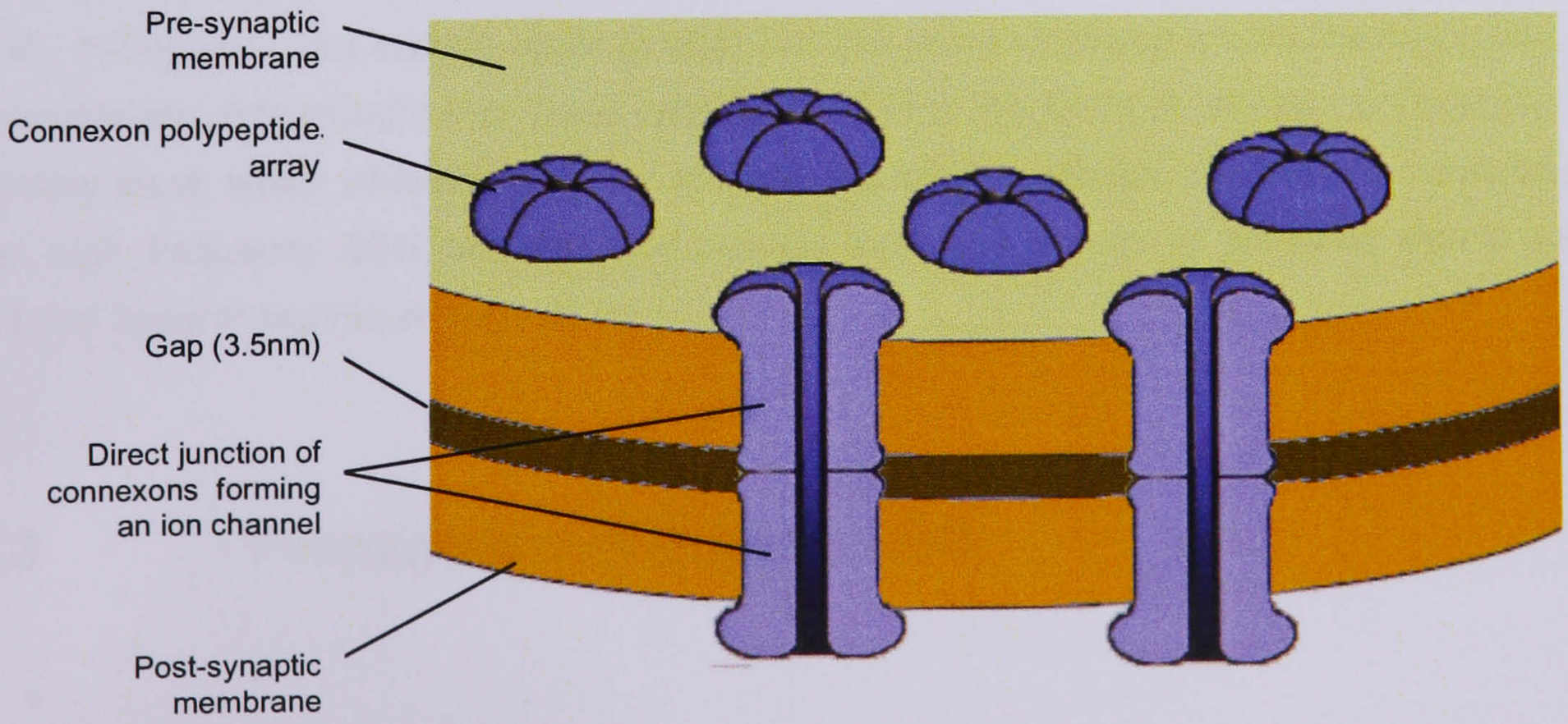

Figure 4.3: Schematic diagram of an electrical synapse.

The significance of electrical synpasing in the study of consciousness is yet to be fully realised, but there are compelling indications that relevance will be found. At least 10 different gap junction connexon proteins have been identified in the mammalian central nervous system (Bennett 2004), each requiring specific sets of analyses to elucidate their function within each region. Deans and colleagues (2001) have shown that dipole oscillations (of frequencies across the EEG spectrum up to 600Hz) in the neocortex are an intrinsic property of inhibitory interneurons, but their spatial synchrony can be associated with widespread coupling by electrical synapses. The presence of electrical synapses has therefore been suggested as a mechanism for entrained rhythmic propagation (Blethyn et al., 2007; Mancilla et al., 2007; Merriam et al., 2005).

The synchronous firing and oscillations identified originally in the inferior olive by Llinas and Ribery (2001), have now been identified in regions widespread throughout the brain including the locus coeruleus, visual cortex, somatosensory cortex, hippocampus, striatum, thalamic reticular nucleus, and cerebellum (Bennett, 2004), and will almost certainly be discovered in many more.

Some work has been carried out to classify neurons by the characteristics of their electrical activity (Myers, 2000). Tonic neurons operate at high frequencies or even continuously (Millar and Atwood, 2004); phasic neurons are more often inactive delivering only short bursts of impulses (Millar and Atwood, 2004); fast-spiking (Morris et al., 1999) and thin-spiking (Del Negro and Ederline, 2002) are identified as their names suggest. Human research in the area is not extensive as it is technically difficult to conduct at this time, however, Celio (1986) has shown with microelectrode EEG that the stellate cells of the cerebral cortex of the rat are of the GABAergic type that contain calcium-binding parvalbumin. Morris and colleagues (Morris et al., 1999) have also shown, again in rats, that this strain of neuron shows the fast-spiking characteristic. It is thought that these cells play a part in the focus of attention on important sensory input, whilst inhibiting attention to more mundane feedback. It is therefore possible that high frequency EEG analysis may provide indication of loss of attention where the isolated forearm technique may not.

4.3 Propagation of Surface EEG

Investigations into the arrangement of the cells nearest the outer surface of the brain allow some assumptions to be made as to where the greatest influence on the EEG originates. The two large hemispherical lobes of the cerebral cortex form the outer layer of the brain. There

are six neocortical layers that lie parallel to the meninges. The closest to the surface, the *plexiform*, is a relatively thin matrix of axonal and dendritic processes. The second, again rather thin *external granular layer,* comprises mostly interneuron stellate cells with some pyramidal cells. The third level is almost exclusively formed of pyramidal cells with some stellate cells. Level four is mostly stellate and layers five and six are again predominately pyramidal with a greater mix of other neuron variants in layer six. Layer three and six are the thickest with the long dendrites of the more prolific pyramidal cells of both layers lying perpendicular to the brain surface and reaching into the plexiform. Subsequently anatomists talk of cortical functional units as 'vertical columns'.

Braitenburg and Schuz (1991) estimate that the complexity of the mesh of cortical axons is such that all cortical neurons are connected by a path of only two or three neurons. Given that approximations to the amount of neurons contained in the cortex are in the region of 10^{10}, the level of neural networking implied can be appreciated.

Sem-Jacobsen (1956) reported that during predominantly periodic electrical activity, potentials recorded several centimeters depth apart within the brain are of similar magnitude to those measured at the cortical surface. Such measurements are consistent with Nunez and Srinivasan's (2006) presentation of neuronal current flow approximating to a current dipole where a current source at the neuron pre-synaptic dendrites is reciprocated with a current sink of equal proportions at the neuron soma.

Between the cortex and surface EEG electrode there exists a complex of cerebral spinal fluid, the skull and scalp that will affect the magnitude of the potentials measured at the scalp. If, for example, cortical dipole activity were responsible for a 100μV potential at the surface of the brain, the inverse square law would suggest a 1μV potential would be recorded 1cm away from the source. In fact measurements show scalp surface potentials to be around a quarter of the magnitude recorded at the brain's surface. There are several factors that are thought to be contributing here. The first is that rather than recording the dipole behaviour of a single neuron, the signal must reflect the spatial and temporal summation of many parallel dipoles in what may be termed a 'dipole layer' (Creutzfeldt et al., 1966) as described in figure 4.4.

Ebersole (1997) concluded that in the region of $6x10^7$ neurons are required to be acting synchronously at the surface of the cortex to provide sufficient additive potential to be recorded at the scalp. Given that the surface of the cortex is comprised of ridges or *gyri*, and invaginations or *sulci*, this translates to surface gyri forming an area in the order of $6cm^2$. Depending on the application, this spatial spread, whilst reducing the spatial resolution that is possible from surface recordings, may be thought of as providing convenient data reduction although this is not without its penalties. Where invasive needle or microelectrode EEG recordings can be used to show how single or small groups of neurons behave in laboratory

experimentation, such techniques cannot be used to identify the presence of widespread rhythmic activity or its phase distribution. Conclusions of functional anatomy drawn from needle EEG studies are not, therefore, easily transferred to expectations of surface EEG characteristics.

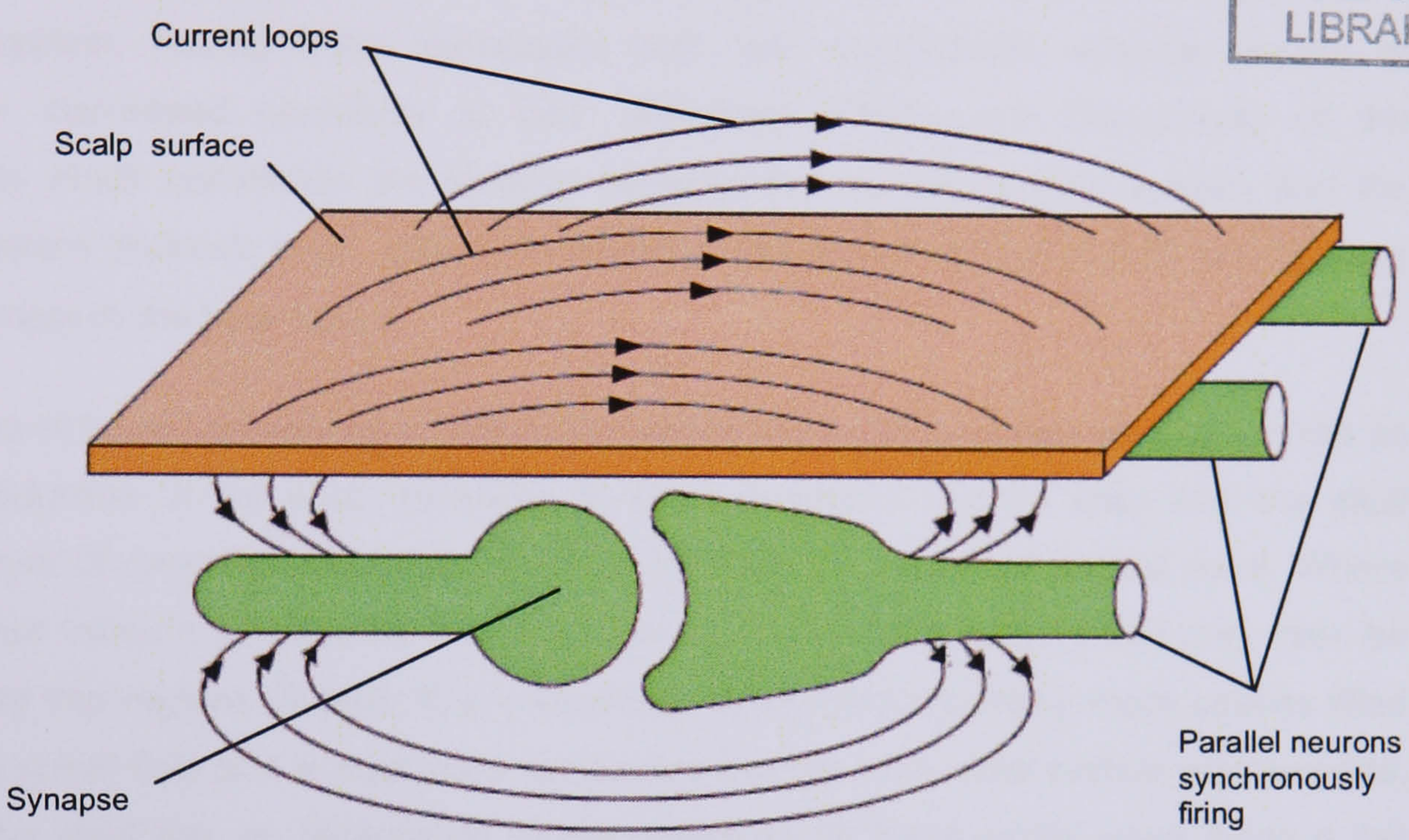

Figure 4.4: Parallel neurons forming a synchronous dipole layer.

Where electric currents alternate within the cortex, they cannot, of course, continue beyond the scalp. Nunez and Srinivasan (2006) suggests that this current boundary increases the potentials observed at the surface with a near doubling of magnitude to an equivalent dipole potential observed in a homogenous medium.

The reduction in potential is due to the inhomogeneous materials found between the brain and the surface of the scalp. The outer most layer of skin, the 'stratum corneum' consists mainly of dead cells and is therefore of relatively high impedance. It is common practice to either remove or penetrate the stratum corneum when applying surface electrodes to the skin and it is thus not considered further here. Below the stratum corneum, skin varies in impedance primarily as a result of altering blood flow through the dermis capillaries. Measurement of skin impedance in response to some stimulus is termed the galvanic skin response (GSR). Studies of the galvanic skin response show that impedance is altered by physiological variations linked to, for example, emotional changes (although it has not proved

possible to identify particular emotions from recordings). In an awake and calm subject the impedance of skin is in the region of 10,000Ωcm but this can vary from between 5,000Ωcm during heightened arousal and 25,000Ωcm during deep depression. The GSR was not thought to contribute useful information in the monitoring of depth of anaesthesia (Kirnö et al., 1991) but Ledowski and colleagues (2006) have found good coherence of the GSR with awareness of intraoperative pain. Due to a decline in general use of the measure in the late 1970's the derivation of the GSR is not well understood. It is known that it forms part of the autonomic system, having been associated both with sympathetic nervous control of increased or decreased sensitivity to pain (Edelberg, 1961), and the activity of the hypothalamus which constitutes the junction between the central nervous system and the endocrine system (Petrovic et al., 2004). A re-emergence of interest in the GSR seems likely to elucidate more in the near future.

The thickness of bone can vary by a factor of 6 across the same skull and yet there is not an equivalent reduction of the scalp potential. In cross section it can be seen that the skull contains a layer of cancellous bone sandwiched between two layers of cortical bone. Where bone thickness varies it tends to be with the depth of the cancellous layer that may even be absent in very thin regions of skull. The cancellous region contains many more spaces filled with cerebral spinal fluid and is thus more conductive than its more solid cortical counterparts. When dry, the skull has an impedance in the region of 10^{13}Ωcm whilst when living it lies somewhere around 15,000Ωcm at 20Hz (Akhatari et al., 2002) and in the region of 5,000Ωcm at 10Hz (Hoekema et al., 2003).

Cerebral spinal fluid has a low resistivity in the order of 60 Ωcm due to its rich dissolved salt content.

The resistivity of tissue varies with frequency but where only narrow bandwidths are of interest it is not deemed important. The same is true of the varying capacitive effective of tissue in narrow EEG bandwidths. Ranck (1963) identified a maximum capacitive-to-resistive current ratio of 0.12 in experiments on rabbit cerebral cortex at frequencies less than 100Hz. Traditionally wideband EEG recordings used an upper bandwidth limit of 80Hz. Clark (in Webster, 1998) suggests that the resolution of the ink-drawn trace display used in traditional EEG monitors was the reason for this practical bandwidth limitation, but it is probable that the low-pass filtering effect of the material complex between source and electrode would have negated efforts to identify ways of increasing the displayed resolution. If variation in skin impedance were disregarded, capacitive and resistive variations would only be significant in studies that compare absolute measures of the EEG.

An example of raw surface EEG data is given in figure 4.11 along with examples of a number of the artefacts that may be observed in a typical recording.

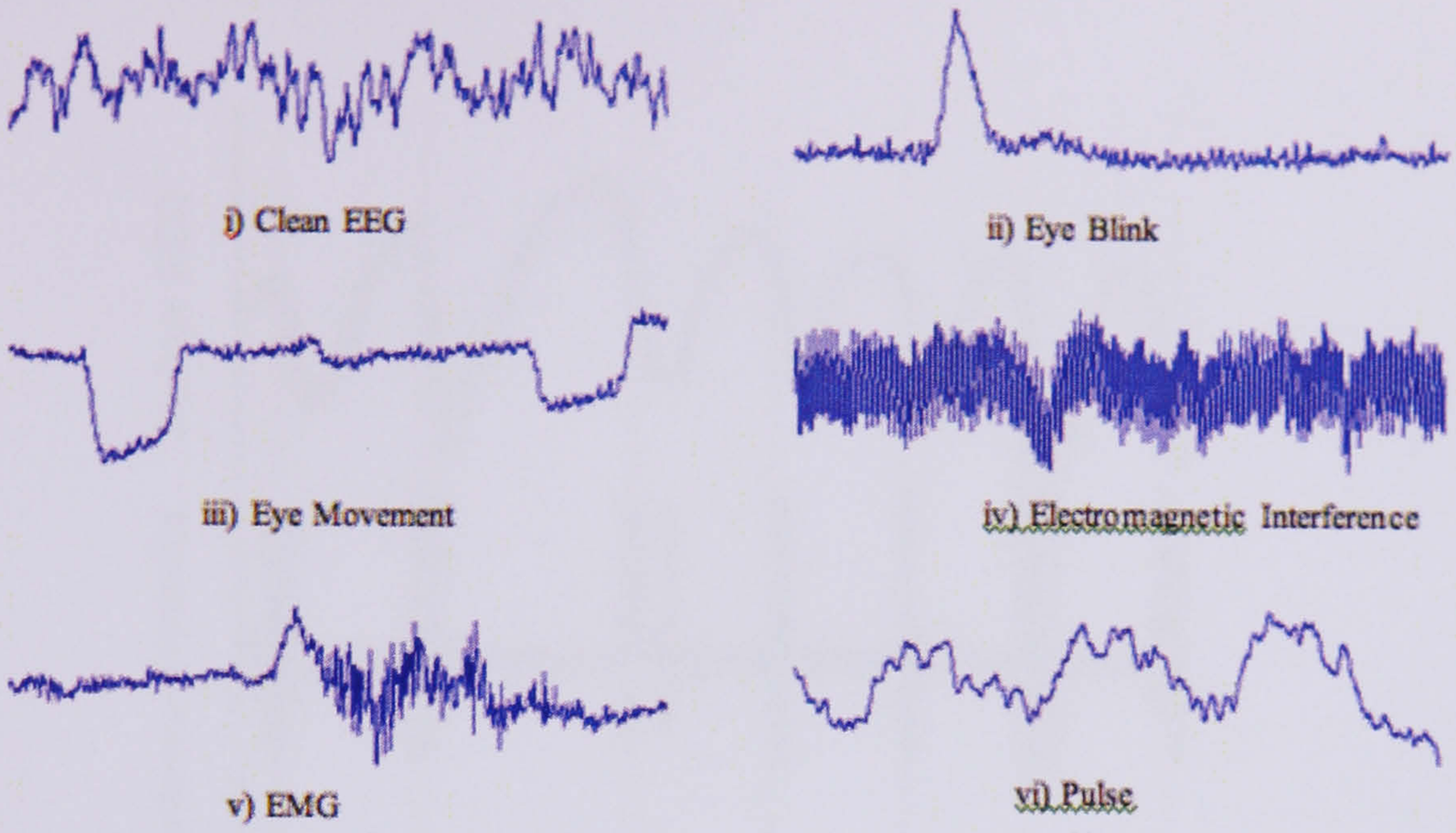

Figure 4.5: Typical EEG signals and artefacts.

Figure 4.5 gives indication of the major challenge that signal artifacts present to the EEG. Artifacts that display frequencies within the bandwidth of interest are of course the most disruptive to analyses. Mains or other electromagnetic interference can often be removed with filtering and high common mode rejection in the front-end electronics, whilst eye blinks, for example, affect high amplitude distortion within the EEG pass-band even on electrodes positioned to the rear of the head. Eye movement 'nystagmus' artifacts often occur simultaneously with eye blinks adding further contamination to the resulting waveform. EMG signals emanating from the various muscles of the face and neck cover a broad bandwidth and are often considerably larger than EEG signals. In addition, when electrodes are positioned near blood vessels, low frequency distortion is observed.

As discussed, the voltage fluctuations observed at the neuronal cell membrane as described in figure 4.2 are not easily translated to large populations of neurons or the surface EEG. However, in studies on the visual cortex of the cat, Gray and Singer (1988) reported that the positive peak recorded on the neuronal membrane potential during action potential propagation is synchronous with the negative peak of surface oscillations as shown in figure 4.6. This implies that if a population of neurons presents rhythmic oscillations at the scalp surface, it is the period of the resting potential phase that determines the frequency of oscillation. Since anaesthetics are known to assert effects on neurotransmission, it might be assumed that changes in oscillation frequency observed during anaesthesia would be the result of EPSP and IPSP interventions modifying the period of synaptic membrane resting potential.

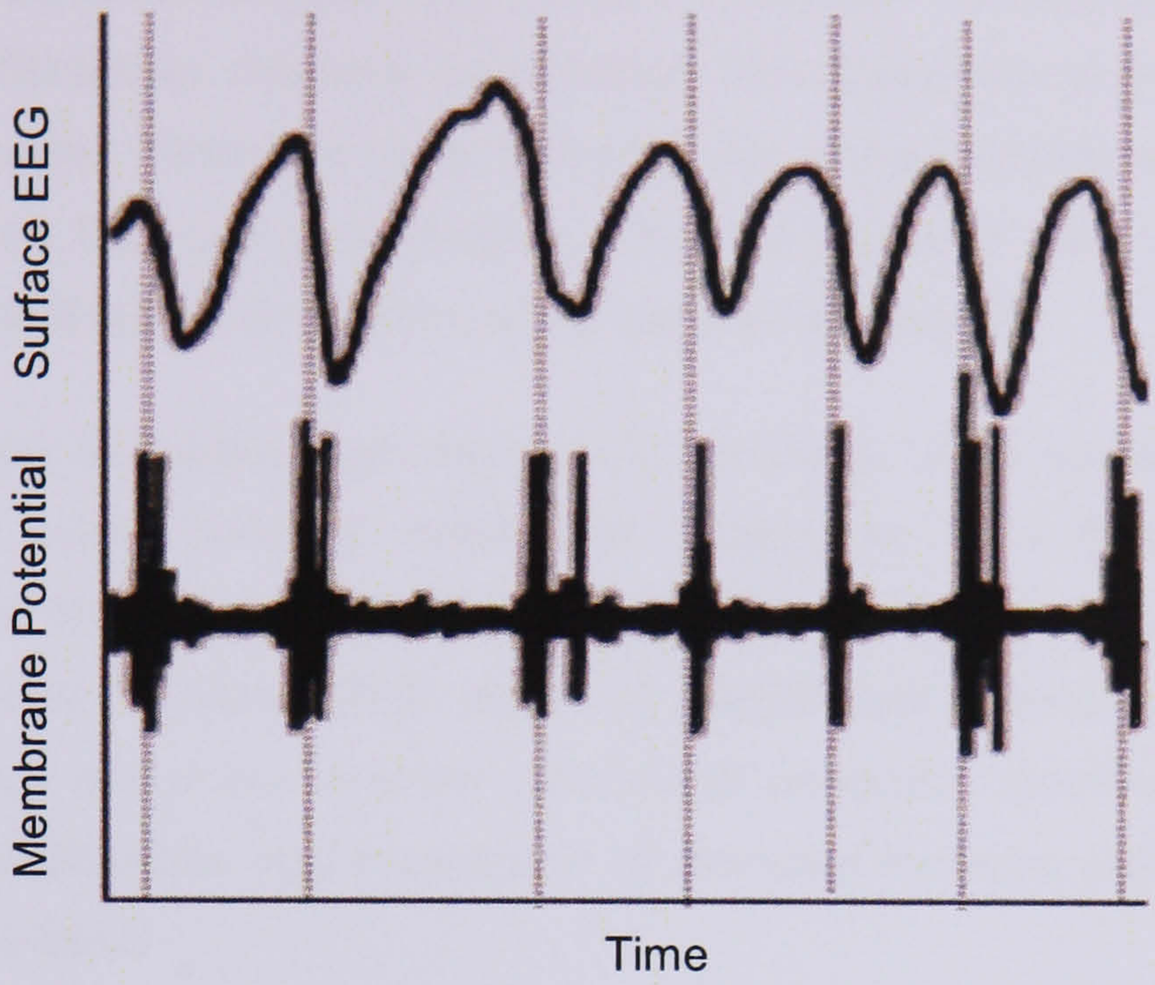

Figure 4.6: Phase relationship between membrane potential and surface EEG oscillations. Adapted from: Gray and Singer, 1988.

In summary, although other structures and processes are implicated, it is primarily the flux of ions consequent of synchronous synaptic neurotransmission of action potentials across populations of neurons that is observed in the surface EEG signal. The balance of excitory post-synaptic potentials (EPSPs) and inhibitory post-synaptic potentials (IPSPs) at the neuronal cell membrane determines when an action potential is propagated. This is convenient to the study as anaesthetics are known assert their effects by modulating synaptic transmission processes. It is thus reasonable to conclude that a profile of the neurotransmitter pathways each anaesthetic agent affects may commute to understanding of the changes in the EEG observed by Clark and Rosner (1973) during anaesthesia.

The orientation of neurons in the brain implies that the major contribution to the surface EEG signal is the pyramidal and, to a lesser extent, stellate cell activity in the outermost plexiform layer of the cortex. Thus if the firing pattern of pyramidal and stellate cells represented in the plexiform holds a correlate of consciousness, the surface EEG may indeed present a method of monitoring consciousness. It is of considerable interest that high frequency firing stellate neurons that mediate attention can be found in the plexiform, not only because loss of attention may undermine the efficacy of the isolated forearm assessment technique, but also because the study of high frequency EEG is relatively new. The evolution of the high-speed and high-resolution technologies needed to study high frequency EEG are becoming available and may thus provide valuable research potential.

The relatively poor spatial resolution at the scalp combines the activity of tens of millions of neurons to give the potentials observed on each electrode. This implies that the surface EEG signal will be affected by neuronal transmission associated with a great many tasks being performed in parallel. Since it is likely that particular characteristics of surface EEG may be the result of more than one phenomenon, distinguishing each may only be possible when there are significant temporal or phasic differences between them.

Although electrical synpasing does not directly contribute to the surface EEG signal, phasic relationships in action potential propagation subsequent to sufficient electrical synapse activity does. The formation and loss of synchronous action potential firing is a key element to the analyses used in some EEG depth of anaesthesia monitor solutions. If electrical synpasing plays a role in the temporal control that underpins synchronous activity then it is likely that any anaesthetic agent mediation of electrical synapse activity will impact on the recorded surface EEG.

It is also of interest that galvanic skin response measurement may contribute more to anaesthetic depth assessment than early experimentation revealed. The intuitive link between noxious stimulation and stress responses in the skin make this an inviting area for further research.

Chapter 5

Functional Anatomy of Three States of Awareness

In chapter 4 it was established that the alternating electrical potentials recorded on the surface of the scalp are primarily the derivation of synchronous synaptic transmission across regions of pyramidal dendrites in the plexiform layer of the cerebral cortex. Through surgical removal it has been shown that the absence of the cerebral cortex does not affect a global abolition of consciousness; provided the brainstem is intact a level of basic vigilance functionality is maintained (Nolte, 2002). In the domain of the anaesthetist the EEG and its derived parameters are termed 'direct measures' of consciousness. The occurrence of EEG burst suppression (discussed further in section 6.14) can be thought of as a binary indication of deep unconsciousness giving the direct measure viewpoint some validity, but unless the brainstem ascends a sufficiently spatial correlate of consciousness to the plexiform, surface EEG would more likely be considered an indirect measure of consciousness by the neuroscientist.

Needle EEG studies have provided a mass of information that relates functionality to neuroanatomical structures and neuronal pathways. Since, as discussed, observed needle EEG phenomenon cannot be directly commuted to expectations of surface EEG characteristics, the possibility of identifying indirect links between the functional anatomy associated with states of consciousness and the emanating surface EEG is of fundamental importance in the evaluation of surface EEG applied to depth of anaesthesia monitoring.

5.1 Consciousness

The question of what constitutes consciousness has been a topic of postulation for millennia. Some theories emanating from the worlds of philosophy, religion, psychology, and

neuroscience can seem somewhat eccentric but the increasing sophistication of techniques used in modern studies of consciousness, the relevance of the conclusions drawn, along with their correlation to the observations and theoretical models developed in the field of anaesthesia, warrants their treatment in this study.

Neuroscience identifies a number of 'neural correlates of consciousness'. The natural assumption made by an anaesthetist might be that a neural correlate of consciousness would indicate, when present, a state of consciousness, and in its absence, would indicate unconsciousness. However in neuroscience, the term relates to subjective experience. For example, Leopold and Logothetis (1996) showed that whilst the primary visual cortex is the destination of afferent visual information, needle EEG studies reveal the 'experience' of visual information resides in the subcortical inferior visual cortex. This suggests that although electrophysiology directly associated with visual perception is observable in surface EEG recordings, visual experience may only be detected indirectly using surface EEG apparatus if at all.

Whilst the goal here is to identify a surface EEG correlate of awareness, the example of visual experience is useful as experiment designed to identify the neuronal communication links involved in this straightforward feature of consciousness are relatively simple in comparison to the design requirements needed to elucidate the same of more complex functionality such as memory. The neuronal map of visual processing substrates and communication links developed through neuroscience research shows a complex network reaching across several regions of the brain that are also implicated in other functionality. It seems unlikely, therefore, that the low spatial resolution of the surface EEG monitoring technique will permit presentation of a strong correlate of visual experience or any other single feature of consciousness unaffected by other cortical activity.

Figure 5.1 presents the neural map of visual perception communication links. The complexity of the network implies that significant temporal control of communication must exist to ensure correct functionality. It seems intuitive when extrapolating this to all functionality of conscious experience, that the temporal marshalling of the communication involved will be fundamental to the existence of a single conscious awareness. This concept appears in neuroscience as the binding by synchrony theory that describes the temporal organisation of communication between regions of the brain. There are two other binding theories: binding by convergence and binding by assembly. The theory of convergence describes the transmission of sensory information from primary neural processing units to a mediating hub. The binding by assembly theory describes development of neuronal pathways and relationships that result

from repeated experiences. This principle of the assembly theory shares commonality with the neurophysiological concept of neural pathway plasticity.

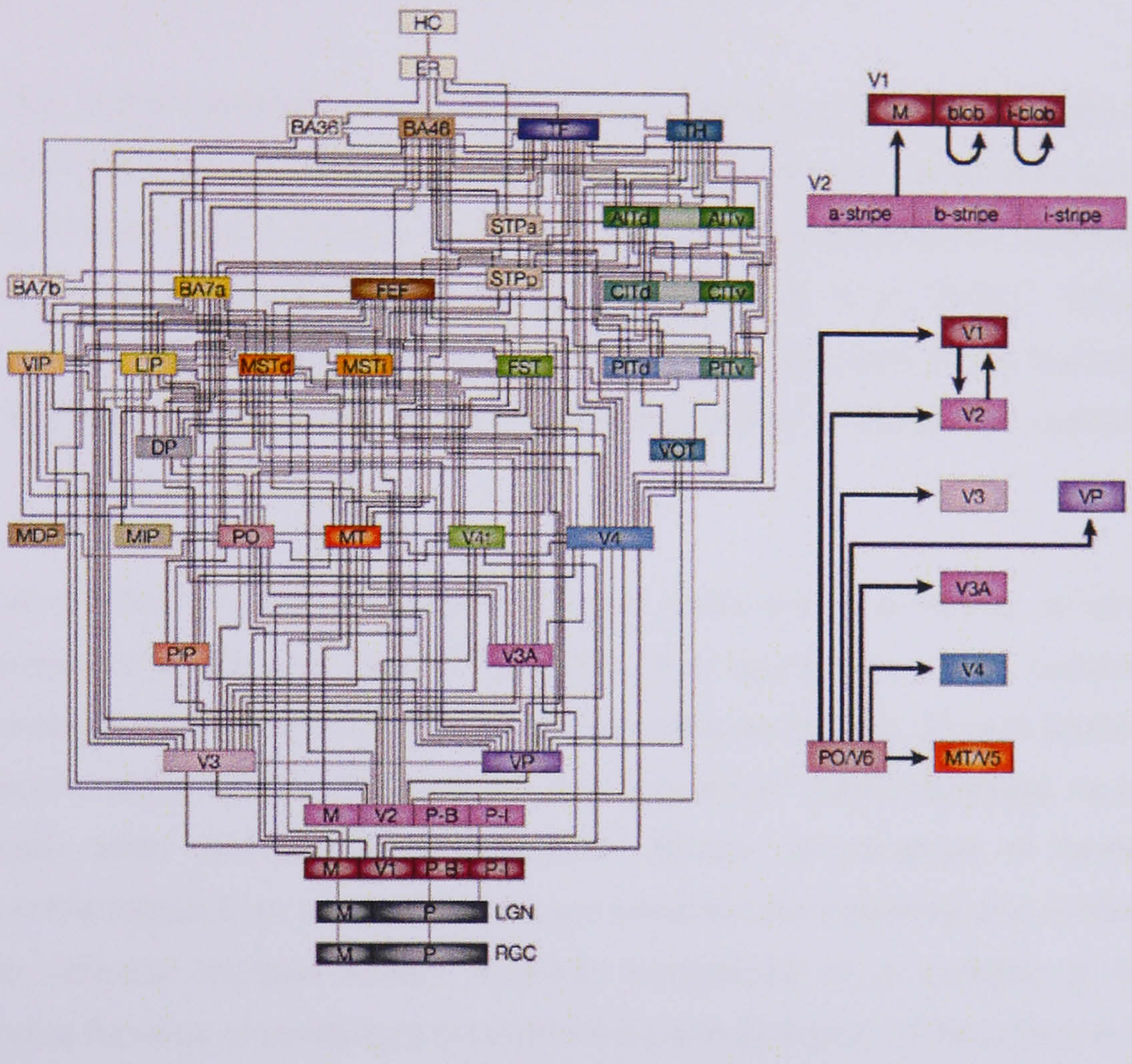

Figure 5.1: Anatomical hierarchy of visual areas in human and non-human primates. AIT, anterior inferotemporal cortex; BA, Brodmann area; CIT, central inferotemporal cortex; d, dorsal; DP, dorsal prelunate area; ER, entorhinal cortex; FEF, frontal eye fields; FST, floor of superior temporal cortex; HC, hippocampus; LGN, lateral geniculate nucleus; LIP, lateral intraparietal area; M, magnocellular regions; MDP, mediodorsal parietal area; MIP, medial intraparietal area; MSTd, dorsal part of the medial superior parietal area; MSTi, inferior part of the medial superior parietal area; MT, middle temporal cortex (visual area 5); P, parvocellular regions; P-B, parvo-blob; P-I, parvo-interblob; PIP, posterior intraparietal area; PIT, posterior inferotemporal cortex; PO, parieto-occipital area (visual area 6); RGC, retinal ganglion cells; STPa, anterior superior temporal polysensory cortex; STPp, posterior temporal polysensory cotex; TF–TH, temporal areas; v, ventral; V1–V4t, visual areas; VIP, ventral intraparietal area; VOT, visual occipitotemporal cortex; VP, ventroposterior visual area. Reproduced with permission from Rees et al., 2002.

Mashour (2004) proposes that it is the summation of binding processes that form consciousness, and instances of unbinding that underlie unconsciousness. Binding might therefore be considered a global neural correlate of consciousness, where vegetative states

might be thought of as 'disconnection' syndromes (Laureys, 2005). If this view is true then it is possible that identification of centres of temporal control may contribute to a greater understanding of the action of anaesthetic agents, and, since their functionality affects all others, may offer a measurable correlate of consciousness.

As early as the 1940s modulation of conscious functionality had been attributed to structures of the brainstem (Mozurri and Magoun, 1949). Although many cell assemblies are thought to have primary roles in consciousness review of the literature indicates the reticular formation and the thalamus to be fundamental (Chalmers, 2002; Rees et al., 2002). Whether either region may be the source of a correlate of consciousness available in the surface EEG will depend on the spatial spread and temporal footprint of their influence on cortical neuronal activity.

The temporal control of communication has been attributed to a variety of structures; of primary importance appears to be the thalamus, the hippocampus and cerebellum. In a review of the structure and function of the thalamic reticular nucleus, Pinault (2004) observes that the predominantly GABAergic thalamic neurons assert spatio-temporal neuronal firing dynamics over open and closed loop circuits. Phasic relationships of communication propagated in the region thus persist in pathways between the thalamus and cortex. Although the thalamic reticular nucleus shows rhythmic oscillations at a number of frequencies determined as a function of mediatory neurotransmission (Steriade, 2004), Pinault and others report that neurons in the region display a mean firing frequency of 40Hz. The combination of regional firing frequencies being propagated across the cortex with stable phase relationships presenting the possibilities of frequency or phasic correlates of consciousness in the surface EEG.

Pathologies of the hippocampus cause memory problems and disorientation. Not all forms of memory are affected, but episodic, short and long term memory formation are known to be impaired by hippocampus depression (Tesche et al., 1996; 2000). The formation of memory is thought to be the manifestation of a cooperation between the hippocampal, anygdala, prefrontal cortex, dentate gyrus, precuneus, annular gyrus, parietal and occipital regions (Badgaiyan et al., 1999; Buckner et al., 1995; Berns et al., 1997; Elliott and Dolan, 1998). Memories themselves appear to exist across the cortex and memory retrieval appears to be a function of the hippocampus (McIntosh et al., 1999; Gabrieli et al., 1998) although not exclusively (Buckner et al., 1995; Tranel et al., 1997).

Hebb (1949) first proposes a neuronal mechanism that relates the formation of memories with long-term increases in synaptic efficiency (Morris et al., 1986). This phenomenon has been

confirmed in many studies and is thought to be primarily mediated by NMDA glutamatergic neurotransmission in the hippocampal and dentate gyrus regions of the brain.

Hippocampal neuronal activity displays two distinct modes in needle EEG studies. During alert consciousness and some stages of sleep hippocampal neuronal activity presents firing frequencies between 6Hz and 9Hz. When in a resting state, the hippocampus propagates large, irregular, high frequency (150Hz to 200Hz) bursts of activity. GABA is also known to affect the response times to stimulation of the hippocampus where excitation depresses activity (Pearce, 1996).

Given the wide neuronal spatial spread of memories there exists the possibility that hippocampal activity may be represented in the surface EEG. As well as a 6 to 9Hz phasic characteristic, a high frequency relative amplitude analysis of the EEG may hold an indication of hippocampal activity.

Various cognitive functions have been attributed to the cerebellum including the attention to and processing of language and other sensory temporal stimuli (Rapp, 2001). Neuronal firing patterns display periods of synchrony in the EEG (Welsh et al., 1995) and are known to be influenced by glutamic and GABAergic excitation (Lang, 2001). Stimulation of cerebella functionality are thus likely to propagate definable characteristics in the surface EEG and may present some indication of the glutamic or GABAergic influences of the anaesthetic agents.

There are two distinct systems involved in the perception of pain. Afferent pain neurons terminate in the ventral posterior nucleus of the thalamus, which ascends associated pathways contralaterally into the somatosensory cortices. This lateral pain system is thought to be responsible for the discrimination and localisation of pain. The second medial pain system ascends thalamic projections to the insular cortex, the prefrontal and anterior cingulated cortices and the cerebellum. These pathways have been associated with the cognition of pain. Mediation of motor reflexes in response to noxious stimuli is a function attributed to the reticular formation with wide spread innervation across the cortex. Perception of pain has been associated with monoamine (serotonin, noradrenalin and dopamine) and acetylcholine neurotransmission.

Given the innervation associated with pain is to be found across the cortex it is possible that an evoked response to noxious stimuli will present itself in surface EEG studies. Of course this would not be an ideal indicator of awareness during anaesthesia as perception of pain is to be avoided. However the loss and return of the perception of pain during anaesthesia may be represented more generally through the inhibition or excitation of the neurotransmitter

pathways implicated. An analysis of the known neurotransmitter pathways anaesthetic agents are known to affect will follow in section 5.2.

Immobility may be caused by intervention at various points in the motor functional anatomy. As their name suggests the neuromuscular blockades operate at the neuro-muscular junction exciting inhibitory acetylcholine receptors for example. Central nervous system mediation of mobility has been located to the reticular formation, thalamus, anterior cingulate cortex and cerebellum as each cause immobility when inhibited. Review of the neurotransmitter pathways known to innervate these cell assemblies may allow some inference of interpretation of the surface EEG recorded during anaesthesia.

5.2 Anaesthesia

The pharmacodynamic profile of respiratory, cardiovascular and neurological effects of modern anaesthetic agents varies considerably giving the anaesthetist a range of features from which to select. Patient age, weight, any respiratory issues such as asthma, risk of epileptic episodes, term of gestation, and the likely content of the stomach will, along with many other possible factors, need to be considered before an appropriate selection can be made. An anaesthetist will also gain experience and confidence in the use of particular combinations of agents, concentrations, and methods of administration with respect to particular patient physiologies and pathologies. As such a wide variety of anaesthetic techniques are in use. Tables 5.1 and 5.2 present the inhaled and intravenous anaesthetic agents in current or recent use.

Halothane, Enflurane, Isoflurane, Sevoflurane and Desflurane constitute a group commonly referred to as the ‘volatile’ agents because each has a boiling point close to room temperature. The volatile inhaled agents superceded ether and other early agents with lower flammability and toxicity. All can irritate the respiratory system and so they are often mixed with air, oxygen or nitrous oxide to reduce this problem.

The motivations for using intravenous anaesthetic agents are compelling; rapid onset, rapid recovery and reduced atmospheric pollution make them a desirable choice. However, control of delivery is greater with inhaled agents and thus maintenance of intravenous anaesthesia can lead to higher doses being used than are required, deteriorating their superior recovery features and increasing the risk of overdose. If comprehensive monitoring were available, agent titration would be preferable to gaseous delivery.

Inhaled Agents	Description
Halothane	Introduced in the 1950s, Halothane has largely been replaced by Sevoflurane as it has lower hepatic toxicity.
Enflurane	Introduced in the 1950s, Enflurane has largely been replaced by Isoflurane as it has lower hepatic toxicity.
Isoflurane	Irritates the respiratory system and so use is in decline.
Sevoflurane	Preferred as it only mildly irritates the respiratory system.
Desflurane	Has rapid onset and offset.
Nitrous oxide	Nitrous oxide does not produce complete anesthesia on its own but is often combined with other agents. The advantage of nitrous oxide is that it only minimally affects the cardiovascular and respiratory systems.

Table 5.1: Inhaled anaesthetic agents and their features.

Intravenous Agents	Description
Barbiturates	Barbiturates are frequently used in the induction of anaesthesia as in low doses they have rapid onset and are comfortably tolerated.
Benzodiazepines	Although very similar in effect, benzodiazepines are often preferred to barbiturates as they have lower toxicity.
Propofol	Propofol has both rapid onset and offset. Improved recovery and amnesic properties have made Propofol popular.
Etomidate	Etomidate is short-acting and does not affect cardiovascular changes in contrast to other agents. It is thus used often in emergency trauma treatment.
Ketamine	Profound and cataleptic analgesia is reached at lower doses of ketamine than other agents. Ketamine causes minimal respiratory depression and, unlike other agents, cardiovascular excitation. This allows ketamine to be used in some trauma treatments where cardiovascular depression may compound the inherent problems of blood loss.
Opioid Agents	Opioids do not produce complete anaesthesia; they are used for their analgesic properties.

Table 5.2: Intravenous anaesthetic agents and their features.

Both inhaled and intravenous agent groups contain apparently disparate compounds with large variations in potency. For example the three atoms of nitrous oxide form a molecule that

has a potency some 10,000 times less than the 14 atom molecule of Sevoflurane. It is thus likely not only that effector sites of each agent will be varied, but also that not all effects of each agent will be additive when used in combinations. Heinrichs (2008) confirms this with observations of combined Remifentanyl and Propofol anaesthesia.

Animal and in vitro studies have established that the 'A" class of gamma-aminobutyric acid receptor (GABA-A) is the major effector site of many anaesthetic agents. GABA is the major inhibitory neurotransmitter of the central nervous system and its various classes of receptor can be found in most neurons of the central nervous system. Many isoforms of GABA-A receptor sub-unit proteins have been identified and their structures profiled, however, the differences in effect of anaesthetics that may preferentially bind with GABA-A receptors appears to be in their potency as opposed to qualitative differences in receptor preference (Harris et al., 1995). That said some agents have been shown to require two or more isoforms to act, most notably Etomidate, the barbiturates and the benzodiazepines (Barnard et al., 1998) and are thus likely to affect different pathways to other GABA acting agents. In addition, particular isoform combinations present resistivity to some agents, notably Propofol (Davies et al., 1997).

GABA-A acting anaesthetics are known to enhance GABA activity and enhance receptor affinity to GABA mediating trans-synaptic membrane chlorine ion movement slowing the deactivation phase of action potentials (Li and Pearce, 2000; Zhu and Vicini, 1997; Bai et al., 1999) for up to seconds (Celentano and Wong, 1994). With sufficient coherence across a population of cells this may manifest at the surface EEG level as a slowing of frequency as described in section 4.3. It has also been shown that GABA can disrupt the occurrence of widespread 40Hz rhythmic activity and hippocampal theta activity associated with memory (Larson et al., 1986).

Inhibitory acetylcholine receptor variants are widely distributed throughout the central nervous system and neuromuscular junctions. Nicotinic cholinergic receptors have been attributed amnesic properties, as they appear to mediate activity in the hippocampal region. Cholinergic modulation of serotonin, dopamine, glutamate, and GABA reception is known to be associated with arousal (Woolf, 1991). The neuromuscular blockade asserted by curare and other agents is known to be a function of cholinergic inhibition. Cholinergic inhibition is an operational feature of anaesthetic agents.

Glutamic acid is the major excitory neurotransmitter of the nervous system. There are three families of the glutamate ligand-gated ion channel receptor: alpha-amino-3-hydroxy-5-methyl-4-isoxazolepropionic acid (AMPA), Kianate, and N-methyl-D-aspartic acid (NMDA). Both

NMDA and AMPA receptors are to be found throughout the central nervous system whilst kianate receptors are differentially distributed but can be found in abundance on pathways leading to the hippocampus. The depression of glutamatergic responses is known to be a major feature of many anaesthetic agents (Richards and Smaje, 1976) but there are some exceptions.

Glycine is a further inhibitory neurotransmitter mediating synaptic chlorine ion exchange, in common with GABA. There are at least four structurally distinct families of glycine receptor each with varying distribution across the central nervous system.

Contrary to the conclusions drawn in early studies it has been shown that volatile anaesthetic agents can directly inhibit sodium ion channels by up to 50% in the rat brain (Rehburg et al., 1996). Calcium ion channels are also known to be inhibited by anaesthetics at clinically relevant concentrations. It has been reported that calcium ion channel inhibition enhances anaesthetic potency in mice and rats (Dolin and Little, 1986; Wu et al., 2004). Potassium ion channels in the brain are not thought to be directly affected by anaesthetics at clinically relevant concentrations (Franks and Lieb, 1994), although interaction has been noted in potassium ion channels of the spinal cord (Nicoll and Madison, 1982; Kim et al., 2007) and may thus contribute to immobility.

Various studies by Rampil and colleagues locate the mediation of movement to the spinal cord. Movement responses were shown to remain after removal of the rat cortex, thalamus and after hypothermic transection between the rat brain and spinal cord (Rampil et al., 1993; Rampil, 1994). Antognini confirms this in studies using Isoflurane and Propofol (Antognini et al., 2000; 2007).

Research opportunities presented by the development of positron emission tomography have given rise to a greater understanding of where anaesthetic agents assert their effects on memory. Amnesic agent properties have been associated with a slowing of firing frequency in the hippocampus, thalamus and prefrontal cortex. This is confirmed with observation of lower cerebral blood flow in these regions (Veselis et al., 1997; 1997b; 2000; 2000b).

Although both the opioids and nitrous oxide are known to act on widely distributed regions of the central nervous system Antognini has shown that the thalamus, midbrain reticular formation and anterior cingulated cortex are primarily involved in their analgesic effects (Antognini, 2002; Carstens and Antognini, 2005).

Table 5.3 presents anaesthetic agents used in modern practice along with the major neurotransmitter pathways they are known to affect. The numbers assigned to each represents the interactions of the agents on each pathway. Positive numbers indicate excitation where a '2' represents a strong excitation, whilst negative numbers indicate inhibition with '-2' representing strong inhibition. Blank spaces are left where no specific interaction has been identified in the literature.

	GABA-A	Glycine	Acetylcholine	Serotonin	AMPA	Kianate	NMDA
Etomidate	2	1	-1	0			
Propofol	2	2	-1	0	-1	0	-1
Barbiturates	2	1	-1	-1	-2	-2	0
Ketamine	1	0	-1	1	0	0	-2
Isoflurane	2	2	-1	2	-2	2	-1
Sevoflurane	2	2	-1				
Nitrous Oxide	1	1	-2	-2	-1	-2	-2

Table 5.3: Neurotransmitter pathways implicated in the action of various anaesthetic agents. Positive numbers indicate the agent effect is excitory, whilst negative numbers indicate inhibitory behaviour. Adapted from Jurd et al., 2004, with further contributions from: Krasowski and Harrison, 1999; Yamakura and Harris, 2000.

In conclusion, if as discussed, removal of the cortex does not necessarily assert unconsciousness it might be argued that a direct correlate of consciousness cannot exist in the neuronal activity of the plexiform. Whilst this may be true, there remains the possibility that brainstem pathways that ascend into the cortex may present direct representation of consciousness.

The literature indicates that of the neurotransmitters GABA-A, acetylcholine and glutamic acid are of primary importance in the action of the anaesthetic agents. Although all are to be found widespread across the central nervous system it is of note that the major centres of temporal communication control are predominantly innervated by pathways of these primary neurotransmitters. It seems intuitive that the patterns of major neurotransmitter inhibition and excitation displayed by each anaesthetic agent should provide a discernable footprint in the EEG. For example, recent studies identify suppression of brainstem arousal (Heinke and Schwarzbauer, 2002) and disturbances in thalamocortical brain activity to be the principle mechanisms in the pharmacological assertion of unconsciousness (Mashour, 2004; 2005;

Antowiak, 2002). This is supported in a report by John and colleagues (2001) who noted a dissociation of synchronized gamma bandwidth activity during anaesthesia. As such, anaesthetic agents shown to strongly affect GABA-A pathways, which innervate the thalamus, are likely to be well represented in the phasic characteristics of the surface EEG.

The effects of anaesthetic agents on glutamic neurotransmitter pathways may also be present in the surface EEG reflecting disruption to the temporal control of communication asserted by the hippocampus. This effect may be supplemented by disruption to the activity of the stellate cells near the surface of the brain that together with the hippocampus form part of the neural network associated with memory.

It is also noted that electrical synpasing may be affected by anaesthesia. Electrical synapsing is dependant on the balance in concentrations of calcium ions across the neuron membrane. The observation that calcium ion channels are blocked by anaesthetics at clinically relevant doses indicates a probability that the communication synchrony engendered with electrical synapsing will be disturbed.

There is evidence to suggest that direct correlates of components of consciousness reside in plexiform neuronal activity. Various primary sensory activities have been mapped to areas of the cortex with evoked surface EEG characteristics that have been used with some success to monitor depth of anaesthesia. However, these characteristics may not be ideal metrics as they indicate when functionality has returned during anaesthesia, which may be too late to prevent traumatic awareness.

If neither a direct correlate of consciousness or component of consciousness can be found, the EEG signal may well only present indirect information pertaining to depth of anaesthesia. Indirect correlates certainly exist in the activity of the plexiform but may be difficult to distinguish or may not be reliable metrics across all anaesthetic techniques.

5.3 Sleep

Many note that the loss of consciousness observed during normal sleep shares features with pharmacologically asserted unconsciousness (for example Massimini, 2005). The EEG generated during sleep has been extensively researched and characterised, as has the functional anatomy associated with the mediation of the circadian sleep cycle. If EEG is a direct measure of consciousness it should be possible to draw parallels between the EEG of

a sleeping subject and that recorded during agent-induced unconsciousness. Given the neurophysiological derivation of the EEG signal a profile of the neurotransmission and functional anatomy known to be associated with sleep will support conclusions drawn.

For many years the industry standard classification of the stages of sleep was that presented by Rechtschaffen and Kales (1968) in their publication 'A Manual of Standardized Terminology, Techniques and Scoring System for Sleep Stages of Human Subject'. Three main stages are identified:

Wakefulness;
Rapid Eye Movement (REM) sleep;
Non-REM sleep.

Measures of cerebral blood flow and glucose utilisation show that the brain is as metabolically active during REM sleep as it is during wakefulness (Lydic and Baghdoyan, 2005) hence the term 'paradoxical sleep' is sometimes used to describe REM sleep (Jouvet 1965).

Gottesmann (2002) reports that the onset of sleep is initiated by gamma-aminobutyric acid (GABA) inhibition of wake promoting neurons of the posterior hypothalamus and activation of the preoptic area of the anterior hypothalamus. This is supported by administration of GABA enhancing hypnotics amplifying this effect (Lancel, 1999). Regulation of early Non-REM stages of sleep has been located to the laterodorsal and pedunulopontine tegmental nuclei that ascend projections to the thalamus, basal forebrain and the cortex (Daniel et al., 2006).

Arousal can first be observed in the reticular activating system where much of the body's afferent sensory pathways converge (Sarter et al., 2006). The locus coeruleus (Daniel et al., 2006), and dorsal raphe nucleus (Bjorvatn, 1997) are also implicated.

Sleep modulation is known to involve glutamergic, serotonergic, dopaminergic, noradrenergic, cholinergic, histaminergic and orexin neurotransmitters. Serotonin (5-HT)-containing neurons in the midline raphe nuclei and noradrenergic neurons in locus coeruleus contribute actively to the generation of wakefulness, slow during Non-REM sleep and have been shown to cease activity during REM sleep (Baghdoyan and Lydic, 2002). When the synthesis of noradrenalin is disrupted in mice, a decrease in levels of action potential activity during wakefulness and REM sleep can be observed; indicating noradrenergic neurotransmission also contributes to the generation of wakefulness and REM sleep (Ouyang et al., 2004). Similarly, acetylcholine levels have been noted to be higher during wakefulness and REM sleep than Non-REM (Baghdoyan and Lydic, 2002), whilst glutamate levels drop during both REM and Non-REM

sleep (Hudspith, 1997). Cholinergic agonists have been shown to ablate sleep spindles, an EEG phenomenon of sleep discussed further in section 7.3 (Sleigh et al., 1999). The inhibitory action of adenosine in the reticular formation laterodorsal tegmental and pedunculopontine tegmental nuclei has been shown to contribute to the promotion of sleep (Porkka-Heiskanen et al., 1997) whilst orexins have been shown to participate in arousal (Lees and Coyne, 2004; Peyron et al., 1998). As stated, arousal can first be observed in the reticular activating system where noradrenergic and cholinergic neurotransmitter pathways dominate. Histamines are known to play a significant role in vigilance, and the correlation between action potential frequency of histaminergic neurons in the hippocampus at sleep onset is clear, showing slower frequencies during tiredness and complete cessation during REM and Non-REM sleep (Sansom, 2000; Haas and Panula, 2003). Table 5.4 gives a summary of the neurotransmitters implicated in the control of sleep and their principle centres of innervation.

Neurotransmitter	Principle Innervation Pertinent to the Sleep Cycle
Glutamate	1. Hippocampus (Hudspith, 1997) 2. Dentate gyrus (Pöschel et al., 2002)
GABA	1. Hypothalamus (Gottesman, 2002) 2. Pontine reticular formation (Gottesman, 2002) 3. Dorsal raphe nucleus (Gottesman, 2002) 4. Locus coeruleus (Gottesman, 2002)
Acetylcholine	1. Basil Forebrain (Steriade, 2004) 2. Coritcthalamic and Thalamicoritcal pathways (Steriade, 2004) 3. Pedunculopontine Tegmental Nucleus (Kodama et al., 1999) 4. Caudomedial medulla (Kodama et al., 1999)
Seratonin	1. Raphe Nucleus (Sallanon et al., 1985)
Noradrenalin	1. Locus Coeruleus (Hirota and Kushikata, 2001)
Dopamine	1. Substantia Nigra (Montia and Montib, 2007) 2. Ventral Temgmental Area (Montia and Montib, 2007)
Adenosine	1. Pedunculopontine Tegmental Nucleus (Porkka-Heiskanen et al., 1997) 2. Laterodorsal Tegmnetal Nucleus (Porkka-Heiskanen et al., 1997)
Histamine	1. Tuberomamillary Nucleus (Haas and Panula, 2003)
Orexin	1. Lateral to Posterior Hypothalamus (Lees and Coyne, 2004)

Table 5.4: Principle neurotransmitters and anatomy implicated in the control of sleep.

To conclude, it is of note that GABA-A inhibition of the hypothalamus is thought to contribute to the onset of sleep. The hypothalamus provides a link between the central nervous system and the endocrine system and so it is likely that hypothalamus inhibition is a major feature of the sleep cycle. If GABA-A inhibition suppresses the release of wake promoting hormones, it is possible that suppression of hormone release is a feature of GABAergic agent anaesthesia.

It is also of note that cholinergic pathway excitation is implicated in wakefulness and REM sleep. During Non REM sleep the cholinergic thalamocortical pathways are suppressed. As

one of the major neurotransmitters implicated in the action of anaesthetic agents, it is possible that a dissociation of phase relationships in the region of 40Hz may feature in the EEG recorded during sleep as well as cholinergic anaesthesia.

The inhibition of glutamic pathways in the hippocampus is a major feature of anaesthesia. Since inhibition of these same pathways is also a feature of sleep, it is possible that a common feature of the EEG exists between the two states.

Chapter 6

Data reduction

Many real-world signals can be completely characterised with a thorough understanding of the underlying physics of the system generating the signal. System-modelling techniques can then be employed to derive data reduction techniques appropriate to particular applications. The EEG signal combines many different contributions and whilst advances in EEG modelling continue to evolve, it has yet to be shown that it is possible to predetermine the form of this complex signal. Data reduction techniques have nonetheless been applied to the signal in efforts to identify useful features.

All data reduction techniques have axioms to their proper function and limitations to their interpretation. If either an inappropriate technique is employed or improper interpretation of data is applied, conclusions drawn may misrepresent the efficacy of EEG to the application. It is thus necessary to critically review the mathematical foundations of methods that appear in the literature such that where possible, the validity of the research can be ascertained. Particular attention is paid to Parametric Spectral Estimation methods as it forms the basis of the patented mathematics.

6.1 Time Domain Analyses

6.1.1 Amplitude

As has been established, there are numerous factors such as skull thickness and skin resistivity that will contribute variability to absolute amplitude measurements of the EEG signal. Subsequently where measurement of total EEG amplitude is used in depth of anaesthesia monitors it is displayed as a trace that varies over time. This method allows direct interpretation of raw data.

The Cerebral Function Monitor (CFM) from Lectromed Devices Ltd. (Letchworth, UK) takes peak-to-peak measurements of the EEG signal and calculates the mean total amplitude. The mean is displayed as a trace with the variance (a statistical measure of data dispersion discussed further in section 6.1.2) alongside. A typical print out from the CFM is given in figure 6.1. The signal mean is shown in the figure as the central trace alternating about a peak-to-peak amplitude of 9μV. The variance of the signal is shown above and below the mean trace.

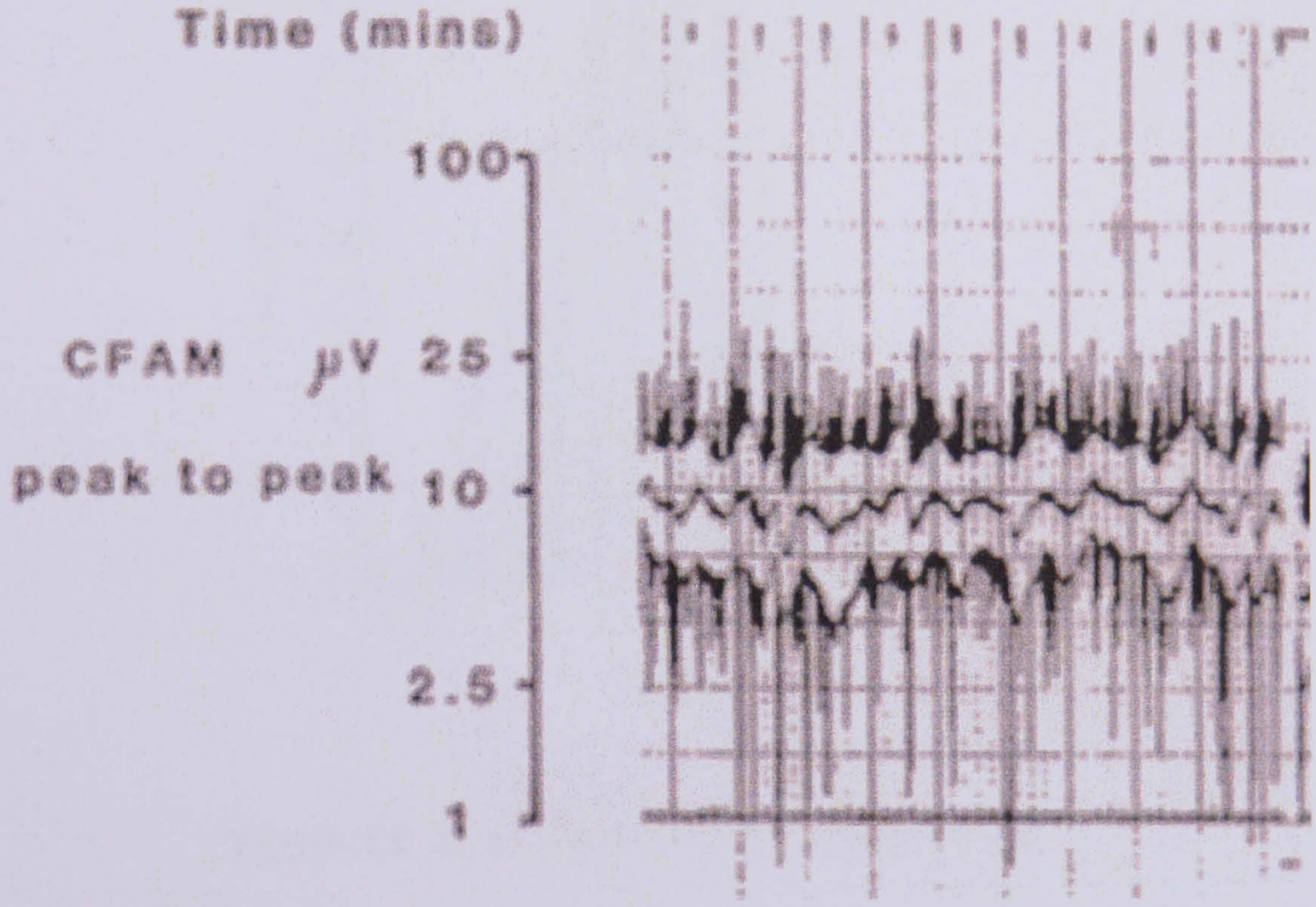

Figure 6.1: Averaged total peak-to-peak voltage output from the Lectromed Devices Ltd. (Letchworth, UK) CFM monitor.

The CFM display thus provides a useful and mathematically stable measure together with indication of how reliable interpretation of the data might be.

6.1.2 Statistical Measures

There are many statistical descriptors that can be applied to a signal. Commonly used in time domain analyses of the EEG are those that characterise commonality in sample amplitudes.

By adding up how many times each sample amplitude occurs within a data set and plotting them on a graph, an amplitude probability distribution is given. An example is given in figure 6.2. In the figure a red line has been added to high light the shape of the probability distribution across the sampled values. If a sample were selected at random from the data set, the probability distribution would allow the amplitude to be predicted with a known probability of being correct.

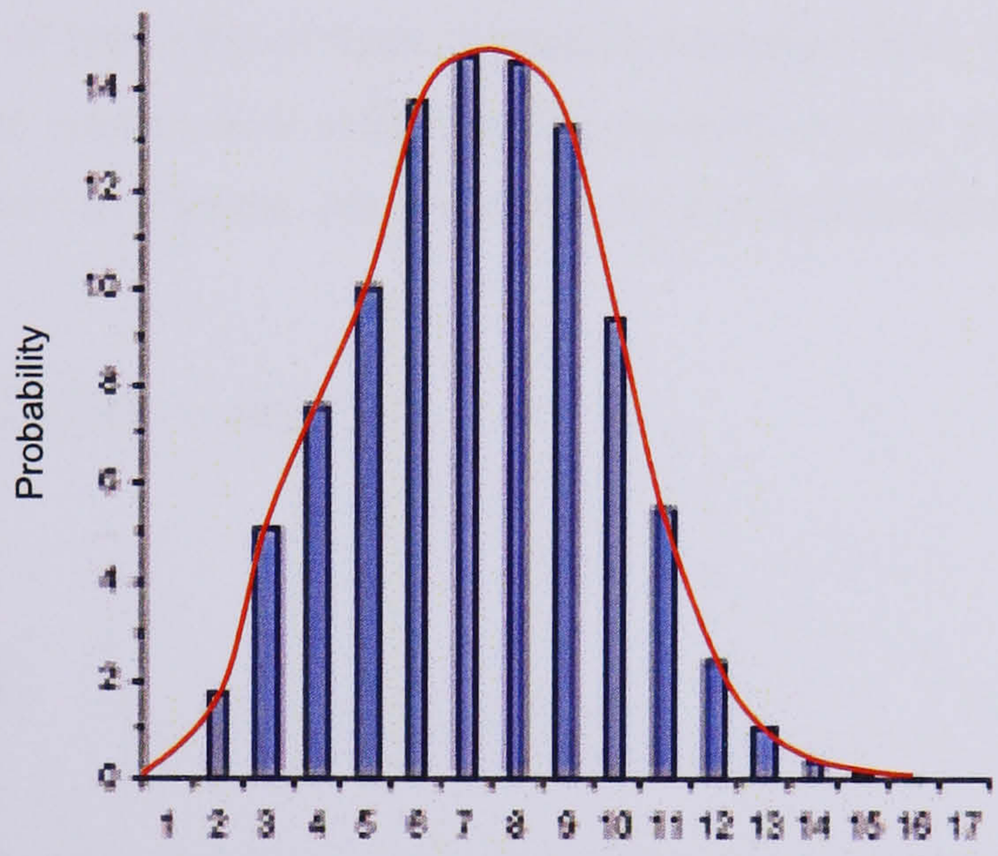

Figure 6.2: Example of a probability distribution.

Tone of the most useful and simplest of the statistical measures used is the amplitude mean. With a discrete time series $x[n]$, the series mean m_x is given by:

$$m_x = \frac{1}{N}\sum_{n=1}^{N} x[n]$$

where N is the total number of samples in the series.

Of course, the mean tells nothing about how dispersed the data samples are about the mean. As the average of all the distances of the samples from the mean will always equal 0, a measure termed the 'variance' is used that instead presents the mean of the squares of each deviation. As such the variance (sometimes called the 'second moment about the mean') can be calculated by:

$$\sigma^2 = \frac{1}{N}\sum_{n=1}^{N}(x[n] - m_x)^2$$

The variance is a robust mathematical method and is used in the CFM monitor discussed in section 6.1.1. The square root of the variance is termed the standard deviation and is also commonly used in statistical analyses.

Neither the mean nor the variance describes the shape of the distribution of data amplitudes. By taking the average of the cube of each sample's deviation from the mean (termed 'the third moment about the mean') it is possible, by dividing by the cube root of the signal variance, to identify where, in general, the deviations lie in the probability distribution.

$$\sigma^3 = \frac{1}{N}\sum_{n=1}^{N}(x[n] - m_x)^3$$

$$\beta_1 = \frac{\sigma^3}{(\sigma^2)^{3/2}}$$

where β_1 is termed the skewness of the sample magnitude distribution. Negative values of skewness present a distribution with a greater probability of high values, whilst positive values show a high probability of lower values as described in figure 6.3.

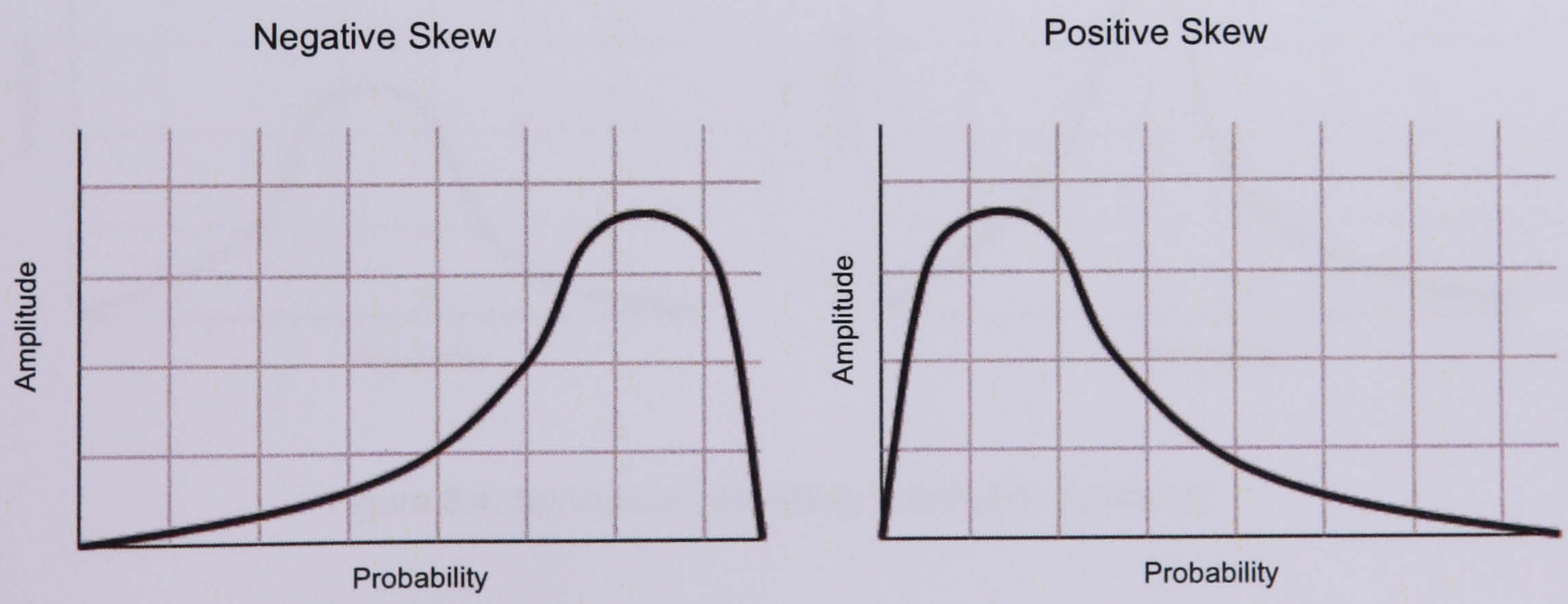

Figure 6.3: Skewed probability distribution functions.

If the variance of a data set is small, it is reasonable to infer that the data samples are generally of a similar magnitude and are thus closely grouped around their mean. If data samples show close grouping around a value that is not the mean, the variance will not represent this. The skewness of the data set will indicate at where in the probability distribution the grouping occurs, but it does not indicate how similar the values are within the grouping. This is termed the 'kurtosis' of the data sample distribution.

By taking a fourth moment about the mean:

$$\sigma^4 = \frac{1}{N}\sum_{n=1}^{N}(x[n] - m_x)^4$$

the kurtosis of data set, β_2 , can be found by:

$$\beta_2 = \frac{\sigma^4}{(\sigma^2)^2}$$

High values of β_2 show a more pronounced peak in the probability distribution to lower values as presented in figure 6.4.

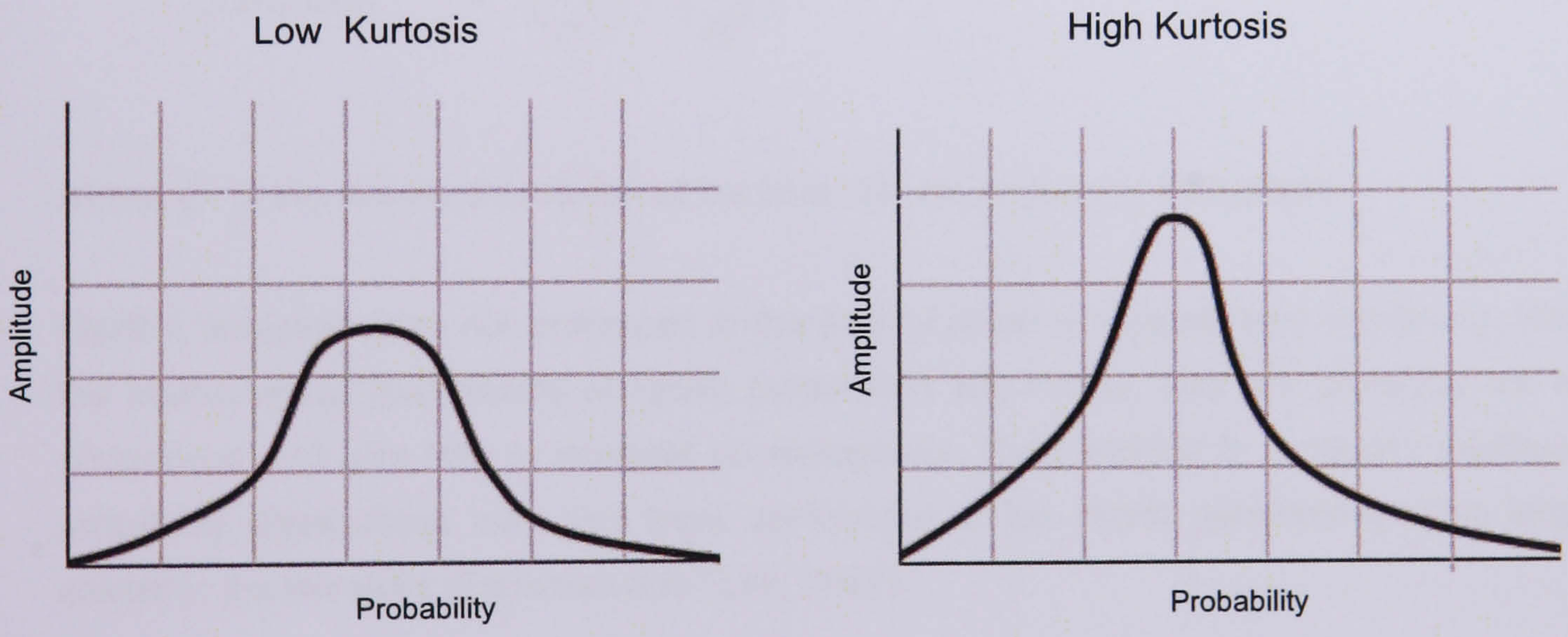

Figure 6.4: Kurtosis of probability distribution functions.

Although the statistical measures are discussed here with respect to time-domain analyses, they can of course be applied to any data set, including, for example, a series of frequency

component amplitudes. If there is more than one grouping of amplitudes within a data set, referred to multi-modal data, the statistical analyses described do not present this information.

6.1.3 Hjorth Descriptors

Hjorth's set of parameters (Hjorth ,1970), referred to as 'normalised slope descriptors', provide information that saw some popularity in the 1970s. The analyses share much commonality with the statistical measures described above, but in a form that could be implemented in analogue circuitry at a time when digital solutions were not fast enough to provide real-time equivalence.

Hjorth defines the normalised slope descriptors as follows:

$$\text{Activity} = \sigma^2$$

$$\text{Mobility} = \left(\frac{\sigma^3}{\sigma^2}\right)$$

$$\text{Complexity} = \left(\frac{\sigma^4}{\sigma^3}\right) / \left(\frac{\sigma^3}{\sigma^2}\right)$$

where σ is the standard deviation of the time domain probability distribution.

Hjorth's analyses were not embraced in the field of depth of anaesthesia monitoring. Whilst the mathematical foundations of Hjorth parameters are robust, they are generally not well understood and give little to interpret physiologically. Their inability to represent multimodal probability distributions may also have contributed to the Hjorth parameters being largely absent in the literature (Bankman and Gath, 1987).

6.1.4 Burst Suppression Ratio

The Burst Suppression Ratio is a measure of how much of a selected epoch of data is built of burst or suppression activity. Figure 6.5 shows a data set showing burst suppression behaviour. The periods of suppression seen in the figure represent cerebral inactivity as may

be observed during deep anaesthesia. The periods of suppression are easily identifiable and several studies relate lengthening periods of suppression to increasing depth of anaesthesia (for example Riker et al., 2003). Recent studies (for example Särkelä et al., 2003) have shown that the amplitude of burst activity provides additional detail to the measurement of depth of anaesthesia when used along side the ratio of the period of burst activity to the period of suppression (known as the Burst Suppression Ratio),

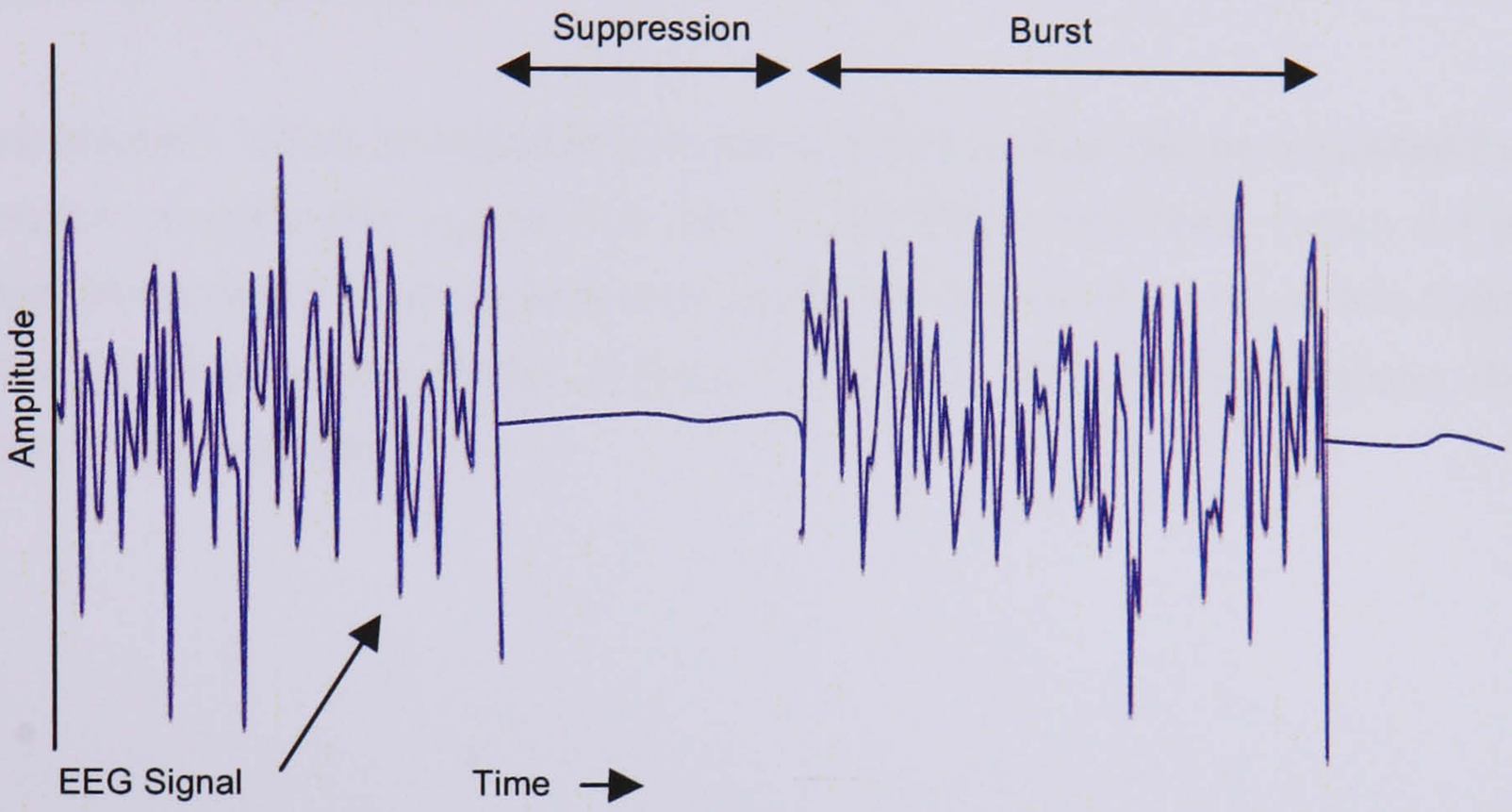

Figure 6.5: Burst suppression signal.

Typical embodiments of the ratio parameter identify periods of suppression as being longer than 0.5 seconds with an alternating voltage of less than +/- 5μV. The period over which EEG suppression may occur can vary considerably and so the parameter is often smoothed using a moving average algorithm with epochs in the order of 60 seconds so as to derive a meaningful parameter with a reasonable refresh-rate.

As will be discussed in section 7.2, the amplitude of the signal during the burst phases of the characteristic may provide additional information about the patient state. Periods of suppression are often referred to as isoelectric. Whilst this may be true under some circumstances, evidently it is not always. Given the appearance of periods of suppression it is entirely possible that many may refer to isoelectric EEG when in fact it is not. No studies have been found that characterise low amplitude suppression signals.

The burst suppression ratio is a mathematically reliable measure and, given its physiological importance, is a useful measure.

6.1.5 Zero Crossing Frequency

The simplicity of the Zero Crossing Frequency parameter derived by incrementing a counter on each occasion when a signal crosses the 0 volt line over a fixed period epoch makes it conceptually easy to visualise.

The parameter's virtual obsolescence in more recent studies can be explained by the loss of information incurred with signals that drift, as the EEG often does. Figure 6.6 presents the problem. In the figure it can be seen that some alternations of the signal are suspended such that there is no signal intersection of the zero volt axis over significant periods, degrading the reliability of the analysis.

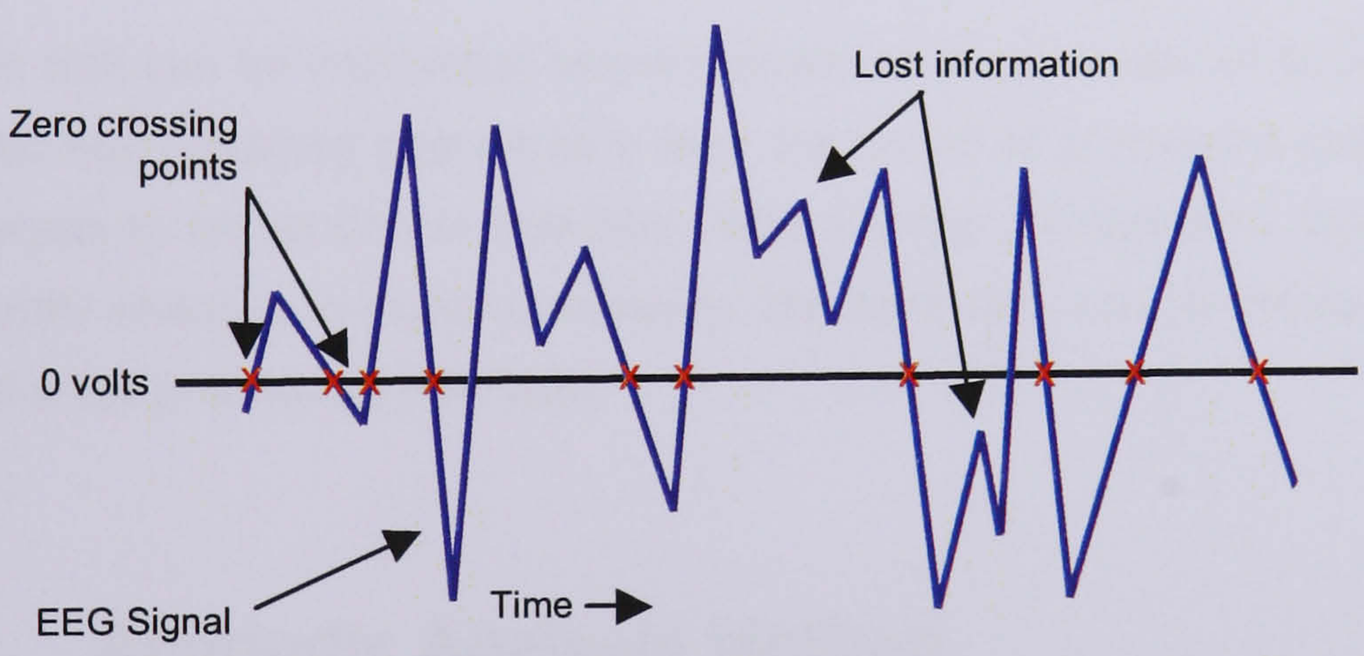

Figure 6.6: Zero crossing algorithm limitation.

6.1.6 Turns Ratio

A more sophisticated approach to the Zero Crossing Frequency analysis interrogates each data sample with respect to its predecessor to identify signal maxima and minima

incrementing a counter with each to give a 'turns per epoch' index or ratio. Figure 6.7 presents the turns counter.

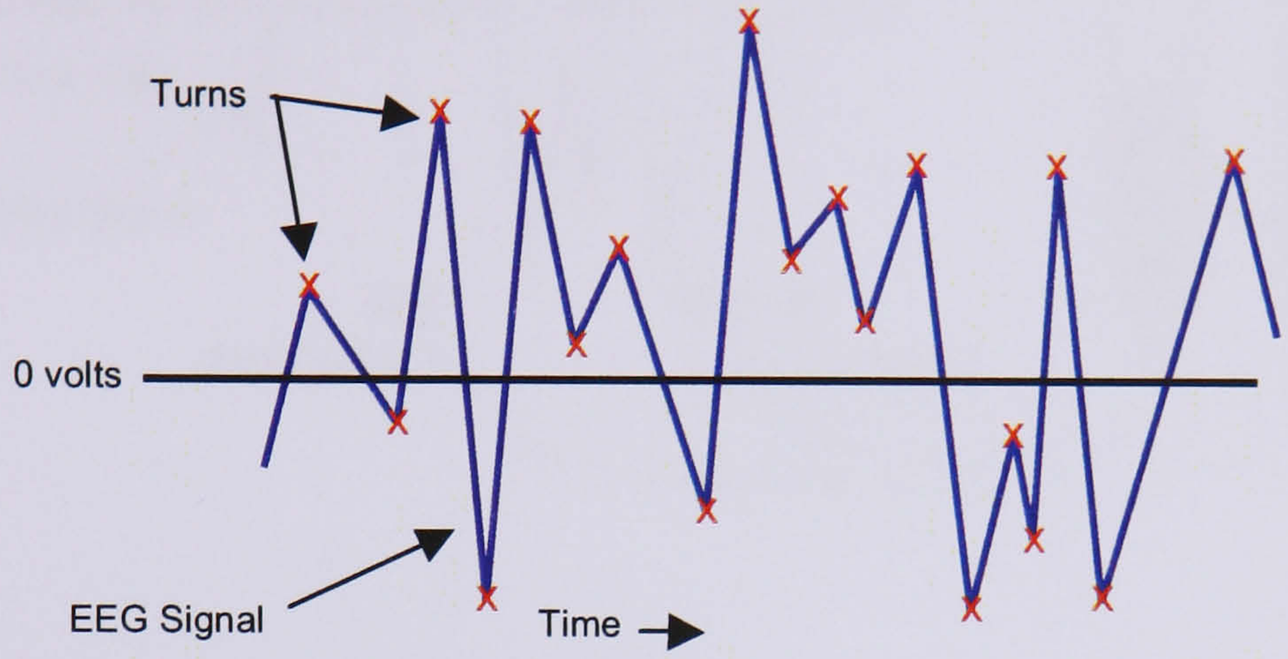

Figure 6.7: Turns Ratio.

There is little that can be interpreted physiologically by a parameter of such abstraction but the turns ratio has remained popular long after the arrival of processing power that enables spectral analysis to be applied in real-time. Where more sophisticated algorithms are now used to quantify changes in signal complexity, the turns ratio can be thought of as a useful analysis with a low processing overhead.

6.1.7 Aperiodic Analysis Method

The aperiodic analysis method was embodied in a product named the Lifescan EEG Monitor from Neurometrics Inc., (California, USA). The algorithm extends the turns ratio analysis by logging inter-maxima and minima intervals (Demetrescu, 1975). The embodiment continues by allocating each interval into two subcategories of magnitude termed 'slow wave' and 'fast wave' ready for histogram display. The is presented in figure 6.8 where the quantity of short and long periods recorded of the signal to the left are represented in the histograms on the right of the figure.

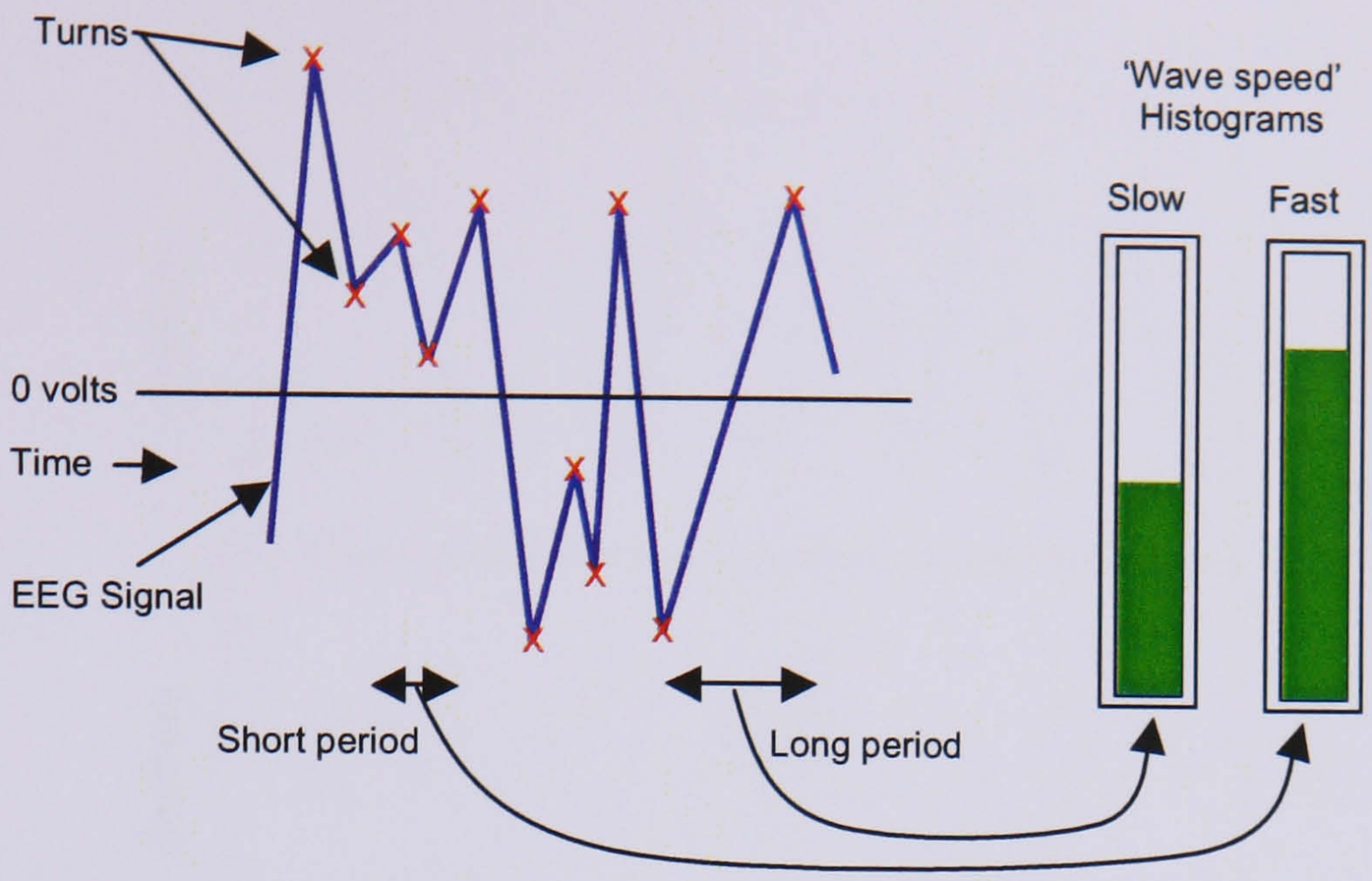

Figure 6.8: Aperiodic analysis method.

Whilst the aperiodic analysis presents additional information to the turns ratio, the complex nature of the EEG signal will yield results that are difficult to interpret. Figure 6.9 presents a waveform of frequency *f* Hz superimposed onto a slower 0.4*f* Hz sinusoid. The lower frequency component will not be represented with the aperiodic method. The lower graph of the figure shows the same wave combined with a further frequency of 4*f* Hz. Neither lower frequency component will be represented correctly with the aperiodic method. Although the figure uses contrived signals, the unreliability of the method is clear.

In fact the somewhat misleading wave speed assignations were developed further to include a greater number of interval length subdivisions. Sebel and colleagues (1983) discuss a 'modified Zero Crossing Frequency' as the basis of their analysis, whilst Gal'chenko and colleagues (1999) refer to a 'modified amplitude-interval algorithm'. Both elucidate their algorithms with descriptions of intervals as frequency periods and also frequency analysis, further exacerbating the misrepresentation by using the same nomenclature for the interval subdivisions as those established for the true spectral bandwidths originally identified and named by Berger (1929) and others (Gibbs et al., 1937; Walter and Dovey, 1946; Jasper and Andrews, 1938).

The information delivered by the algorithm would present an amount of useful information that may even closely correlate with properly calculated EEG spectra under certain conditions, however, consideration of the mathematical foundations should be exercised when interpreting data from this algorithm.

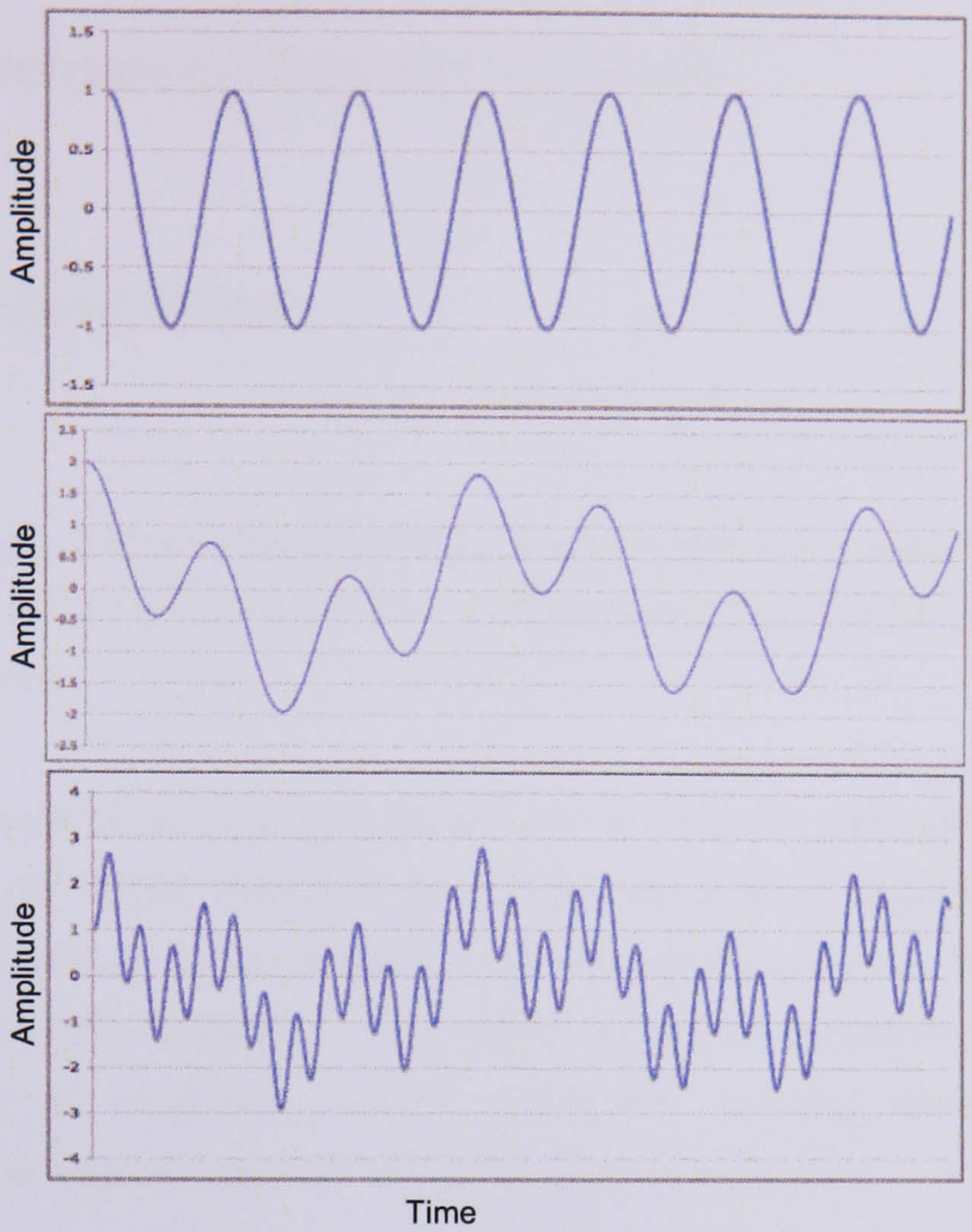

Figure 6.9: Examples of aperiodic analysis limitations. The top graph shows a single sinusoid of frequency f Hz. The middle graph shows the same sinusoid added to a second of frequency 0.4f Hz. The bottom graph includes a further frequency of 4f Hz.

Similar algorithms were embodied in the medical device product market with continued misrepresentation of the output data. Subsequently, a significant quantity of research has been conducted, the results of which draw misleading conclusions on the efficacy of EEG spectral analyses with respect to particular applications (for example Koumoundouros et al., 1989; Spackman et al., 1987).

6.2 Frequency Domain Methods

6.2.1 Tuned Filters

In the pre-digital age, narrow bandpass filter array circuits were used to produce display of bandwidth root mean square voltage. The relative power found in each selected bandwidth could thus be inferred.

An awkward trade-off of such electronic circuitry is that the narrower the bandpass filter design employed (12^{th} order filtering is not uncommon in EEG applications), the longer its signal transient will take to decay affecting phase delays in the output. Similarly, steep roll-off filters affect a ringing characteristic on the output. Thus the requirement of an application to detect emergence of short-term, narrow bandwidth, spectral characteristics must be measured against its required spectral and time-domain resolution.

With proper research and development around design requirements, analogue circuits simply require the incoming signal to be of peak amplitude that will not be clipped through its path to the display circuitry to produce meaningful results. The well-designed analogue filter circuit might therefore be seen as the gold standard for identifying the spectral components of a signal albeit at greater cost and inflexibility of analysis.

6.2.2 Digital Frequency Domain Analysis

Digital frequency analysis was conducted in off-line studies with good effect in the years preceding the development of processing power that would enable real-time implementations. Upon inception of such technology the cheaper, faster and more flexible research and design implications of working with software processing algorithms rather than electronic circuit design, saw rapid proliferation of the technology into a wide range of applications.

All such techniques have their trade-offs, and subsequently a vast range of algorithms have been developed that show characteristics suitable for particular applications. For the

purposes of the present study, the categories of algorithms are presented such that discussion of their generalised strengths and limitations may be expressed.

Frequency analysis algorithms have axioms to which data statistics must conform. Linear analyses require signal statistics to be independent of time origin, termed 'stationary'. Whilst this is not true of an ensemble of EEG data, it is possible to select an epoch period over which, in the absence of significant artefacts, the less strict conditions of wide-sense stationarity will be met where only the mean and correlation functions are assumed to be independent of time origin. Wide-sense stationarity is sufficient for many algorithms to propagate reasonable results provided the epoch is of sufficient length and can be considered 'ergodic'. Ergodicity is the assumption that a particular time series is truly representative of an ensemble, a condition that is often difficult to prove.

6.2.3 Non-Parametric Spectral Analysis

Jean Baptiste Joseph, Baron de Fourier's ubiquitous time-frequency transform tools first entered the digital world in the form of the Discrete Fourier Transform (DFT). The principle behind Fourier's techniques is that any signal can be decomposed into a set of sine and cosine waveforms, the frequency and amplitude of which will describe the signal completely. For this study only the main concepts of the analysis as applied to digital signals need be presented, a full treatment of Fourier analysis methods can be found in numerous texts.

In the analogue world distinction is made between the Fourier techniques used with periodic or aperiodic signals. Using the Fourier Series, periodic analogue waveforms can be completely described by harmonically related sinusoidal components, whilst the Fourier Transform, as is applied to aperiodic analogue signals, propagates a continuous frequency spectrum of sinusoidal components. With sampled signals no such distinction is made; all signals are assumed periodic for the purposes of calculation. The limitations subsequent to this assumption will be discussed later in this section.

Using the more convenient complex radian form, the Fourier Series takes a periodic signal $x[t]$ and effectively sweeps through the integral multiplying here by the Euler representation of sine and cosine waves, of angular frequency indexed by t with values of t. In this way, the Fourier Transform can be viewed as an infinite series of bandpass filters.

$$X(\omega) = \int_{-\infty}^{\infty} x[t]\, e^{-j\omega t}\, dt$$

where $\int_{-\infty}^{\infty} x[t]\, e^{-j\omega t}\, dt \neq 0$

$|X(\omega)|$ is termed the Fourier Coefficient and describes the amplitude of the sine or cosine wave of angular frequency ωt.

The DFT assumes the sampled data inside of the windowed epoch of $x[n]$ to be a single cycle of an infinite periodic signal. With discrete samples there is no requirement for integration and so the transform simply sweeps through values of $x[n]$ multiplied, as in the Fourier Transform, with the Euler representation of sine and cosine waves of angular frequency related to n, with values of n as opposed to the continuous time variable, t.

$$\Omega_k = \sum_{n=0}^{N-1} x_n e^{-\frac{2\pi i}{N} kn} \qquad \text{where} \quad 0 \leq k \leq (N-1)$$

where N is the number of samples in the epoch of data to be analysed (necessarily a power of 2), and the values of Ω_k form a sampled spectrum periodic at Ω with a period of 2π. The initial phase of each spectral component ϕ_k can be found using the real and imaginary parts of Ω_k:

$$\phi_k = \arctan\left\{\frac{imag(\Omega_k)}{real(\Omega_k)}\right\}$$

Increasing the size of N improves spectral resolution. If spectral components of close frequency are expected, longer data epochs may be required as well as high values of N to ensure they are distinctly represented.

The computational implementation of the DFT carries a considerable processing cost. Within the algorithm calculation of up to $4N^2$ multiplications may be needed, each of which, depending on the processor architecture and data types used, may require several dozen processing steps. Fortunately, there are many calculation repetitions that may be dynamically identified and removed from iterations of the algorithm. There are a range of techniques that may be used to do this, the most well known is embodied in the Cooley-Tukey Fast Fourier Transform algorithm (FFT) (Cooley and Tukey, 1965), which first decomposes the time series into smaller transforms, and then identifies calculation repetitions through a process of

recursion. A look-up table populated with results calculated on each iteration is then interrogated to locate appropriate results. This method can reduce the multiplications required to calculate an FFT to:

$$\frac{N}{\log_2 N}$$

For the Fourier Transform to operate correctly the following conditions must be met:

1. The sampling frequency must meet the Nyquist limit;
2. The signal should be stationary;
3. Each data epoch should contain only integer numbers of periodic components.

Nyquist's theorem states that the signal sampling frequency used should be at least twice that of the highest frequency component of the signal. If the Nyquist Limit condition is not met, frequency components above half the sampling frequency will be misrepresented in a spectral analysis at related but incorrect frequencies; a phenomenon termed frequency aliasing. It is usual to ensure that all frequencies above the Nyquist limit are removed with hardware filtering and so need not be considered further here.

The extent of the problem resulting from condition 2 not being met depends on a number of factors. Figure 6.10 describes the problem with a signal that doubles in frequency twice during a single epoch. The Fourier transform of the signal is presented below the signal in the figure. The principle frequency components are represented but are flanked by severe side lobe characteristics.

Condition 2 presents a limitation that is virtually impossible to avoid when dealing with signals with multiple unrelated frequency components. The problem is easy to visualise; as the data being analysed is 'windowed' there is no appreciation of the signal before or after the window period i.e. it is assumed to be '0'. If a signal with a periodic component is truncated by the data window at a point in time other than at the end of a complete cycle of the periodic component, a discontinuity occurs in the time series data that will give rise to a less well defined frequency spectrum. Figure 6.11 shows the Fourier transform of a single sinusoid using an ill-fitting data window. Whilst the signal contains only a single sinusoid the spectral transform shown in the figure presents significant power in neighbouring frequencies. This misrepresentation of power distribution is termed 'spectral leakage' and not only clouds interpretation, but also depletes the calculated amplitude of the real frequency components.

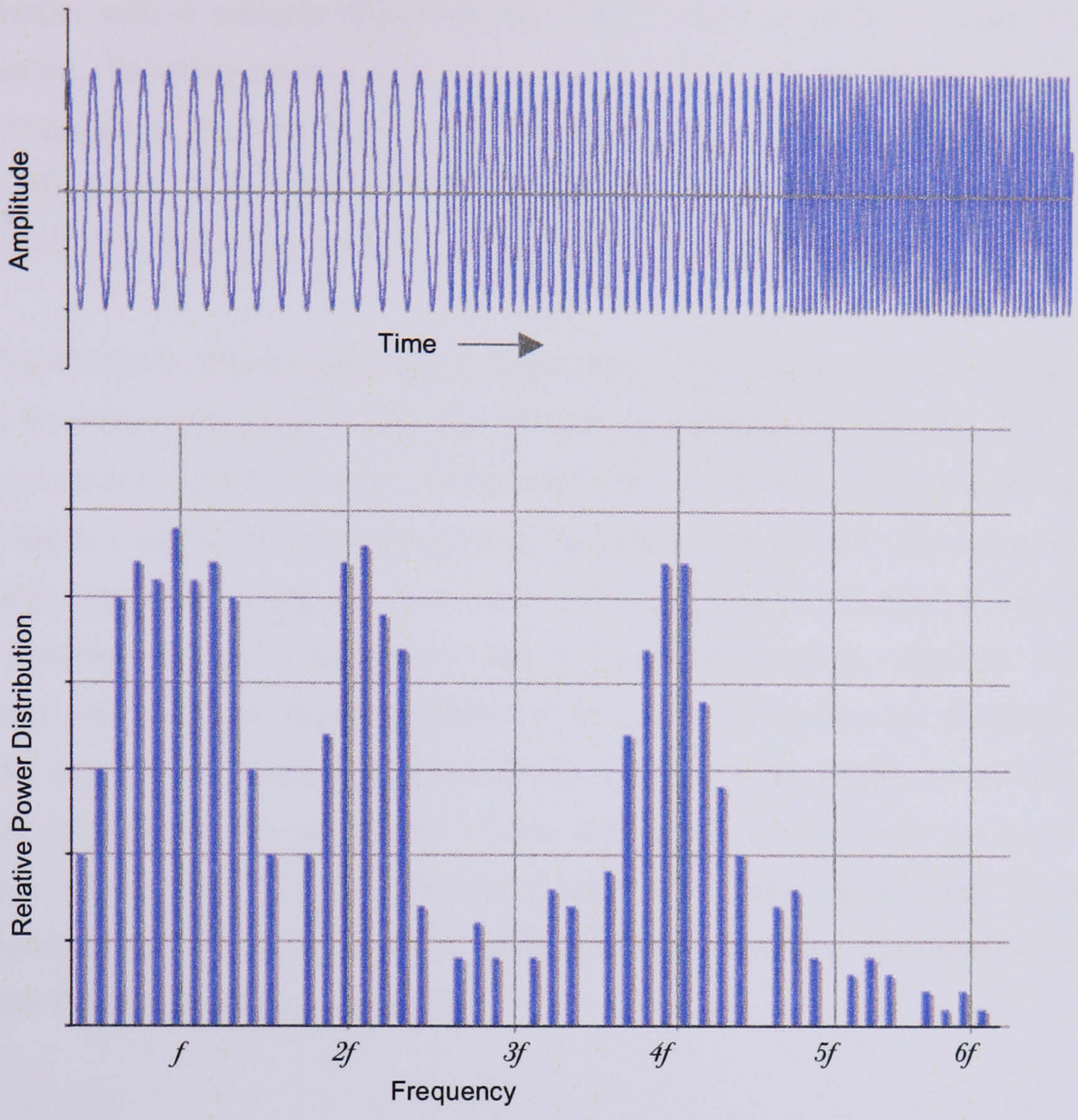

Figure 6.10: Fourier transform of epoch of a single sinusoid with changing principle frequency. The signal shown in the top graph propagates the Fourier transform given in the lower graph.

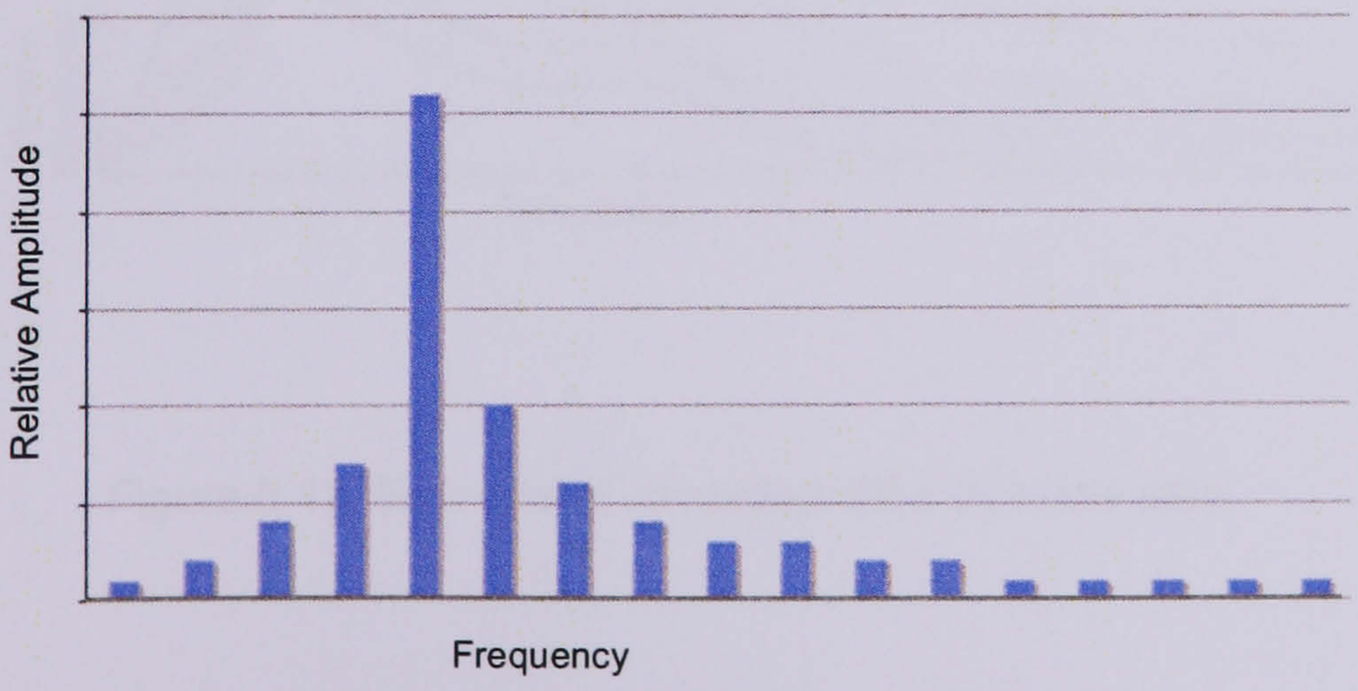

Figure 6.11: Fourier transform of a single sinusoid truncated with an ill-fitting data window.

Techniques to reduce this effect focus on the shape of the data window. By weighting each data sample with a variable that over the epoch forms a window shape, the spectrum is manipulated. Tapering each end of the data window to reduce the discontinuity disruption, affects changes in the spectrum output that need to be accounted for when interpreting the results. Window manipulation can prove useful when a signal is stationary and contains components of known frequency, but do not offer advantage otherwise.

Short Term Fourier analysis was born of the need to generate a higher resolution of temporal detail in the frequency domain. Standard Fourier analysis shows only the temporal changes in frequency content from one epoch to the next. Each spectrum generated can be cascaded to give a clearer view of temporal changes in frequency composition as shown in figure 6.12. If constraints on epoch length are such that useful temporal information is lost, the time series epoch window can be moved such that it overlaps previous windows. The subsequent transforms can then be pieced together to form a spectrogram that presents the additional detail. An example is given in figure 6.13. As a time axis is needed to convey the additional temporal information the amplitude of the frequency components is colour scaled. The technique comes with a high processing cost and does not answer the issue of data truncation and so the same trade-off exists between time and frequency resolution as with any of the Fourier techniques described.

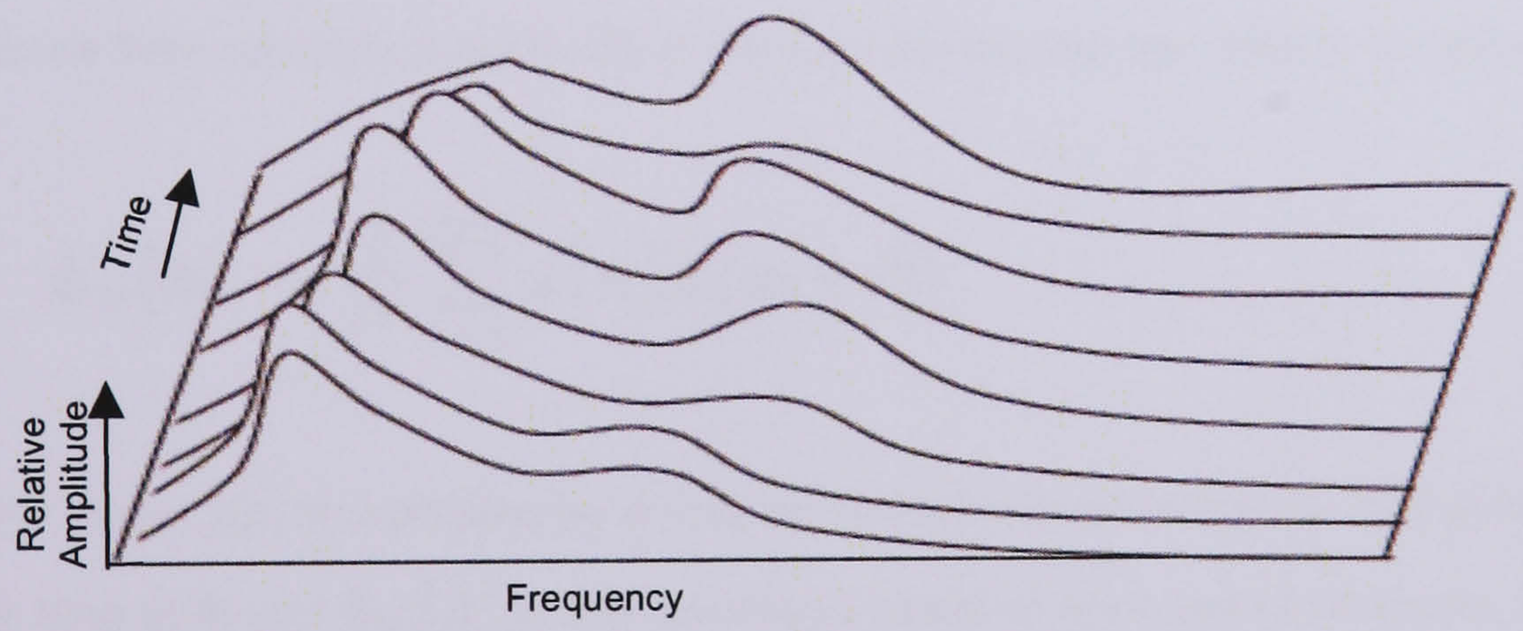

Figure 6.12: Example of cascaded EEG spectral data.

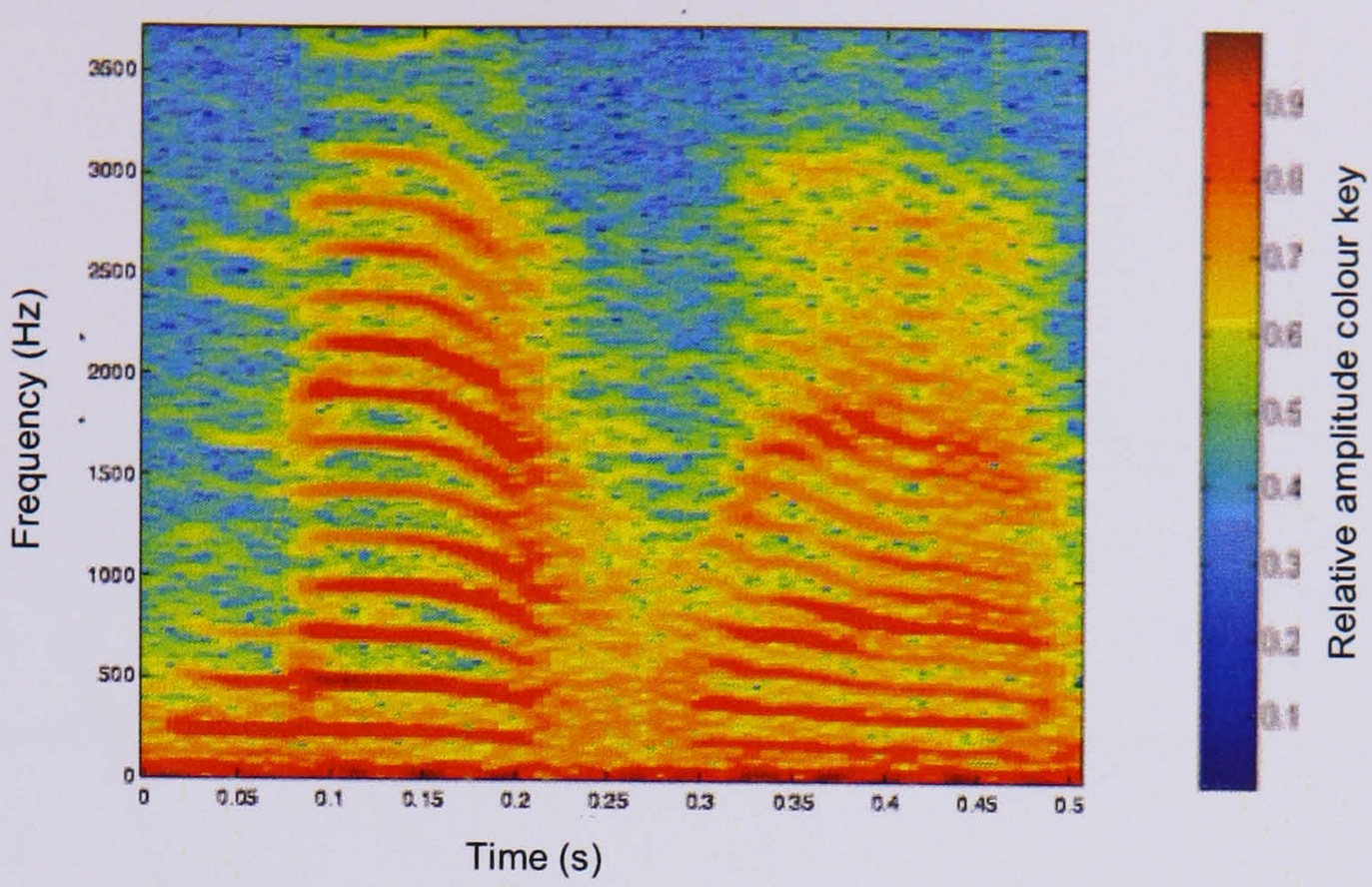

Figure 6.13: Example of a short term Fourier analysis spectrogram.

6.2.4 Autocorrelation

Central to the principles of modern spectral analysis is the concept of autocorrelation (sometimes referred to as the second-order cumulant), as it either directly forms the basis of many practical algorithms, or is related to other techniques such as Linear Prediction where divergence from correlation is identified. Mathematically autocorrelation is defined as:

$$\phi_{xx}[k] = \frac{1}{N}\sum_{n=1}^{N-k} x[n]x[n+k]$$

Thus the signal $x[n]$ is multiplied by a time shifted windowed image of itself of length N, where k is the time shift and $\phi_{xx}[k]$ is the averaged result of each set of products. In this way the presence of deterministic trends within $x[n]$ are revealed in a form that, whilst not leading to power distribution identification directly, can be manipulated to do so in a number of ways. Figure 6.14 shows plots of $\phi_{xx}[k]$ for two signal autocorrelations. The left plot in the figure shows a decaying oscillation typical of an autocorrelation of a strongly periodic signal. The plot on the right of the figure is representative of an autocorrelation function of data with several frequency components of amplitudes that remain constant over the period of the time series epoch.

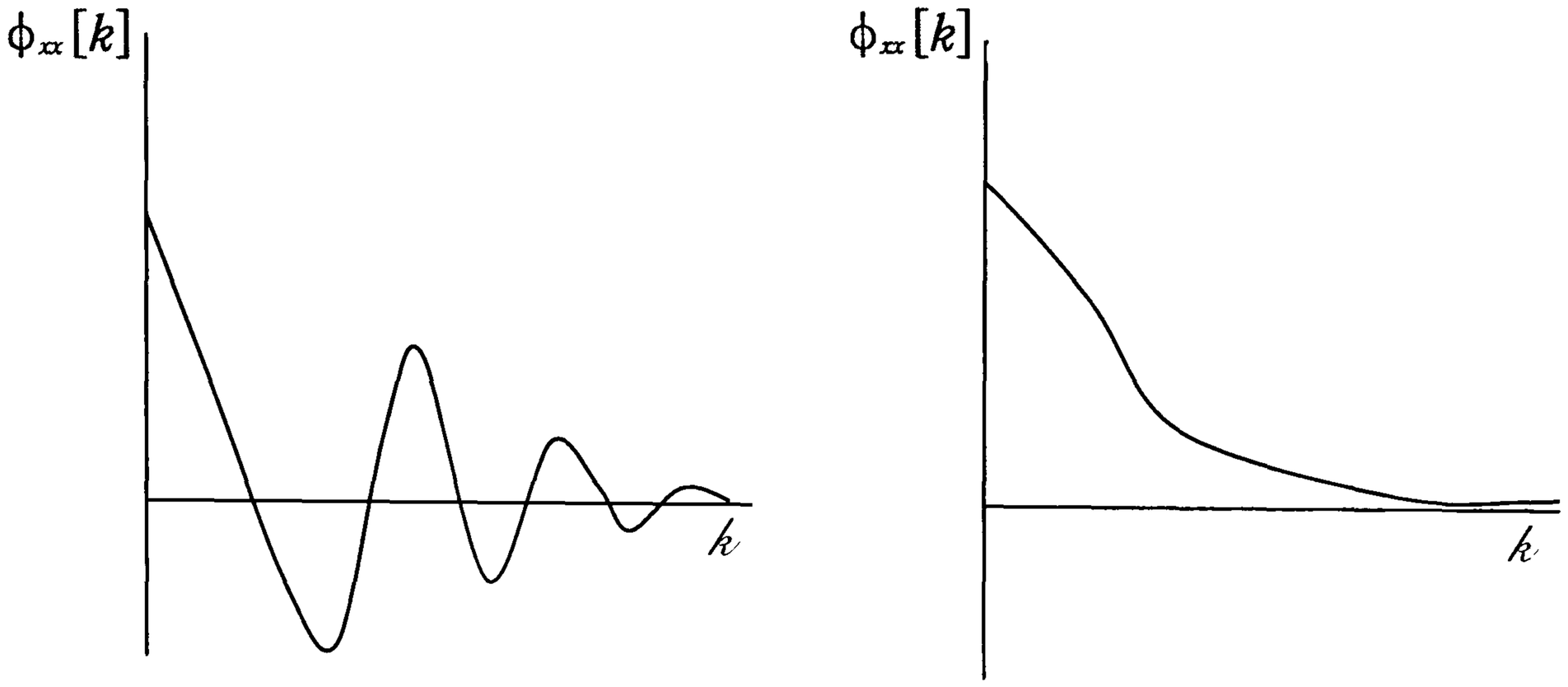

Figure 6.14. Example autocorrelation plots.

6.2.5 Parametric Spectral Estimation

Spectral Estimation constitutes a set of related tools that can usefully be employed when analysing time series signals that contain both noise and deterministic periodic components. Although not popular until the 1960s, Yule (1927) first developed model-based parametric spectral estimation in the 1920s as an approach for weather analysis. There are now a variety of parametric methods available, each with characteristics that must be considered when choosing which is best suited to the application. When well selected, such techniques are said to provide high-resolution spectra with a lower processing over-head than the FFT, as they are able to operate using less time series data. Modeling techniques achieve this advantage by using past data from within a time series to predict current values, not only increasing resolution but also improving noise handling without the spectral leakage problems associated with the FFT that may obscure low-amplitude periodic components. The analysis method on which the study patent is based is a parametric spectral estimation method.

The general principle behind spectral estimation techniques is to identify a parametric model that will best fit the characteristics of the signal to be analysed. The complexity of the signal determines the appropriate order of the model such that sufficient detail will be possible of the output. The parameters (and hence shape) of the model may then be determined by minimising the errors between the data set and the model. If white noise were applied to the

derived model as an input, the output should be a close match to the signal. The model is in effect a filter and as such standard techniques may be applied to its transfer function to identify its spectral output, and thus the spectral content of the signal.

There are three principle forms of model from which to choose: Autoregressive (AR), Moving Average (MA), Autoregressive Moving Average (ARMA). Each can be used to describe the same signal equally well but the complexity of the calculations required of each to do so will vary widely. It is usual to select a model using the principle of parsimony i.e. the less parameters required of a model to represent the signal, the better. The general form of the transfer function provided by each strain of model presents the characteristics of signal to which they may most parsimoniously be applied. Z-plane poles positioned on or near to the unit circle will give rise to sharp spectral peaks, thus if a signal is expected to be mainly composed of distinct spectral components an AR model should be selected with estimation coefficients in the transfer function denominator.

The MA model has estimation parameters in its transfer numerator; with Z-plane zeros on or near to the unit circle, the MA model will produce sharp troughs in the spectral output. The ARMA model has estimation parameters in both the transfer numerator and denominator. ARMA z-plane poles and zeros that approach the unit circle are thus able to represent spectra with both sharp peaks and sharp troughs. Intuition may lead to selection of the apparently more flexible ARMA model in all cases but unless the signal is likely to present itself in the form described, the model order required may affect high model complexity. If a model is poorly selected with an inappropriate order the output will present inaccuracies as the model will, to some degree, assert its own characteristics. Figure 6.15 presents the form of AR, MA and ARMA models when applied parsimoniously. The top left graph in the figure shows a typical AR spectral output with spectral peaks rather than troughs, the top right graph gives an MA output describing a signal with spectral troughs and the bottom graph shows a typical ARMA output where both peaks and troughs are well represented.

AR models are the most commonly used in low-bandwidth EEG signal analysis as they are of relatively simple linear form (unlike MA and ARMA variants) and can be parsimoniously applied to the EEG signal. AR techniques are causal linear models and thus assume wide-sense stationarity. Subsequently only relatively short epochs of EEG data can be used so as to maintain quasi-stationarity. This does not necessarily affect a limitation to spectral resolution as it would if using an FFT, as parametric models use past data to make estimations of the current output. The result is a continuous line spectra that achieves a best fit spectra in a least-squares sense (i.e. the variance of data about the spectral output is of a minimum). The errors between the actual spectral component amplitudes and the spectra

given by the model will be Gaussian white noise, provided the model and model order are appropriately selected.

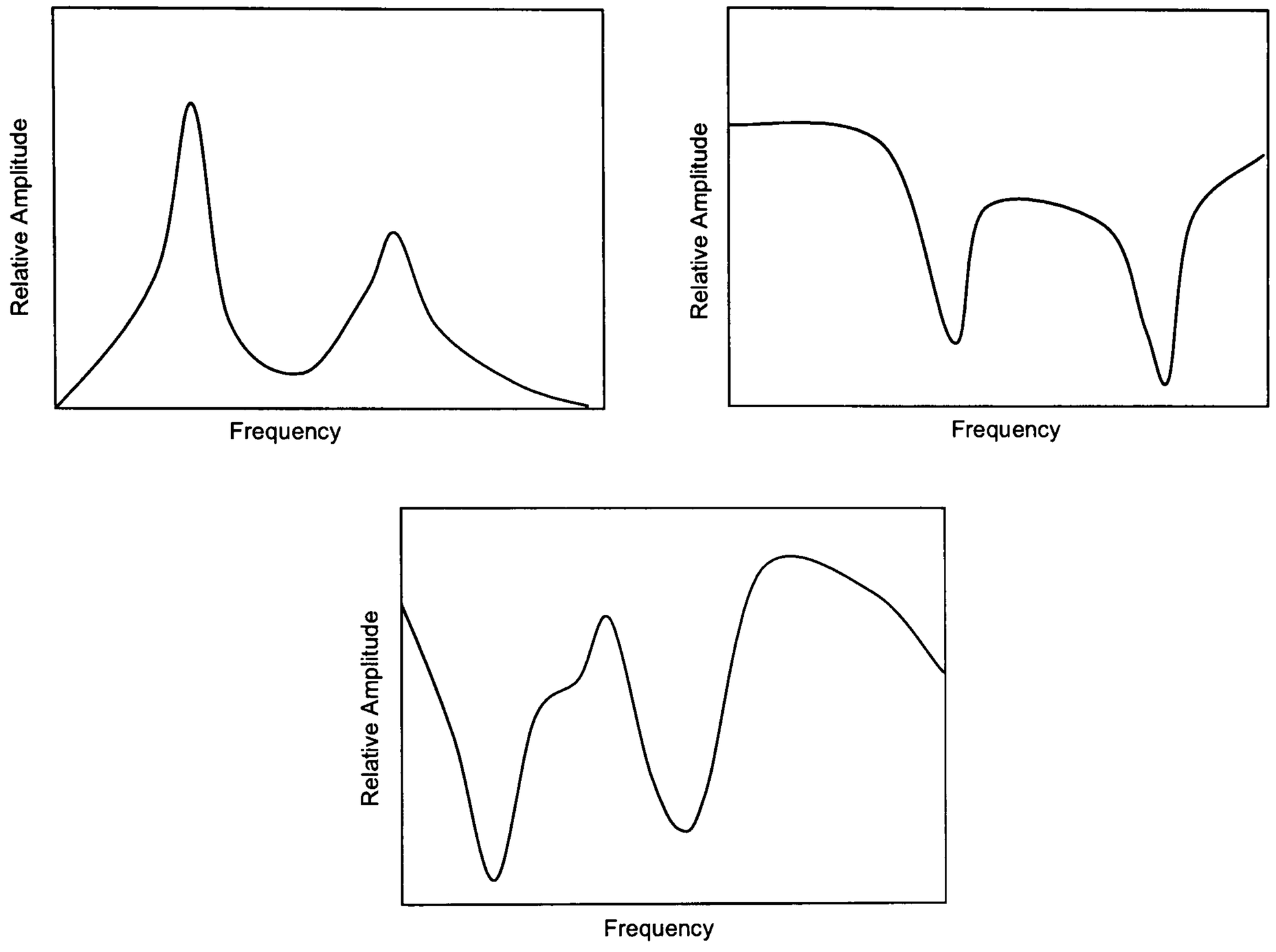

Figure 6.15: Forms of parametric model.

An AR model can be described using the general difference representation of a causal, infinite impulse response, linear time invariant filter:

$$y[n] = \sum_{-\infty}^{\infty} h[k]x[n-k]$$

where $y[n]$ is the output of sample n, $h[k]$ is the filter impulse response, and $x[n\text{-}k]$ introduces the current and past values of the input. To enable computation, k is necessarily limited to a model order, M giving:

$$y[n] = \sum_{k=1}^{M} h[k]\,x[n-k] \tag{6.1}$$

In the case of the AR model, solving $h[k]$ will determine a series of constants, a_k, known as predictor coefficients, from which the spectrum of the time series epoch $x[n]$ will be determined. Since the model will propagate a 'best fit' spectra based on the model order, it can be expected that equation 6.1 will not give an output $x[n]$ that exactly matches the EEG signal and so a prediction error term $\varepsilon[n]$ is also introduced. Equation 6.1 can therefore be rewritten to give the general formula for an AR model:

$$x[n] = \sum_{k=1}^{M} a_k x[n-k] + \varepsilon[n] \tag{6.2}$$

Equation 6.2 shows that the current term $x[n]$ of the series can be estimated by a linear weighted sum of previous terms in the series. The AR model can therefore be described in terms of the recursive filter with a white noise input and the data series, $x[n]$, as the output, as shown in figure 6.16.

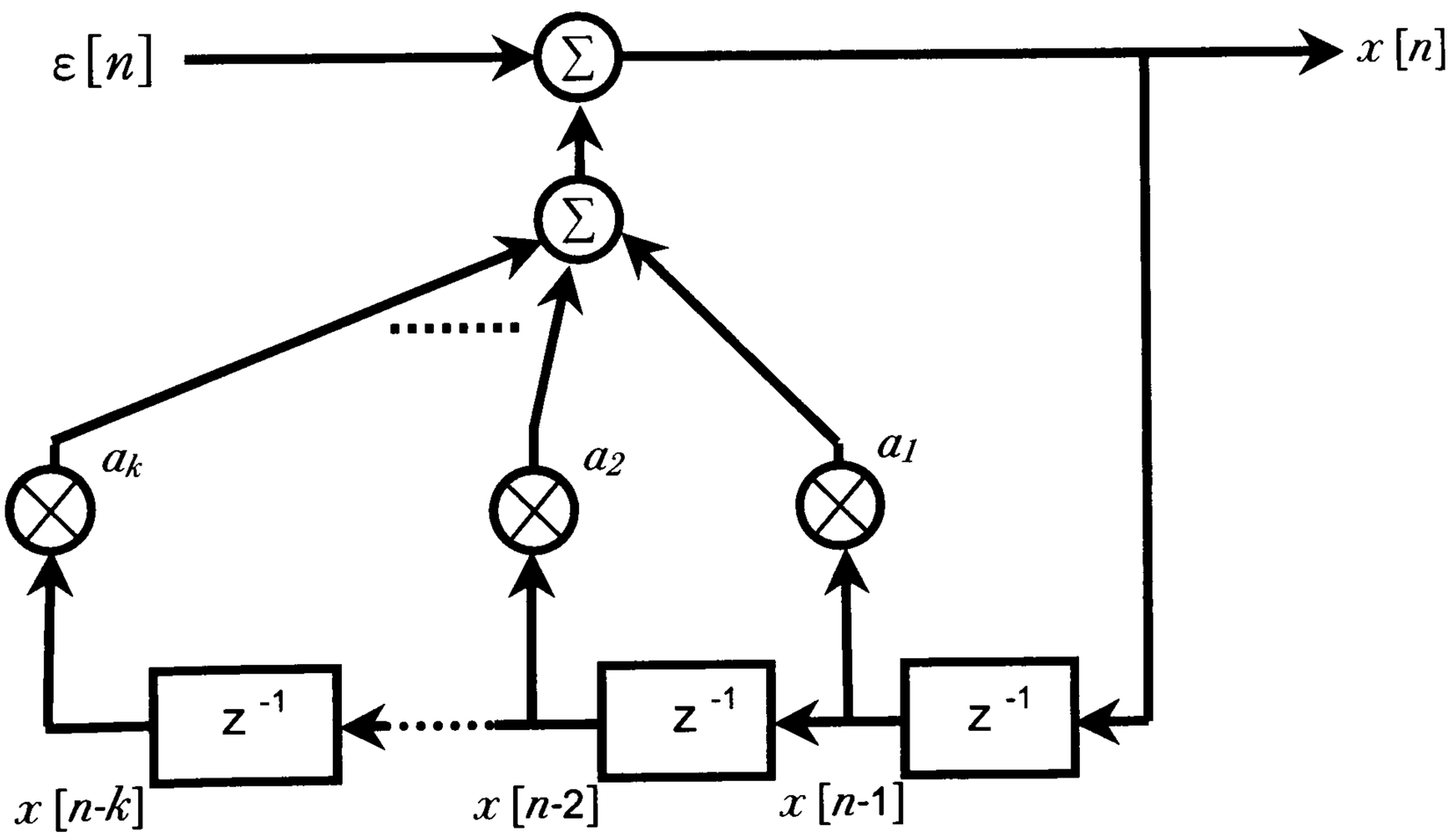

Figure 6.16: All pole filter characterisation of autoregressive model.

The error term $\varepsilon[n]$,is assumed to be Gaussian white noise, if it is not the implication is that the model is not a good fit. $\varepsilon[n]$ must be minimised in order that the prediction coefficients a_k match the EEG signal as closely as the model order selected will permit. This can be achieved using least-squares minimization (i.e. identifying values of a_k when the gradient of the squared error term is at a minimum). Since the error term $\varepsilon[n]$ is dependant on the values of a_k, the squared error term, S, is given by:

$$S(a_k) = \sum_{n=1}^{N} \varepsilon[n]^2(a_k) \tag{6.3}$$

By differentiation the gradient of S is thus given by:

$$\frac{dS}{da_k} = 2\sum_{n=1}^{N} \varepsilon[n]\frac{d\varepsilon[n]}{da_k} = 0 \qquad k = 1,2,3,...,M \tag{6.4}$$

Rearranging 6.2 to give an expression for $\varepsilon[n]$:

$$\varepsilon[n] = x[n] - \sum_{k=1}^{M} a_k x[n-k] \tag{6.5}$$

which gives the differential:

$$\frac{d\varepsilon[n]}{da_k} = -\sum_{k=1}^{M} x[n-k] \tag{6.6}$$

Substituting 6.5 and 6.6 into 6.4 removes the prediction error term giving:

$$\frac{dS}{da_k} = -2\sum_{n=1}^{N} x[n-k](x[n] - \sum_{k=1}^{M} a_k x[n-j]) = 0 \qquad (j = 1,2,3,...,M) \tag{6.7}$$

which expands to give the estimate:

$$\sum_{n=1}^{N}\sum_{k=1}^{M} x[n-k]x[n-j]\hat{a} = \sum_{n=1}^{N} x[n-k]x[n] \qquad (j = 1,2,3,...,M) \tag{6.8}$$

where $\hat{a}$ is a vector of the estimated values of a_k. Written in the more general matrix form (x[n - j] being the transpose of x[n – k]) equation 6.8 gives a set of simultaneous Normal equations, which in this case, as they are populated with autoregressive data, are referred to as the Yule-Walker equations:

$$(X^T X)\hat{a} = X^T x \tag{6.9}$$

In practice, the Yule-Walker equations can be populated with data from an autocorrelation of x[n] :

$$\phi_x[k] = \frac{1}{N}\sum_{n=1}^{N-k} x[n]x[n+k] \tag{6.10}$$

Whilst the matrix will be different, relative amplitudes are the same and thus the approach will propagate valid results. The left hand expression in equation 6.9 is directly equivalent to the prediction coefficients being multiplied by the autocorrelation of *x*[*n*] (shown on the right hand side of equation 6.10), whilst the right hand expression is equivalent to the first column vector of the autocorrelation matrix ranging from n=1 to n=N. This alternative, and in practice simpler, calculation can be summarised as:

$$\phi\underline{a} = P \tag{6.11}$$

where

$$\phi = \begin{pmatrix} \phi_x(0) & \phi_x(-1) & \cdots & \phi_x(-M+1) \\ \phi_x(1) & \phi_x(0) & \cdots & \phi_x(-M+2) \\ \vdots & \vdots & & \vdots \\ \phi_x(M-1) & \phi_x(M-2) & \cdots & \phi_x(0) \end{pmatrix}$$

$$\underline{a} = \begin{pmatrix} a_1 \\ a_2 \\ \vdots \\ a_M \end{pmatrix} \quad \text{and} \quad P = \begin{pmatrix} \phi_x(1) \\ \phi_x(2) \\ \vdots \\ \phi_x(M) \end{pmatrix}$$

By combining equation 6.5 with equation 6.10 the error term is re-introduced:

$$\begin{bmatrix} \phi_x(0) & P^T \\ P & R \end{bmatrix} \begin{bmatrix} 1 \\ -\underline{a} \end{bmatrix} = \begin{bmatrix} \varepsilon[n] \\ \underline{0} \end{bmatrix} \tag{6.12}$$

which, when expanded gives :

$$\begin{pmatrix} \phi_{xx}(0) & \phi_{xx}(-1) & \cdots & \phi_{xx}(-M+1) \\ \phi_{xx}(1) & \phi_{xx}(0) & \cdots & \phi_{xx}(-M+2) \\ \vdots & \vdots & & \vdots \\ \phi_{xx}(M-1) & \phi_{xx}(M-2) & \cdots & \phi_{xx}(0) \end{pmatrix} \begin{pmatrix} 1 \\ a_1 \\ \vdots \\ a_M \end{pmatrix} = \begin{pmatrix} \sigma_w^2 \\ 0 \\ \vdots \\ 0 \end{pmatrix}$$

where σ^2_w is the variance of the error. These are Yule-Walker equations and as such will give the same spectral output as equation 6.9.

Solving the Yule-Walker equations will present the optimum values of a_k. There are very many approaches to solving Normal equations; Gaussian elimination is probably the best known but is inefficient with larger sets of equations. In essence the Gaussian approach reorganises each Normal equation below the first such that each unknown quantity is eliminated with expressions based on the Normal equation above. In this way only the top Normal equation contains all the unknown quantities, with each subsequent equation below having one less unknown. This leads to the development of a triangular matrix the values of which can be back-substituted from the bottom to the top to give the complete set of solutions. Iterative methods such as the Jacobi method improve on the Gaussian approach by making successive approximations to identify the solutions more efficiently. The recursive Levinson-Durbin approach can be used when the matrix X is Toeplitz (i.e. values in the top left to bottom right diagonals are equal) as will be found here. This method is described in equation 6.13 below. Its efficiency makes the Levinson-Durbin the method of choice for small and moderately sized matrices.

Initialisation:

$$\varepsilon_0 = \bar{\phi}_0$$

Recursion:

for $m = 1, 2, 3, \ldots p$:

$$k_m = -\frac{\left[\bar{\phi}_m + \sum_{i=1}^{m-1} a_{(m-1)i}\bar{\phi}_{m-i}\right]}{\varepsilon_{m-1}}$$

$$a_{mm} = k_m$$

$$a_{mi} = a_{(m-1)i} + a_{mm}a_{(m-1)(m-i)}, \qquad \text{for } 1 \leq i \leq m$$

$$\varepsilon_m = (1 - k_m^2)\,\varepsilon_{m-1} \tag{6.13}$$

where ε_x are the prediction errors, a_{xx} are the model predictor coefficients, k_m are intermediate quantities called reflection coefficients, and $\bar{\phi}_x$ are the ACF coefficients. In essence the principle of the Levinson-Durbin method is the recursive tuning of the filter model parameters to the ACF such that prediction error is minimised. This approach reduces computation to N^2 multiplications rather than N^3 when using the more common Gaussian Elimination.

The response of the linear time invariant causal filter can be described most simply in the z-domain as:

$$X(z) = H(z) * W(z) \tag{6.14}$$

where * denotes convolution, $X(z)$ is the z-transform of the system response, $H(z)$ is the z-transform of the filter transfer function, and $W(z)$ is the z-transform of the prediction error input signal.

Equation 6.14 can be rearranged to give an expression for the filter transfer function:

$$H(z) = \frac{X(z)}{W(z)} \tag{6.15}$$

Taking z-transforms of equation 6.5:

$$W(z) = X(z)\left(1 - \sum_{k=1}^{M} a_k z^{-k}\right) \tag{6.16}$$

equation 6.14 becomes:

$$H(z) = \frac{1}{1 - \sum_{k=1}^{M} a_k z^{-k}}$$

As expected the AR model has terms of a_k in the denominator only, hence the model has an all-pole response. In the same way that the frequency response of filters can be found in the z-plane using:

$$z^{-k} = e^{-jk\omega T}$$

the Euler expression for the spectral output of $H(z)$ is:

$$H(\omega) = \frac{1}{\left(1 - \sum_{k=1}^{M} a_k e^{-jk\omega T}\right)} \tag{6.17}$$

The power density spectrum of a filter is given by:

$$\Gamma_{xx}(\omega) = \left| H(\omega) \right|^2 \Gamma_{\rho\rho}(\omega)$$

where $\Gamma_{xx}(\omega)$ is the power density spectrum of the output, $\Gamma_{pp}(w)$ is the power density spectrum of the input, and $H(w)$ is the frequency response of the filter. Since the input is white noise it can be described in terms of its variance and so using equation 6.17:

$$\Gamma_{xx}(\omega) = \sigma_\rho^2 \left| H(\omega) \right|^2 = \frac{\sigma_\rho^2}{\left| 1 - \sum_{k=1}^{M} a_k e^{-jk\omega T} \right|^2}$$

If a signal changes its statistical properties beyond the scope of complexity determined by the model order, information will be lost, and potentially without indication. Thus the selection of an appropriate order is of considerable importance, however, in analyses of quasi-stationary signals such deviations are likely and to some extent permissible. Provided such instances

are relatively few, an epoch of artifact ridden time series data will be forced by the model to present an output of expected form. To optimally exploit this property the model order needs to be sufficiently high to enable all forms of normal signal behaviour to be characterised, but minimal such that the model does not artificially or reactively assert spurious spectral detail. The application of some form of averaging algorithm to the current and previous epochs is thus necessary to maintain spectral stability. Whilst this adds further meaning to the term 'spectral estimation', the ability of parametric modeling to reveal spectral trends remains powerful.

There are a number of approaches that may be used to identify a suitable model order. With a time varying signal such as the EEG this should be conducted using a good deal of data covering all system behaviours. Studying correlogram plots can provide a useful indication; the AR model is most suited to correlograms that show a near exponential drop towards zero without a subsequent increase in absolute amplitude. The point at which the correlogram is first significantly close to zero identifies the appropriate order. Use of an algorithm that presents the distribution of orders over numerous epochs will allow identification of a median solution. There are several more formal criterion analysis techniques that can be used, an example of which is Akaike's Information Criterion (AIC) which is recommended for small data epochs (Proakis and Manolakis, 1996):

$$AIC(M) = \ln(\sigma_w^2) + 2M/N$$

where M is the model order, N is the number of samples in the epoch, and σ_w^2 is the variance of the prediction error. Assuming the number of data samples to be constant as would be the case here when N is determined by the constraints of epoch length showing wide-sense stationarity, the Nyquist limit and analogue-to-digital conversion hardware used, if the AIC is plotted with model order the AIC decreases until it reaches a minima before increasing again (the AIC thus penalizing non-parsimonious results) or reaching a plateau. The AIC value at the minima or beginning of the plateau indicates the optimal order needed to model the signal. Of course, because the model must be implemented for each M to identify values of AIC, such methods are not suited to on-going assessment of model order during real-time signal analysis.

As the AR model is effectively an infinite impulse response filter, it can be expected that issues of stability pertaining to one can be applied to the other. Proakis and Manolakis (1996) discuss three areas that may cause instability of the infinite impulse response filter:

1. Parameter quantization in digital filters;
2. Round-off noise in multiplication;
3. Word length overflow.

If a signal tends towards pure sinusoidal content the poles of an AR model selected to fit the signal, will tend towards the z-plane unit circle. Inaccuracies of the kind listed each have the potential to place a pole outside of the unit circle and thus fail the condition of stability. In the instance of the AR model, this will propagate model coefficients with more than one solution and a distorted output which may not be immediately obvious to the observer.

The issue of AR model stability is treated practically in the analysis of the patented mathematics in section 8.6.

6.2.6 Wavelet Analysis

Wavelet theory as applied to signal analysis has much in common with the Short Time Fourier analysis. In the case of Fourier analysis, a signal is decomposed into sinusoidal components of frequency and amplitude that determine a frequency domain spectrum. In Short Time Fourier analysis the data window is then moved along the time series such that an epoch overlap of fixed length is maintained. Subsequent transforms provide indication of each sinusoidal component on a temporal plane with a resolution determined by the epoch length and overlap. In engineering terms, a wavelet signal analysis convolves the incoming epoch with a high-pass filter (mother wavelet) of a specification to suit the application, interleaved with its conjugate-mirror low-pass filter positioned either side of the half-bandwidth point. The high-pass filtering propagates high frequency detail coefficients, whilst the low-pass filter output provides coarse approximation coefficients. The high frequency components are then removed and the process is repeated using only the low-pass filter output data. This is continued to form a cascaded bank of filters as shown in figure 6.17.

At each filter stage, or level, the remaining signal has been reduced in bandwidth by a half. The signal can then be re-sampled at a minimum frequency half that of the previous level, referred to as 'downsampling'. The low frequency content is then filtered in the ssame way as the original signal but with a rescaled wavelet (child wavelet) with a rescaled wavelet. This next stage gives rise to a frequency resolution twice that of the previous level. Hence the wavelet analysis is referred to as 'multiresolution'.

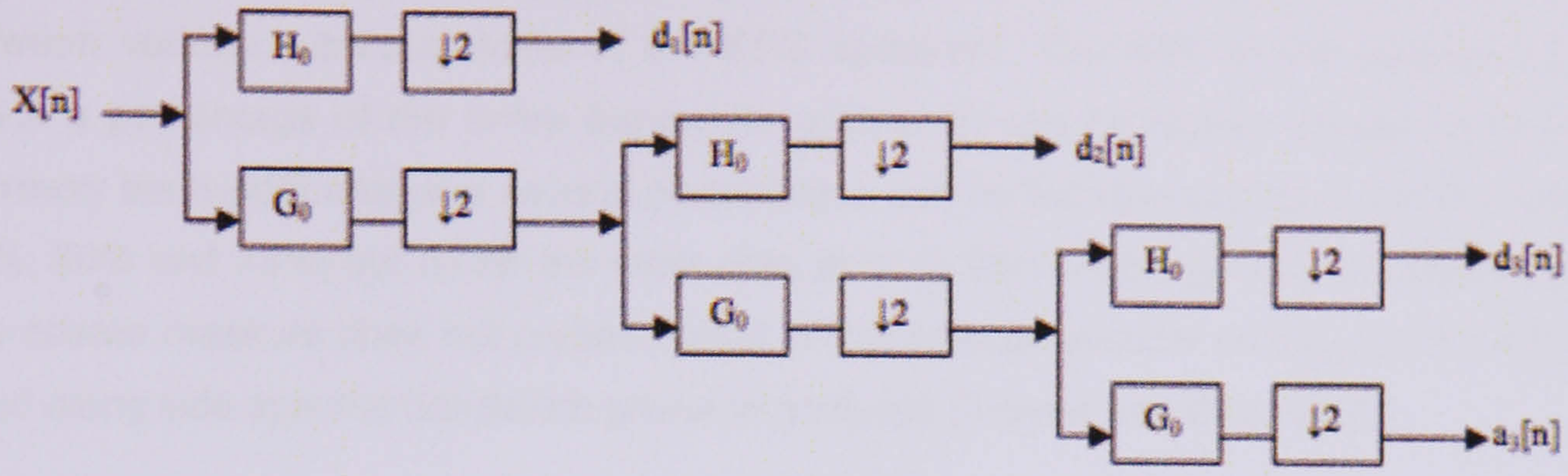

Figure 6.17: Wavelet cascaded decomposition. The signal x[n] is filtered such that high frequency components $d_x[n]$ are isolated at each filtering stage whist the low frequency components $a_x[n]$ are passed on for further filtering.

Wavelet signal decomposition techniques supercede the performance of Fourier analyses in a number of ways:

1. Discontinuities at data window end points do not give rise to spectral distortion;
2. No distinction of linearity is made;
3. Presents high resolution time-frequency information within each data epoch;
4. Improves spectral detail even with noisy signals;
5. Can be implemented with greater computational efficiency than the Short Term Fourier analysis.

6.2.7 Frequency Domain Parameters

A great many parameters derived from frequency domain analyses have been used in EEG. Some of the more common are:

Relative spectral power median;

Relative spectral power mean;

Relative peak power frequency;

Relative sub-bandwidth spectral power ratios;

Spectral Edge Frequency (SEF).

Numerous analyses have been carried out using algorithms that provide power comparisons between various sub-bandwidths of the EEG spectrum. The SEF is the frequency below which a percentage of the entire bandwidth of interest can be found. Usually used on the narrower bandwidth analyses several percentages can be found in common use (for example 25%, 50% and 75%) but by far the most ubiquitous is 95%. Although mathematically robust, this coarse measure does not present detail of multi-modal spectral activity and so it is often used along side spectral bandwidth power in analyses (Tonner and Bein, 2006).

6.3 Non-Linear Analyses

The field of non-linear system modeling presents a broad spectrum of techniques that are evolving rapidly at this time. Successful implementation of a general model that can be applied to non-linear systems began in the 1980s although the conceptual foundations can be attributed to French mathematician Poincaré whose theories on moments of synchronicity began exploration into characterisation of complex deterministic systems.

There are several methods of determining a state space form that will characterise a non-linear system. One of the simplest is that of 'time-delay embedding'. Three equidistant points in a time series are each used as the mapping coordinates of a point in three-dimensional space. By advancing the three points along the time series a further point is determined. This is repeated for some model dimension, d, and propagates a three dimensional representation of the system called an 'equivalent attractor' where an attractor is a form to which all vector trajectories converge provided the system is not chaotic. Although formal methods have been developed, the time lag between each point in the time series is often determined by the point of convergence of the time series autocorrelation. The dimension, d, of the model can be determined as that at which the attractor does not change form to previous values of d. Formal methods for identifying both model lag and dimension are reviewed in by Celluci et al. (2003). Flexibility of the model to accommodate changes in system dynamics is provided by such concepts as 'attractor landscape deformation' and bifurcation. The form of an attractor can be characterised spatially by its dimension, in terms of its energy loss by its entropy, and convergence (or divergence) by its Lyapunov exponent. Numerous additional characterisation methods have been developed with novel approaches being proposed on a regular basis.

The bispectrum is a nonlinear technique that has seen much use in the field of EEG. The bispectrum of a signal is said to quantify the degree of phase coupling between all spectral components in non-linear signals. An example bispectrum output for an EEG signal is given in figure 6.18. By reading off the frequency values of the x and z axis, it is possible to identify

which pairs of spectral components are coupled by synchronous phase as shown by high amplitude on the y axis.

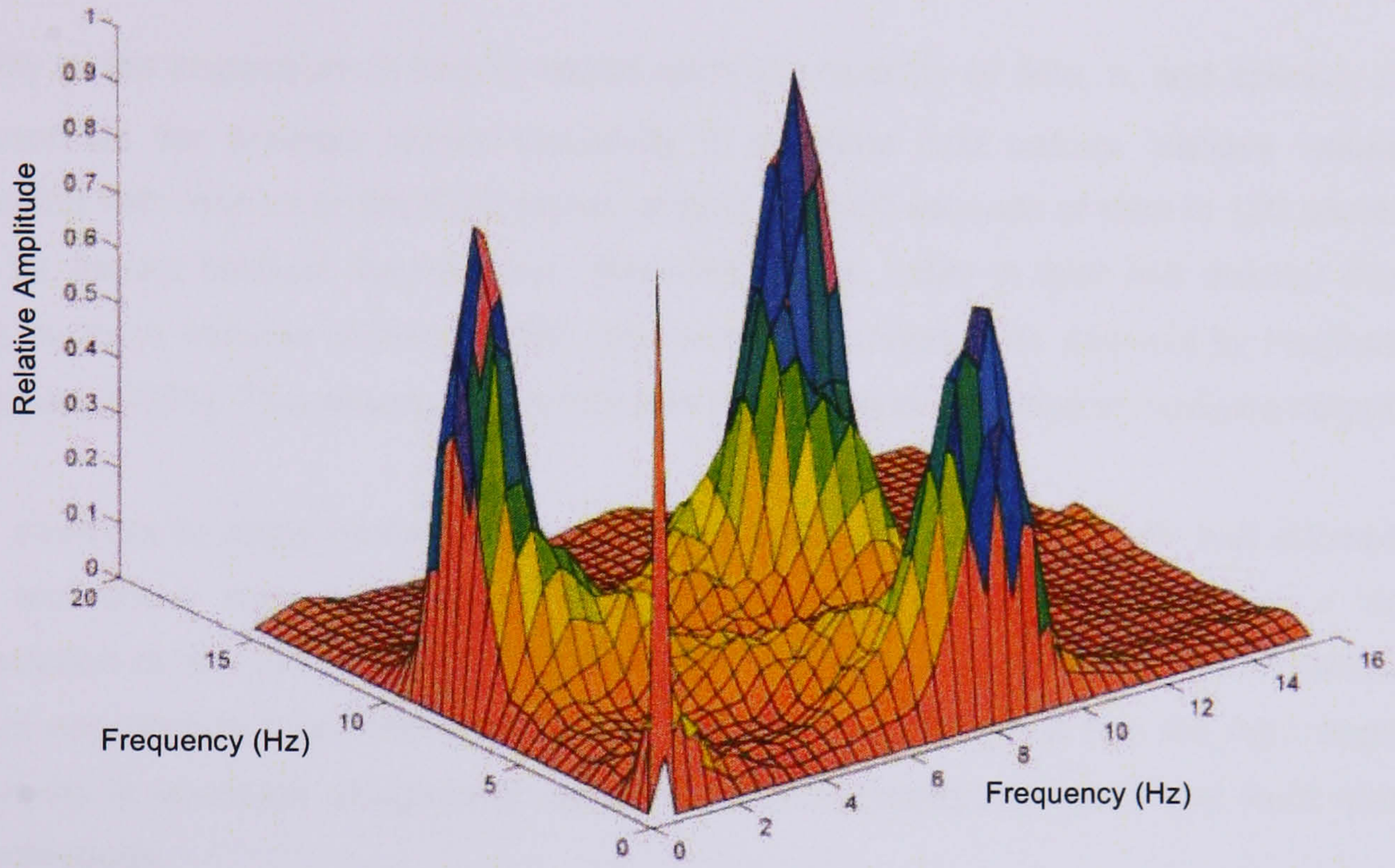

Figure 6.18: Example of a bispectral analysis of an EEG signal

The bispectrum is calculated by convolving spectral outputs and averaging over several epochs. Given a time series $x[n]$ divided into L epochs each with their own Fourier transform, X_l, the phase relationship between spectral components w_1 and w_2 can be found by:

$$B(w_1, w_2) = \frac{1}{L}\sum_{l=0}^{L-1} X_{lw_1} X_{lw_2} X^*_{l(w_1+w_2)}$$

where $X^*_{l(w_1+w_2)}$ denotes the complex conjugate. If w_1 and w_2 share the phase relationship:

$$\text{ø}w_1 = \text{ø}w_2 = \text{ø}\,(w_1 + w_2)$$

where ø denotes 'the phase of', a peak will appear in the bispectrum at these frequencies. As the values of w are dependant on amplitude, the bispectrum is often normalised to values between 0 and 1 giving what is termed the signal's 'bicoherence'. The bicoherence can be calculated by taking the square root of the ratio of the squared magnitude of the bispectrum and the squares of the convolution components in w_1 and w_2 over L epochs.

$$B^2(w_1, w_2) = \frac{L^2 \left| B(w_1, w_2) \right|^2}{\sum_{l=0}^{L-1} \left| X_{lw_1} X_{lw_2} \right|^2 \sum_{l=0}^{L-1} \left| X^*_{l(w_1+w_2)} \right|^2}$$

Stability of the bispectrum is largely based upon the quantity of data, n, and epochs, L, that are used as the analysis shows sensitivity to spurious data values. Various values are suggested with respect to the EEG signal ranging from 60 seconds of data in 120 epochs, as used by Aspect Medical Systems Inc., (Massachusetts, USA) in their BIS monitor (Rampil, 1998), to three minutes of data in 360 epochs as prescribed in an analysis by Hagihari and colleagues (2001). This asserts a considerable time delay in obtaining an updated output.

Early attempts to apply nonlinear techniques to EEG signals gave results that inferred that such techniques were not of use in EEG analysis. The main problem was a lack of appreciation of how bio-noise would deteriorate the quality of the initial dimension calculation. Recent approaches have improved on this, but it is of significance that the high degree of complexity in nonlinear analyses propagated misinterpretation by those that were applying the techniques.

Miller and Atwood (2004) question the information provided by the bispectrum, refuting that the output represents phase coupling. Others talk of the algorithm output providing a spectral characterisation of the time series amplitude probability distribution skewness. It would appear that the complexity of these techniques might lead to incorrect assessment of their output.

6.4 Entropy Measures

There are a number of approaches that may be applied to assess the entropy or 'uncertainty' of a signal. High uncertainty is found when there are a large number of underlying processes contributing to the system, whilst low entropy indicates that there are only a small number of dominating processes. Advocates of the use of entropy measures in the analysis of EEG refer to a set of simple tools that provide fast results.

As an example, to calculate spectral entropy the power spectrum is found and then normalised to 1. The entropy value, H, can then be calculated using:

$$H \equiv \sum_{n}^{N} p_n \log\left(\frac{1}{p_n}\right)$$

where p_n is the normalised power density value at frequency n. Commercial embodiments of spectral entropy use transforms of data from several window sizes to increase stability. GE Healthcare (Buckingham, UK) who have developed an entropy module for their operating theatre physiological signal monitoring systems refer to 'State Entropy' and 'Response Entropy' which arithmetically appear to differ only in that the State Entropy uses a bandwidth of 0.8Hz to 32Hz whilst the Response Entropy parameter uses a bandwidth of 0.8Hz to 47Hz. GE imply that the distinction between the two gives the Response Entropy measure a better indication of patient arousal as the added bandwidth includes more EMG, whilst the State Entropy measure focuses purely on the assessment of the EEG.

The premise of entropy does not introduce any new ideas relating to the physiological processes that underpin changes in EEG. As such it has not been well received by some (for example Jäntti et al., 2004), but nonetheless correlation between entropy metrics and states of consciousness have been reported (for example Ningler et al., 2004).

6.5 Multivariate Methods

Several processing schemes have been devised that combine two or more EEG parameters. Advantage is engendered in the use of parameters that display coherent characteristics distinct in their behaviour under various conditions. Two of the better known EEG monitors marketed as consciousness monitors are based on multivariate designs.

The BIS monitor from Aspect Medical Systems Inc. (Massachusetts, USA) is presented as being based around a bispectrum analysis. Although flow charts of the algorithm have been released into the public domain (see figure 6.19), the mathematical detail has not.

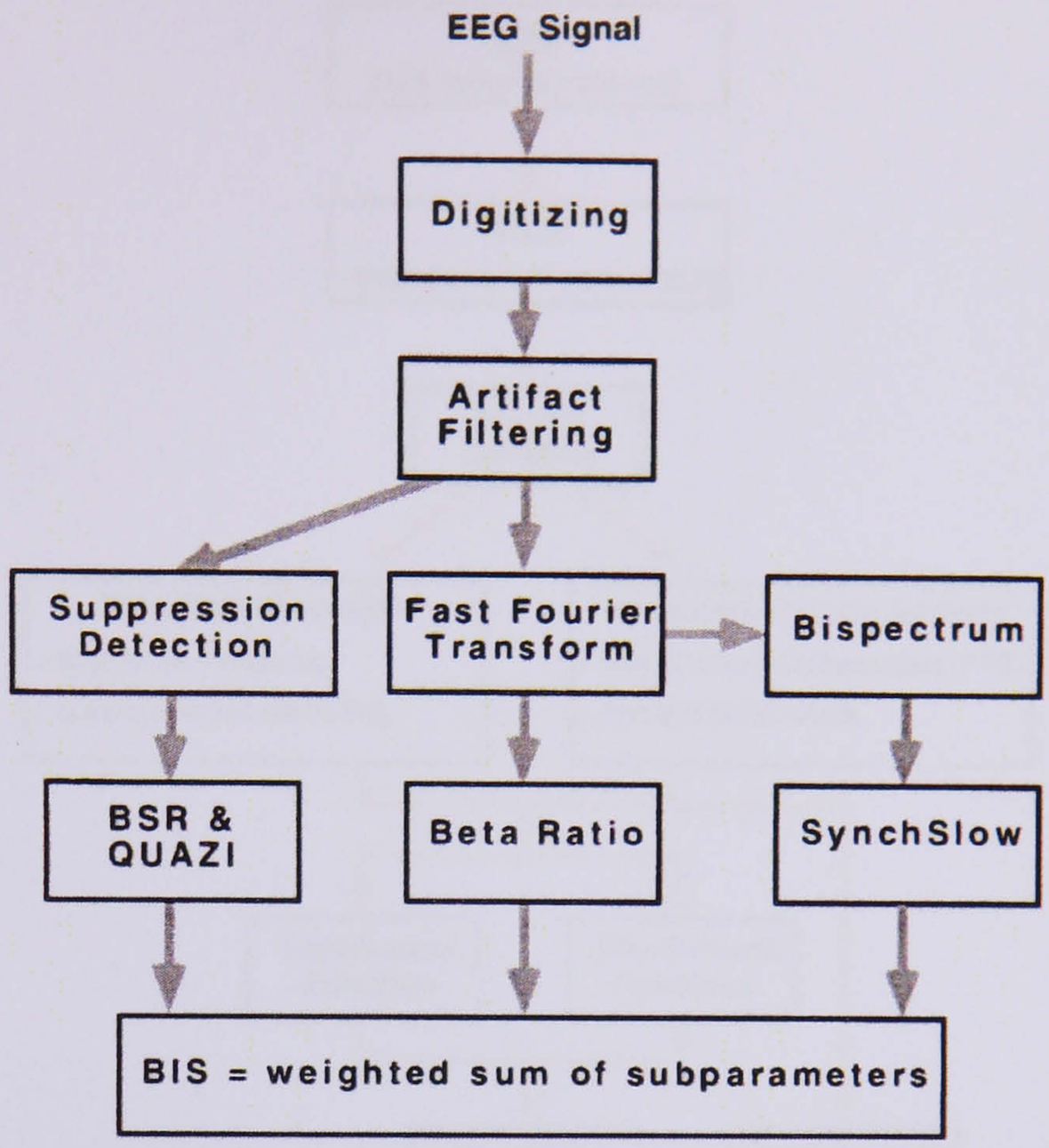

Figure 6.19: Flow diagram of the BIS algorithm from Aspect Medical Systems Inc., (Massachusetts, USA). Adapted from: Rampil, 1998.

The BSR & QUAZI algorithms are combined to give a representation of burst suppression activity. The beta ratio has been defined as the ratio of the spectral power between 30Hz and 47Hz divided by the power between 11Hz and 20 Hz whilst the SynchSlow bispectral derivative is said to present the ratio of bispectral power between 0.5Hz and 47Hz divided by the power in the 40Hz to 47Hz bandwidth. Each parameter contributes to the derivation of a single dimensionless number of between 0 and 100 via an undefined 'weighted sum' scheme.

The Narcotrend monitor from Monitor Technik (Bad Bramstedt, Germany) has also met with some commercial success. Combining time domain and spectral parameters, the Narcotrend monitor, in common with the BIS monitor, displays a single dimensionless number from 0 to 100 (see figure 6.20). Using a bank of EEG data samples known to be associated with different stages of anaesthesia, an undefined automated parameter selection criterion algorithm identified those parameters showing the highest correlation to anaesthetic state. Autoregressive modeling is used to generate the basis on which the spectral parameters are to be found (Krueur et al., 2003).

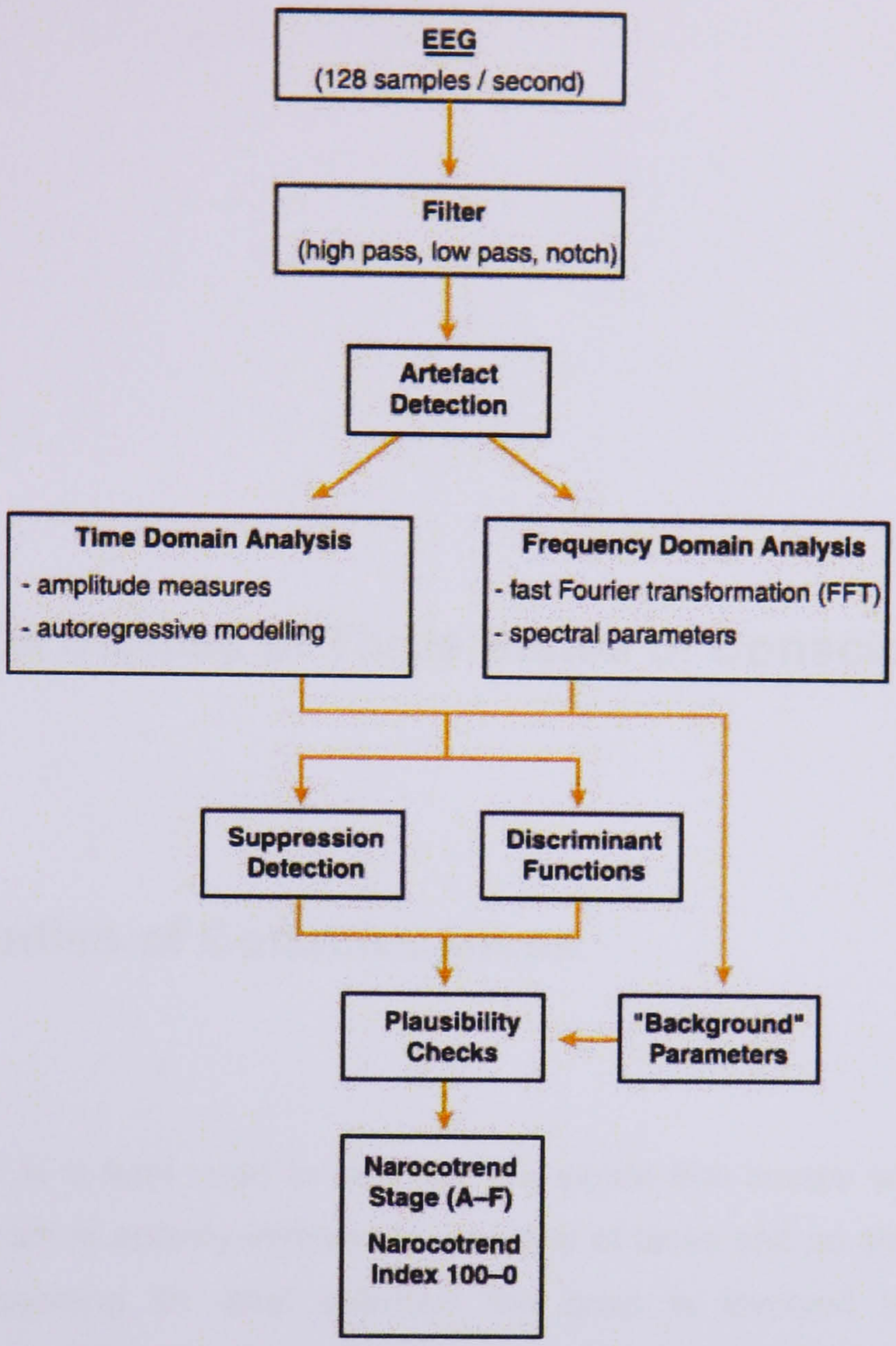

Figure 6.20: Flow diagram of the Narcotrend algorithm from from Monitor Technik (Bad Bramstedt, Germany). Adapted from: Kreuer et al., 2001.

Unless the multivariate methods prove to give a robust output with respect to the application there is little that can be assumed of their shortcomings when neither manufacturer has disclosed the complete algorithms on which their analyses are based. This is unfortunate, not only because the secrecy prevents others contributing to the furthering of the technology, but also because if instances are found where these monitors do not give an expected measurement, the use of EEG in depth of anaesthesia monitoring in general is likely to attract justifiable skepticism.

Chapter 7

Review of EEG Studies of Three States of Consciousness

7.1 EEG Studies of Consciousness

'Spontaneous EEG' is a term used to describe the signal that occurs without intervention. Whilst awake the brain is actively involved in a variety of tasks and so characteristics of the EEG will vary depending on what activities the brain is involved in, the individual's physiological status, and the effects of afferent stimuli. As such, it is difficult to identify a state that may propagate spontaneous EEG true to its definition. The EEG of a healthy and awake subject will be of a constantly varying form. Elul (1969) investigated the variance distribution of EEG amplitude of the awake individual; a Gaussian distribution was observed for 66% of the time series through non-tasked wakefulness, dropping to 32% during a mental arithmetic task.

Whilst there are a wide variety of transient features that can be interpreted in the EEG of an awake individual, certain features do recur. Many such features are more clearly observable in the frequency domain.

Spectral analysis of the EEG signal has been common practice since the discovery of EEG. It was recognised that whilst for much of the time the signal may appear as noise, periods of near pure sinusoidal activity indicate the deterministic content of the signal. In early studies it was thought that the important features of the signal lay between 0.5Hz and 32Hz as associations between sub-bandwidths and neuropsychological functionality could be identified. Modern studies have extended the total bandwidth to include frequencies from

0.1Hz to 1kHz. Figure 7.1 presents the EEG spectral bandwidth with the classic EEG sub-bandwidth divisions marked.

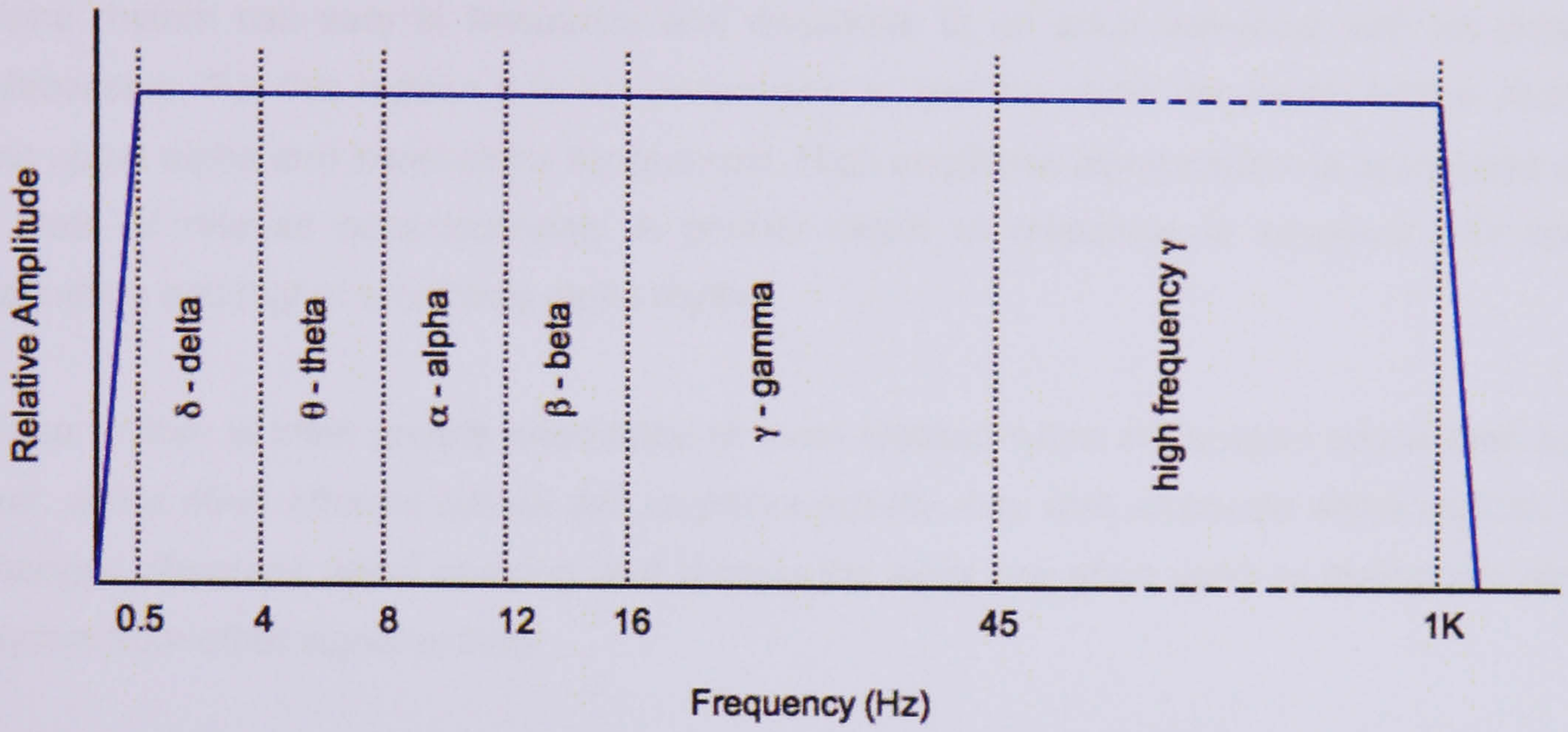

Figure 7.1: EEG spectrum bandwidths.

The phenomenon of alpha rhythm forms one of the most prominent features of human EEG. Its presence was the first characteristic studied by Berger (1929), the generally accepted father of EEG analysis. Alpha rhythm is the central feature of the alpha index method described in the patent that under pins this thesis.

Over the decade following Berger's identification of alpha rhythm, the EEG bandwidth was divided into several subdivisions based on features that appeared distinct in their occurrence. As it contained the first feature identified, the 8 to 12Hz bandwidth subdivision was termed alpha. Thus the alpha bandwidth is the spectral region in which 'alpha rhythm' can be shown to occur. That is not to say that all spectral power found between 8 and 12Hz is alpha rhythm, nor, as Berger's subsequent studies showed, does alpha rhythm appear exclusively within these limits (Berger, 1929). The term alpha rhythm describes a psychophysiological phenomenon, whilst alpha bandwidth is more a physicist's expression. The distinction is frequently unclear in the literature where the term alpha is often used. Assumptions can be made of the author's intended meaning of the term, but it is often not possible to identify whether the author has excluded the possibility, for example, that activity noted in the alpha bandwidth being something other than alpha rhythm.

Berger identifies alpha rhythm as a feature prominent in the awake but relaxed adult individual. Under optimum conditions the waveform of the entire EEG resembles a pure sinusoid in the alpha bandwidth. It is therefore a feature that does not necessarily require processing in order to directly identify it in the time-domain. Its magnitude varies considerably from one individual to the next but typical peak amplitudes are between 20μV and 80μV. Alpha rhythm can vary in frequency and amplitude in an adult individual with an inverse relationship. For this reason it is not uncommon to see the alpha bandwidth further divided into upper alpha and lower alpha for example. High amplitude alpha rhythm is associated with a state of relaxed consciousness. A greater depth of relaxation is assumed with lower frequency and higher amplitude alpha rhythm.

Alpha rhythm is often greatly attenuated or even blocked when the subject opens their eyes and, whilst other afferent stimuli and cognitive activity may also attenuate alpha rhythm, the changes observed when opening and closing the eyes are often used to distinguish alpha rhythm from other signal activity.

Nunez and Srinivasan (2006) observe that high alertness attenuates alpha with an increase in higher frequency activity, whilst the onset of drowsiness will attenuate alpha with an increase in lower frequency activity. If this is a stable relationship then alpha rhythm may indeed provide a useful feature of the EEG in monitoring depth of anaesthesia.

The amplitude and frequency of the alpha rhythm feature has been shown to change over the life cycle. EEG components showing alpha rhythm characteristics can be observed at frequencies as low as 4Hz in the infant. Through childhood both the frequency and amplitude of alpha rhythm increase up to adulthood whereupon those expected in adult EEG may be exceeded before settling back to the classic EEG alpha rhythm bandwidth. Nunez and Srinivasan (2006) note that the development of the skull and skin during maturation will have bearing on such measurements although no detail has been found to define this relationship.

It has been reported that in later life there is a decline in the prevalence of alpha rhythm. Nunez and Srinivasan (2006) make the point that by far the largest proportion of EEG recorded is that taken during clinical assessments of elderly patients. The increased anxiety experienced by elderly patients undergoing EEG examination, some of whom may have neurological conditions, will inevitably result in attenuated or blocked alpha. Alpha rhythm has been shown to occur in the elderly and so the observation that alpha rhythm diminishes in later life may simply be the result of biased data sets.

Although no definitive answer has emerged, EEG topographical mapping studies have established that the source, or sources, of alpha can be found in the posterior region of the brain. Positron emission tomography (PET) studies lend support to this (for example Larson et al., 1998) indicating alpha rhythm is generated in the lateral geniculate body and medial pulvinar of the thalamic nuclei. Hence there are many theories relating thalamic control and cortical propagation of alpha rhythm. Anaesthetic agents that modulate thalamic neurotransmission might therefore impact on alpha rhythm propagation to the surface EEG.

When the eyes are opened during high alpha bandwidth activity some sources are immediately attenuated whilst others are not. This suggests that some sites identified as sources of alpha may in reality be regions that show susceptibility to alpha frequency entrainment.

An asymmetrical relationship exists between alpha amplitudes recorded on either side of the scalp. When a subject opens one eye it is the alpha rhythm of the opposing hemisphere that is most greatly attenuated. This is perhaps not surprising given the contra-lateral wiring of the ocular system. Studies have shown that the asymmetrical alpha rhythm amplitude does not relate to whether the subject is left or right handed (Shaw, 2003).

The phase distribution of alpha rhythm is relatively stable and thus provides source location information for mathematical modeling. Nunez and Srinivasan (2006) derive a multiple source theory from this information. In addition, the phase stability means that distinct regions of the skull will show in-phase alpha activity. Electrode pairs sited at positions linked in this way will present a heavily attenuated alpha rhythm due to the common-mode rejection of the recording equipment front-end electronics. Neidemayer and da Silva (1993b) identify bipolar electrode recordings across the International 10-20 electrode positions P3 – O1 and P4 – O2 will have an increased likelihood of such an occurrence.

It should also be noted with respect to the present study, that some individuals show no signs of alpha activity. Davis (in Neidemayer and da Silva, 1993b) categorised the population by the prominence of their alpha rhythm: dominant alpha (20% of population), subdominant alpha (35%), mixed alpha (20%), and rare alpha (25%). Saul and colleagues (1937) reported a reasonable correlation between the prevalence of alpha and personality types where anxious or hyperactive individuals show low alpha activity, whilst nonchalant or highly focused individuals show heightened alpha activity. Charles and colleagues (2006) report that subjects showing higher alpha activity tend to be more resilient to pain.

Also of note is the observation that large amplitude alpha may be recorded in comatose patients as well as those in trauma or with certain diseases (Nunez and Srinivasan, 2006).

Whilst would appear that it is of some use, whether alpha rhythm is a reliable indicator of depth of anaesthesia seems doubtful. If alpha rhythm is a characteristic of the EEG that is found in only a subsection of the population, it cannot form the central component to a consciousness-monitoring scheme. Similarly, if the feature can persist for pathological reasons, it is unlikely that it would be accepted as a generalised solution.

High delta bandwidth activity is usually linked to inattention, drowsiness and deep sleep although it has been shown to persist in brain injury and coma. The mixed frequency and phasic content of delta activity has been attributed to the depression of thalamic rhythmic control centres (John et al., 2005). As the thalamus activity is a known site of influence of anaesthetic agents, it might be assumed that some indication of the influence might be presented in delta activity.

Theta was defined by Walter and Dovey (1946) as a bandwidth showing distinct behaviour to the neighbouring delta and alpha bandwidth activity. In general theta activity can, in the EEG of healthy awake adults, be swamped in relative amplitude studies, as delta and alpha are usually of much larger magnitudes. Theta appears in some stages of sleep and has been observed during deep relaxation (Aftanas & Golosheykin, 2005) although this may alpha rhythm occurring at a lower frequency propagated by modulated thalamic activity. There is also evidence to suggest that cognition may generate theta bandwidth activity in the surface EEG (John et al., 2005). This observation links well with the discussion of hippocampal activity in section 5.2 where it was suggested that a phasic characteristic in the theta bandwidth may exist during wakefulness but cease when the subject is unconscious. There is a likelihood that the feature would only be weakly represented in the surface EEG, which may cause issues in its mathematical extraction.

The possibility of alpha rhythm appearing at lower theta bandwidth frequencies would confuse analysis and may render theta monitoring inappropriate to the application. Theta activity during stages of sleep may also disrupt successful interpretation, however theta monitoring may be of use as part of a multivariate monitoring solution.

Perhaps unsurprisingly Berger's identification of beta bandwidth activity was successive to his observation and profiling work of alpha bandwidth characteristics. The beta bandwidth is often defined with a lower limit of 12Hz and an upper limit determined by the overall

bandwidth of analysis, which may be as low as 32Hz in clinical EEG assessments or as high as 1KHz in modern wideband studies (for example Klostermann et al., 2002).

Beta bandwidth activity is generally of lower amplitude than alpha for example, with peaks of around 30μV. Some authors refer to a 'beta rhythm' but it is often considered that the frequency content in the bandwidth is too irregular to be termed a 'rhythm'.

Berger's observations of beta activity revealed the link between increased beta bandwidth power and active concentration (Berger, 1938). Beta bandwidth activity in the pre-frontal region has been proposed as an indication of consciousness (Ingvar, 1987) as it is both prevalent in almost every healthy adult (Brazier and Finesinger, 1994), and displays reasonably stable associations with mental processing. It is therefore thought that beta bandwidth activity is propagated by functional groups of cortical neurons, a view confirmed in a recent functional magnetic resonance imaging study (Laufs et al., 2003).

Given the multiplicity of beta rhythm sources, phasic relationships in the beta bandwidth are unlikely to present a robust indication of return of consciousness. This would be compounded by the low spatial resolution of the surface EEG. However, amplitude analysis may present a reasonably robust indication of return of consciousness as beta activity appears to be attributed to a general increase in cognition. This characteristic should be independent of which agent or agents are being administered.

The classification of a gamma bandwidth was first used by Jasper and Andrews (1938) to describe the 35Hz to 45Hz region of the EEG spectrum. In the literature the term gamma appears interchangeably with beta to accommodate descriptions of high frequency phenomenon linked to mental activities and responses. Some make a distinction between the terms using beta to refer to spontaneous high frequency activity and gamma to describe induced phenomenon (Bullock et al., 1997; Fitzgibbon et al, 2004).

Gamma activity has been shown to exist as a feedback feature between the cortex and thalamus and is noticeably more prominent during arousal and some stages of sleep. There are many studies that suggest a link between 40 Hz gamma bandwidth activity and the binding of modes of subjective experiences to form the basis of consciousness (Mashour, 2004; Joliot et al., 1994; Rodriguez et al., 1999). It is possible, therefore, that both amplitude and phase analyses of the 40Hz region of the gamma bandwidth may reveal useful components to this application.

The study of 'wideband' EEG shows promise in diagnostic and monitoring applications. Curio (2004) reviews a number of studies and concludes that conspicuous and stable bursts of EEG activity in the region of 600Hz can be observed in response to stimulation or motor activity. Multiple distinct sources are thought to exist including cuneothalamic and thalamocotical relay cells, cortical bursting pyramidal cells and possibly, fast-spiking inhibitory neurons (Klosterman, 2002b). Few studies have employed such wide frequency bandwidths but the results presented by Curio and Klosterman suggest they may be of some significance to the application.

Spectral parameters such as 95% spectral edge frequency (SEF), the frequency below which 95% of the spectral energy is observed, tend to vary to a degree that prevents their use as an early predictor of changes from the state of consciousness (Schwarz et al., 2004). Due to signal variability, the mean SEF calculated over periods of 1 minute or more provides a more meaningful indication of consciousness. In general the SEF is expected to be lower in an unconscious individual than when conscious. Gajraj and colleagues (1998) showed that the SEF of a conscious individual can vary between 16.1 and 29.1Hz, giving a mean of 24.2Hz. In the same study the SEF of a bupivacaine induced, Propofol maintained, anaesthetised subject was shown to vary between 12.5 and 26.5Hz with a mean of 18.7Hz. Such wide and overlapping deviation supports the lack of SEF reliability concluded by Schwarz. Gajraj and colleagues (1998) also show that the degree of fluctuation of the median frequency of an awake individual varied between 1.5Hz and 18.9Hz with a mean of 10.9Hz; when unconscious values varied between 1.7Hz and 13.7Hz with a mean of 8.8Hz. Thus it is concluded that both SEF and Median frequency cannot solely be relied upon in the real-time assessment of consciousness (Gajraj et al.,1998).

Bullock and colleagues (1997) report that although occurrences of bicoherence do present themselves they are generally absent in the awake individual. Where coherent bispectral relationships emerge they are often unstable, local to relatively small regions of the cortex, and of variable character.

Entropy studies can be expected to deliver results similar to the bispectrum. Over long epochs, entropy analyses will approach a maximum whilst shorter epochs will reveal transient periods of coherence in response to particular activities and stimuli.

In experimentation conducted by Gajraj et al. (1998), the BIS analysis used by Aspect Medical Systems Inc. (Massachusetts, USA), is shown to provide an output that varies between 98 and 56 (mean 85.1) for a conscious individual. Although the mean of the BIS given over periods of 1 minute or more may reduce the problem, the BIS still gave outputs

above 70 indicating consciousness during deep anaesthesia when the 'mean smoothing' function was switched off. Gajraj and colleagues suggest that this may be a result of artifact interference. In experimentation the BIS analysis is shown to provide an output that varies between 98 and 56 (mean 85.1) for a conscious individual. Although the mean of the BIS given over periods of 1 minute or more may reduce the problem, the BIS still gave outputs above 70 indicating consciousness during deep anaesthesia when the 'mean smoothing' function was switched off. Gajraj and colleagues suggest that this may be a result of artifact interference. As a result of this variability, the numerical output of the BIS algorithm cannot directly be interpreted as indication of a particular state of consciousness. Thus a patient context must be maintained.

7.2 EEG Studies of Anaesthesia

Changes in the EEG resulting from particular stimuli are known as event related potentials (ERPs). Where the stimuli are deliberately applied, ERPs are known as evoked potentials. The evoked potential signal is often smaller than the spontaneous EEG activity. The classic approach to handling the adverse signal-to-noise ratio in the time-domain is to use a train of stimuli, at a frequency unrelated to dominant EEG frequencies. By averaging the equivalent data samples within recorded epochs phase-locked to the stimulus, the mean noise component will tend towards '0' and so variation in the sample means will correspond to the evoked potentials. This simple approach has its limitations, for example, to reduce noise sufficiently 1000 or more samples may be required and hence there will be a time lag in the output.

There is some debate over source of the evoked potential, the more populous theory is that they are the result of neuronal pathways becoming active as a result of the stimuli, but Sayers and Beagley (1974) show that they are the product of a spatial reorganization of 'normal' EEG activity as the intensity of the stimuli affects spectral component phase relationships rather than amplitude. Given the technical challenges involved in recovering low amplitude signal features from noisy environments, measures of bicoherence over the bandwidth of the evoked response may equate to an advantage in earlier identification of evoked potential response characteristics.

Somatosensory, auditory and visual stimuli have been found to be of use. Electric pulse somatosensory evoked potentials make use of the pathway from peripheral nerve to the brainstem and then cortex. Click-track auditory evoked potentials excite the eighth cranial

nerve pathway to the brainstem with subsequent distribution to the cortex. Visual evoked potentials, stimulated by light flashes, show the retinal and optic nerve pathway to the cortex.

Somatosensory responses have been shown to present considerable inconsistency between individuals and anaesthetic agents. Analgesic agents are also known to dissociate the somatosensory response from depth of anaesthesia correlation (Thornton, 1991).

Retinal evoked potentials are recorded using contact lens electrodes and have been shown to provide a useful indication of anaesthesia onset but a considerable latency in reflecting the termination of anaesthesia (Iohom et al., 2004).

Auditory evoked potentials (AEP) have been the most commonly used evoked potentials in depth of anaesthesia monitoring and have been embodied into commercially available products. The characteristic of the potential has been divided into three stages; the brainstem latent evoked potential (BLEP), the mid-latency response (MLEP) and the late-latency cortical response (LLEP). The BLEP has not been shown to vary with the concentration of any anaesthetic agents and so is not considered further. The LLEP only unreliably presents itself as it may exist as a function of attention as well as consciousness. The LLEP has been shown to be absent in wakeful subjects who are inattentive to the stimulus (Newton et al., 1989). The MLEP presents the activity of the primary auditory cortex (Tooley et al., 2004) and is characterised by 3 positive and 3 negative deflections in the EEG time series as shown in figure 7.2.

In the figure AEP1 shows the MLEP of an wakeful subject. AEP2 shows the MLEP during Propofol administration of blood concentration 1.5µg/ml where the subject was responsive to stimuli. AEP3 shows the MLEP of an unresponsive patient with a blood concentration of 3.8µg/ml of Propofol. AEP4 shows the MLEP of an unresponsive subject with a blood concentration of 8.9µg/ml of Propofol. The markers bs, Na, Pa and Nb indicate the features of the AEP waveform complex. The figure shows the AEP response slows with increasing doses of propofol, with the amplitude of the response after the initial spike (labeled bs in the figure) weakening in amplitude such that the response after the feature labeled Na is not significantly distinguishable from the background EEG at high doses.

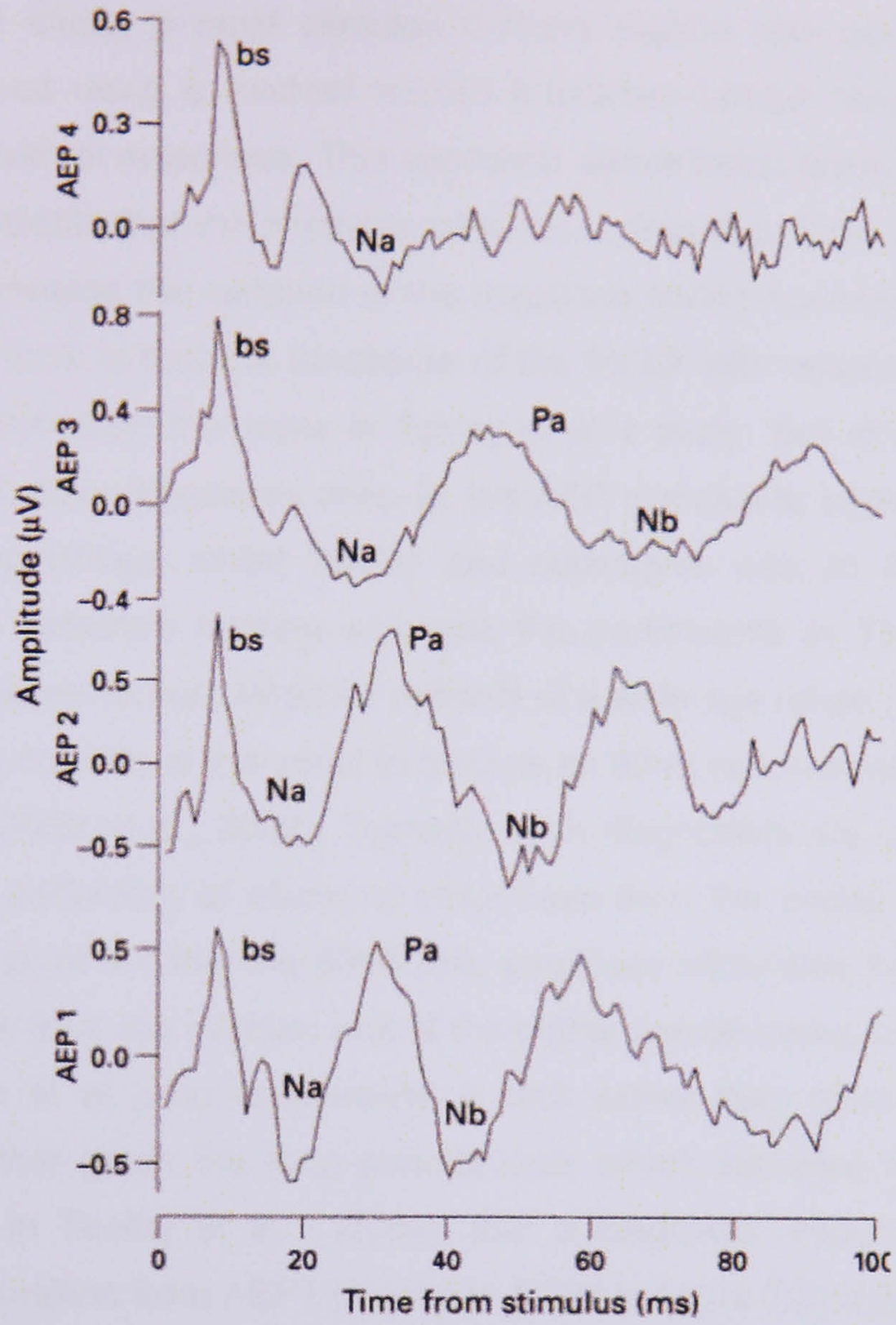

Figure 7.2: Variation in auditory evoked response. From: Tooley et al., 2004. Reproduced with permission.

Thornton and Newton (1989) note that whilst the latency of the MLEP tends to increase with anaesthetic dose, considerable interpatient variability exists. The decrease in MLEP amplitude again suffers from interpatient variability, but its presence has been shown to be an indication of implicit memory functionality (Sebel et al., 1986). In addition to amplitude and latency measures the click frequency at which the auditory evoked potential complex merges with previous complexes, presents the maximum stimulating frequency of the evoked response. In an awake individual this occurs somewhere between 30Hz and 40Hz. According to some, the frequency at which the auditory evoked potential complex merge can be seen to slow with increasing dose of anaesthetic (Plourde and Picton,1990).

Whilst AEP measurements might appear to be of some use to depth of anaesthesia monitoring, the proposal is not without some controversy. In a recent study Bell and colleagues (2006) report that the MLEP does not hold a stable characteristic with agent

concentration. In the study, a rapid stimulus delivery regime was used with over-lapping responses deconvolved using a method termed Maximum Length Sequences (Bell et al., 2001) to give the individual responses. This approach allows much faster data collection. The authors suggest it possible that the intensive stimulus regime may have caused stress to the auditory pathway increasing the variance of the response during anaesthesia. Also of note in Bell and colleagues' work is that the amplitude of the MLEP with respect to the background EEG is somewhat lower than the same in Tooley et al.'s study. Bell et al. use a 60dB nHL (normal hearing level) rising frequency chirp as the AEP stimulus to subjects showing a wide range of hearing capabilities, whilst Tooley and colleagues use an 80db nHL click. No mention is made of defective hearing amongst the participants in Tooley et al.'s study, suggesting that they were normal, albeit for patients of a wide age range (up to 71). In clinical diagnoses of auditory conditions it is usual to provide an 80dB nHL repeating click for patients with normal hearing (Katz et al., 2002). Typically such diagnostics are carried out using the electrocochleograph (recording of electrical responses from the cochlea of the inner ear). Katz and colleagues point out that the 80dB nHL amplitude stimulates the clearest response in the signal response from the cochlea end of the eighth cranial nerve and is thus discussed as a minimum. Katz et al. also recommend a click rather than chirp stimulus. Bell and colleagues suggest that given the long periods over which standard AEP data collection occurs (90 seconds in Tooley et al.'s study), that a catgorical response of the MLEP to anaesthesia (i.e. a transition from AEP1 directly to AEP4 in figure 7.2) may be represented as a dose-dependant progressive characteristic in data averaged over longer periods.

Noxious stimuli, body temperature, blood concentrations of glucose and carbon dioxide, as well as age and gender all effect evoked potential responses, as do hearing disorders, demyelinating diseases (multiple sclerosis), ischemia, coma, and tumors. A patient context must therefore be maintained when interpreting evoked response measurements.

Most agents evoke a drop in the total EEG signal amplitude upon onset of agent delivery. Increasing doses show a concomitant rise in amplitude. The barbiturates, opiates and nitrous oxide do not show the initial decrease in total amplitude noted with use of other agents but they all show a rise in total amplitude with further increases in dose. As discussed in section 6.1.1, total signal amplitude is an absolute parameter and as such actual measurements will vary significantly between patients. Monitors that show the parameter tend to display the mean total amplitude as a trace that varies over time. In this way relative changes can be visually assessed and interpreted. This approach is not ideal. Recent monitors combine various parameters to derive a dimensionless index, values of which are assigned to states of consciousness. Whilst this may make them more susceptible to interpatient and circumstantial output variability, operator training is minimised. Use of the physiological

signal trace requires study of the field of EEG in order for it to be understood. EEG training does not currently form part of anaesthesia training and so monitors that require interpretation of EEG traces have not generally been adopted. Thus, whilst total amplitude may be of some use, it is unlikely that it could form a generalised solution. Measurement of relative changes in total amplitude, however, may constitute a useful alternative.

Upon reaching deep anaesthesia a subject's EEG will begin to present bursts of electrical hyperactivity increasing mean amplitude. Bursts can last between 1 to 3 seconds. Bursts alternate with periods of heavily attenuated or isoelectric EEG. Suppression periods are often significantly longer than the bursts typically lasting from 5 to 10 seconds. An index for the period of burst and period suppression is provided by the burst-suppression ratio. Halothane, nitrous oxide, ketamine, the opiates and the benzodiazepines do not produce burst suppression and are thus thought not to assert complete anaesthesia.

Burst suppression is a phenomenon that is of more use in the assertion of prolonged sedation in the intensive care of patients with brain trauma. The technique used involves titration of the anaesthetic agent to some burst suppression ratio end point. The ratio of burst suppression is then maintained by pulling back the level of agent titration. The parameter is not generally used as a metric in general anaesthesia as burst suppression in EEG signifies a level of anaesthesia not usually required in the operating theatre. That said, occurrence of the phenomenon can be considered a clearly identifiable flag of approaching overdose and it therefore remains an important metric of depth of anaesthesia. A method of detecting and presenting burst suppression characteristics is a common component in monitoring solutions.

Burst suppression in EEG is a feature of a number of cerebral conditions that include brain trauma, brain ischemia, epilepsy, Creutzfeldt-Jakob disease and brain death. A patient context is therefore needed when interpreting the parameter. In addition Dwyer and colleagues (1994) note in experimentation with Isoflurane anaesthesia, that the relationship between anaesthetic concentration and the ratio of burst suppression is not stable. Both of these observations cast considerable doubt on whether the EEG can realistically be used as a depth of anaesthesia monitoring solution.

Both time domain amplitude skewness and kurtosis can be calculated with stability and are conceptually easy to visualise in the context of neurophysiology. Despite these advantages, and positive indications of their use (Bronzino et al., 1981; Ningler et al., 2004; Schwilden et al, 2005) the measures do not appear extensively in the literature however, recent wideband studies show both parameters strongly correlate with depth of anaesthesia (Ningler et al, 2004).

Clinically, the Zero Crossing Frequency parameter has been dismissed as much as it has been extolled. Where some have noted reasonable correlations between the parameter and clinically tested levels of sedation (Herregots, 89), others have shown insensitivity to other agents (Kaneda et al., 1995; Wauquier et al., 1988, Rampil and Laster, 1992). Whilst its mathematical derivation is usefully simple, it is unlikely that the parameter can contribute to a generalised solution.

Shannon entropy has been shown to correlate well with changes in consciousness (Sleigh et al., 2004) and has been embodied in a product aimed at anaesthesia monitoring, but Bein (2006) and Bruhn et al. (2001) note that wide variation in measurements between patients. Whilst useful, the unclear data interpretation required of entropy-based monitoring solutions has meant they have not been generally adopted.

The agents that strongly excite GABA and glycine receptors: Propofol, Isoflurane, Sevoflurane and Desflurane, all show similar spectral characteristics. Since both neurotransmitters can be found in abundance in the cortex, local agent effects are strongly represented in the surface EEG. Increases in delta and beta bandwidth activity are accompanied by a decrease in alpha activity at the onset of agent delivery. The differences in glutamate receptor interaction between these agents shows either glutamate pathways do not present significant differences in spectral EEG analysis or that the excitory effects may be masked by the effects generated by GABA and glycine pathway excitation. It seems intuitive that the inhibition of excitory glutamate receptors should lead to a depression of total power. Whilst this remains true for many of the agents, nitrous oxide, which inhibits all three glutamate receptors, affects an increase in total EEG power.

The relative spectral characteristics of many agents have been profiled extensively and are presented in table 7.1.

	Dose	Delta	Theta	Alpha	Beta	Total Power	Burst Suppression
Propofol	Low Medium High	 Inc inc		Dec	Inc	Dec Inc Inc	Yes
Etomidate	Low Medium High	 Inc		 Inc	Inc	Dec Inc Inc	Yes
Isoflurane Desflurane	Low Medium High	 Inc	 Inc Inc	Dec	Inc	Dec Inc Inc	Yes
Enflurane	Low Medium High	 Inc	 Inc	Dec	Inc	Dec Inc Inc	Yes
Halothane	Low Medium High	 	 Inc		Inc Inc	Dec Inc Inc	No
Nitrous Oxide	Low Medium High				Inc	Inc	No
Barbiturates	Low Medium High	 Inc		 Inc	Inc	Inc Inc Inc	Yes
Opiates	Low Medium High	Inc Inc Inc	Inc Inc		Dec	Inc Inc Inc	No
Ketamine	Low Medium High	 Inc	 Inc	Dec		 Inc Inc	No

Table 7.1: Classic EEG bandwidth characterisation of various anaesthetic agents. 'Inc' indicates an increase, whilst 'Dec' describes a decrease in each parameter. Adapted from: Holt, 1997.

Table 7.1 shows that activity in alpha bandwidth is not a consistent feature of all the agents. Delta bandwidth activity generally increases with deepening anaesthesia although not with nitrous oxide or halothane. These anomalies of delta bandwidth activity do not constitute a direct relationship with the anomalies of alpha. This suggests that the observations made by Griffiths et al. (1991), do not translate to uniform a characteristic of the EEG in depth of anesthesia monitoring.

The table also shows that relative beta activity appears to increase in the use of several agents but not the opiates, or ketamine. Total power in narrow band studies appear to increase with dose of all agents although there are some differences in the concentrations required to elicit the characteristic.

Both nitrous oxide and ketamine show similar principle neurotransmitter interactions and yet show different spectral characteristics. The only narrowband spectral change that occurs with nitrous oxide administration is a rise in beta bandwidth power.

Both Ruiz-Gimeno et al. (2005) and Ningler et al. (2004) report a good correlation of beta, gamma and high frequency suppression during Propofol or Sevoflurane anaesthesia. Whilst Willmann and colleagues (2002) suggest that high frequency analysis are more prone to movement artefacts and electromagnetic interference from other equipment.

Large slow potential oscillations have been reported in gerbils during Halothane anesthesia (Roughan and Laming, 1998).

In summary, the lack of uniform EEG sub-bandwidth characteristic across all agents would suggest that these parameters are not direct measures of consciousness. It might therefore be assumed that spectral components provide a measure of the processes by which the various agents assert their effects. Similarly, the relationship between the neurotransmitter pathways associated with the action of each agent and the spectral content of the surface EEG derived from each agent is not consistent.

Whilst this would indicate that use of spectral components is not appropriate to the application, some characteristics may prove of some use as a component to a multivariate algorithm design. The increase in beta activity at low agent doses appears in the literature as a uniform characteristic across all the agents except the opiates and ketamine. The exception of the opiates might not constitute a problem, as it is unlikely that an anaesthetic procedure would consist of opiates alone. Although this is not true of ketamine, the very low concentrations of ketamine required to induce analgesia (see table 1.2) means awareness with pain is very unlikely at clinically relevant concentrations of the drug. For this reason beta activity may usefully be included in such a design but with the understanding that the measure may represent only particular drug actions rather than loss of consciousness.

Similarly delta bandwidth activity may be used as a representation of high doses of all but nitrous oxide and Halothane. However, the exception of Halothane may constitute a problem as it may be used with nitrous oxide as a complete anaesthetic.

The decrease in alpha activity seen at the onset of agent delivery is not a feature across all agents. Some agents even give rise to an increase in alpha activity during delivery onset. It is therefore not a useful parameter to the application.

Total power across the narrow EEG bandwidth (0.5 to 32Hz) may contribute a useful measure of increasing dose beyond low doses except in the instance of nitrous oxide. Again, nitrous oxide is unlikely to be used as a sole agent in an anaesthetic procedure, and so this may not be a problem if the parameter is interpreted in the context of drug action as opposed to the state of consciousness.

Spectral parameters such as the spectral edge frequency show overlapping standard deviations between values representing different known states of consciousness. This necessitates long moving average analyses to lower the mean error of the spectral parameters making this set of tools insensitive at the threshold of loss of consciousness (Dwyer et al., 1994; Gajraj et al., 1998; Langford and Thomsen, 1994).

As with time domain spectral entropy, interpatient variability presents a problem in the use of spectral entropy methods as a generalised solution (McKay et al., 2006). Successful correlation with loss of consciousness was found to be between 82% and 84% (Ellerkman et al., 2006). High frequency studies present a good correlation between spectral entropy and return to consciousness (Gunawardane et al., 2002) although anomalies have been noted (Gjerstad et al., 2007).

Despite the compelling idea that loss of cortical connectivity may provide a stable correlate at the scalp surface (Massimini et al. 2005; Myles et al., 2004), Schwilden and Jeleazcov (2002) show that bicoherence is not a strong correlate of consciousness with only 10% of all epochs presenting nontrivial bicoherence. Sleigh et al., (2001), reported that the BIS monitor is no more effective a correlate of consciousness than a beta rhythm monitor. This suggests that the bispectrum component of the BIS monitor algorithm may not constitute the predominant component of its index.

Various studies have shown a correlation between the spatial dimension of nonlinear analyses and anaesthesia (Watt and Hammeroff, 1987; Kumpf, 1997). Schwilden (2006) gives 74% prediction success.

Anderson and Jakobsson (2004) suggest that neither the State Entropy or Response Entropy parameters were sensitive to nitrous oxide. Two groups led by Zhang et al. (2001) and Ningler et al. (2004), have reported a 93% prediction success rate during the use of several agents using Lempel-Ziv signal complexity in wideband studies. No study of the effects of nitrous oxide on Lempel-Ziv measures has been found.

As discussed in section 6.5, the various components of the BIS algorithm are combined to deliver a single, dimensionless number between 0 and 100. Values of above 85 are said to indicate wakefulness, between 65 and 85 indicates sedation, 40 to 65 indicates general anaesthesia and values below 40 signify burst suppression. Values of 75 and below are said to represent a low probability of awareness (Iselin-Chaves et al., 1998).

The commercial success of the unit is related to the statistical evidence of efficacy derived from observations across large trials (for example Myles et al., 2004, Sebel et al., 2004). The occurrence of awareness is reported to be reduced by 82% with use of the system. However, various conditions have been identified in which the BIS does not perform well. Several studies have shown that BIS values as low as 50 can be accompanied by awareness (Glass et al., 1997).

Questions have been posted about the derivation of the algorithm, which Drummond (2000) indicates was developed in single agent studies. Sensitivity to noise has been noted (Kim et al., 2001) and even the burst suppression algorithm appears to be unreliable (Bruhn, 2000). Large interpatient variability has also been reported (Roustan et al., 2005). Nitrous oxide (Rampil et al., 1998; Sice, 2005), the opiods (Brunner et al., 1994) and ketamine (Suzuki et al., 1998) do not affect changes in the BIS even when sufficient agent has been delivered to ensure deep sedation.

The Narcotrend monitor from Monitor Technik (Bad Bramstedt, Germany) catagorises the stages of anaesthesia in the manner presented in table 7.2.

Kreuer and colleagues (2001) present a review of the Narcotrend monitor in which a comparison is made with the performance of the BIS monitor. The correlation of both monitors to clinical signs are presented in table 7.3. The clinical signs listed in the left hand column represent a complete anaesthetic procedure. Of interest is the variance of both the Narcotrend and BIS monitors at the assumed point of loss of consciousness belying the state labeled loss of eyelash reflex. The variances observed at this point merge with the variances noted at loss of verbal response and the opening of eyes. Errors will thus occur although the Pk values given alongside each set of variances indicate that these are relatively unlikely. The study indicates that the Narcotrend monitor may present advantage in detecting return of consciousness with more accuracy than the BIS monitor.

Depth of Anaesthesia	Narcotrend stage	Narcotrend index
Awake	A	95–100
	B0	90–94
Sedated	B1	85–89
	B2	80–84
Light anaesthesia	C0	75–79
	C1	70–74
	C2	65–69
General anaesthesia	D0	57–64
	D1	47–56
	D2	37–46
General anaesthesia with deep hypnosis	E0	27–36
	E1	20–26
	E2	13–19
General anaesthesia with increasing burst suppression	F0	5–12
	F1	1–4

Table 7.2: Key to the index derived from the Narcotrend monitor from Monitor Technik (Bad Bramstedt, Germany). Adapted from: Kreuer et al., 2001.

Clinical Signs	Narcotrend Index	P_K	BIS-XP Index	P_K
Baseline	94.4±5.6		91.4±7.7	
Loss of verbal response	80.1±6.8	0.97	81.6±9.7	0.97
Loss of eyelash reflex	71.8±8.9	0.93	77.2±11.0	0.95
Opens eyes spontaneously	80.3±5.8	0.97	76.7±9.2	0.95
Extubation	86.8±7.4	0.98	82.5±5.0	0.98

Table 7.3: Comparison of Narcotrend monitor from Monitor Technik (Bad Bramstedt, Germany) performance and the BIS monitor from Aspect Medical Systems Inc., (Massachusetts, USA). P_K is the prediction probability. Adapted from: Kreuer et al., 2001.

Figure 7.3 presents the practical benefits in the use of both monitors in reducing the quantity of agent used during a procedure. The dark orange bars represent the doses used when no monitor is used, with the lighter bars indicating doses administered when using the BIS monitor, and the pale bars indicating that when the Narcotrend monitor is used. This study indicates the Narcotrend monitor to be more effective.

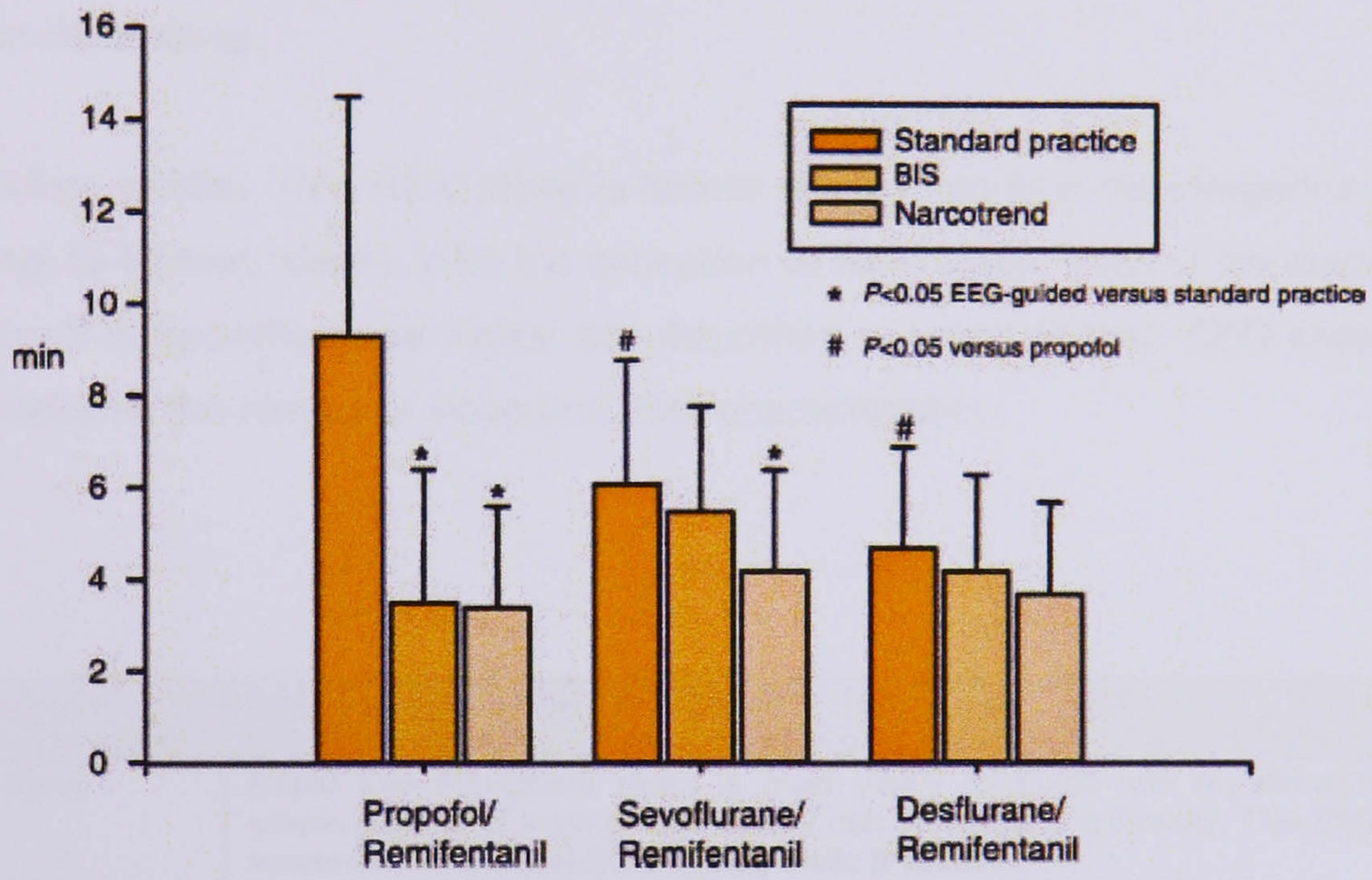

Figure 7.3: Comparison of time taken from termination of agent delivery to eyes open recovery using the BIS monitor from Aspect Medical Systems Inc., (Massachusetts, USA) and the Narcotrend monitor from Monitor Technik (Bad Bramstedt, Germany). Adapted from: Kreuer, 2001.

Various studies have been conducted to confirm the results presented in table 7.3 and figure 7.3 of which several have found that the resolution of the Narcotrend system is unreliable at moderate depths of anaesthesia (Russell, 2006; Bauerle et al., 2004) and may not be relied upon when using multiple agents (Bauerle et al., 2004).

The results from the multivariate design approaches indicate that they do not accurately measure loss of consciousness, but do nonetheless provide a useful measure.

7.3 EEG Studies of Sleep

As discussed in section 5.3, three main stages are identified in the standard classification of the characteristics of sleep (Rechtschaffen and Kales, 1968):

Wakefulness;
Rapid Eye Movement (REM) sleep;
Non-REM sleep.

In more modern studies, Non-REM sleep is further divided into four subcategories, numbered 1 (light sleep) to 4 (deep sleep). With the exception of REM sleep, each of the stages of sleep described by Rechtschaffen and Kales' are described in terms of their EEG characteristics. Table 7.4 presents the stages of sleep and their characteristics.

Sleep Stage	EEG Characterisation
REM Sleep	Rapid Eye Movement sleep is most easily identified with an electroculargram where periods of such ocular activity can be measured directly. The EEG is often recorded with parallel EOG in diagnostic practice.
Stage 1	During the onset of sub-REM sleep the EEG is usually of a low amplitude (75 μV) and low median frequency in narrow bandwidth analyses. High theta activity increasing in frequency towards the alpha bandwidth signifies the transition in to stage 2 Non-REM sleep. It is noted that K complexes may be observed during stage 1 Non REM sleep.
Stage 2	K complexes and occasional sleep spindles mark, along with increased alpha bandwidth power, stage 2 Non-REM sleep. The frequency of K complexes is used to distinguish between stages 1 and 2 Non-REM sleep, where intervals of 3 minutes or less indicate stage 2 Non-REM sleep.
Stage 3	Delta bandwidth power begins to increase.
Stage 4	Where delta activity reaches a relative power (in narrow bandwidth analyses) of 50%, the subject is considered to have entered stage 4 Non-REM sleep.

Table 7.4: Rechtschaffen and Kales' characterisation of sleep stages.

There are a number of time domain EEG features that are of use in sleep monitoring. K-complexes are low frequency (0.5 to 2Hz) and high amplitude (>100 μV) EEG signal fluctuations that occur over periods of around 0.5 seconds. K-complexes often occur as isolated single periods of low frequency oscillation and are thus unlikely to be represented in

a frequency analysis with long data epochs.

A second phenomenon, termed 'sleep spindles' occur as bursts of globally synchronous oscillations in the 12 to 14Hz range displaying increased amplitude with a tapering envelope. K-complexes and sleep spindles cannot reliably be detected in the frequency domain and so both are more commonly captured using time-domain analyses. Figure 7.4 shows an example of both the K-complex and a sleep spindle. Although the mean amplitude tends to lower during onset of sleep, the increasing frequency of higher amplitude K-complexes deteriorates reliability of mean amplitude measures. Both sleep spindles and K-complexes represent increases in the phasic synchronization of action potential firing in the plexiform layer of the brain.

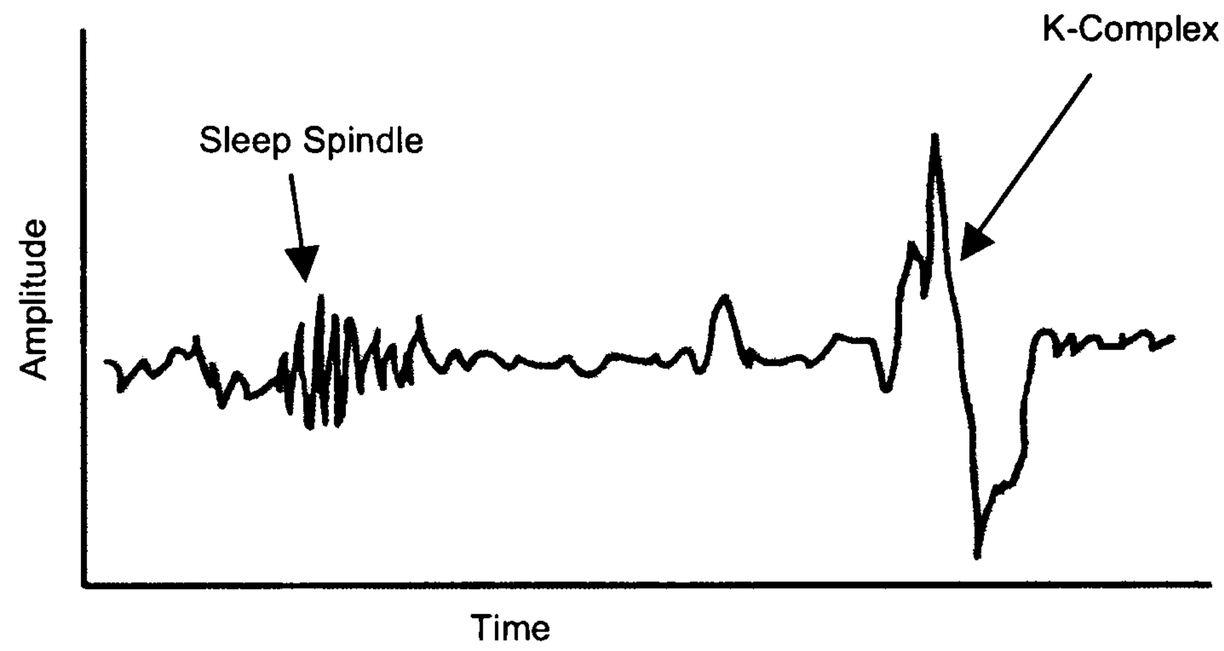

Figure 7.4: Example of a sleep spindle and a K-complex.

The skewness of kurtosis of amplitude variance plots show some coherence to sleep stages (Dumermuth et al., 1972) but this has been shown to be limited and thus an unreliable measure (Rémond, 1973). Dumermuth and colleagues (1972) also showed that the correlagraph shows considerable coherence with all stages of Non-REM sleep in narrow bandwidth studies but not elsewhere.

During the course of a single period of sleep, physiological indicators show there is oscillation between stages of sleep at increasing frequency when approaching arousal (McCarley 1975). The cumulative display of spectral power distributions presented in spectrograms have been shown to enable direct sleep stage identification by observation, but the variety of routes through the stages of sleep that a particular subject might take through a complete period of sleep has prevented an automated system from being based solely on bandwidth

power variation (Santamaria and Chiappa, 1987).

It would appear from table 7.4 that a number of frequency domain parameters should contribute usefully to an automated sleep classification scheme. Sleigh and colleagues (1999) have shown that variances of the 95% spectral edge frequency, relative delta bandwidth power and relative alpha bandwidth power are considerable.

Variance in individual epoch values of the parameter makes real-time spectral edge frequency (SEF) potentially misleading. A moving average of the spectral edge analysis provides an indication of some value as it drops fairly constantly, but not substantially, throughout deepening sleep (Sleigh et al., 1999). The mean and standard deviations of relative delta and alpha power are given in table 7.5 along with the SEF.

	SEF	*Delta*	*Alpha*
Awake	21 ± 3	50 ± 5	52 ± 8
REM	14 ± 4	59 ± 4	44 ± 3
Stages 1-3	12 ± 2	50 ± 4	49 ± 6
Stage 4	17 ± 2	50 ± 4	46 ± 7

Table 7.5: Power band and spectral edge frequency characterisation of sleep stages. Mean values are given with the standard deviation. Adapted from: Sleigh et al., 1999.

Several classification systems have been developed to supercede the detail of sleep stage identification. Dement (1998) presents a seven stage scheme:

1. Alpha wave train;
2. Alpha wave intermittent A;
3. Alpha wave intermittent B;
4. EEG flattening;
5. Theta wave;
6. Saw tooth wave – indicates increased harmonic activity;
7. Movement.

Dement suggest that as EEG flattening and theta wave patterns are the most frequently presented features, they may be the most useful EEG indicator of REM sleep.

A number of groups have focused research on higher frequency bandwidths (Ferri, 2000; Sing et al., 2005). Ferri showed that whilst there are no direct relationships between activity in the 15Hz to 45Hz bandwidth and the sleep continuum, indices derived by the relative power in the 15Hz to 25Hz bandwidth divided by the relative power found in the 35Hz to 45Hz bandwidth, and similarly the relative power in the 25Hz to 35Hz bandwidth divided by the relative power found in the 35Hz to 45Hz bandwidth to be of use. High values give good indication of REM sleep and low values correlate well with non-REM sleep. Sing and colleagues (2005) use a much broader bandwidth split into 5 sub-bandwidths: 1-15Hz, 16-50Hz, 50-100Hz, 101-200Hz & 201-500Hz. When viewed relative to a much wider bandwidth Sing and colleagues were able to show that the combined power in the classic delta, theta and alpha bandwidths could present a metric of sleep onset through to stage 3 sleep.

Spectral entropy has been successfully used to distinguish stages 1 to 3 Non-REM sleep, but does not provide a complete solution to automated identification of REM and stage 4 Non-REM (Feng and Chen, 2005).

Non-linear analyses have also been shown to identify only Non-REM stages of sleep. Šušmáková recommends that if non-linear analysis is to be used, it should be in combination with linear techniques (Šušmáková, 2004).

In congruence with the effects observed during anaesthesia, the bispectrum shows a decrease in synchronicity during deepening sleep (Steyn-Ross, et al., 1999). This implies a loss of cortical phase connectivity (Massimini et al., 2005). REM sleep presents increased synchronicity.

The BIS monitor from Aspect Medical Systems Inc., (Massachusetts, USA) tends to decrease over deepening sleep. Standard deviations are again relatively high but an averaged output will provide useful indication of depth of sleep up until REM sleep, which the algorithm represents with an increase in output to an index representative of consciousness.

Other multivariate approaches to monitoring the conscious continuum of sleep have proven somewhat successful. Carli and colleagues (in Angeleri, 1997), choose an eight feature classification system presented in table 7.6. The analyses employed were used to form an automated characteristic recognition process. The indication of sleep stage provided by each feature is weighting on a basis given by analysis of previous recordings by an expert prior to

automation. Through this method Carli and colleagues found an 83% average in successful prediction of sleep stage. This is a similar success rate to those found using other schemes.

Feature	Analysis
Quantity of high-amplitude delta	Identified using an appropriate finite impulse response filter
K complex detection	Identified using an appropriate finite impulse response filter
Sleep spindle detection	Identified using an appropriate finite impulse response filter
Band power in delta, theta, alpha and beta bandwidths	Identified using appropriate finite impulse response filters
Measure of desynchronization	Using bispectrum analysis
Quantity of muscle artifacts	Indicated by epochs of severe variance from a moving average of real time data
Quantity of muscle activity	Electromyogram observation
Quantity of slow and fast ocular movements	Identified using cross-correlation with prior waveforms

Table 7.6: Eight-feature classification scheme as proposed by Carli and colleagues (in Angeleri, 1997).

In summary, whilst it would appear to be convenient to the present study that since the 1960's sleep stage classification has been based on EEG characteristics, it does present some problems. The reasonably stable characterisation of sleep EEG waveforms provides a powerful tool in the diagnosis of sleep abnormalities. However, it could be argued that the generally accepted categorizations of sleep stages have detracted research from identifying whether there is a direct link between EEG and the neurophysiology of consciousness. With sufficient characteristics available in the EEG for diagnostic purposes there is little motivation to identify a parameter of the EEG that directly monitors consciousness in the context of sleep.

As changes between the stages occur over relatively long periods (30 to 60 minutes) epoch lengths of 60 seconds or more are often used in sleep analyses. For applications in sleep abnormality this has been proved sufficient but caution must be given to any stage classification of a continuum, especially one so coarse as that presented by Rechtschaffen and Kales. Shorter epochs, modern recording equipment and advances in signal processing

techniques provide additional information that has, in general, been obscured by traditional classifications in studies of EEG recorded during sleep.

However, of note is that during sleep, phase relationships within the EEG desynchronise during the onset of sleep but then reassemble during REM sleep indicating that the neurophysiology of the surface EEG during dreaming is much the same as during wakefulness. It should therefore be of no surprise that monitoring systems that utilise bispectral analyses as their central algorithm do not distinguish between these two states reliably. The same appears true of other non-linear analyses and entropy measures which are also confounded by REM sleep, however, since dreaming is not generally a feature of surgical anaesthesia, this may not undermine the approach for use of EEG during anaesthetic procedures. Sleep studies make clear however, that the bispectrum is not a measure of consciousness. If consciousness is defined with terms like “aware of one’s environment” then REM sleep is clearly a sate of unconsciousness, and so these EEG tools might be thought of as brain function monitors as opposed to monitors of consciousness.

Chapter 8

Monitor Development

8.1 Design Theory

Figure 8.1 gives a functional block diagram of the key components that comprise a typical EEG monitoring system. Each component shown in the figure will be reviewed.

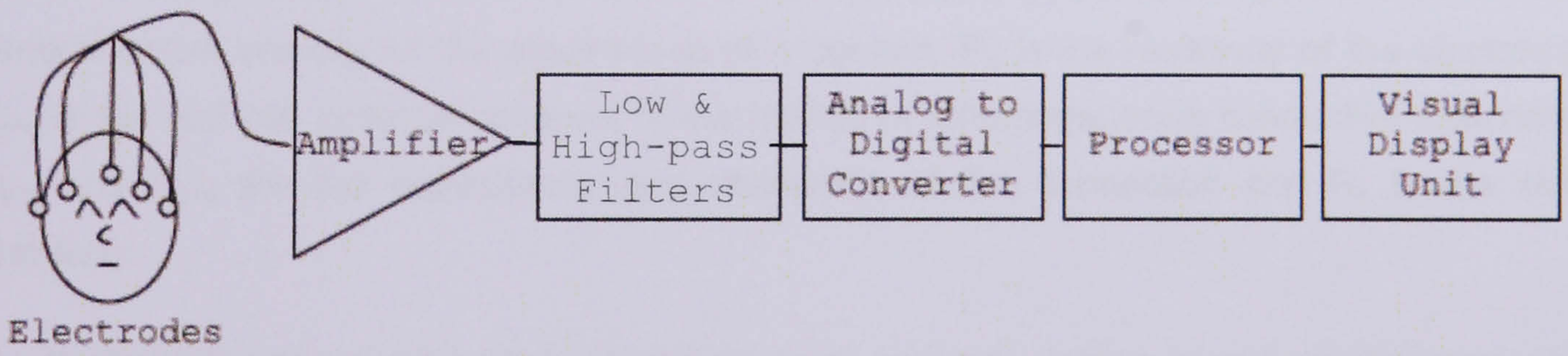

Figure 8.1: Basic bock diagram of key EEG monitor functional subunits.

To acquire the EEG signal it is first necessary to convert ionic current to electrical current. This is done with electrodes.

Electrodes take many forms appropriate to particular applications. Needle microelectrodes can be used to retrieve signals from within a single nerve fibre for example, whilst surface electrodes are designed to maximally conduct the ionic signal from the less than ideal

conditions of the skin's surface. An example of a traditional and typical surface electrode is described in figure 8.2.

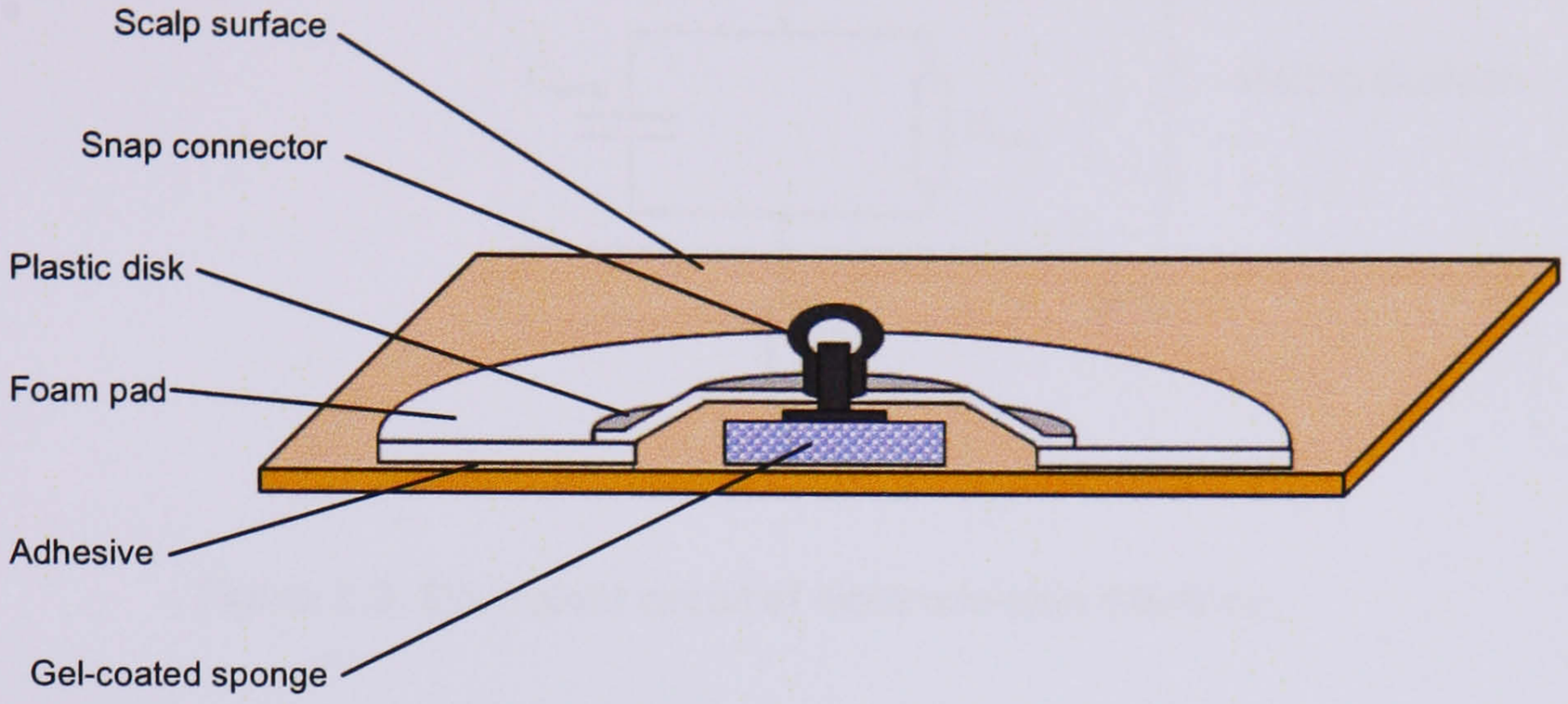

Figure 8.2: Cross section schematic of a traditional surface EEG electrode.

The example in figure 8.2 employs a silver electrode disc coated, using electrolysis, with silver chloride (AgCl). This is a common form as the impedance of silver chloride closely matches that of the epidermis of the skin. Any difference between the potentials of the two surfaces will give rise to a half-cell direct current (DC) offset potential. Figure 8.3 shows the general circuit analogy of the electrode-to-skin contact. R_e is the resistivity of the electrode, E_{e+s} is the half cell potential inherent in the mating of inhomogeneous conductive materials, C_{e+s} and R_{e+s} are the capacitance and resistance of the connection and R_s is the skin resistivity.

Ideally the half-cell potential would remain at some constant voltage level such that it may be removed by common mode rejection and filtering in the analogue circuitry, but changes occur for a variety of reasons including electrode movement and changes in skin resistivity, often yielding a relatively large signal on which the EEG will be superimposed. To minimise half-cell disturbances caused by electrode movement, an electrolytic gel of high chloride ion content is used to make and maintain contact with the abraded skin.

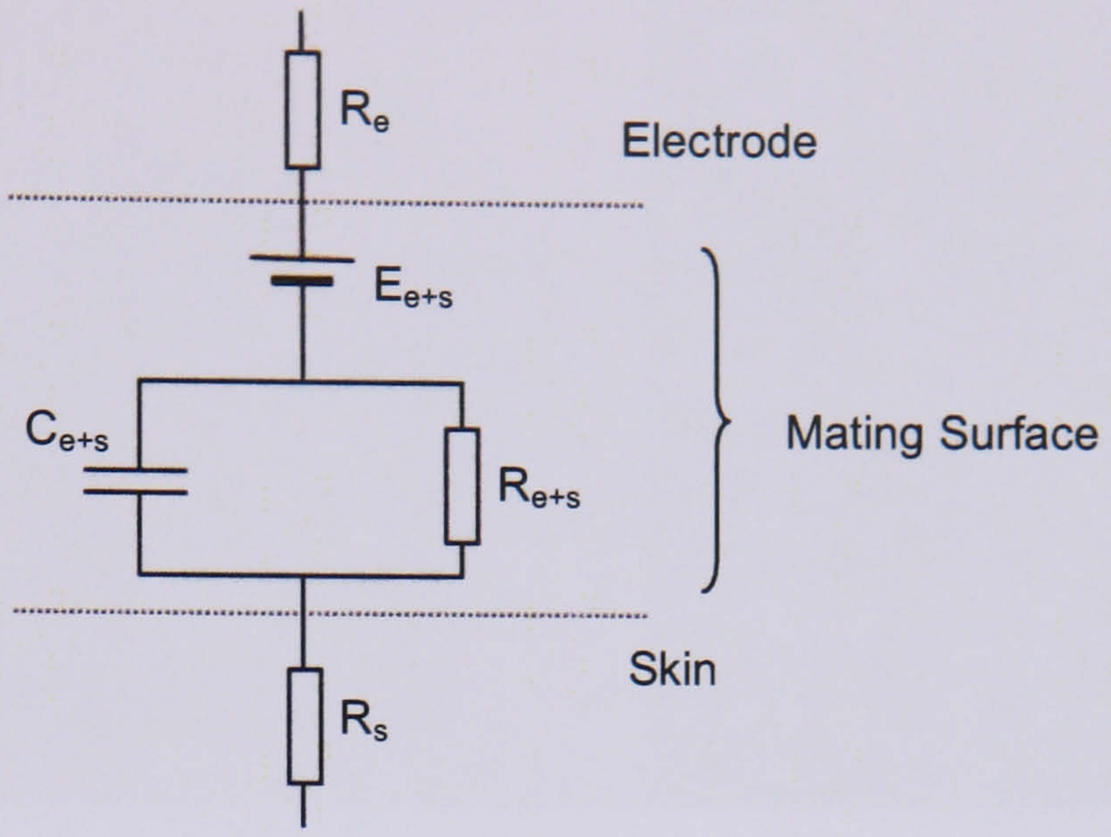

Figure 8.3: Equivalent circuit of electrode-skin interface.

To reduce the impedance between skin and electrode some skin preparation is required before electrode placement as the stratum corneum can increase electrode contact impedances by as much as 100kΩ. Scrubbing the dead skin cells of the stratum corneum away with an abrasive glass paste can be poorly tolerated by the patient and may take some time, especially if many electrodes are to be used.

Modern surface electrode designs have been developed to minimise half-cell potential disturbances and reduce the preparation time required to achieve acceptable skin contact impedances. Aspect Medical Systems Inc., (Massachusetts, USA), the company that produce the BIS monitor, have developed proprietary electrodes for use with their systems (see figure 8.4). Each electrode is positioned on a flexible plastic strip such that upon application the electrodes are located as prescribed by the manufacturer. Covering the electrode contact is a fairly stiff polymer mesh of roughly hexahedral subunits to hold the electrolytic gel. When pushed, the free end prongs of the polymer network pierce the stratum corneum improving contact impedance. Whilst this technique gives suitably low impedances, electrolytic gel dries after a few hours and can cause irritation when the dermis of the skin has been pierced (Hemmerling, 2004; Muzed et al., 2004).

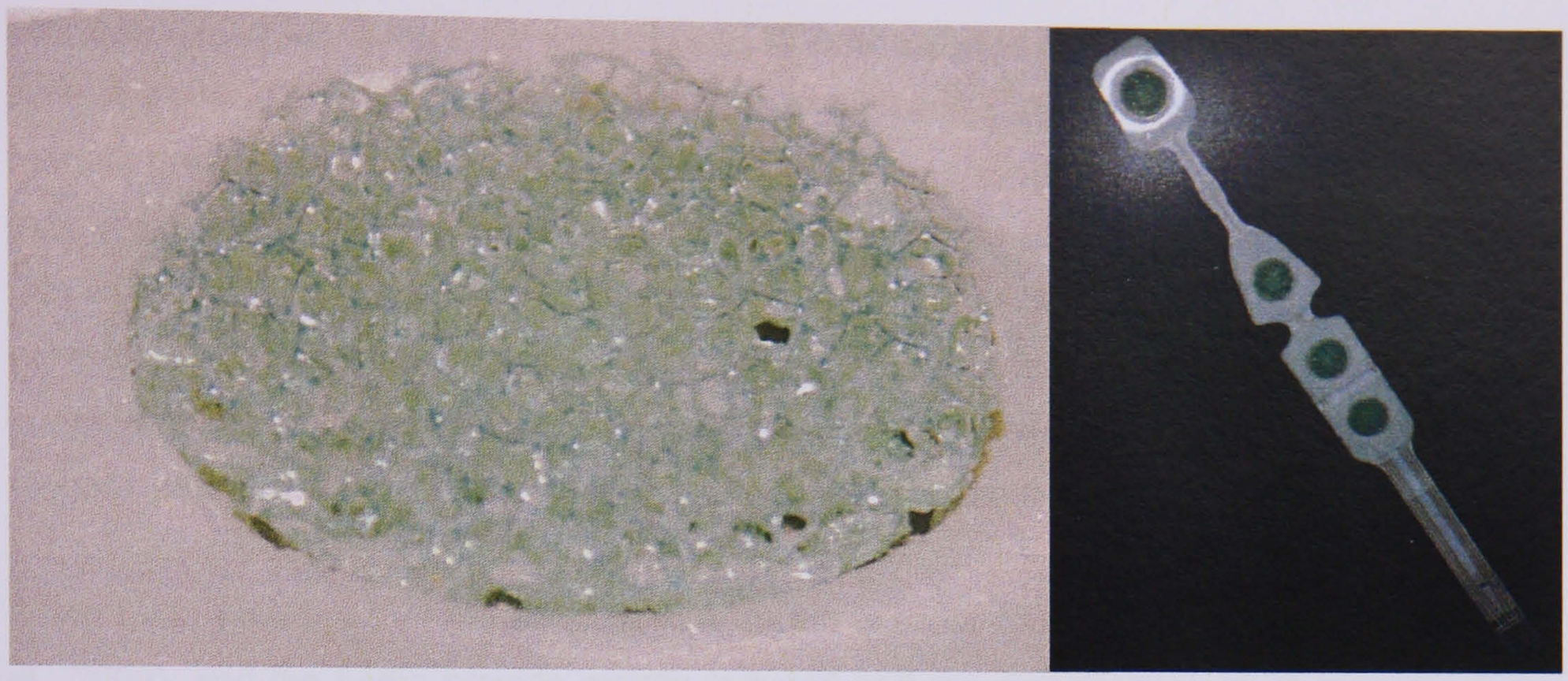

Figure 8.4: Close-up (left) and complete (right) views of a Quattro electrode strip as sold by Aspect Medical Systems Inc., (Massachusetts, USA) for use with their BIS monitor. Each electrode is 15mm in diameter and the entire strip is 280mm.

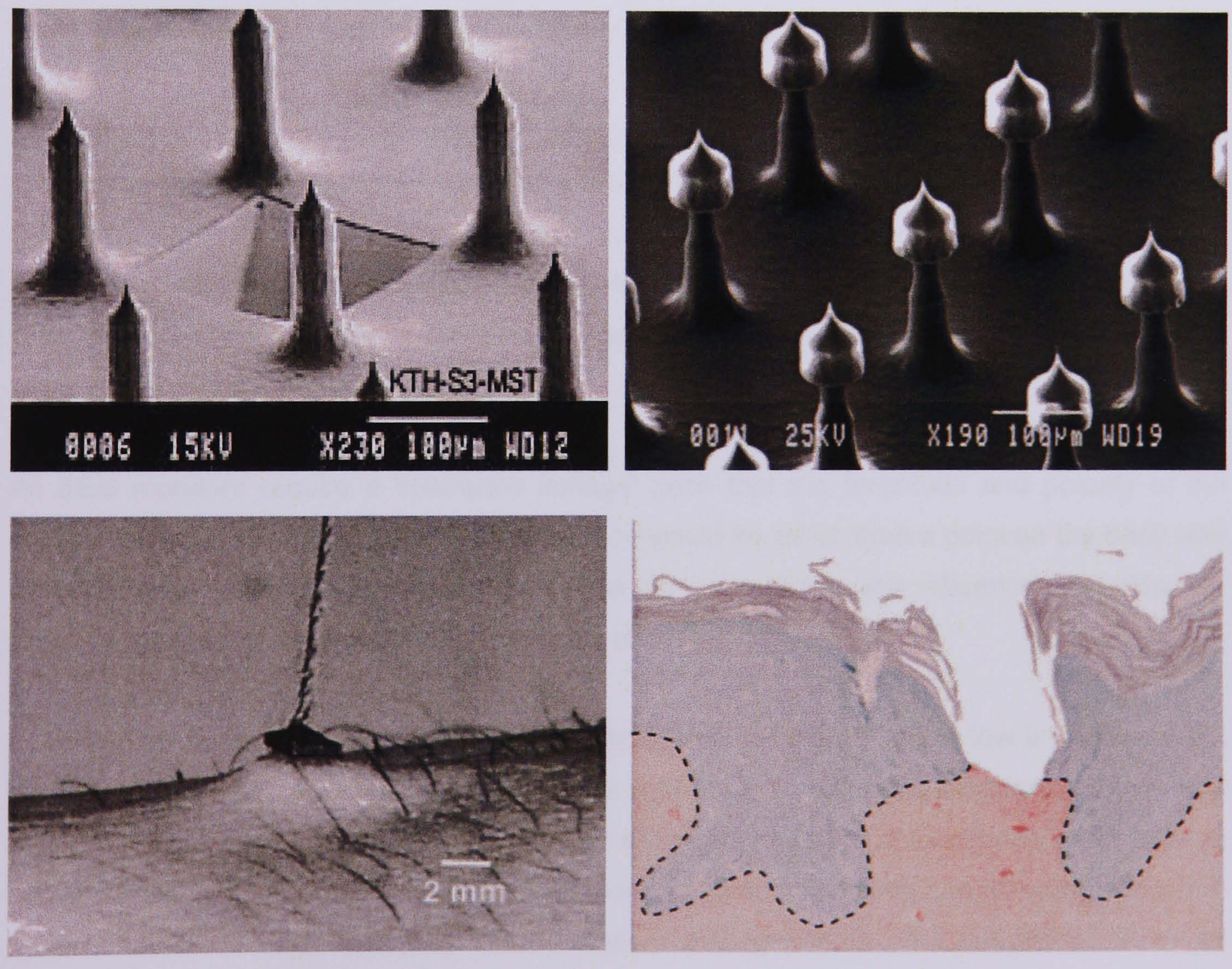

Figure 8.5: Micromachined electrodes. From: Griss et al., 2002. Reproduced with permission.

Micromachining techniques have been used to form needles on the surface of the standard surface electrode in order to pierce the high impedance stratum corneum. Silex Microsystems have improved on this with barbed points on 150 µm long, 40 µm diameter spikes. An example is shown in figure 8.5. The bottom left photo shows the superior attachment properties of this type of solution. The bottom right photo shows a section of skin previously penetrated by a barbed microspike. The grey region is the stratum corneum, the blue region is epidermis and the pink region is the dermis. It can be seen that the barb breaches the stratum corneum and extends fractionally into the dermis below.

It has been reported that the small spikes do not present discomfort to the patient (Griss et al., 2002), and the barbs provide greatly reduced half-cell disturbances upon movement. As such, these technologies do not require electrolytic gel and are thus termed 'dry' electrodes.

Ferree et al., (2001) suggest that skin abrasion or piercing of the stratum corneum will increase the risk of infection. The articles cited in Ferree and colleagues' study to substantiate the view present individual cases where transfer of blood-born pathogens occurred through improper electrode re-use procedures. No statistical evidence is available that indicates the problem is widespread. This is probably due to the increase in use of disposable solutions.

Laboratory EEG studies will usually employ the International 10-20 surface electrode placement standard of up to 21 electrodes and a 'reference' electrode as described in figure 8.6. In the figure 'Z' refers to the midline of the head, 'C' to the lateral central line, 'Fp' is the frontal polar region, 'O' is occipital, 'P' is parietal and 'T' is the temporal region. Odd numbers refer to the left hemisphere, whilst even numbers refer to the right. A1 and A2 are sometimes used as reference electrode positions.

All EEG monitors require a 'reference voltage' such that the amplitude and polarity of the signals can be determined. Ideally the reference would be taken from a point on the body with no variation in potential. Such a position does not exist and so the reference is traditionally taken from a central position on the forehead, or the earlobes.

Care in skin preparation and application of electrodes is taken to make low impedance and consistent electrode electrical contact with the skin so as to minimise impedance losses and half-cell potential disturbances. Careful preparation of 21 traditional electrodes could take an hour or more. This is impractical for applications such as anaesthesia monitoring where the human resources and operating theatre patient throughput are the subject of continual organisational review, however, assessments using only three electrodes are possible

provided no abnormal activity is expected. As long as each electrode is positioned in accordance with the 10-20 arrangement, cross-compatibility of data is maintained.

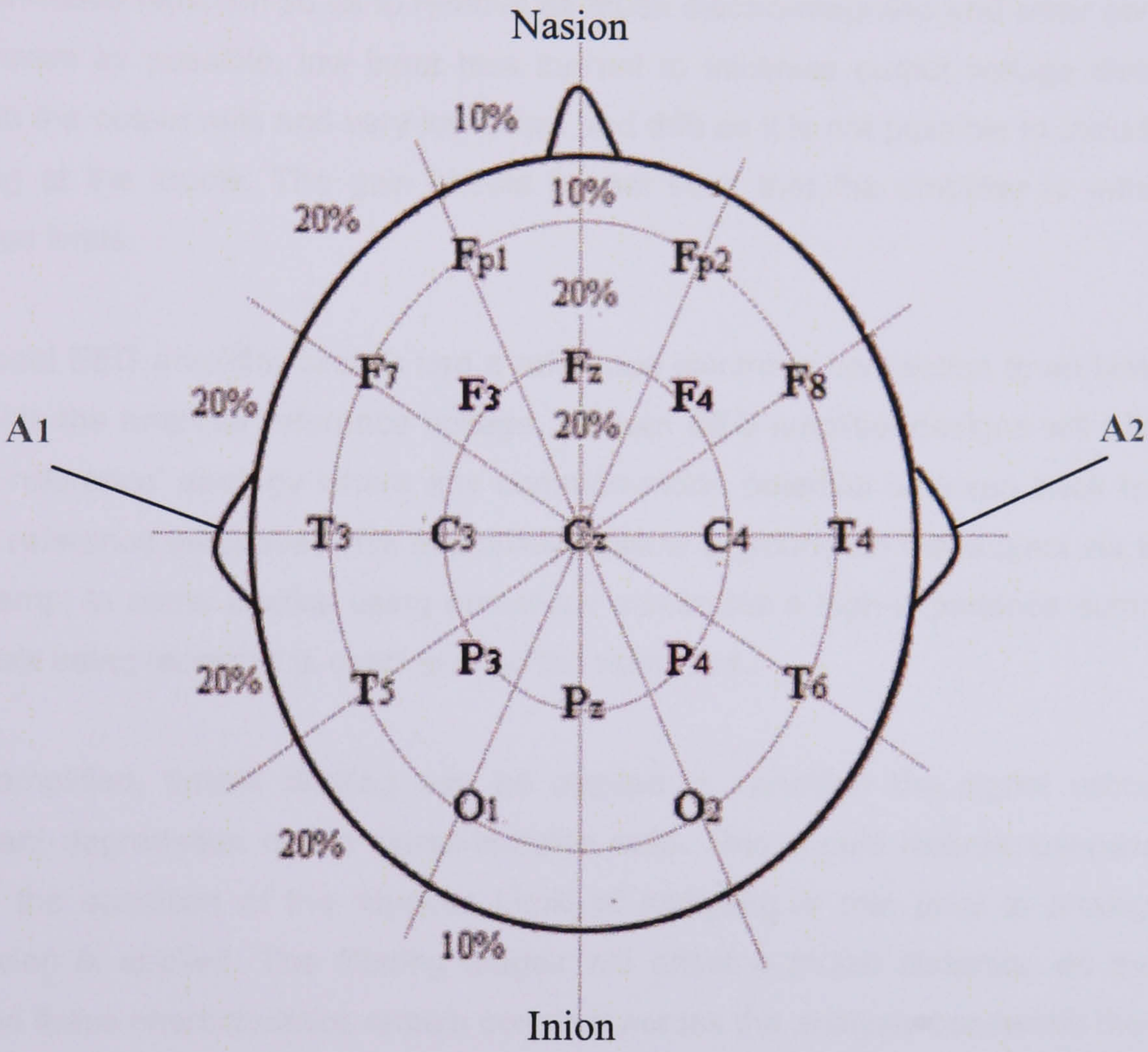

Figure 8.6: The 10-20 international convention of electrode placement.

To carry the signal from the electrodes to the front-end electronics, a high quality, low impedance twisted wire loom is used with a ground 'screen' to reduce electromagnetic field interference. The wires are twisted to minimise magnetic-field pickup, and the loom screen, continuous with an isolated ground to which enclosure and printed circuit board screens are connected, assists with electric field dissipation.

The half-cell potentials generated by differing materials dictates that the joint between electrode contact and wire should not be soldered. Rather they should be welded or mechanically clamped. Where high frequency analyses are required, the looms are kept short such that their shunt impedance does not oppressively attenuate frequencies of interest. To ensure a high signal-to-noise ratio, the electrode and loom impedances must be small in

comparison to the amplifier circuitry. Some manufacturers have developed analogue circuitry that forms part of the electrodes themselves so as to negate loom capacitance issues.

The front-end electronic design of an EEG monitor will usually begin with a current limiting circuit protection arrangement. The signal is then passed to a precision difference amplifier. The specification for the amplifier should include very low noise, low-gain stability, high common-mode rejection so as to remove as much electro-magnetic and other common-mode interference as possible, low input bias current to minimise output voltage distortion, good swing to the output rails and very low offset and drift as it is not possible to include capacitive coupling at the inputs. The gain should be set such that the amplifier is within its stable response limits.

Traditional EEG amplifier circuits use a reference electrode connection to an isolated ground to provide the amplifier reference voltage. Modern EEG amplifier designs will often employ a 'driven reference' strategy where any common-mode potential is driven back to the subject via the reference electrode. This effectively asserts a ground on the subject via the output of an op-amp. In some studies using numerous electrodes a high-impedance summation of all potentials being recorded is used to drive the reference.

Once amplified, further filtering can be applied to condition the signal without incurring significant degradation of the signal-to-noise ratio. This should include low-pass filtering to ensure the condition of the 'Nyquist Limit' of sampling is met prior to analogue-to-digital conversion is applied. The filtering stages will affect a phase distortion on the signal but provided these characteristics remain constant across the analysis bandwidth they are of little consequence. The signal suitably conditioned, it can then be digitised.

To maximise the performance of digital EEG monitors, the amplification of the signal should be low enough to minimise the possibility of signal 'clipping' but high enough to provide the analogue-to-digital conversion hardware with a large enough signal to ensure that useful information is not lost through 'quantization'. Signal clipping occurs whenever the amplitude of the signal reaches the supply voltage of the electronic components in the signal path. Quantization is a source of error inherent in the digital representation of an analogue signal. Digital signals represent analogue signals using fixed values. Where an analogue signal makes smooth amplitude transitions over a period of time, a digital representation of the same signal will step up and down in amplitude. This is termed quantization. Information is inevitably lost with digital representations of analogue signals and so it is incumbent on a design engineer to ensure that quantization errors are small enough to be of no significance.

The use of high-resolution analogue-to-digital conversion relaxes the amplification gain required although resolution is a parameter of the analogue-to-digital converter that is traded with maximum sampling frequency and thus measurable bandwidth. Once digitised the signal can be passed over a suitable interface to a central processing unit where signal processing, if required, and graphics generation can take place. Sufficient resolution is also required of the graphical representation of data such that useful information is not lost.

Of course the subject must be properly isolated from any potentially dangerous electrical supply. The current requirement for compliance to European Union standards is the provision of isolation that will maintain integrity to at least 1000Vrms. Typical arrangements include optical isolation of signal pathways and DC-to-DC converter isolation of supply rails and the ground reference.

8.2 Engineering Prototype Development

The project plan for this study initially required research and development of an EEG monitor based on the performance of a monitor that had been developed some 15 years previously, the TM-20 from Transmed Ltd (Bristol, UK). This stand-alone EEG monitor, pictured in figure 8.7, was based on dated transputer technology and subsequently consisted of parts that had since become obsolete. Apart from a circuit diagram of an early revision of the amplifier board used in the TM-20, the design records of the TM-20 were not available. An amplifier board design based on the TM-20 arrangement was built such that its performance could be tested. The amplifier board could then be used to develop a complete PC-based engineering prototype.

Figure 8.8 shows a picture of the engineering prototype development. As can be seen, the system consists of a 5-electrode loom, shown to the left of the picture, connected to an amplifier unit. The amplifier unit also contains interface hardware such that data can be transferred to a computer with keyboard, mouse and visual display unit.

Although the computer interface could be used to provide power to the amplifier board the power consumption of the board with its near obsolete components was shown to be too high and so an additional power source was provided in the form of internal batteries. Figure 8.9 presents the design of amplifier board circuit used.

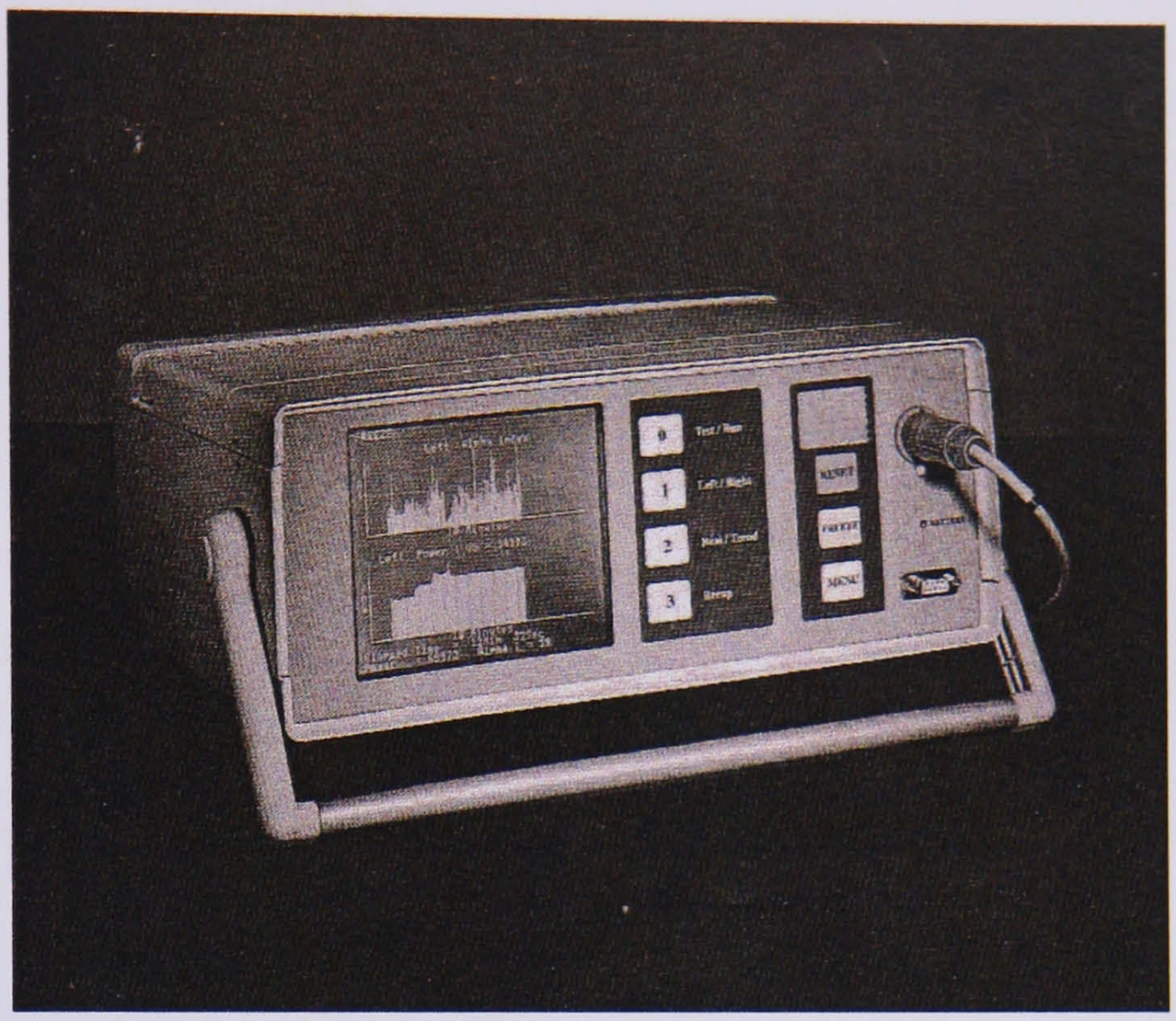

Figure 8.7: The TM-20 from Transmed Ltd (Bristol, UK).

Figure 8.8: Engineering prototype development.

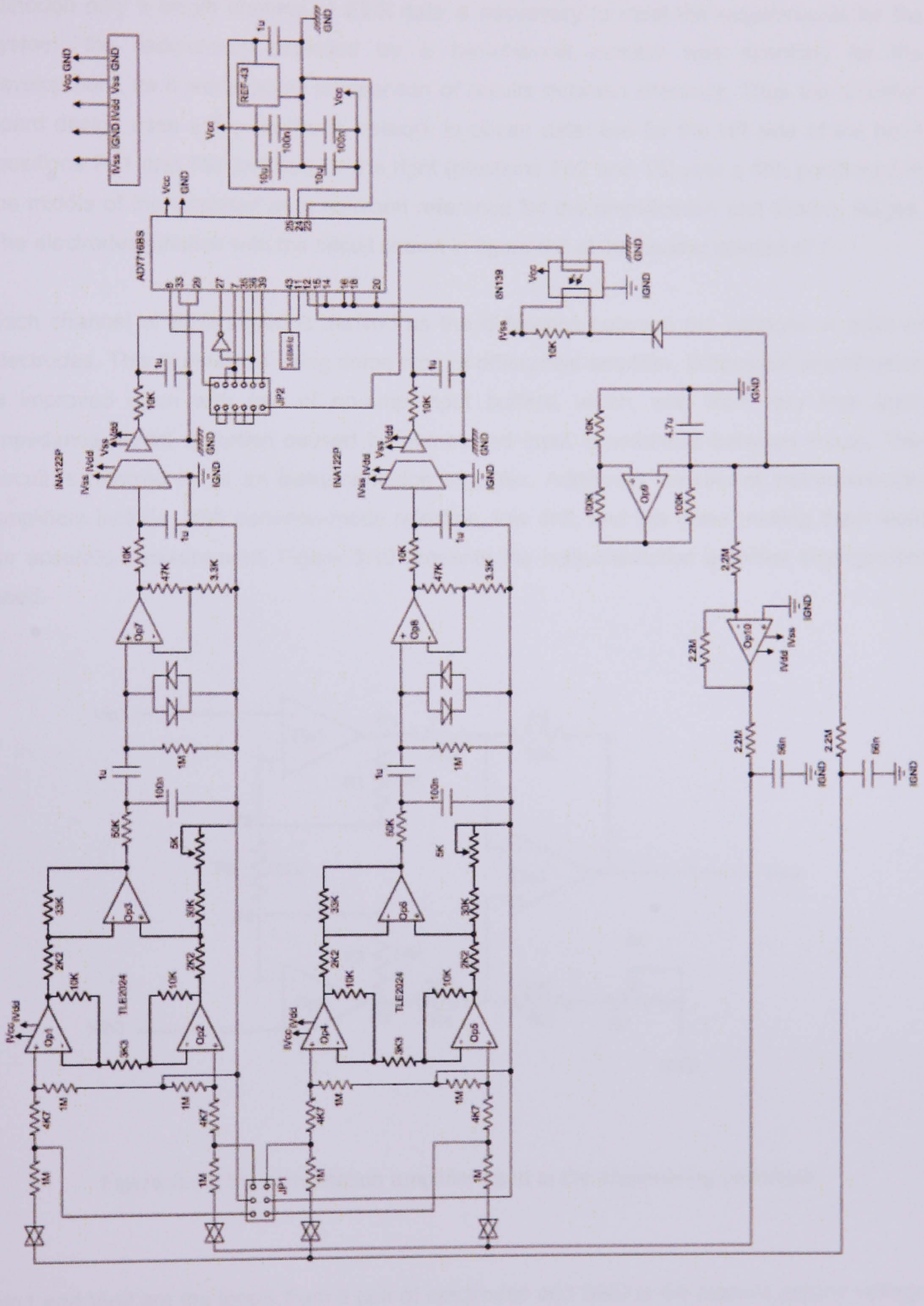

Figure 8.9: Circuit diagram of engineering prototype amplifier board.

Although only a single channel of EEG data is necessary to meet the requirements for the system, the redundancy provided by a two-channel monitor was specified for the development, as it would allow comparison of results between channels. Thus the amplifier board design uses a five-electrode network to obtain data: two for the left side of the head (positions Fp1 and T5) and two for the right (positions Fp2 and T6) with a fifth positioned in the middle of the forehead as a common reference for the amplification and filtering stages. The electrodes junction with the circuit shown in figure 8.9 at the header labeled JP1.

Each channel of EEG signal is derived as the difference between the voltages at pairs of electrodes. This is obtained using some type of differential amplifier. Differential amplification is improved upon with use of op-amp input buffers, which, with their very high input impedance, avoid distortion caused by unmatched input impedances between inputs. This circuit is referred to as an instrumentation amplifier. Additional benefits of instrumentation amplifiers include, high common-mode rejection, low drift, and low noise making them ideal for accurate measurement. Figure 8.10 presents the instrumentation amplifier arrangement used.

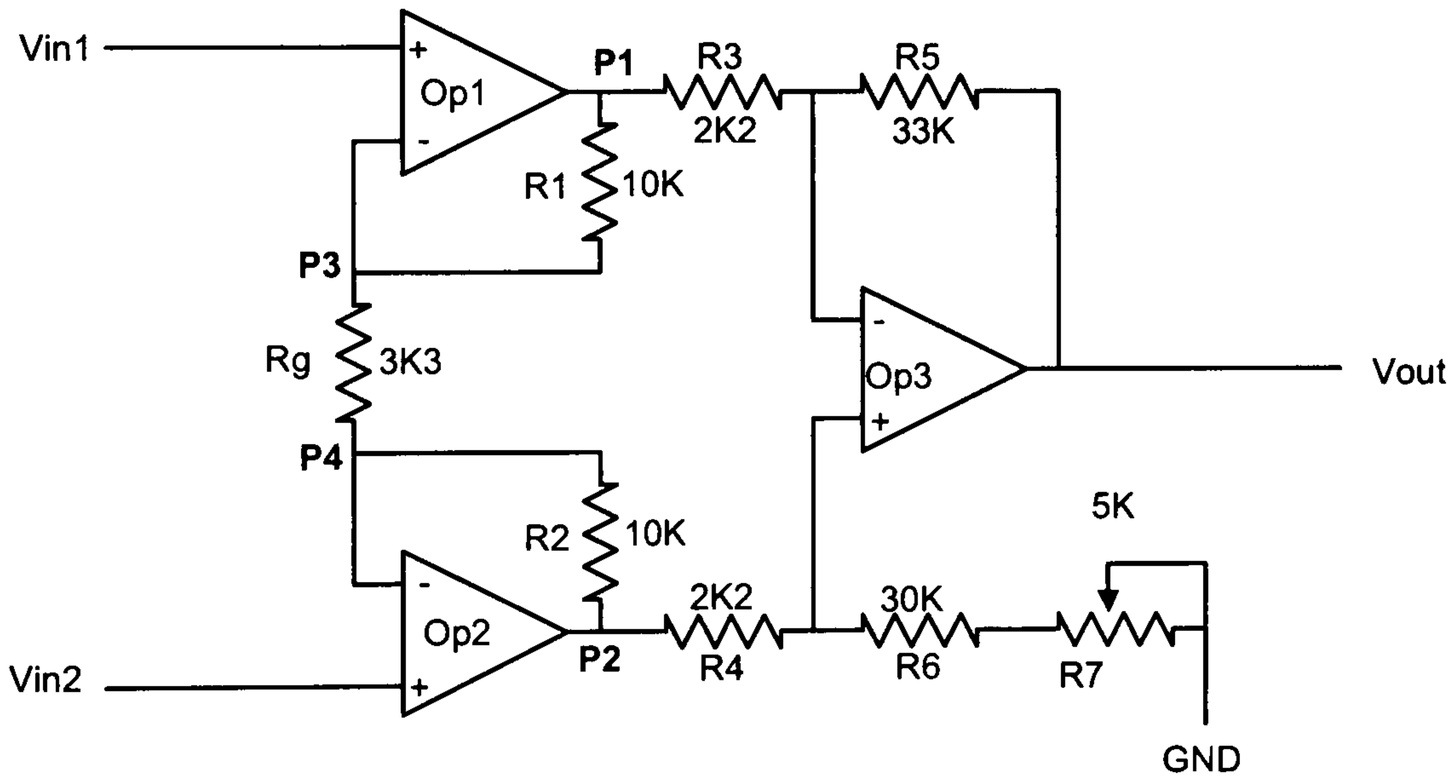

Figure 8.10: Instrumentation amplifier used in the engineering prototype.

Vin1 and Vin2 are the inputs from a pair of electrodes and GND is the passive ground voltage taken from the reference electrode. Considering the op-amp labeled Op1, the inverting feedback loop, puts the input voltage Vin1 at point P3. Similarly the input voltage Vin2 will be given at P4 by op-amp Op2. Since the feedback loops of both op-amps draw no current, the

current observed over Rg, will be the same as that seen between points P1 an P2. The magnitude of the differential output is thus given by:

$$V_{p1-p2} = (V_{in2} - V_{in1})(1 + \frac{(R_1 + R_2}{R_g})$$

The gain of the first stage of the arrangement is therefore set by a single resistor, Rg, which in this case equates to a gain of 24.4. The third op-amp, Op3, is the differential amplifier, the gain of which is determined by the potential dividers formed between P2 and Ground (GND in the figure) such that V1 is amplified by the ratio of R5 and R4:

$$\frac{R_5}{R_3} = \frac{33}{2.2} = 15$$

To avoid signal distortion R3 must equal R4 in value, as must R5 equal R6 + R7 hence R7 is included as a trim potentiometer such that adjustments can be made in the built circuit. With R7 appropriately trimmed to 3KΩ, V2 is attenuated by the same ratio to give a difference output gain of 15.

The gain of the complete arrangement is therefore given by:

$$\frac{V_{out}}{V_{in2} - V_{in1}} = (1 + \frac{(R_1 + R_2)}{R_g})\frac{R_5}{R_3} = 24.4 \times 15 = 366$$

Figure 8.9 shows the instrumentation amplifier stage is followed by resistor and capacitor low-pass and then high-pass filter arrangements on both channels. The time-constant of the charging characteristic of a capacitor varies with its capacity. Forming a potential divider between a resistor and a capacitor provides a means of attenuating unwanted frequencies in a signal. Although RC filter networks alter the phase of the signal component frequencies they do so with a time-independent characteristic. As such frequency component phase relationships remain constant and so the alterations are not considered important. The frequency and phase responses of both the low-pass (R = 50KΩ, C = 100nF) and high-pass (C = 1μF, R = 1MΩ) filters are given in figure 8.11. The red lines in the figure gives the frequency gain response; the green line presents the phase characteristic.

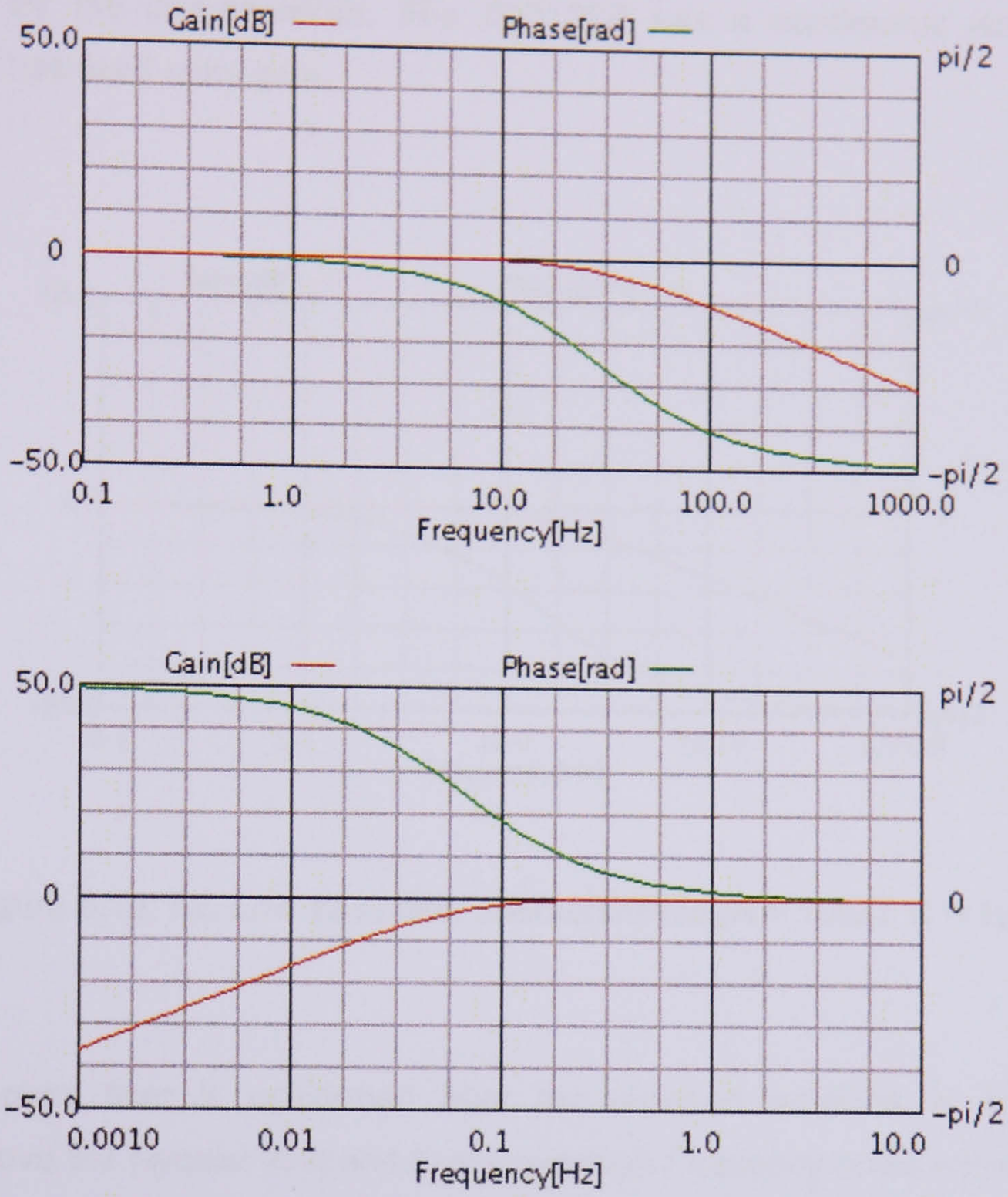

Figure 8.11: Low and High-pass filter characteristics. The upper graph gives the low-pass filter gain and phase responses, the lower graph gives the high-pass filter characteristics.

Back-to-back diodes are positioned after the amplification stage to provide an amplitude limit to the signal such that the signal pathway cannot become overloaded. A final stage of amplification that employs a single op-amp with gain set to 14.2 giving an overall gain of approximately 5,000. This is followed by a further resistor-capacitor low-pass filter (R = 10KΩ, C = 1μF), the characteristic of which is given in figure 8.12.

As the signal path can itself conduct dangerous currents to the contact electrodes (and therefore the patient) the signal path is broken with an isolating linear amplifier with a required breakdown voltage in excess of the EC-60601 Medical Device Directive minimum. The component used in the arrangement is the ISO122P from Burr-Brown (Arizona, USA). The ISO122P converts the signal amplitude to a modulated pulse duty cycle that is transmitted digitally across a galvanically isolated pair of isolating capacitors. The signal is then demodulated back to an analogue signal that is then filtered to remove any high frequency

ripple caused by the demodulation. The ISO122P has a continuous isolation rating of 1500Vrms and has fixed unity gain.

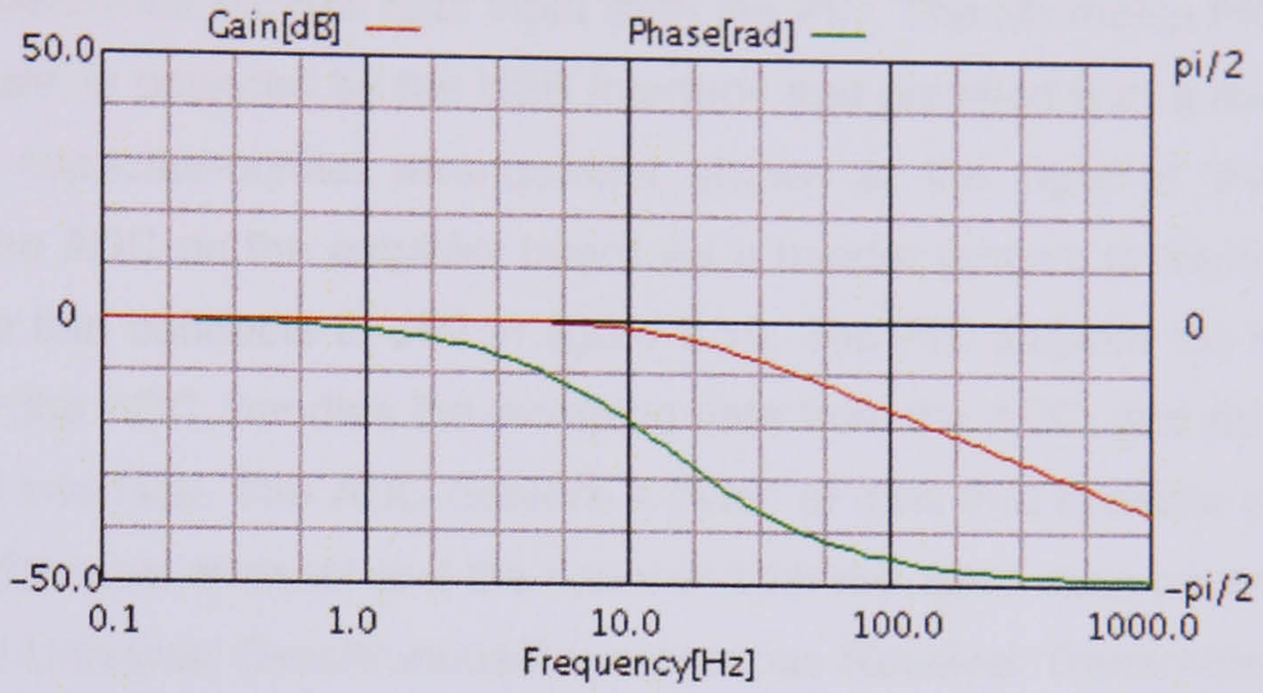

Figure 8.12: RC Low-pass filter characteristics (R = 10KΩ, C = 1μF).

A further low-pass filter is positioned after the isolation amplifier to further attenuate frequencies above the Nyquist limit and to remove high frequency noise introduced along the signal path. The specification and characteristics of this filter are identical to those given in figure 8.12.

The analogue-to-digital converter (ADC) used is the 22-bit AD7716 from Analog Devices (Massachusetts, USA). The device over-samples the signal at high frequency using a modulated pulse duty cycle representation of the signal. This is then averaged down to the sampling rate programmed into the AD7716 by the user. This approach minimises quantization errors inherent in the stepped digital values assigned to a smooth analogue signal. The AD7716 also filters the signal after digitising. This removes noise consequent of the conversion process.

A programmable integrated circuit (PIC) is used to programme the ADC as well as read and organise the data from the ADC ready for transmission to the personal computer (PC). Although over-featured for the application, a Microchip Technology Incorporated (Arizona, USA) CMOS FLASH-based 8-bit PIC, part number 18F242 microcontroller was selected as it, and its development tools, would be more useful to the industrial organisation than a minimally equipped device. A processing clock speed of 20MHz enables fast computation of Reduced Instruction Set Computing (RISC) code.

Data transmission from the amplifier board to the PC is handled via a Universal Serial Bus (USB) interface, selected for its common usage, power supply potential and adequate data transfer speeds. Figure 8.13 presents the circuit diagram for the interface between the ADC and the USB hardware. The USB interface is pictured to the right of the diagram with connections for byte-wide parallel data input from the PIC. The Microchip PIC, pictured in the centre of the figure, is powered by the USB interface and provided with a master clock signal from a 20MHz capacitor-crystal arrangement shown to the right of the PIC. The PIC interfaces with the ADC on the amplifier board via a header (shown to the left of figure 8.13) and ribbon cable that connects to JP2 in figure 8.10. The PIC delivers the necessary set-up programming for the ADC, handles the incoming data from the ADC, and delivery of the EEG data to the USB interface. The ADC delivers 4 bytes of data that consists of 22 bits of EEG data for each differential channel and the channel address. Each data packet is then passed via a high-speed Universal Synchronous/Asynchronous Receiver Transmitter series interface to the PIC.

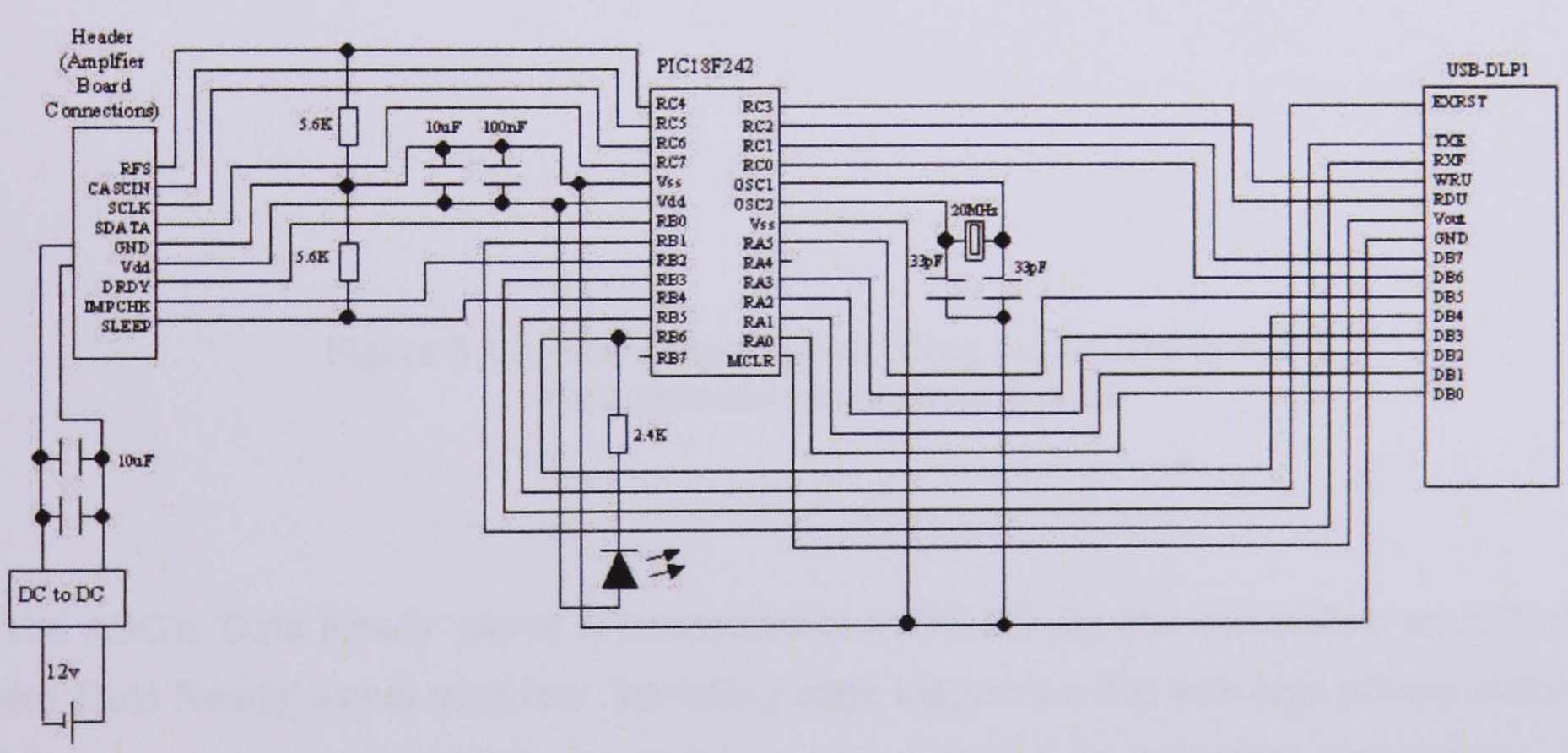

Figure 8.13: Circuit diagram of the PIC-managed, analogue-to-digital converter (ADC) to Universal Serial Bus (USB) hardware interface.

Figure 8.14 presents flow charts of the PIC programming. After a set-up routine that configures all the PIC I/O pins, interrupt service, supporting register allocations and delivery of the ADC set-up data, the PIC simply loops a routine that strobes an LED indicating functionality to the user. Interrupt Service Routines (ISR) are used to handle the reception of incoming data from the ADC and the PC interface.

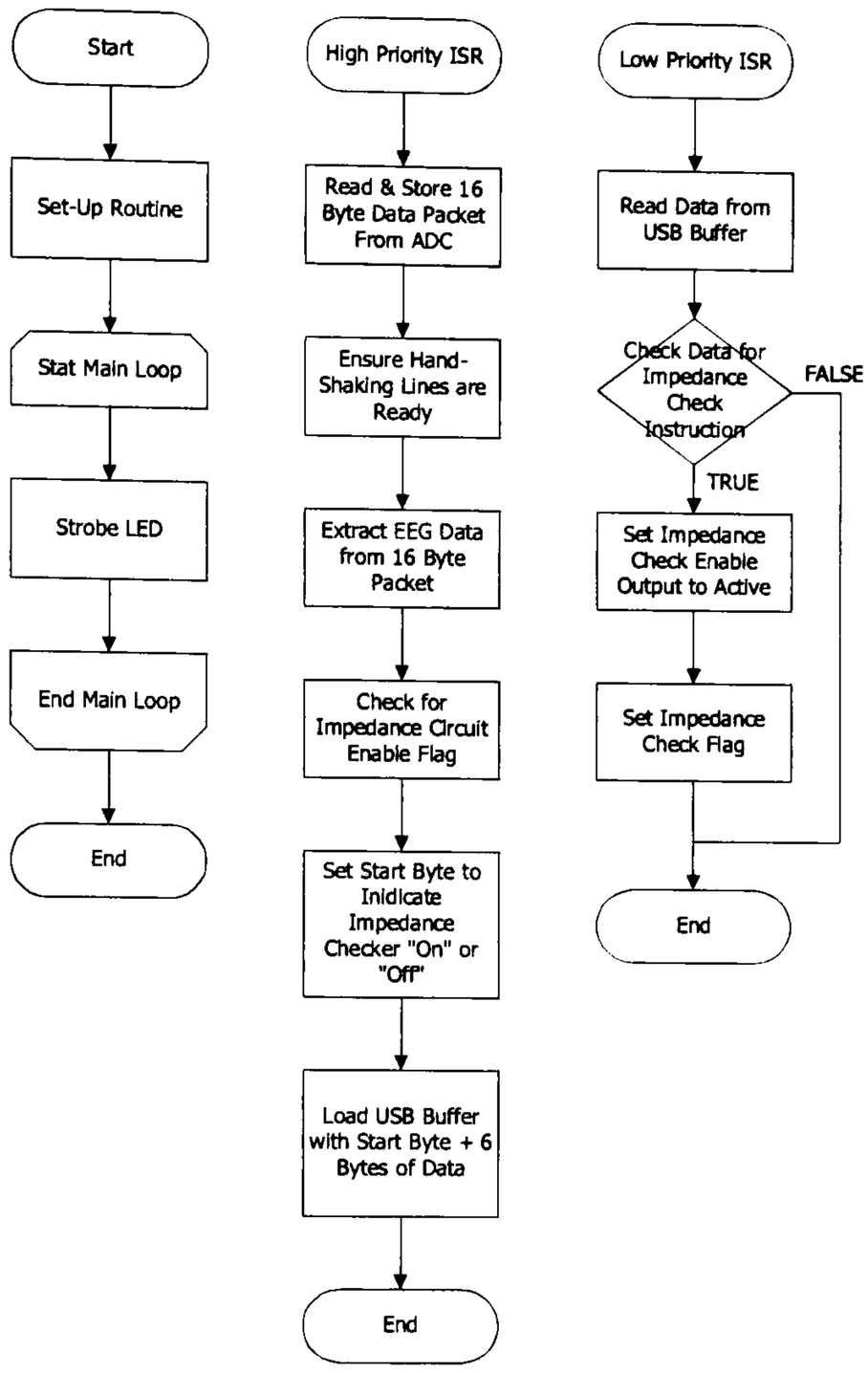

Figure 8.14: Flow diagram describing the operation of the Programmable Integrated Circuit.

The ADC's 'Data Ready' signal is connected to a PIC I/O pin that can initiate an ISR. When the 'Data Ready' signal goes low, the falling edge triggers an ISR with high priority status. All other interrupts are disabled, the registers saved, and data collection commences. Once collected the 6 bytes of 2 channel data are retrieved from the 16-byte ADC data packet by the PIC.

The PIC clocks the data into a 512 byte buffer onboard the USB-DLP1 from DLP Design (Texas, USA) pictured to the right of figure 8.13. Central to the USB-DLP1 is a FT245BM FIFO chip from FTDI Chip Ltd. (Glasgow, UK) capable of delivering data at 1 MByte per second over a standard USB interface to a Personal Computer (PC).

An epoch of data consists of 192 data samples from each channel. As discussed, each sample consists of 3 bytes. A two-channel data packet therefore consists of 6-bytes of data to

which an additional byte is appended by the PIC that is used by the PC software to perform data transfer integrity checks and also labels the data with indication of whether the impedance check circuitry was active during acquisition. Given that each epoch consists of 192 data samples from each channel, a complete epoch of 2 channel data consists of 1344 bytes. The 1 MByte transfer speed provided by the USB hardware selected is thus comfortably sufficient.

The USB interface also presents the PIC with data from the computer controller. Upon reception of incoming data, the PIC outputs connected to the USB-DLP1 are changed in software to inputs so that data can be read. This temporary reversal is only initiated when the user requests an electrode contact impedance test. The impedance test circuit is shown in figure 8.15. Upon receipt of an impedance check command the PIC puts the enabling line, shown to the right of the figure as IMPCHK, to +5volts.

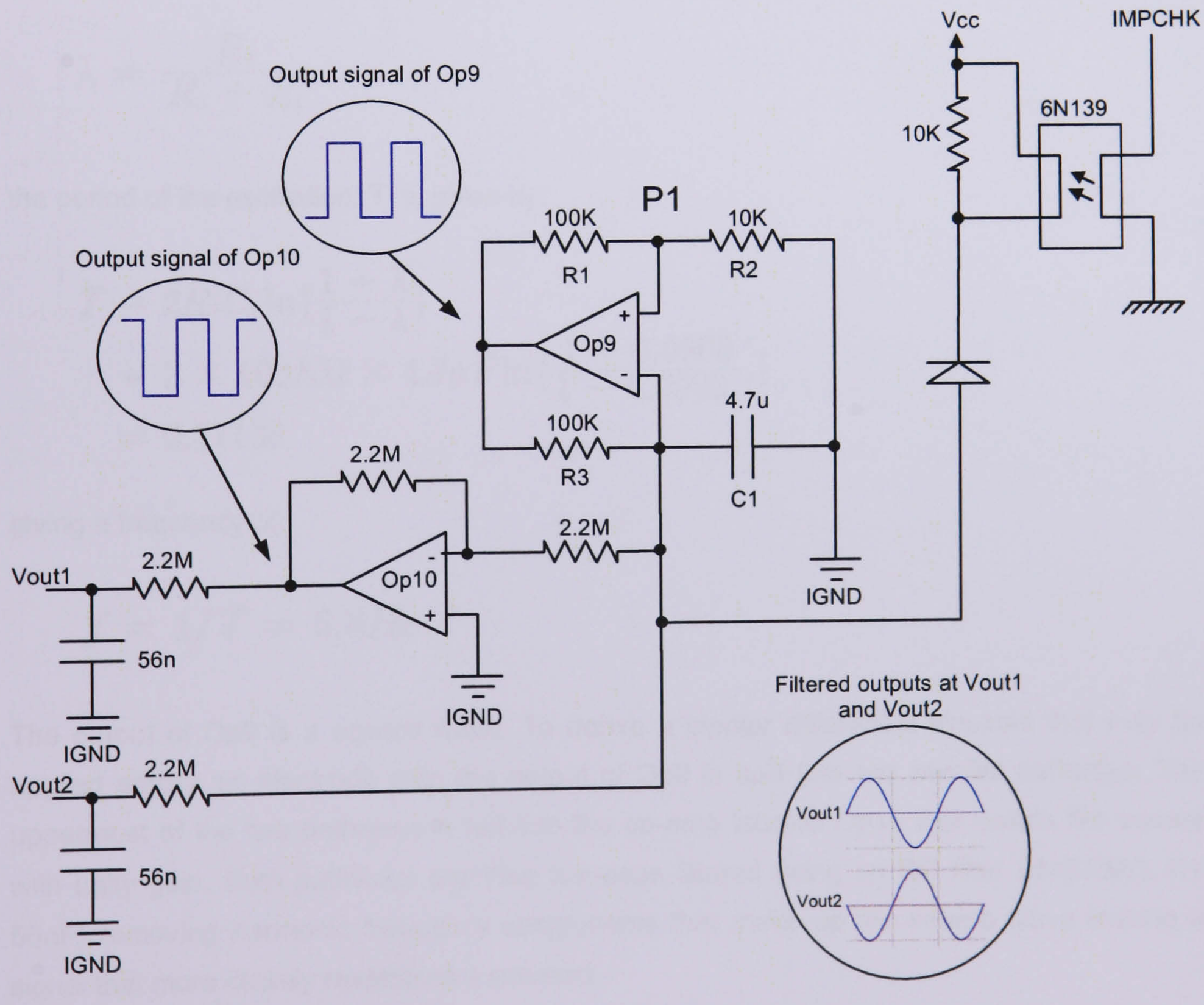

Figure 8.15: Electrode impedance checking circuit.

As the impedance check circuit will apply a current to the patient, the IMPCHK line is isolated from the impedance check circuit with use of a 6N139 photodiode optocoupler from Fairchild Semiconductor Corps, Maine, USA) and current limited by a reversed series diode. When the impedance check circuit is activated the output of op-amp Op9 will be at the positive supply voltage and capacitor C1 will begin to charge. When the voltage across the capacitor C1 reaches the voltage at P1 within the potential divider of R1 and R2, the output of Op9 will snap to the negative supply rail (-5v), thus reversing the polarity across the capacitor and the potential divider. Similarly when the voltage across C1 drops to the negative voltage at P1, the output of Op9 will revert to the positive supply rail and the cycle repeats. The circuit thus acts as an astable multivibrator; the voltage oscillates between the positive and negative supply voltages for as long as the circuit is activated.

It is the values of resistors R1, R2 and R3, along with the capacitor C1 that determine the frequency of the oscillation. Given:

$$\lambda = \frac{R_2}{R_2 + R_1}$$

the period of the oscillation, T, is given by:

$$\begin{aligned} T &= 2R_3C_1 \ln[\frac{1+\lambda}{1-\lambda}] \\ &= 2 \times 100K\Omega \times 4.7\mu F \ln[\frac{1+0.0909}{1-0.0909}] \\ &= 0.17138 \end{aligned}$$

giving a frequency of:

$$f = 1/T = 5.8Hz$$

The output of Op9 is a square wave. To derive a bipolar differential sinusoid that may be applied across an electrode pair, the output of Op9 is split into two parallel pathways. The uppermost of the two pathways is fed into the op-amp labeled Op10 that inverts the square with unity gain. Both pathways are then low-pass filtered using an RC filter (R=2.2MΩ, C= 56nF) removing harmonic frequency components that make up the square wave leaving a signal that more closely resembles a sinusoid.

The filter characteristics used are presented in figure 8.16.

Figure 8.16. RC Low-pass filter characteristics (R=2.2MΩ, C= 56nF).

When the impedance check circuit has been enabled, the PIC-to-USB data lines are reverted to outputs in software with the impedance check circuit remaining enabled for the period of one epoch. Interrogation of the recorded voltages at the ADC allows the maximum amplitude sample in the epoch to be identified which can then be scaled to give a measure of the impedance between the front and rear electrodes on each side of the head. In this way the quality of electrode contact can be monitored.

A low priority ISR is used to enable the impedance check circuitry. When an impedance check request is issued by the PC a byte is delivered to the peripheral's USB receive buffer and a 'Data Ready' line goes high on the USB hardware. This triggers the low priority ISR summarised in the flow chart given to the right of figure 8.14.

As can be seen in figures 8.10, 8.13 and 8.15, power supply rails, the ground and signal pathways are isolated such that there is no direct continuity between mains powered devices and components with direct contact with the patient. The isolating amplifiers, optocouplers discussed keep signal pathways isolated, whilst DC-to-DC converters are used to ensure power and ground lines are similarly isolated. The low power NMH0505SC from C & D Technologies Incorporated (Pennsylvania, USA) was used to give DC-to-DC supply rail and ground isolation of a root mean squared (rms) voltage of 1kV. The battery power supply shown to the left of figure 8.13 provides the 'patient-side' of the circuitry with power.

The data acquisition by the PC is handled by a routine summarised in figure 8.17.

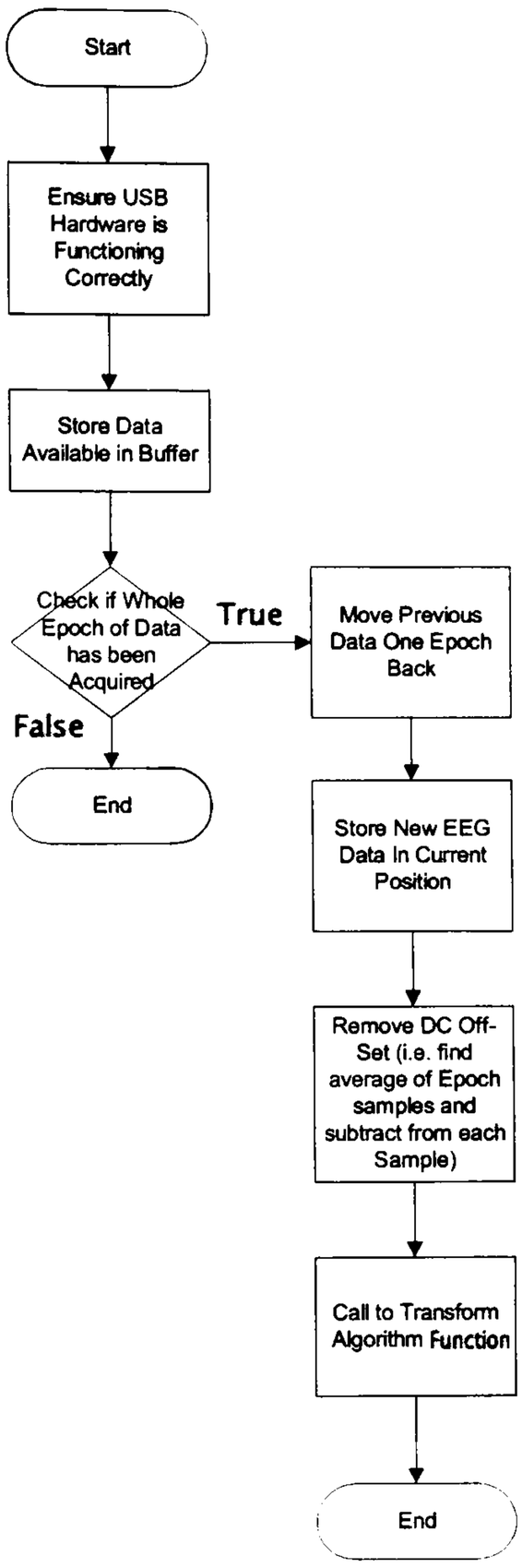

Figure 8.17: PC data acquisition flow diagram.

Once build and debugged the circuit was tested for maximum current leakage to the patient by the local hospital trust medical equipment management organisation using the European IEC 60601-1 Class II medical device standard (maximum of 150μA).

The general specification of the completed arrangement is given in table 8.1.

Number of channels	2
Resolution	22 bit
Input Voltage Resolution	3 µV
Input Voltage Full Scale	+/-5V
Wideband noise	3 µVp-p
Supply Current	510 mA
Isolation voltage	1KVrms (for 1 minute)
Offset handling capability	0.5Vdc
Low frequency CMRR	107 dB

Table 8.1: General specification of head amplifier circuit.

8.3 Production Prototype Development

The engineering prototype design described above needed to be redesigned primarily because the ADC component, which was as used in the TM-20 monitor, was approaching the end of its product life-cycle. In addition, many of the components have been superceded by smaller devices that consume much less power. The engineering prototype required a current source of over 500mA to operate whilst the USB interface protocol includes a 5volt, 100mA source as standard. Reducing the power requirement of the entire circuit to below 100mA would enable the device to be operated without the need for the additional power supply used in the engineering prototype. The circuit design was revised and all components used in the engineering prototype were reviewed to identify lower power solutions. Of the components used, the DC-to-DC converters and the analogue-to-digital converter are the most power hungry. The inefficiency of DC-to-DC converters is proportional to the power they are required to supply, thus a lower powered arrangement will minimise the power consumption of the DC-to-DC converters.

In testing the engineering prototype it was noted that some artifacts generate signals larger than ±1mV, which given the device gain of 5000 causes the signal to be clipped at the ±5V supply rail voltages. Whilst the algorithm was shown to perform well delivering stable spectra with artifact-ridden signals, if the signal became large enough to be clipped, the output became highly distorted. Figure 8.18 presents the problem of clipping. As can be seen in the figure the clipped sinusoid resembles a series of step functions. Any filter algorithm (domain transforms included) will be driven into oscillation by a step function.

To reduce the occurrence of clipping events, the gain of the amplification stage may be reduced, but to maintain similar resolution in the system, the ADC resolution must be increased.

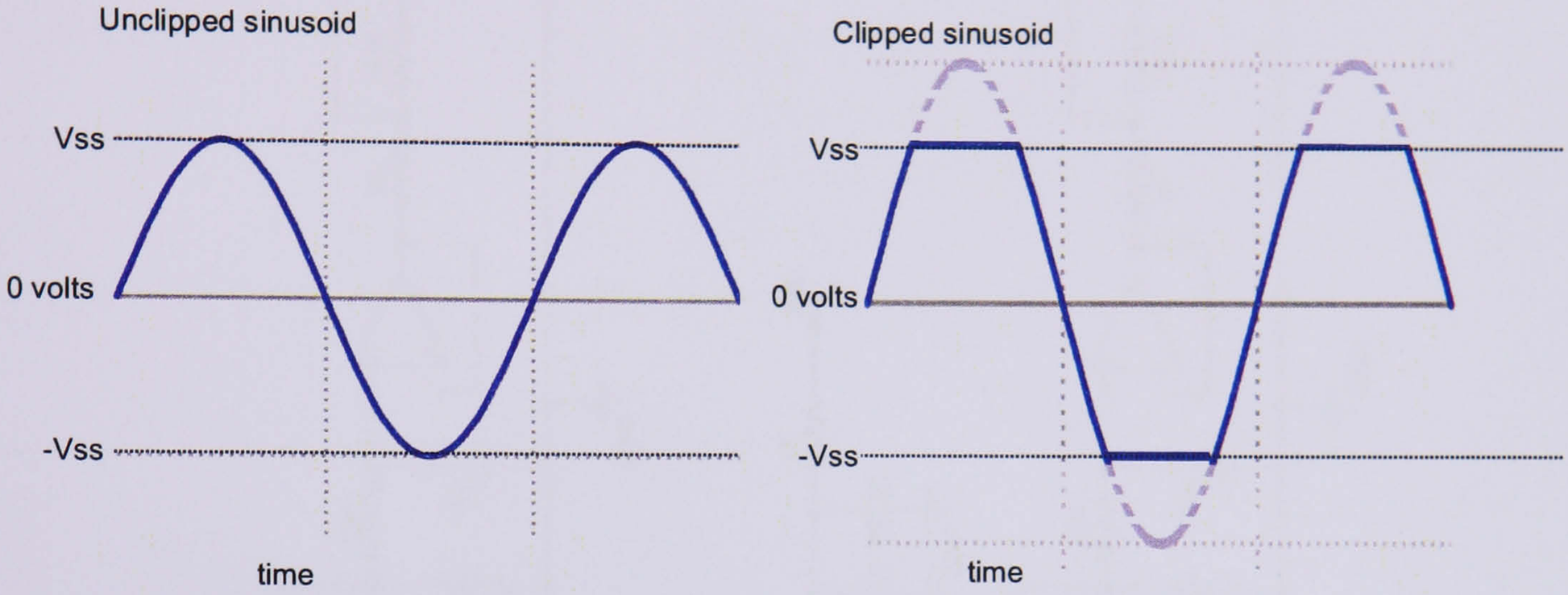

Figure 8.18. Demonstration of signal clipping.

In some environments the mains interference in the system was of an amplitude that would occlude the EEG signal completely. Strategies to minimise main interference were reviewed.

The product prototype amplifier circuit design is shown in figure 8.19.

Surgical diathermy is a modern technique of which there are several variants; the simplest involves the positioning of a large electrode plate under the patient. The plate is connected to one pole of a high power (up to 3000watts), high-frequency (1MHz to 3MHz) sine wave power source with a small-tipped probe connected to the other pole. When the probe is positioned on the patient, current can flow from plate to probe. The current density at the small probe tip is very much higher than the large electrode plate and so heat is generated at the probe tip, which can then be used for making controlled surgical cuts or to stimulate blood coagulation. A 1MΩ input impedance along with back to back pico-diodes from the inputs to the ground reference, provides the circuit with protection against electromagnetic surges and surgical diathermy.

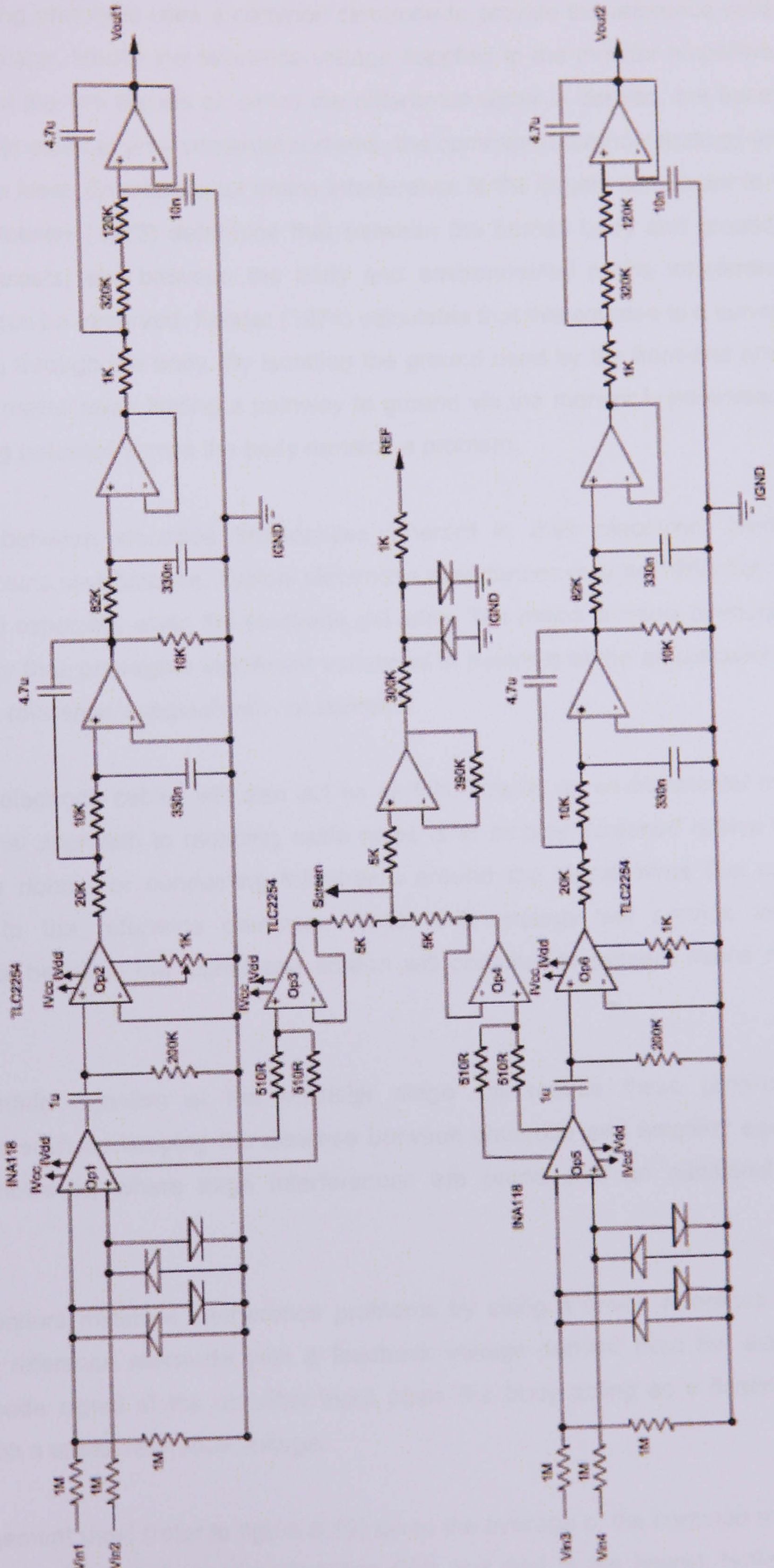

Figure 8.19: Circuit diagram of production prototype amplifier circuit.

The engineering prototype uses a common electrode to provide the reference voltage for the amplification stage. Ideally the reference voltage supplied to the monitor amplifiers would be the midpoint of the two signals on which the differential signal is derived, but because of the body's ability to conduct environmental currents, the common reference strategy will fluctuate away from the ideal. Environmental mains interference is the largest contributor to this effect. Huhta and Webster (1973) determine that between the human body and ground, a 300pF capacitance exists, and between the body and environmental mains interference, a 3pF capacitance can be observed. Forster (1974) calculates that this equates to a current of up to 0.5μA flowing through the body. By isolating the ground used by the front-end amplifiers the possibility of mains noise finding a pathway to ground via the monitor is minimised, however the fluctuating potential across the body remains a problem.

Differences between electrode impedances inherent in their placement compound the problem of mains conductance. Typical electrodes impedances may be 10KΩ but can vary by 50% or more especially when the electrode gel dries. The mains currents conducted through the body may thus propagate significant variations in potential at the amplification stage that the common reference approach will not address.

In addition, electrode cables will also act as aerials, picking up environmental mains noise. The traditional approach to reducing cable noise is to employ screened cables that have a latticed wire ribbon, or conducting foil sheath around the signal wires that can then be connected to the reference common. Whilst this strategy will provide improvement, capacitances between the signal and screen will continue to present mains noise to the amplifiers.

Common mode rejection at the amplifier stage will reduce these problems, as will practicalities such as keeping the distance between electrode and amplifier equal and at a minimum, however, where large interferences are propagated an additional strategy is required.

Modern monitors minimise interference problems by using a driven reference strategy. By driving the reference electrode with a feedback voltage derived from the average of the common mode signal at the amplifier input stops the body acting as a floating ground by driving it with a useful reference voltage.

The arrangement used (refer to figure 8.19) takes the average of the common mode signal of the two differential signal channels (labeled Op3 and Op4 in the figure), buffers the result,

drives it to the screen and then drives it to the reference electrode. Only a few micro-amps are required to achieve 50dB drops in mains interference.

Instrumentation amplifiers contained on a single chip are constructed using laser-trimmed matched resistors and therefore offer an improvement in common-mode rejection and distortion. An INA118 chip from Burr Brown (Arizona, USA) was selected for its high common-mode rejection (110dB), low noise (11nV at 10Hz), low input bias (5nA max) and very low power consumption (350µA at ±5Vss).

This is followed by an RC high-pass filter removing any very low frequency drift (R=200KΩ, C=1µF). The characteristic of this arrangement is given in figure 8.20.

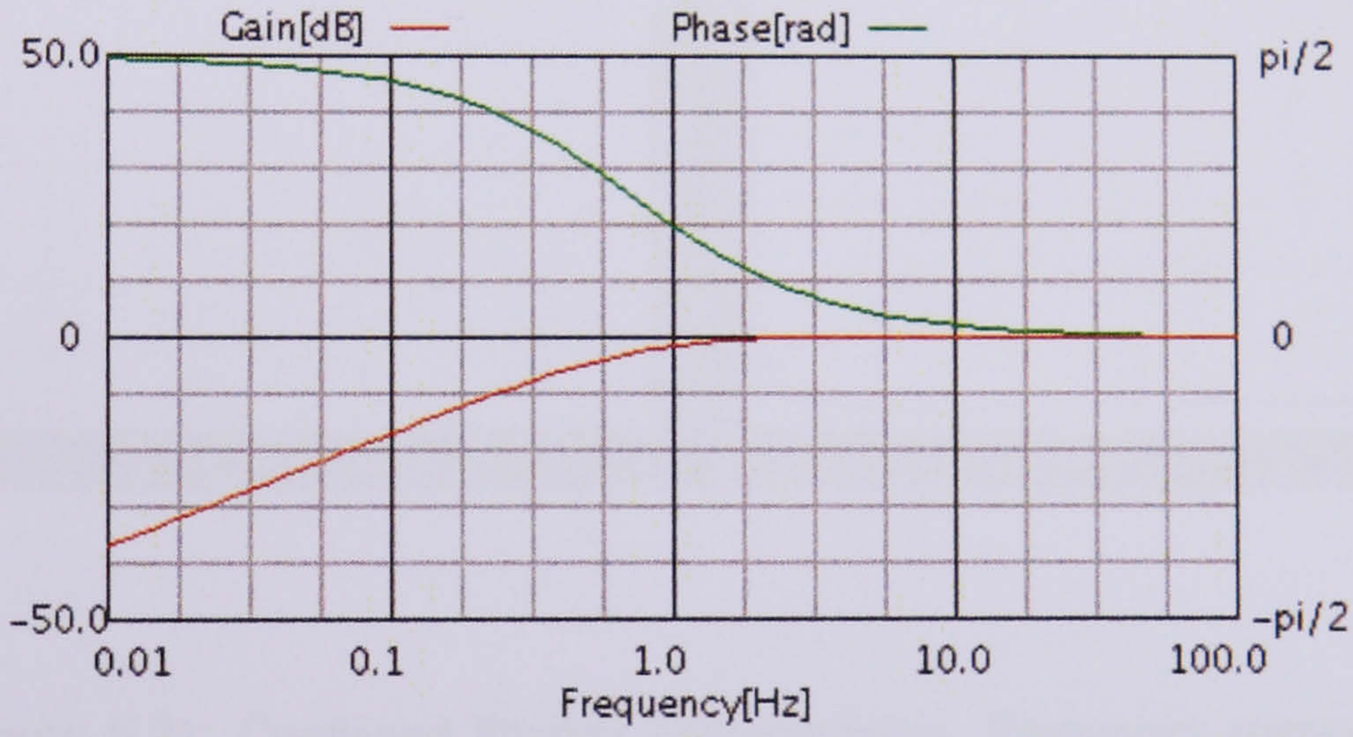

Figure 8.20. Frequency and phase response of RC high-pass filter (R=200KΩ, C=1µF).

Gain control is achieved with the inclusion of an output dividing 5K variable resistor (RV1) at the second op-amp. Low-pass filtering is applied to minimise aliasing. An active 3rd order Butterworth Sallen Key filter design with a 28dB roll-off at 50Hz and -43dB attenuation at the Nyquist limit of 64Hz was developed using a low power precision Texas Instruments Inc. (Texas, USA) quad op-amp part number TLC2254. Figure 8.21 presents the filter characteristics.

Patient isolation is achieved with use of DC-to-DC converters on the component supply rails with opto-amplifiers on the signal lines. The low power NMH0505SC from C & D Technologies Incorporated (Pennsylvania, USA) is used to give DC-to-DC supply rail and ground isolation of a root mean squared (rms) voltage of 1kV, whilst high speed 6N137S

opto-isolators from Fairchild Semiconductor (California, USA) are used to provide signal pathway isolation of 2500Vrms.

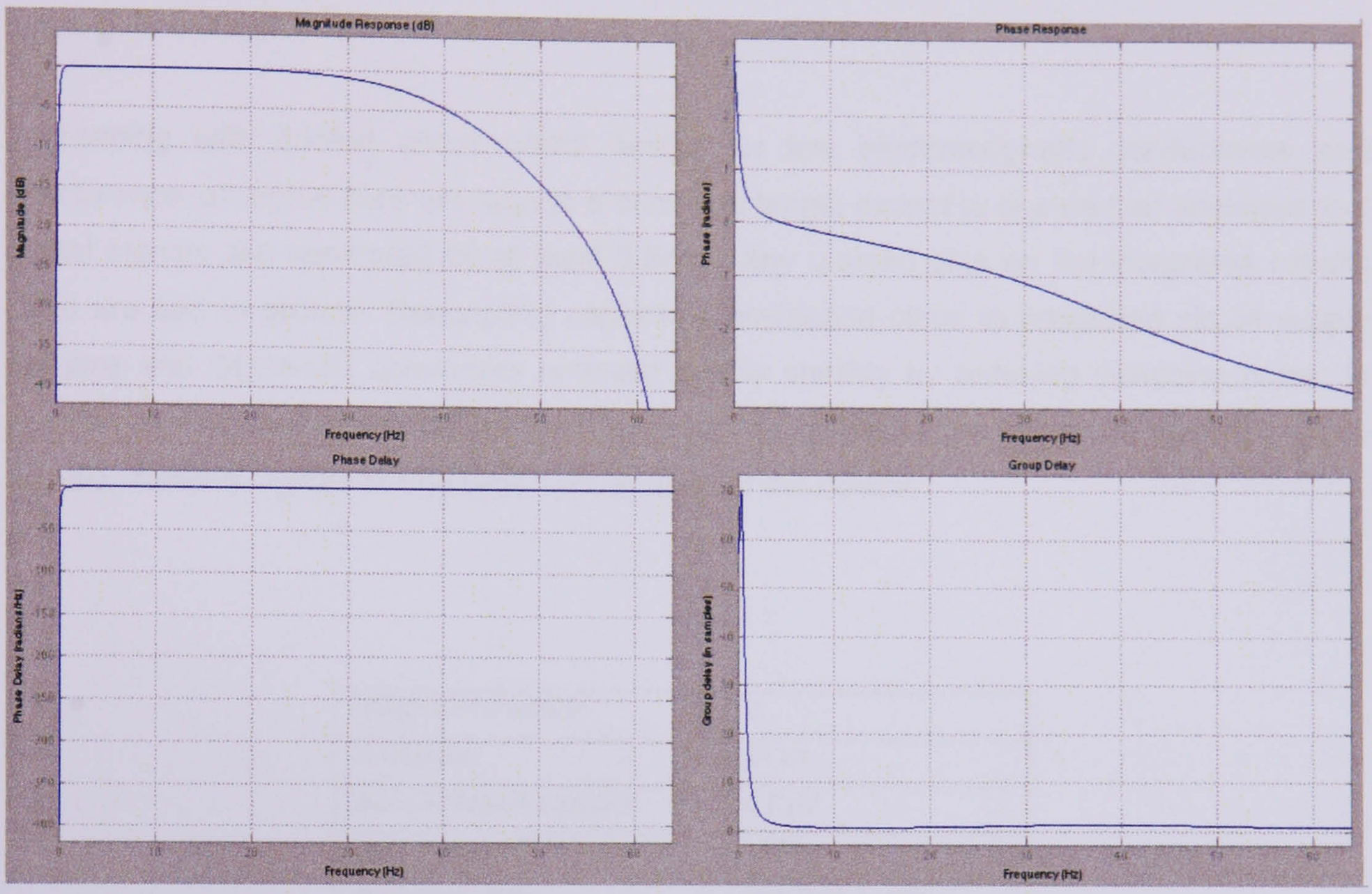

Figure 8.21: Combined filtering characteristics. Frequency response (top left), phase response (top right), phase delay (bottom left), and group delay (bottom right).

The choice of analogue-to-digital converter (ADC) was based on improving on the 22-bit part used in a prototype developed by the inventors. Increased ADC resolution permits use of a lower amplification gain. The advantage here is that signals with larger amplitude artifacts can be digitised without supply-rail clipping or loss of resolution. The 24-bit LTC2442 ADC from Linear Technologies Corp. (California, USA) is used as it has a low power consumption, 2 differential channels, with low offset (<1μV), low noise (220nV RMS at 13.6Hz) and high common mode rejection (120dB). Like the ADS7716, the LTC2442 over-samples the signal to reduce quantization errors given at the selected sample rate. Also data transfer from the LTC2442 is possible with the USART protocol enabling straightforward integration into the interface constructed for the engineering prototype.

A PIC is again used to control the ADC, buffer and organise the incoming data form the ADC, as well as deliver the data to the USB interface and handle impedance check commands from the user. Some reprogramming was required as the set-up programming for the LTC2442 differs from the AD7716 as does the format of the data, but adherence to the flow chart in figure 8.14 is maintained.

In keeping with printed circuit board design for low electromagnetic conductance and interference, all signal lines are kept to a minimum length except to ensure that analogue and digital signals are separated by at least 3.5mm. Any unused pins on the integrated circuits used are tied to ground. Decoupling capacitors positioned close to integrated circuit supply rail pins and DC-to-DC converters optimise supply stability by reducing switching noise. In addition the channels are laid out with symmetry to minimise generation of common mode signals. Table 8.2 gives the general specification of the device.

Number of channels	2
Resolution	24 bit
Input Voltage Resolution	0.5 µV
Input Voltage Full Scale	+/-5V
Wideband noise	less than 1 µVp-p
Supply Current (±5v)	70 mA
Isolation voltage	1KVrms (for 1 minute)
Offset handling capability	0.5Vdc
Low frequency CMRR	110 dB

Table 8.2: General specification of pre-production prototype circuit.

Figure 8.22 presents a photo of the final product based on the production prototype described. The hardware was assembled by Imartec Ltd. (Bordeaux, France) and is marketed by Staplethorne Ltd. (Honiton, UK) under license from the University of Bristol.

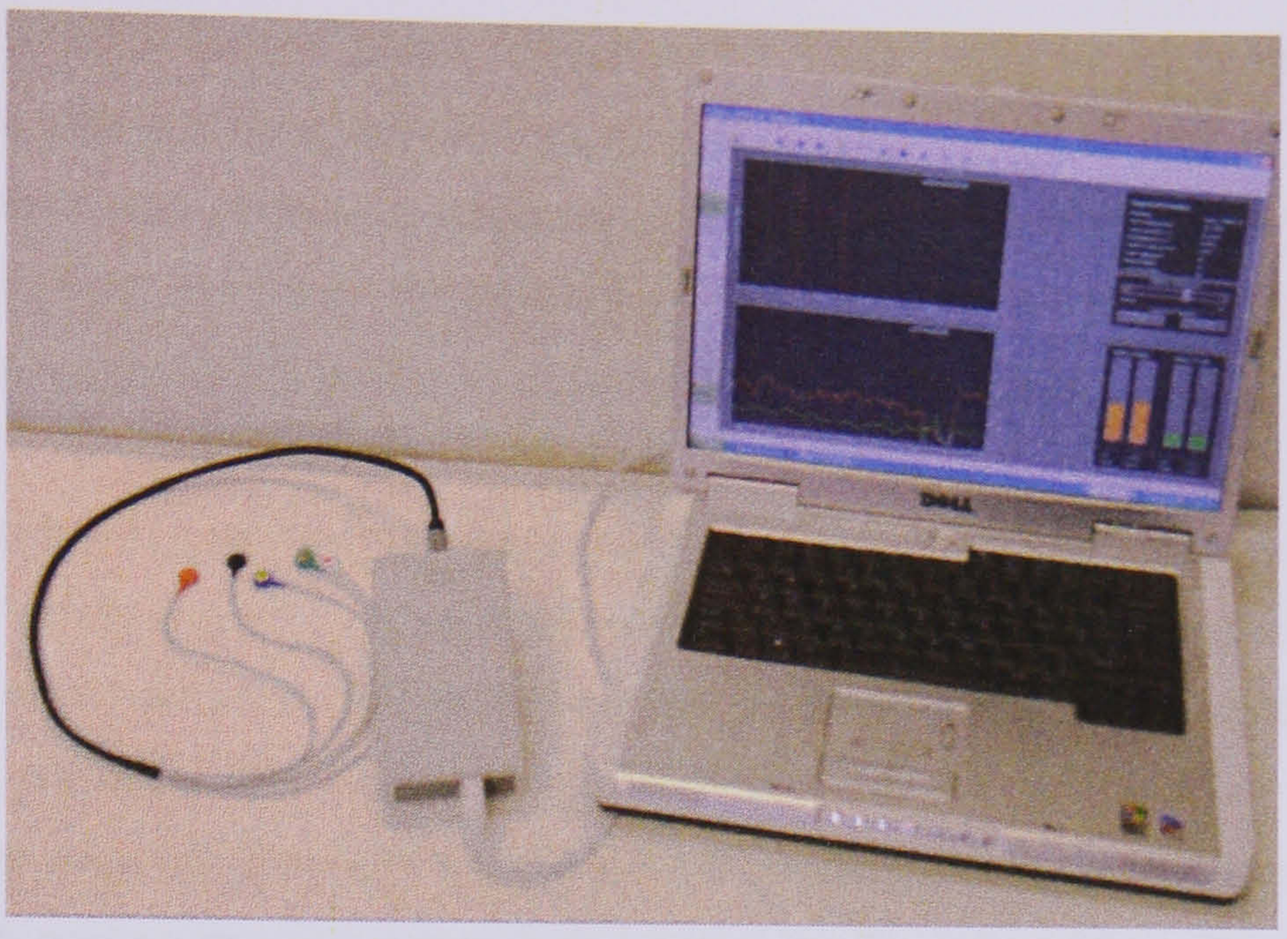

Figure 8.22. Photo of production unit.

8.4 Software Interface Development

An object-orientated software design was developed to embody the signal-processing algorithm described in the patent and a Graphical User Interface (GUI) using Microsoft Corp. (Washington, USA) Visual C++ v6. It has since been updated for compatibility with Windows XP and Vista from Microsoft Corp. (Washington, USA).

The USB-DLP-1 device contains a 512-byte buffer that is progressively filled with data from the PIC. The PC software operates with a clock-initiated interrupt service routine every 5 milliseconds that initiates data transfer from the USB-DLP-1 buffer. The incoming data from the peripheral amplifier unit is interrogated for interface transfer integrity by ensuring that every seventh byte takes the form of a valid data label i.e. that which identifies the data as EEG or impedance check data. If a valid data label is not found in the expected position in the incoming data an error message is shown on the GUI. Valid data is assembled and stored in a temporary storage buffer of 384 'double' 8-byte data. Once the temporary buffer is full, signifying that an epoch of data is available, the contents of the temporary buffer is copied to an array ready for processing either as EEG data or impedance check data such that subsequent incoming data from the USB-DLP-1 can continue to be placed in the temporary buffer. The flow chart shown in figure 8.17 gives a summary of the data acquisition.

With an epoch of EEG data in place, a processing class performs the transform algorithm making several arrays of data available for use in GUI construction as well as for printing. The transform algorithm was coded as appears in the patent and, in implementation, requires 250,000 single instructions for each two-channel iteration. Figures 8.23 to 8.25 presents the three major views given by the software development user interface.

Figure 8.23 shows two graph windows the content of which can be changed using the grey buttons running down the left side of the screen. Along the top of the screen, media-player controls are provided with a record button as well as several navigation controls that can be used during file playback. The name, date and time of the file recorded are given in the top right corner of the screen along with the current file position displayed in the graphs. Playback speed and graph scaling controls are included below the file information. The lower right hand region of the screen presents numerical and histogram representations of the spectral indices generated by the algorithm.

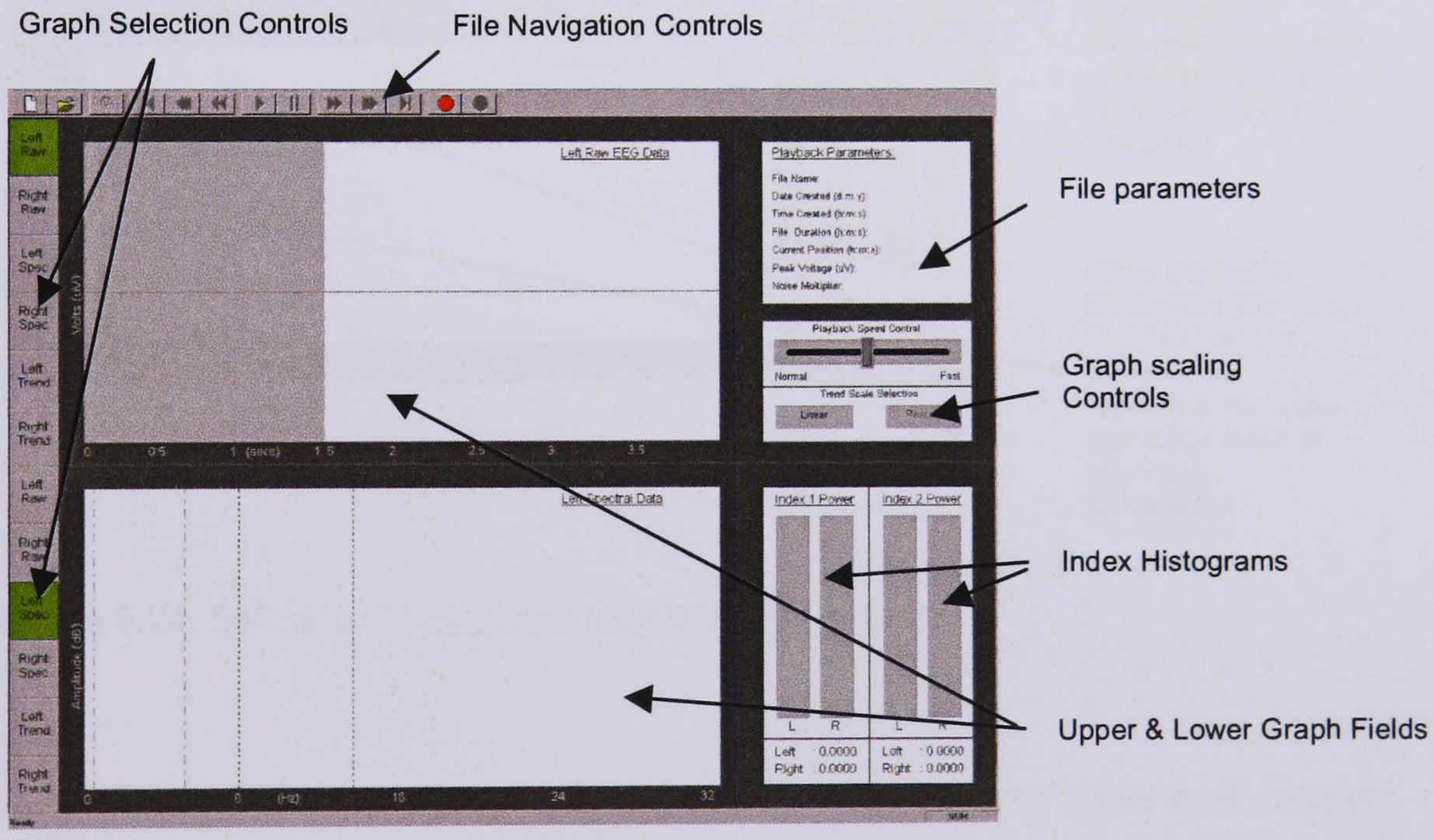

Figure 8.23: Software development user interface. Part 1.

Figure 8.24 presents the software in operation. A raw EEG trace from the left hand EEG channel has been selected for representation in the top graph using the buttons on the left of the screen. The grayed area highlights the current 1.5-second epoch. The raw data view provided by the interface allows immediate assessment of the quality of the signal. The lower

graph has been selected to show the spectral transform of the raw data epoch highlighted in the upper graph. The dotted vertical lines seen in the spectrum graph allow manipulation of the bandwidth limits of the indices generated by the algorithm. The value of each index is numerically represented underneath an associated histogram bar that provides a graphic representation of the index value.

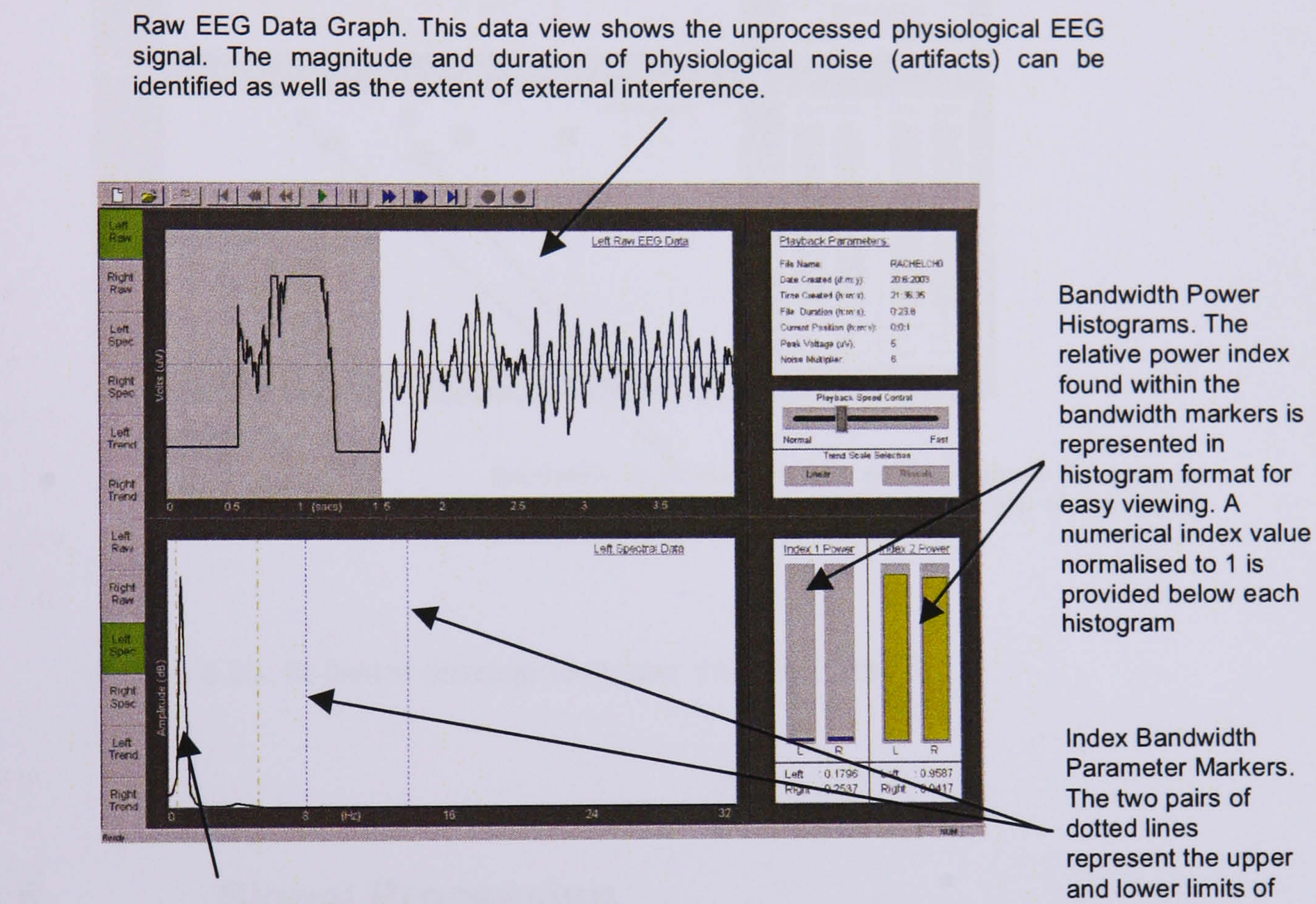

Figure 8.24: Software development user interface. Part 2.

The top graph in figure 8.25 has been selected to present each index value as it changes over time, giving a trend line. The lower graph shows the spectral transform of the current epoch of raw data. Of note are the index bandwidth limit drag-and-drop tabs that allow real-time manipulation of the index bandwidth. These features are among several real-time research tools available to the user, that include automated impedance check intervals, total bandwidth high and low-pass filters, graph scaling, playback speed controls, colour controls, and trace pen size selection, all of which were specified during the development.

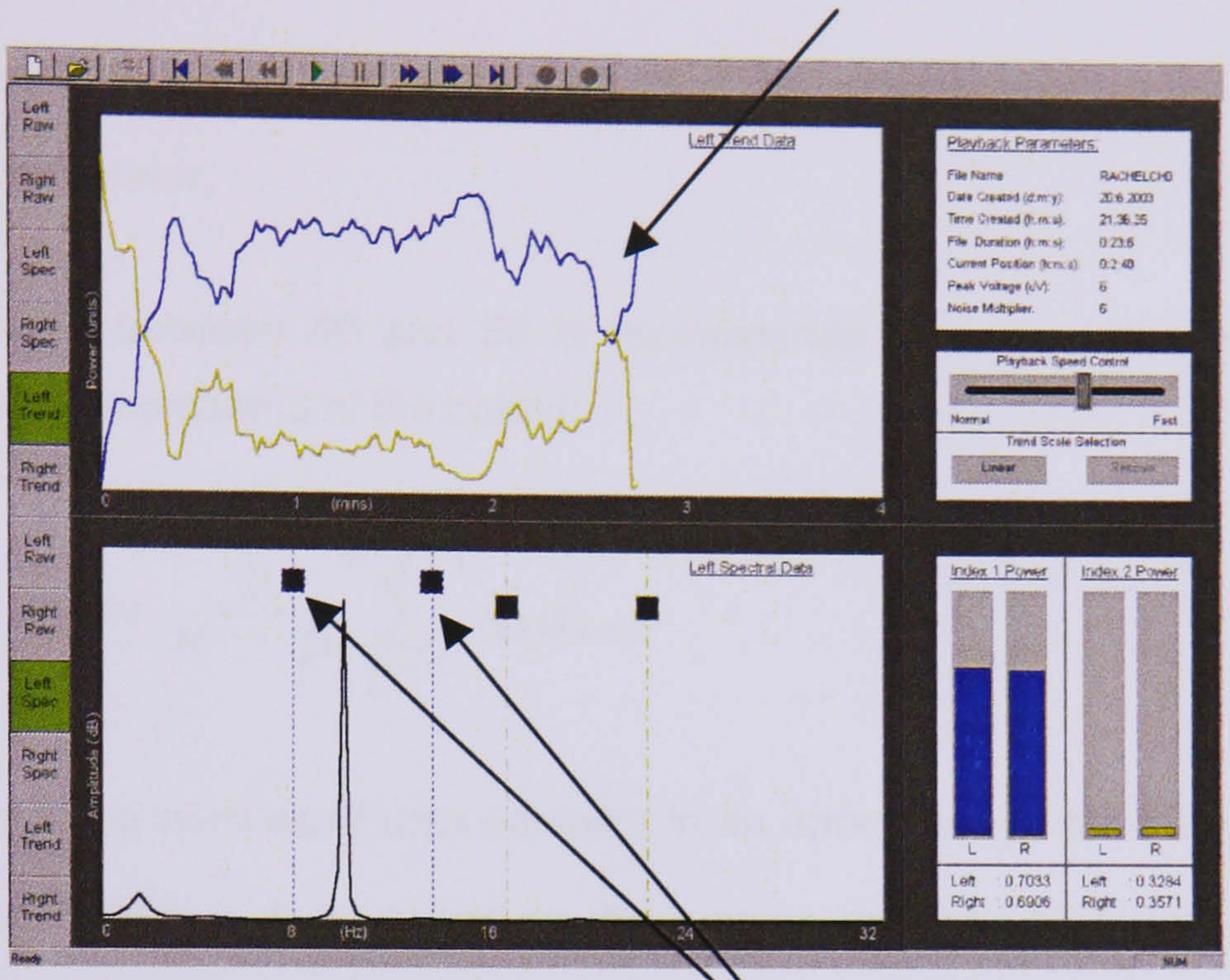

Figure 8.25: Software development user interface. Part 3.

8.5 Signal Processing

The patent offers an embodiment of the novel mathematics to which programming of the signal processing algorithm adhered.

An epoch of 1.5 seconds duration is used to provide sufficient data for the analysis whilst maintaining wide-sense-stationarity. A 0.5Hz to 32Hz bandwidth is proposed with a sampling frequency of 128Hz. No indication is given of a required resolution of the analogue-to-digital conversion but in a personal communication with the inventors it was stated that no less than 16-bit resolution is required for the technique to operate optimally.

Equation 2 of the patent describes the means by which the noise component is added:

$$a_k' = a_k + abs\left(\frac{a_{\max}}{20000}\right)(500 - \text{random}\,(1000)) \tag{8.1}$$

where a_k' is the sampled time series value at a_k added to a scaled output of a random number generator.

An order of between 40 and 50 is recommended for the autocorrelation function (ACF) described in equation 3 of the patent:

$$x_p = \frac{1}{n-p}\sum_{k=0}^{n-p-1} a_k' a_{k+p}'$$

where n is the number of data samples in an epoch and p is the lag of the ACF, giving an output x_p, which is then added to the running average of 7 previous ACF averages as described in equation 4 of the patent:

$$R_p = \frac{7R_p' + x_p}{8}$$

where R_p is the averaged result of the current autocorrelation product, x_p, and the previous 7 averaged autocorrelation outputs, R'_p. Once averaged, the resulting Yule Walker equation is then solved. The Levinson-Durbin (LD) decomposition technique is suggested.

The power density function, D_f, is then found using a squared Fourier transform normalised to 1 as described in equation 6 of the patent:

$$D_f = \frac{1}{\left|1 + \sum_{p-1}^{m} y_p \exp\left(-i.\frac{2\pi f}{64}.p\right)\right|^2}$$

where D_f is the power at frequency f, y_p are the power distribution coefficients and m is the model order. It is recommended that D_f be evaluated at 0.25Hz intervals. The relative power indices discussed in the patent are then found using equation 7 from the patent:

$$a_r = \left\{ \frac{\sum_{k=32}^{48} D_{(k/4)}}{\sum_{k=2}^{96} D_{(k/4)}} \right\}$$

where a_r is the index of relative powers. There appears to be some confusion in the patent as to what the index actually presents. In column 6 line 14 of the patent it is rightly pointed out that the division of the alpha bandwidth power distribution coefficients by those of the entire bandwidth will give indication of what proportion of the total power is contained in the alpha bandwidth. The paragraph ends by stating that the index therefore shows the power in the alpha bandwidth. This is untrue. If, for example, an EEG recording shows predominant alpha rhythm, but after a period there is a growth in delta rhythm, the alpha index will drop even if the power in the alpha bandwidth remains unchanged. Situations of this kind occur often in EEG as the signal changes considerably and can include many transient components. As a result such relationships may not be as easily identified and so it is of importance that interpretation of the output remains in context. The misrepresentation is perpetuated through the patent.

The resulting index is then scaled using a non-linear function described in equation 8 of the patent:

$$a_i = \exp\{S.\ln(a_r)\} \tag{8.3}$$

where S is a scaling factor recommended in the patent to be 0.4, and a_i is the modified component power. The inverse relationship between S and the magnitude of a_r is described in figure 8.26. As can be seen the knee of the gain curve is moved to the right by increasing values of S. Selecting S=0.4 gives a high gain to amplitudes of a_i below 15% of full scale. It might be assumed that the value of S was determined by practical evaluation of the improvement to the display resolution of low amplitude changes in spectral composition.

The scope of the patent is widened with the inclusion of additional system features, such as a keyboard to allow user manipulation of parameters. Epoch length is given as an example of a parameter one might wish to change. Although no circumstances are outlined for when parameter manipulation may be required, the inclusion of such a capability indicates that the inventors do not believe the suggested embodiment will maintain reliability in all circumstances.

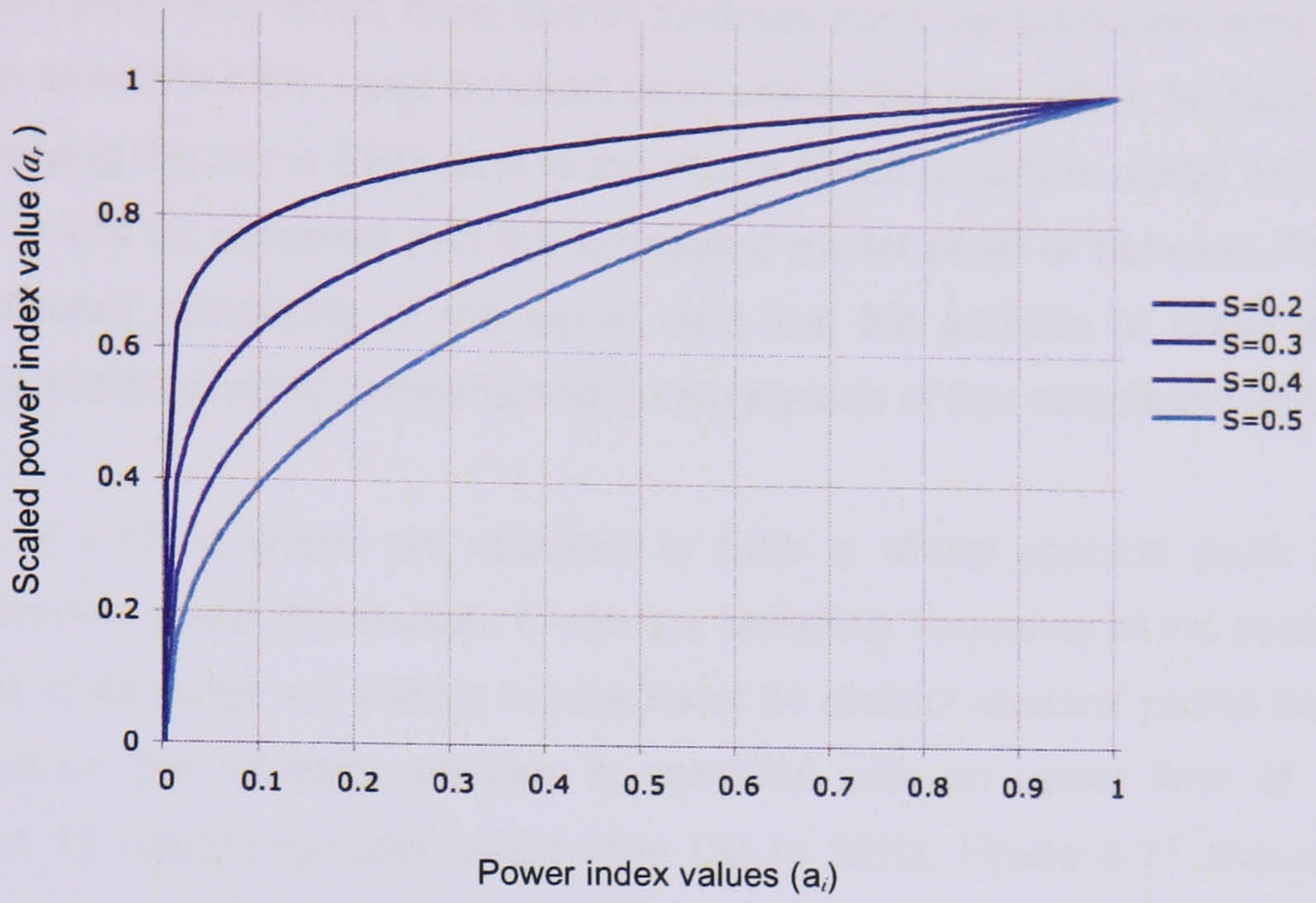

Figure 8.26: Relative power index scaling policy with varying values of the factor S in equation 8.3.

8.6 Algorithm Analysis

An ideal signal to which an autoregressive model can be applied will present an exponential drop to zero in its autocorrelation function (ACF) without a subsequent increase. The model order can be estimated from the point at which the correlogram reaches a close proximity to zero. EEG data sets recorded during wakefulness and relaxation present complex and low complexity data respectively, where the term 'complex' is used to describe a signal with a wide range of spectral components. Visually verified 'artifact free' complex and low complexity data totaling 1124 epochs were run through a taper-compensated autocorrelation algorithm of order 64. The autocorrelation time shift, k, (see figure 6.13) at which the correlogram reached 10% or less of the first value of the correlogram (i.e. k = 1), was added to a running total. If the ACF of an epoch failed to meet this condition a counter was incremented and the running total register remained unchanged. Once the analysis was complete the running total was averaged over the total of 'successful' epochs to give the mean model order.

Of the 1124 epochs of data, 988 autocorrelation functions met the conditions giving a mean model order, M, of 13.9 with a minimum of 6.1 and a maximum of 33. This is lower than the model order of between 40 and 50 prescribed by the patent.

There are several formal methods for identifying model order. Since the objective is a minimal and Gaussian prediction error, most formal methods have the prediction error central to their analysis. An example often used on short data sets is the AIC, which is described in section 6.2.5. In applying the same EEG data to the AIC, a mean minimum model order of 15.23 was obtained. It might be assumed that the suggested model order of between 40 and 50 would require additional complexity in the signal, and that the addition of noise is necessary to ensure sufficient complexity is maintained during periods of low complexity EEG.

In general, 2 z-plane poles are required to form a sharp spectral peak in the Nyquist bandwidth-limited power distribution. Given the sampling frequency of the system is 128Hz, a model order of 48 poles will yield a maximum of 24 distinct spectral peaks between DC and 64Hz. However, the spectral analysis is specified with an upper limit of 32Hz giving a maximum of 12 distinct spectral peaks from DC to 32Hz. Figure 8.27 shows the algorithm output when transforming an optimally complex signal i.e. a signal with 12 frequency components equally distributed across the 32Hz bandwidth. Each spectral peak, whilst clearly identifiable in the figure, presents power across a 2.667Hz bandwidth.

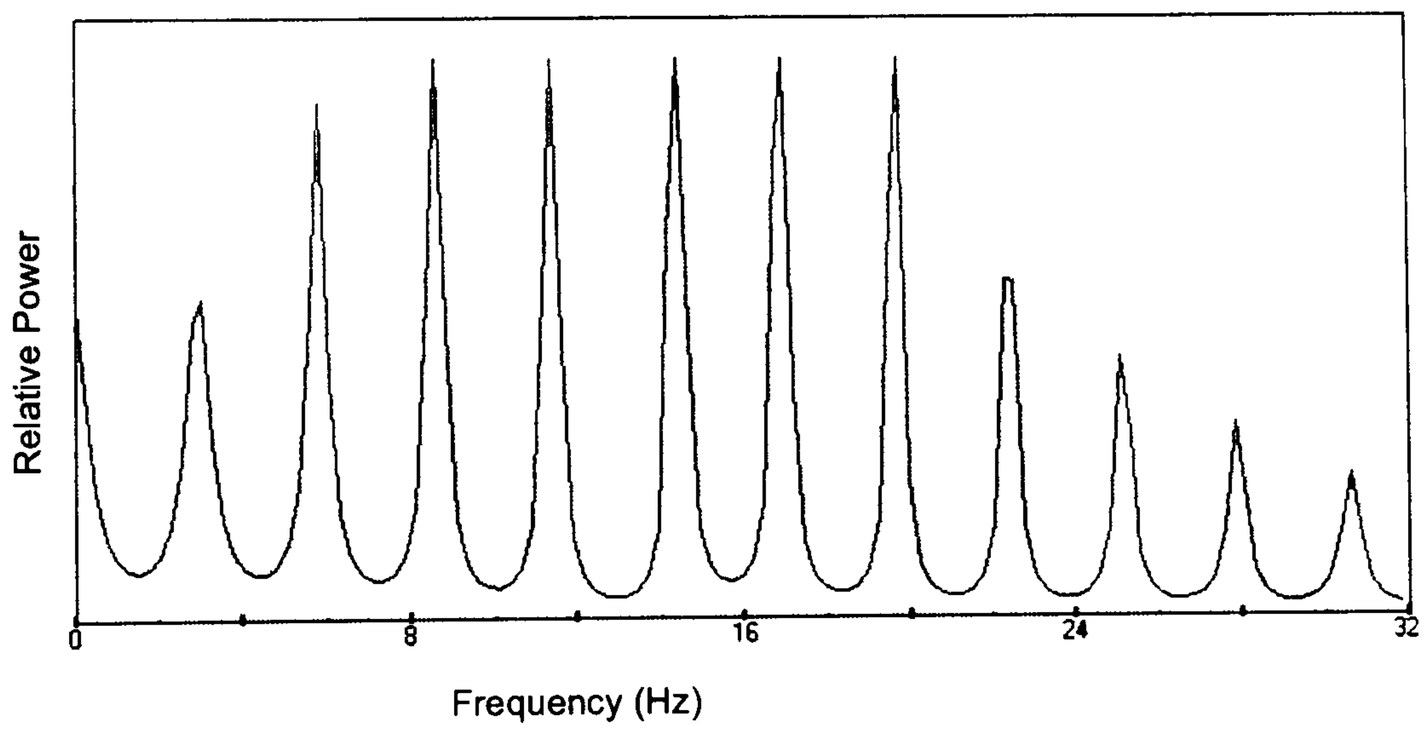

Figure 8.27: Maximum resolution of an optimally complex signal.

In the study conducted by Griffiths et al., (1991) data was obtained using a TM-20 EEG monitor from Transmed Ltd. (Bristol, UK) with ethical committee approval, from a volunteer without epilepsy, no known psychiatric problems or history of drug abuse. After a period of relaxation the volunteer was given 0.5% Enflurane in air for 10 minutes. The data was recorded for a further 10 minutes after cessation of Enflurane delivery. The performance of the algorithm during Enflurane sedation is presented in figure 8.28.

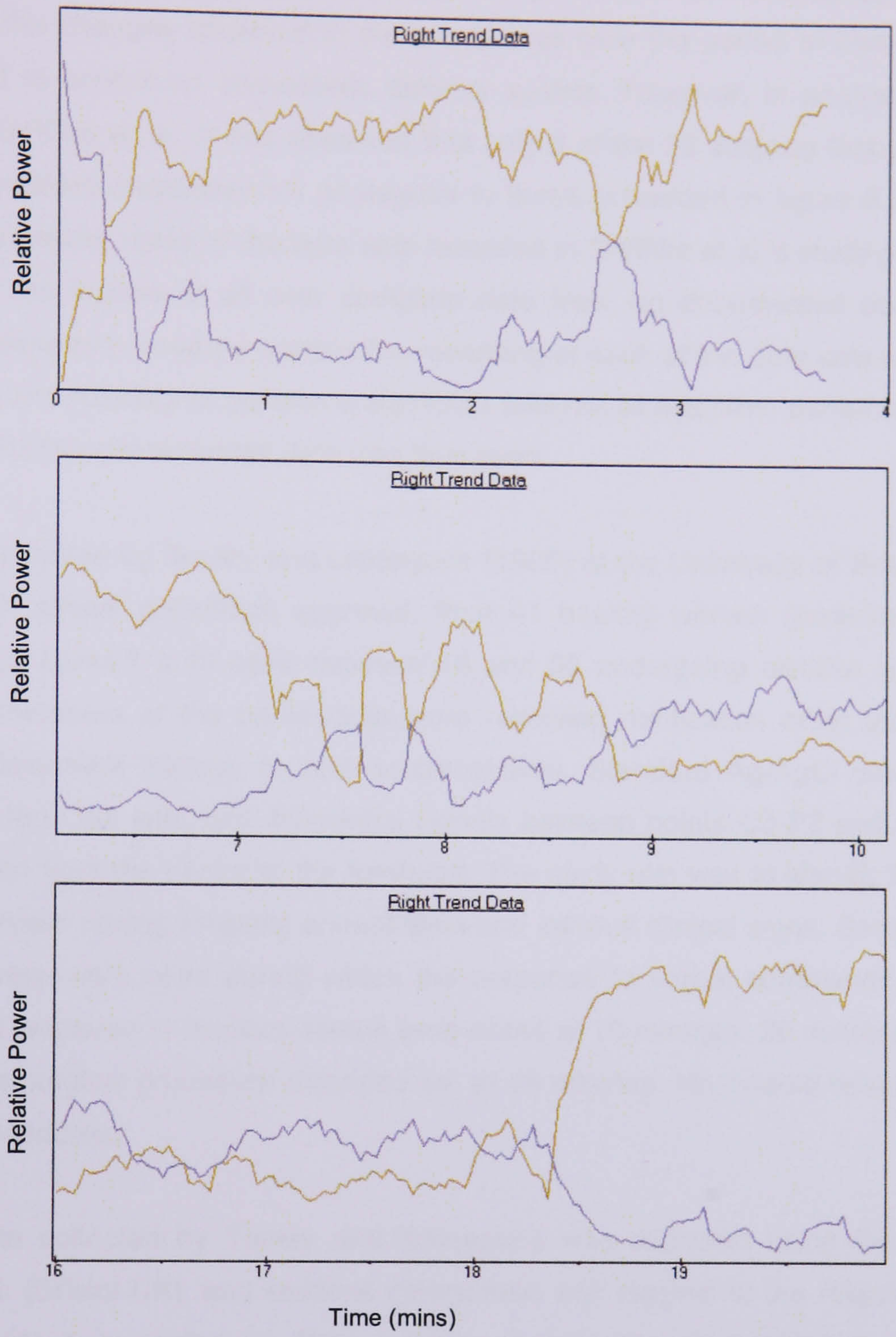

Figure 8.28: Performance of patented algorithm using Enflurane sedation EEG data. Index 1 presents the alpha bandwidth index of 8Hz to 12Hz relative to the entire 0 to 32Hz bandwidth. Index 2 presents a delta index of 0.5Hz to 4Hz relative to the entire bandwidth.

The top graph of figure 8.28 shows four minutes of the index trend display from the right channel of the monitor whilst the subject was in a state of wakeful relaxation. The high alpha index (shown in orange) and low delta index (shown in blue) characterise this state until around 2½ minutes where a noise disturbs the subject. In the middle graph of figure 8.28 the changes to both the alpha and delta indices that resulted during the onset of Enflurane delivery are shown. The bottom graph of figure 8.28 presents the changes that occurred to

both indices at the termination of Enflurane delivery. Griffiths and colleagues (1991; 2005) suggest that the changes observed in the two indices over the period of Enflurane delivery may be used to control an anaesthetic delivery system. However, in analysis of the data recorded by Griffiths et al., it was observed that only 8 of the 20 subjects that participated in the study presented characteristics analogous to those presented in figure 8.28. When run through the software, many of the data sets recorded in Griffiths et al.'s study presented little fluctuation in the indices at all over complete data files. No documented accounts of the anaesthesia delivery procedure used in the recording of each of the data sets were available and so it was not possible to perform a statistical analysis of algorithm performance over the 20 subjects. Further pre-recorded data was thus used.

In a study conducted by Tooley and colleagues (1996) at the University of Bristol, data was collected, with ethical committee approval, from 41 healthy women (American Society of Anesthesiology Class I & II) aged between 16 and 58 undergoing elective gynaecological surgery. No members of the participants were receiving medication other than as part of hormone replacement therapy or oral contraceptives. Standard Ag-AgCl electrodes were positioned to form left and right differential signals between points C3-P3 and C4-P4 with a reference taken from the centre of the forehead. The study aim was to identify links between the EEG observed during Propofol anaesthesia and various clinical signs. Seven regimes of Propofol delivery were used during which the response to verbal commands, the eyelash response and response to noxious stimuli were noted at 10 minutes, 20 minutes, 30 minutes and, when the surgical procedure extended so, at 45 minutes. No muscle relaxant was used during the procedures.

The EEG data collected by Tooley and colleagues was recorded using the TM-20 from Transmed Ltd. (Bristol UK), and sections categorised with respect to the response feedback noted. Data set 1 consisted of 4041 epochs of data recorded whilst the patient was unresponsive to stimuli. Data set 2 consisted of 2770 epochs of data where the subject was shown to be responsive during Propofol delivery. To minimise the possibility of artifact colouration of the analysis an automated artifact rejection scheme was devised based on large transient changes in the optimum autocorrelation time shift calculated for each epoch of data. Taking the optimum time shift, k, as that which the correlogram first drops to 10% of the first value of the correlogram, epochs that showed a greater than 16 point change in k to the previous epoch and persisting for less than 4 epochs were removed from the data analysis along with the subsequent 3 epochs. Visual inspection of the remaining data showed that not all obvious artifacts were removed using this technique. After inspection of the ACFs generated by epochs containing the remaining artifacts, an additional constraint was implemented in the artifact rejection scheme. It was noted that whilst the output of the

correlogram at k = 1 would vary considerably between epochs, the remaining artifact ridden epochs would present a first output of larger magnitude than artifact free epochs. By inspection a value of 135,000 was identified as an appropriate limit above which the epoch would be discarded. It was noted that both artifact rejection techniques removed data that may have been processed without causing a major disturbance to the algorithm along with disruptive epochs. Despite crude in its visual derivation, the scheme provided a useful automated means of removing artifact-laden epochs from the data to be analysed. Data set 1 was reduced by 287 epochs (7.6% of the complete data set) and 190 epochs were removed from data set 2 (7.4% of the complete data set).

After artifact rejection, data set 1 contained 3754 epochs and data set 2 contained 2580 epochs. To ensure the algorithm performance analyses remained comparable, 2580 epochs of data set 1 were used. Running both sets of data through the algorithm gave arrays of alpha and delta indices with mean and standard deviations as shown in Table 8.3.

	Delta Index	*Alpha Index*
Data set 1	0.51 ± 0.21	0.19 ± 0.1
Data set 2	0.32 ± 0.12	0.29 ± 0.14

Table 8.3: Algorithm performance with Propofol anaesthesia data. Data set 1 consisted of 'patient unresponsive' data. Data set 2 consisted of 'patient responsive' data. The mean and standard deviations of both delta (0.5Hz to 4Hz) and alpha (8Hz to 12Hz) indices are given.

To test how useful the alpha index is to the application, a threshold alpha index value can be selected such that values above the threshold are assumed to indicate the patient is awake and values below the threshold show the patient is asleep. A Bayesian diagnostic test of the sensitivity and selectivity of the alpha index can then be found. Assuming the correct prediction of the patient being awake is as important as the correct prediction of the patient being unconscious, then the threshold can be determined by finding the index value that equally divides the probability distribution overlap between the two data sets. This is shown in figure 8.29. The threshold index value is selected such that areas A and B in the figure are equal. With the data described this in effect equates the sensitivity and selectivity measures of the diagnostic test.

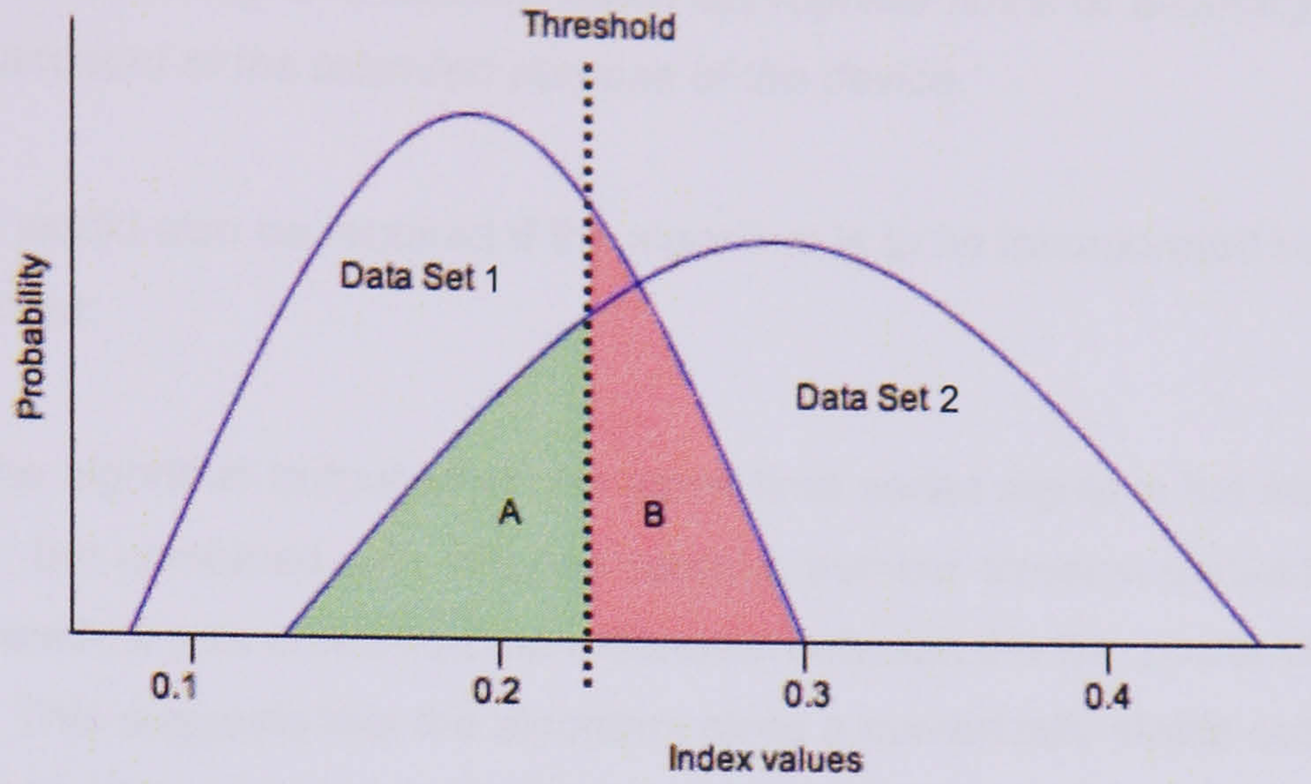

Figure 8.29: Diagnostic test threshold identification

Using the data described, the alpha index threshold is 0.23. Testing the alpha index for its efficacy at determining when a patient is awake, the diagnostic sensitivity and selectivity equate to 65%.

Repeating the same calculations for the delta index, the threshold is 0.39 with a diagnostic sensitivity and selectivity of 72%. These tests show that the proposed indices are not a reliable measure of consciousness during Propofol anaesthesia.

Of the 41 original Propofol patient data sets 13 gave a significant rise in alpha bandwidth activity within 2 minutes of infusion start. Interestingly, the alpha index value did not reflect the increase in 8 of the patients as the feature appeared in parallel with an increase in predominantly delta, and sometimes theta, bandwidth activity. This suggests that early detection of emerging alpha bandwidth activity would not be an advantage in a generalised monitoring solution. In addition the alpha index proposed in the patent may not reveal the characteristic even if it were present.

The graphs of figure 8.28 show that even in data sets that present a strong correlation between the proposed indices and agent delivery, considerable variation will persist during a single known state of consciousness. The contribution to the variance attributable to the recording and processing method needs to be defined as part of the compliance procedure. The Medical Device Directive (EU Council Directive 93/42 EEC) states in section 10.1 of annex 1, such a device should show:

> *'sufficient accuracy and stability within appropriate limits of accuracy and taking account of the intended purpose of the device.'*

Such definition would also be required if the algorithm is to be incorporated into a multivariate processing monitor.

By observing the algorithm output when the same time series signal is fed into both channels simultaneously, but combined with different random number streams derived using equation 8.1, applied to each, it was noted that the difference between the two power distributions is no more than 1%. This suggests that the algorithm gives a numerically stable output and that the deleterious contribution of the noise addition is not of practical consequence as suggested in the patent.

An epoch of moderately complex EEG data recorded when the subject was relaxed and awake was selected and repeatedly fed into the algorithm to form a contiguous time series of repeating identical data. In addition to the noise signal a sinusoid of 29.3Hz was added to the incoming data. The frequency of the added sinusoid was selected to be harmonically unrelated to the sampling frequency such that the epoch data window would truncate the sinusoids in most epoch transforms as would most often be the case with sinusoidal components in real EEG data.

The addition of the 29.3Hz sinusoid provides an opportunity to analyse the representation provided by the algorithm of a frequency component of known magnitude. With the logarithmic band power amplifier function removed, the relative power index given over a 2.667Hz bandwidth (identified earlier in this section as the magnitude of bandwidth influenced by a single sinusoid component) centred at 29.3Hz was observed. The amplitude of the 29.3Hz component was varied with respect to the maximum time series amplitude in the EEG epoch and run through 200 epoch iterations. The different amplitudes of the added sinusoid are represented along the x-axis of the graph in figure 8.30. The y-axis presents the index output.

The variation presented in figure 8.30 suggests that the algorithm does not provide a stable relative power index and that pre-whitening the signal with noise does not constitute a complete solution to the instability. Although the mean amplitude generally rises with increasing amplitudes of the 29.3Hz component, it is noted that the range of values is roughly proportional to the amplitude of the 29.3Hz component. The smaller variance at low amplitudes would be amplified if the scaling policy described in figure 8.26 were applied.

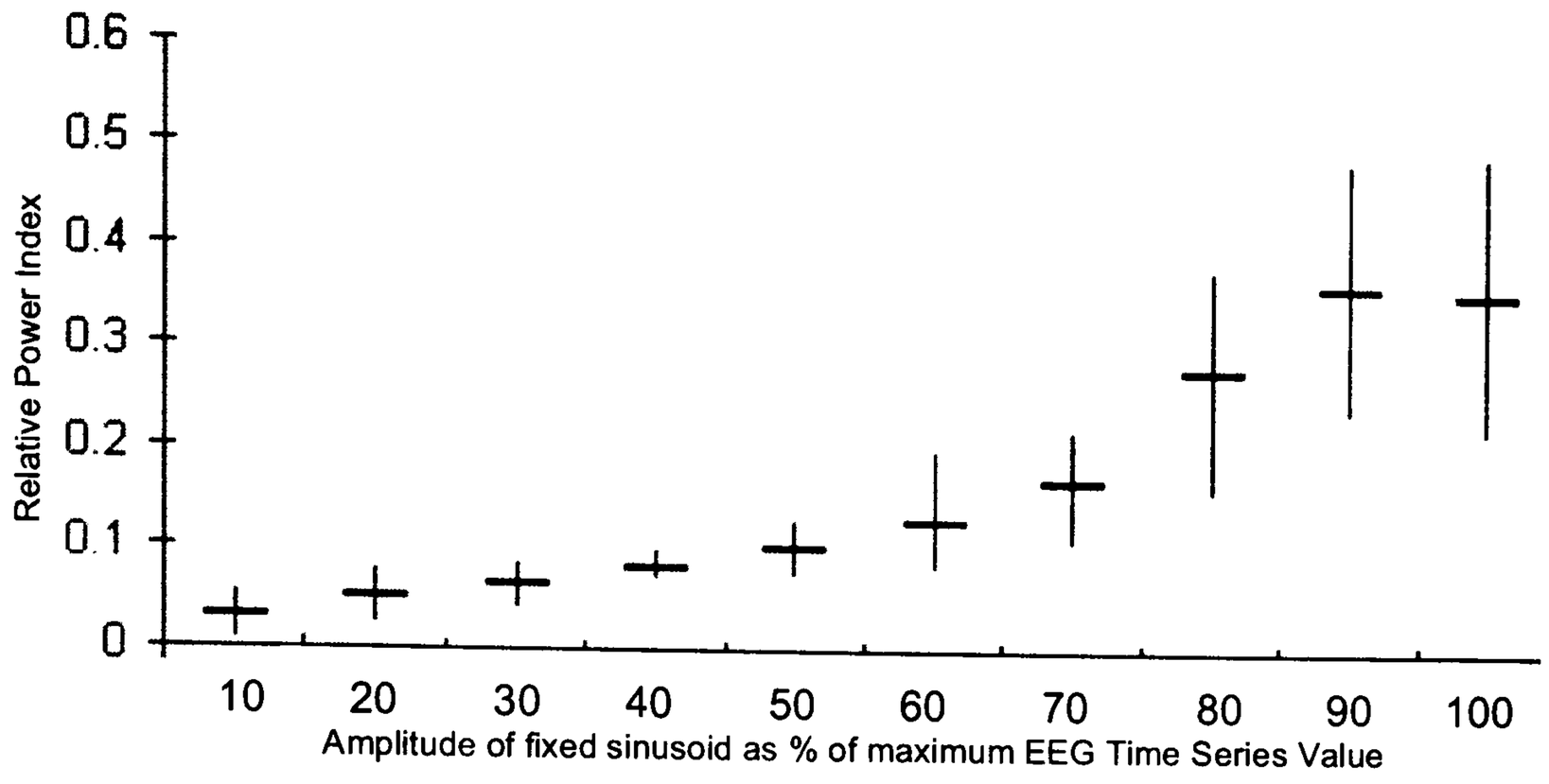

Figure 8.30: Minimum, maximum and mean relative power index output given by various amplitudes of a single sinusoidal component in a signal of noise and a repeated epoch of EEG data.

The known sources of algorithm instability are discussed in section 6.2.5 to which the practical problem in EEG recording of non-stationarity can be added, i.e:

1. Parameter quantization in digital filters;
2. Round-off noise in multiplication;
3. Word length overflow.
4. Periods of non-stationarity

Given that each element of the ACF is the gross sum of N^2 multiplications, the accumulation of quantization errors, round-off errors and word-length overflow may cause instability. The addition of noise of an amplitude indexed to the EEG time series maximum amplitude is unlikely to contribute a solution to the problem.

The double data type used throughout the signal-processing algorithm represents all variables parameters with an 8-byte floating point integer ranging between ±1.79E+308. The 3-byte data from the analogue-to-digital converter used gives a range of ±8.39E+6. Thus even with an epoch of data at full-scale deflection of the analogue-to-digital converter (i.e. when the input voltage is at the maximum or minimum of the analogue-to-digital converter range), the double data type used will more than comfortably permit all calculations to take place right through the signal processing chain without overflow.

Instability can be identified in the elements and symmetry of a given ACF matrix. Under ideal conditions the ACF matrix will display a symmetric Toeplitz form where each diagonal will be mirrored about the main diagonal (from the top left element to the bottom right). Pardey and colleagues (1995) suggest that the value of the prediction error in the model may be used to identify if instability has arisen in the ACF. If instability is found, calculation of the ACF roots by Laguerre's method will enable reflection of the poles back into a stable position on or within the z-plane unit circle. The approach organises a row of the ACF as a product of linear factors the roots of which are assumed to be clustered about some guessed value with the exception of one, which is assumed to be a guessed distance from the cluster. The guessed value of the single root is then iteratively modified. Once convergence of the single root value reaches some acceptable tolerance, the single root can be removed from the polynomial and the process is repeated. Laguerre's method provides a solid mechanism for finding the roots of non-linear polynomials as would be found when instability in the ACF exists.

A further useful measure is provided by a parameter termed the 'condition number' of the matrix. The condition number is the ratio between largest eigenvalue of the matrix and the smallest. An infinite condition number indicates matrix singularity (i.e. there is no single solution to the set of parametric equations). Similarly if the condition number is sufficiently high, quantization errors, round-off errors and word-length overflow will also assert singularity. The matrix in this instance is termed 'ill-conditioned' and will propagate z-plane poles outside of the unit circle and thus more than one solution to the parametric decomposition.

The occurrence of an ill-conditioned matrix can be caused by too little complexity in the signal. Baddour and Beaulieu (2005) suggest a signal with less than (M – 1) sinusoids, where M is the model order, will cause this. Figure 8.31 presents the instability observed when transforming a signal containing less than M-1 sinusoids. Two components were used in this analysis, 4.1Hz and 8.1Hz, again both selected to be harmonically unrelated to the sampling frequency and far enough apart to remain distinct in their spectral representation. As can be seen from the figure, the instability gives multiple spectral outputs.

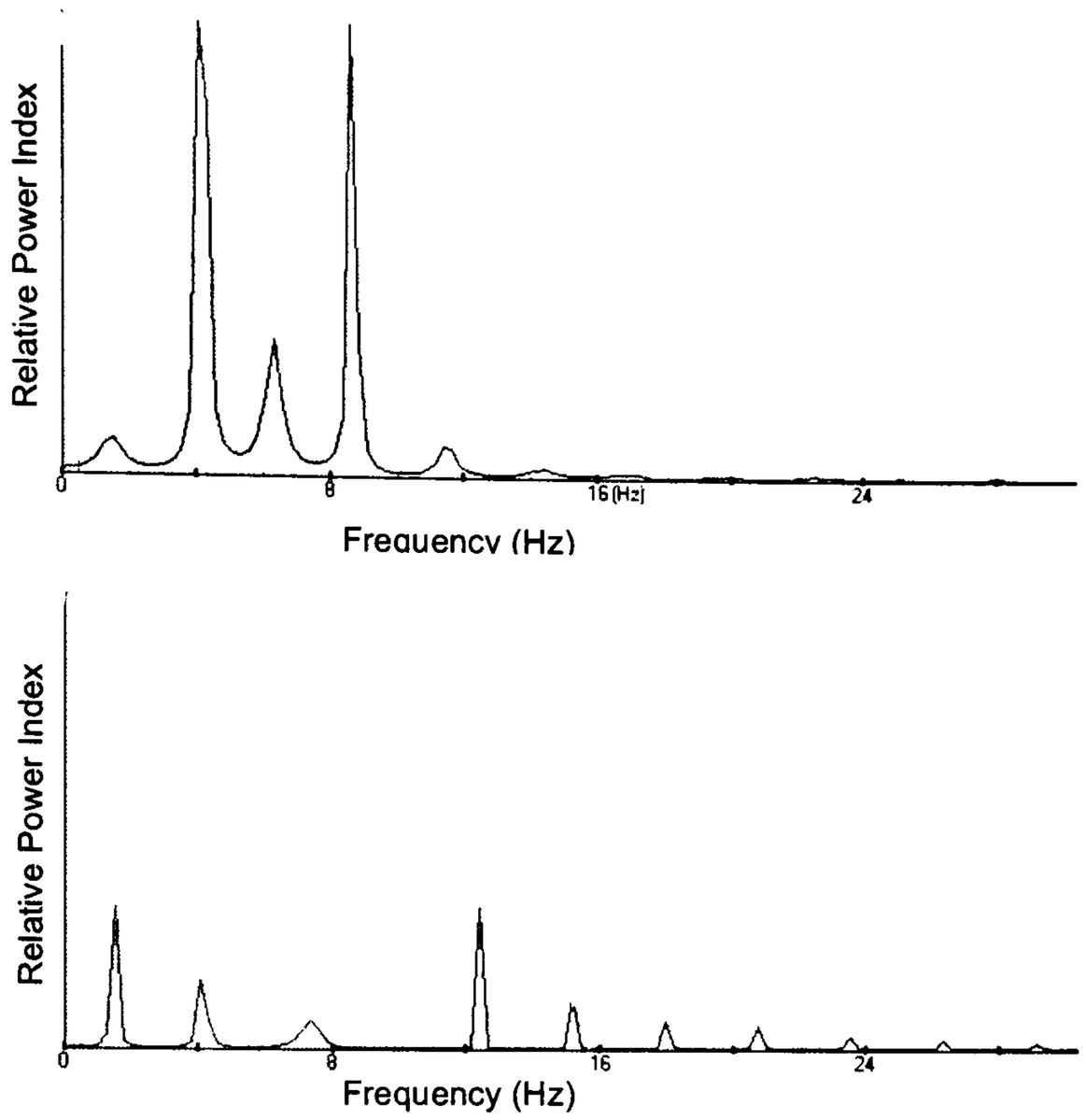

Figure 8.31: Two consecutive epochs of a single consisting of 2 fixed amplitude sinusoids at 4.1Hz and 8.1Hz.

The addition of noise increases the complexity of the time series data with a signal that, with averaging of multiple ACFs, will present a flat characteristic in the resulting power distribution function. This is equivalent to increasing the eigenvalues of the ACF matrix by some amount. Messerschmitt (2006) points out that the eigenvalues of a symmetric Toeplitz matrix closely match the power spectrum of an autocorrelation matrix and so it is possible to improve stability by asserting orthogonality to the matrix by a measured amount through interrogation of the eigenvalues. There are a number of methods that aim to do this. The best known is the Gram-Schmidt process, which asserts orthogonality by projecting the inner product of an ACF vector, q, onto its orthogonal counterpart, r. The vector q is then redefined as the difference between r and its orthogonal projection:

$$proj_q r = \frac{\langle q, r \rangle}{\langle q, q \rangle} q$$

$$q_k = r_k - \sum_{j=1}^{M-1} proj_{q_j} r_k$$

By altering the eigenvalues by a calculated amount the Gram-Schmidt process is thus analogous to the calculation of the 'noise' time series such that stability is maintained. In implementation, the Gram-Schmidt remedies the 1% variance noted above when both

channels are supplied with a repeated epoch of combined EEG and separate white noise signals. Repeating the analysis shown in figure 8.30 using the Gram-Schmidt addition as implemented by Press and colleagues (1992) instead of noise, the results presented in figure 8.32 were given.

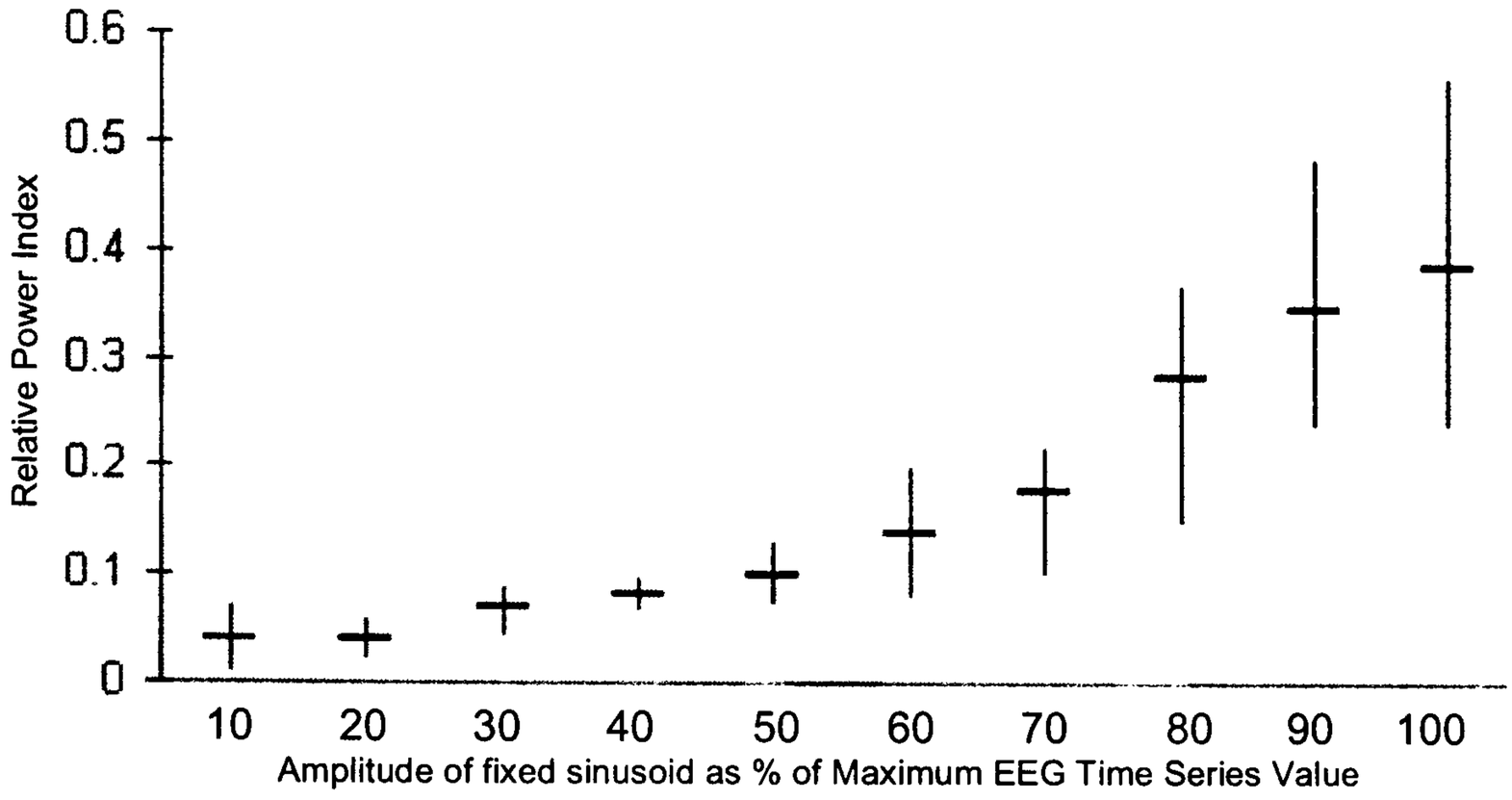

Figure 8.32: Minimum, maximum and mean relative power index output given by various amplitudes of a single sinusoidal component in a repeated epoch of EEG data with an orthogonal ACF asserted by the Gram-Schmidt process.

The results shown in figure 8.32 are similar to those of figure 8.30. The increasing amplitude of the added 29.3Hz component is represented with an increase in the magnitude of the index. Similarly, the range of index values given at each amplitude of the added sinusoid also increases with the amplitude of the sinusoid. This indicates that the variance observed in figure 8.30 is not linked to the stability of the ACF. This can be confirmed by running a low complexity EEG time series, as may be found in an EEG signal of predominant alpha rhythm, through the algorithm. With no noise added, a flag to indicate that prediction error calculation in the autoregressive model (see section 6.2.5) equals zero or less was never raised. This suggests that what may appear as low complexity EEG contains sufficient low amplitude frequency components to be run with stability through a model of the selected order without the noise addition.

Figure 8.33 presents the algorithm power distribution output with an input signal of two sinusoids, 4.1Hz and 8.1Hz, chosen to be more than 2.667Hz apart to ensure their spectral representations would remain distinct. Both additional components were of equal amplitude. 46 sinusoids of various amplitudes and frequencies above 22Hz selected to keep their

spectral representation entirely distinct from the two lower frequency components were also included. In this analysis no further noise is required to maintain sufficient signal complexity for algorithm stability as the condition of M-1 sinusoids is met.

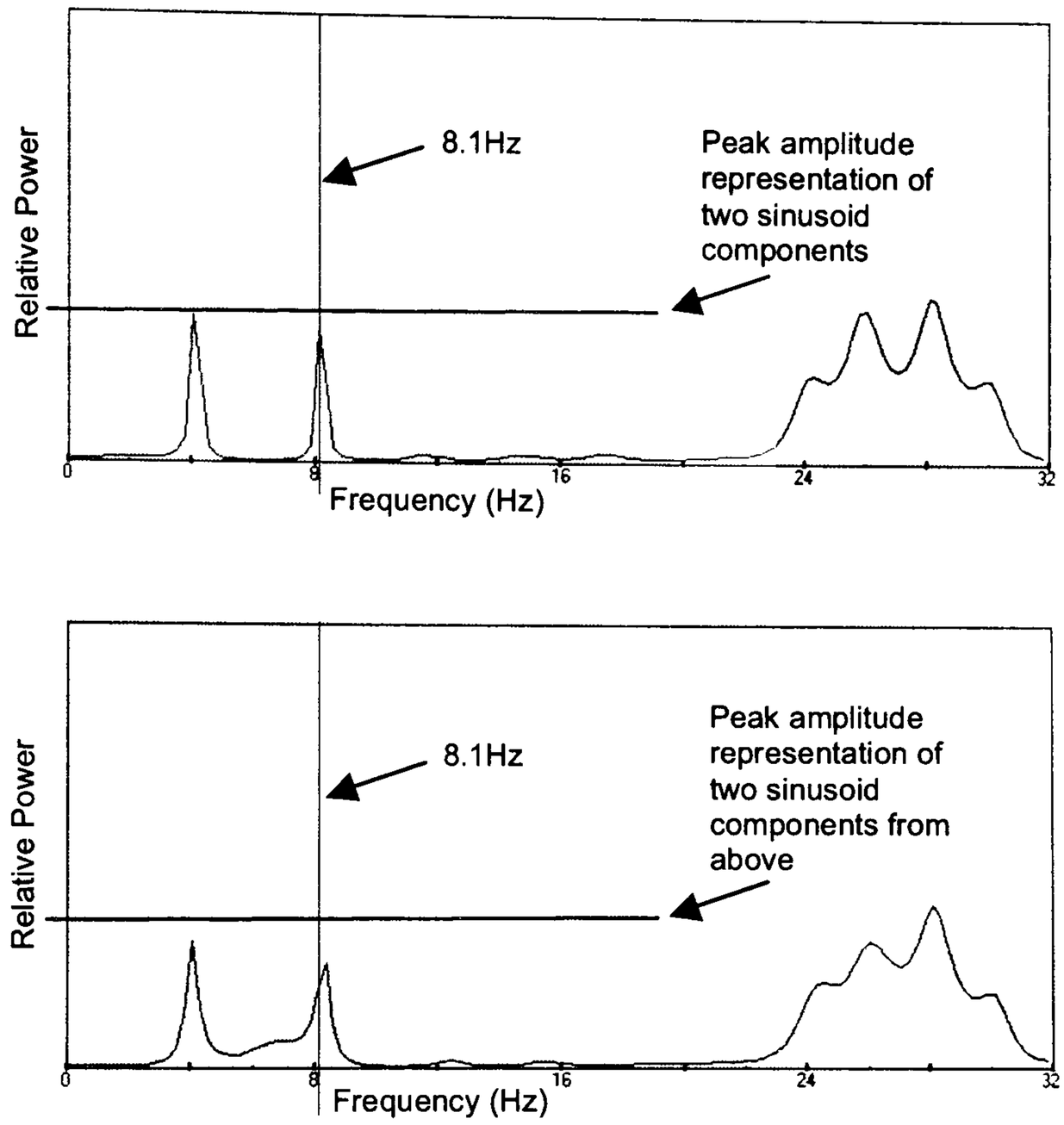

Figure 8.33: Two sinusoid components at 4.1Hz and 8.1Hz in a signal of noise band limited to 23Hz to 32Hz (top graph). The bottom graph shows the same signal as above with an additional 6.4Hz component.

The top graph of figure 8.33 shows a typical power distribution of the signal. As can be seen, although the two low frequency components are of the same amplitude their spectral representations differ. It was noted that the peak amplitude of the power distribution function at the lower sinusoid frequencies varied with each epoch. Using an index bandwidth of 2.667Hz centred at either of the low frequency components gave rise to index values ranging between ±24% of the mean amplitude.

The lower graph of figure 8.33 shows the power distribution representation of a signal with the same 4.1Hz and 8.1Hz components but with an additional third component at 6.4Hz of half the amplitude of the 4.1Hz and 8.1Hz components. The frequency of this third component was selected to be close to, but not within, the 2.667Hz bandwidth centred at either the 4.1Hz

or 8.1Hz sinusoids so as to find out whether the third component would assert influence over their representation in the spectrum. As can be seen in the figure, the addition of the third component lowers the peak amplitude of the 4.1Hz and 8.1Hz components. The 6.4Hz component is also poorly represented with a peak amplitude representation far below half that of the 4.1Hz and 8.1Hz component representations. It is also noted that the peak frequency representation of the 8.1Hz component is increased by 0.2Hz with the addition of the third component. Figure 8.34 describes this behaviour in greater detail.

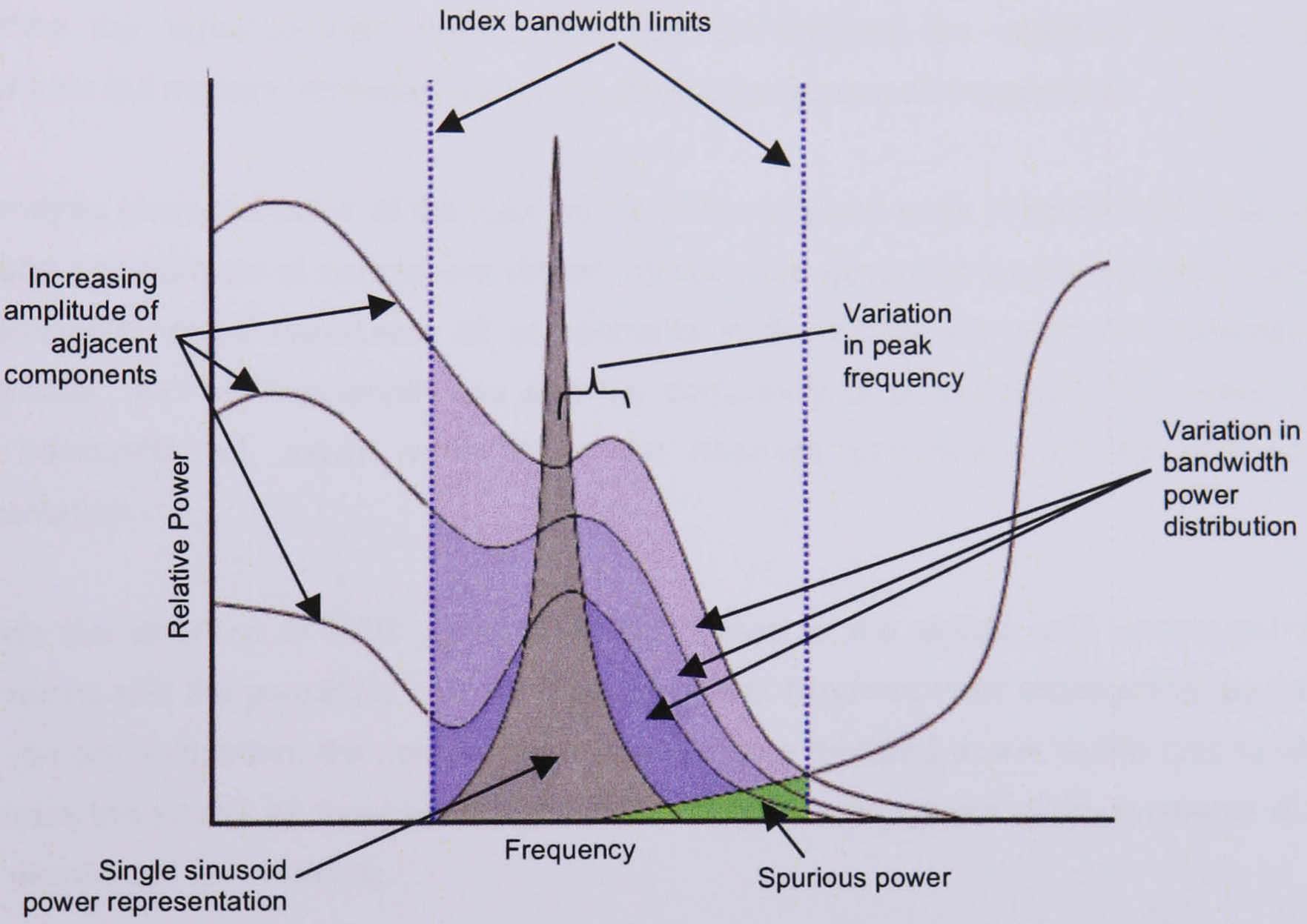

Figure 8.34: Variance asserted by model geometry. The model representation of a single sinusoid component is shown in grey. Adjacent component(s) alter the integral of the signal within the index bandwidth (shown in blue). The area in green demonstrates the possibility of entirely spurious bandwidth power.

The grey region shown in figure 8.34 presents the shape of the representation of a single sinusoidal component by the AR model. When further components are added at frequencies close to, but lower frequencies to that shown in grey, the amplitude peak of the single sinusoid drops (shown in dark blue). Increasing the amplitude of the lower frequency components increases the peak of the single sinusoid (shown in lighter shades of blue). The two vertical blue dotted lines mark a bandwidth that might be used to derive an index value.

As can be seen, without any change in the amplitude of the single sinusoidal component, the blue areas vary considerably thus affecting variability to the index measure. The green region shown to the right of the single sinusoid representation presents the possibility of frequency components a little further away from the index bandwidth limits can cause entirely spurious measurements in the index.

Spurious components can also be seen in figure 8.34, between the 8.1Hz component and the sinusoids positioned at 22Hz and above. The addition of white noise at a signal-to-noise ratio of 30dB removed the spurious peaks from this region of the power distribution function and reduced the standard deviation of the 4.1Hz and 8.1Hz index representations to ±11%. Degrading the signal-to-noise ratio further did not improve the variance of the fixed components but instead increased the power distribution across all frequencies.

This analysis gives indication of the main cause of the variance seen in figure 8.30. The peak amplitude and kurtosis of component representations are governed by the manner in which the parametric model represents all components in the signal. As such the proximity of components, their relative amplitudes and the complexity of power distribution across the entire bandwidth will assert variation to the absolute parameters of the component representation.

Although the variance in EEG spectra will be related to the signal, with undeterminable contributions and the possibility of more than one set of circumstances propagating the same power density fluctuation, the possibility of determining a modified power distribution function that relates the impact of changes in signal complexity to manipulation of the gradients of the power distribution is unrealistic.

The implication of the above analysis is that making detailed assessment of bandwidth power trend emergence or relative power using the patented algorithm is unlikely to yield accurate results.

8.7 Improvements

Rapid detection of sub-bandwidth power trend emergence is discussed as the succession to the earlier methods in the patent. The difference between the mathematics and the text of the patent of what the index represents gives two paths to the possible improvements that might be made to present a more robust analysis. If, as the patented mathematics suggest, it is the

changes in sub-bandwidth power with respect to the power over the total bandwidth that is the feature considered to be of interest then it has been shown that the algorithm introduces significant artifacts to the index output. All parametric estimation methods aim to reduce the prediction error across the entire bandwidth to a white noise component of minimum amplitude. When a sub-bandwidth is being observed the prediction error will not be white unless the signal varies in frequency content with time, and the index is averaged over long periods. An additional averaging regime over longer periods would propagate more stable results but this will diminish the resolution of emerging power distribution trends.

Alternatively coarse scaling of the output that accounts for the variance observed in the output might be employed. This will reduce the apparent resolution provided by the algorithm, but will increase the validity of the output. Figure 8.35 describes a scheme that uses the standard deviations observed in the representation of the fixed amplitude sinusoid seen in figure 8.30. Where the standard deviations overlap, the probability of an index value being related to a particular amplitude of the fixed component is used to identify where the graduations are positioned.

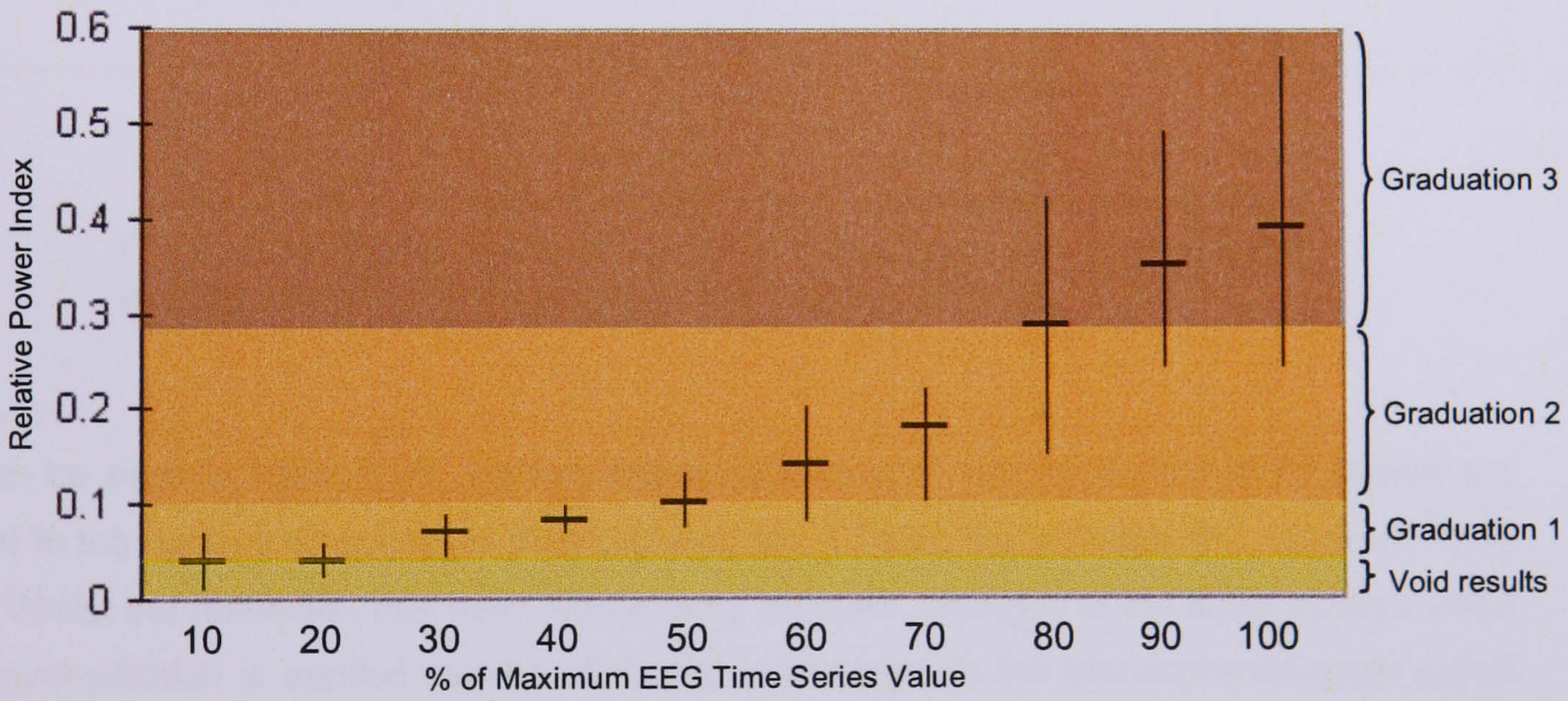

Figure 8.35: Graduation scheme devised to increase the physiological validity of the index method.

With this approach the resolution is significantly reduced but the output provides a clear representation of the changes in the index with minimised algorithm colouration. This is demonstrated in figure 8.36. The same sections of data presented in figure 8.28 are presented in the left hand graphs of figure 8.36 whilst the graphs on the right of the figure present the same data with the graduation policy applied.

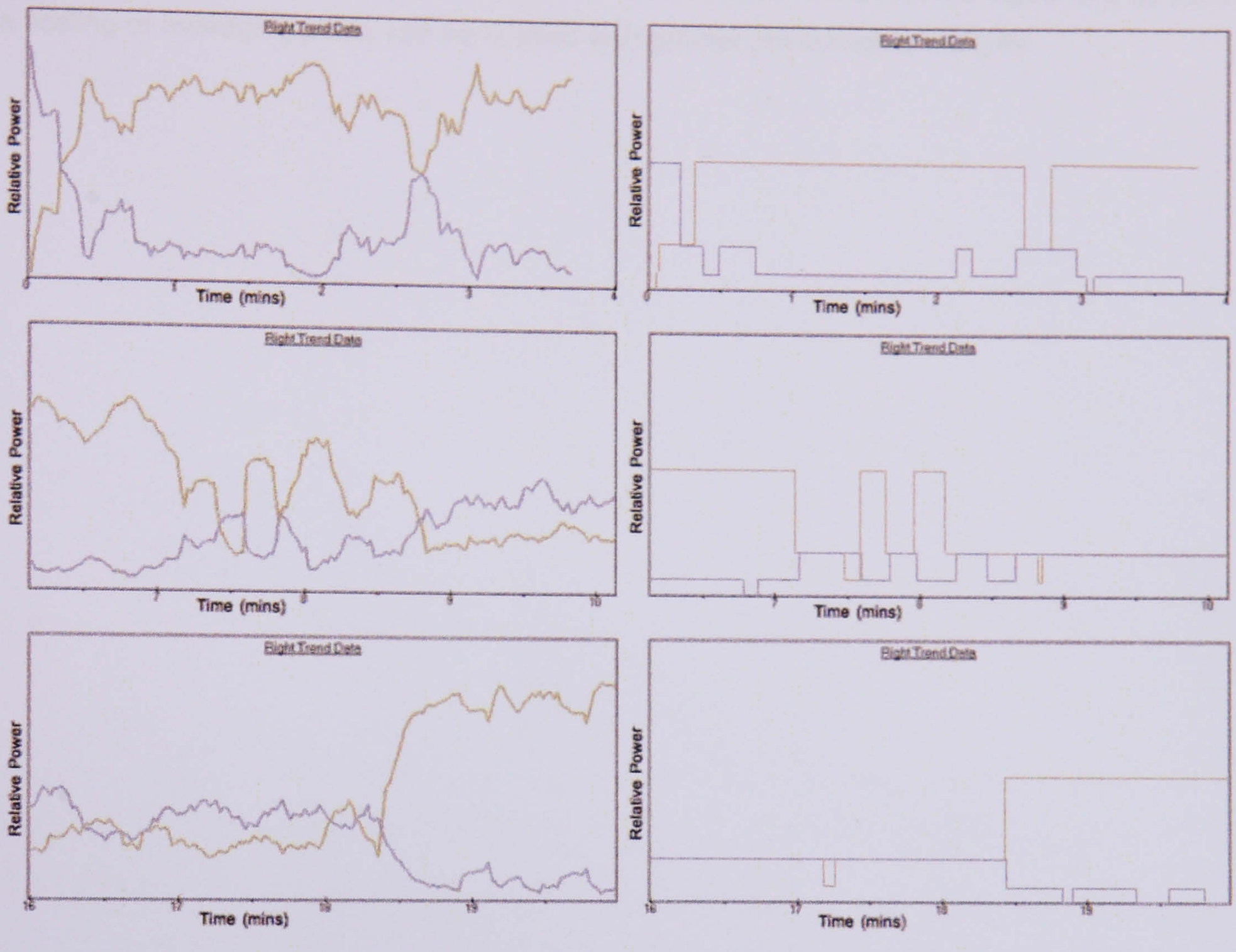

Figure 8.36: Performance of algorithm with relative power graduation applied using Enflurane sedation EEG data.

As can be seen in figure 8.36, the two indices plotted over time in the left hand graphs are scaled in the right hand graphs to step between the 4 index value thresholds shown in figure 8.35. Whilst the resolution has been significantly reduced, changes in the index powers when the novel addition is applied can be attributed to changes in the electrophysiological signal with greater confidence. The improved approach incurs no time lag associated with the calculation of means for example and so assessment of the metrics can be made based on the real-time context of the patient.

If the analysis described in the patent text is of interest then it is the changes in relative power in the bandwidth subdivisions that is considered of interest. Given that an increase in power outside of the index bandwidth might reduce the index output even if the index bandwidth power has itself increased, the approach can be considered fundamentally flawed. Assuming this to be the case, the gold standard method is to use a steep roll-off bandpass filter with high attenuation characteristics outside of the pass band. Using a stable linear filter design,

the output variance can be attributed to the variable spectral content of the signal and as such a scaling or averaging policy can be applied with greater physiological integrity.

Chapter 9

9.1 Conclusions

The patent on which this study is based presents the early identification of emerging alpha and delta bandwidth activity as a unique aspect of the protected mathematics. Aside from the doubt conveyed with regard to whether rapid detection of spectral trend emergence would constitute a useful advance in the application field, the reliability of domain transform algorithms and the susceptibility of the surface EEG signal to various environmental factors would make any measure based on small changes in signal detail inappropriate for a robust monitoring solution.

Changes in alpha bandwidth activity have been shown to occur in relation to anaesthetic dose but the premise that the parameter provides a uniform metric for the monitoring of depth of anaesthesia appears to be untrue. Whilst some patient context is required in the interpretation of all patient assessment techniques, it has been shown that the characteristic described does not occur across the population or the range of anaesthetic procedures currently in use. Any metric based on this characteristic will therefore be unreliable. The same is true of the delta bandwidth measurement and in addition, without a direct relationship between the alpha and delta bandwidth measurement characteristics across the agents, there is no indication that a parameter derived from both metrics would offer any further information.

It has also been shown that as well as the limitations of its performance, the interpretation of the algorithm output may be flawed. The method is therefore not appropriate for the development of a closed-loop anaesthesia delivery system based on this analysis as proposed by Griffiths et al. (1991). The evidence provided to this effect, along with the improvements offered, are novel and may be considered advances in the science of depth of anaesthesia monitoring.

This thesis has also set out to evaluate the use of EEG in depth of anaesthesia monitoring and to identify how the company set-up to exploit the precision technology developed should

proceed with regard to the depth of anaesthesia monitor application. Taking a pragmatic approach, the literature has been reviewed in an effort to link signal derivation, field-related functional anatomy, pertinent neuropharmacology and relevant EEG studies. The conclusion to this work must be that whilst the link between the pharmacological affects on the neurophysiology of pertinence to the derivation of the surface EEG signal is strong, the information available in the signal has yet to be shown to provide a complete profile of the physiological changes that occur during anaesthesia. Advice to the company set-up to market the device developed in the project must be that the method is not appropriate for proceeding with the expensive compliance procedures required of a medical device intended for use in the operating theatre environment.

9.2 Discussion

The maturation of digital recording techniques during the 1970s provided a platform for the development of what has become a vast array of algorithms aimed at reducing EEG data in a manner that will expose features that characterise changes in depth of anaesthesia. However, the current view of both the American Society of Anesthesiologists and the UK's Royal College of Anaesthetists is that brain function monitors should not currently form the sole basis for depth of anaesthesia monitoring. Despite the availability of a variety of EEG-based products that propose to meet this need, the advice remains that close vigilance to all patient and equipment variables should be maintained. Acknowledgement of EEG as a useful source of data is given in advising EEG to be used as an adjunct to standard vigilance during anaesthetic procedures in high-risk cases. In addition, it is noted by both bodies that the potential for EEG to become a useful measure warrants continual review of the technology.

It becomes apparent when reviewing the literature that the absence of hard-lined definitions clouds interpretation of evidence. The potential rewards for developing a robust technique suitable for routine depth of anaesthesia monitoring are almost unimaginably high and so perhaps it should be of little surprise that some present such ambiguities with misleading conjecture in support of a commercial project.

This approach may not be entirely divisive; the commercialisation of medical devices is expensive and is thus done so at considerable risk, especially to an industry newcomer. In a field with so few hard facts and yet so many promising indications, a marketing strategy that seeks to embellish positive results and disregard all else may be the only route to establish a product on the market. Although a complete solution to the problem of depth of anaesthesia

monitoring has yet to be identified, many studies show some value to the use of the devices that have been developed and so misrepresentations of this kind may not be an immediate cause for scorn. However there is evidently a need to maintain both a critical approach when reviewing the literature and considered expectations of the products available on the market.

Contradictory evidence of the efficacy of EEG in this application is widespread, and yet when properly carried out, EEG is thought of as a robust clinical assessment tool. Poorly designed techniques propagate such problems and thus undermine the premise that EEG might be used to monitor depth of anaesthesia. It has been shown in this study that it cannot be assumed that the algorithms being used are of sound mathematical foundation. All algorithms have caveats to their correct operation and limitations to their interpretation. Whilst a visual display of an algorithm output may present features that appear to have an intuitive connection to their application, awareness of the limitations of algorithm operation must be maintained to ensure validity of conclusions drawn. This asks a lot of the clinicians who are publishing literature on the subject but the quality of literature that does not breakdown the mathematical techniques before embarking on presentation of the study is limited.

Industrial practice also introduces ambiguity. Intellectual property law dictates particular courses for medical device manufacturers to protect their commercial interests. A model of current prevalence is the guarding of proprietary algorithms without public domain declarations of their form. This is less than ideal for the field as in the event that the technique does not form a complete solution to the problem, the anaesthetist has justification to be skeptical of EEG approaches in general. One such manufacturer has recently released 'Version 3.12' of their monitoring system. Incompatibility of data between versions of this single product has been noted, again deteriorating the quality of the literature.

It seems unlikely that any signal other than the EEG would have had so many signal processing techniques applied to it without clear understanding of what signal features are sought. The absence of even agreed clinical endpoints for a monitoring method is indicative of the complexity of the problem. Many studies of EEG analysis techniques in the literature therefore proceed directly towards aligning algorithm outputs with poorly defined psychophysiological characteristics, or worse still, with the output of other algorithms.

In this context it is of no surprise that research has as yet to identify a feature of the signal that presents a uniform characteristic across the population and all anaesthetic procedures. It is of course possible that such a parameter does not exist and thus a multivariate processing approach may be the only way to proceed, but there remains argument that the constituent components of such a design should be related to the signal's physiological derivation if acceptance within the field of anaesthesia is expected.

What is known of functional anatomy lends an understanding of what structures are likely to ascend characteristics to the outermost regions of the brain. The most compelling accounts of what constitutes consciousness discuss the phenomenon as a temporal orchestration of neuronal activity over an anatomical network of exceptionally high functional integration. It has been shown that the electrophysiological characteristics of cortical communication reflects functionality at subcortical temporal communication control centres. The study of the pharmacology of anaesthesia and the relevant functional anatomy affected by the anaesthetic agents reveals many agents assert disruption to the temporal organisation of consciousness.

Neuronal firing in the 40Hz region of the spectrum has been identified as a common feature of unmodified activity at these centres. If a direct link between EEG neurophysiology, the neuropharmacology of anaesthetics and the neurophysiology of consciousness exists, theory would therefore suggest that representation should be found in the 40Hz region of the surface EEG spectrum. The review of the literature has not indicated that such a feature exists in the signal, but without complete profiles of the mathematics employed in their analyses, it is difficult to disregard the possibility that this is an issue of the analysis techniques used.

As large areas of in-phase cortical activity are required to propagate strong characteristics in the surface EEG signal, neuronal activity associated with a wide range of functionality will be represented in the surface signal and will almost certainly make extraction of such a feature more complex. However, designing a recording and signal analysis method specifically for extraction of a theoretical signal characteristic of a known physiological phenomenon is likely to be a more successful research approach than simply applying such techniques in the hope that a feature may be found serendipitously.

Review of the results given when different algorithms are applied to the signal show that it is possible to identify features that present changes in electrophysiology concomitant with agent titration. Time domain techniques offer robust simplicity in their mathematical foundation and, although limited, interpretation of their output is reasonably straightforward. Statistical analyses and time domain entropy methods also present useful information. Their inclusion into a multivariate algorithm would therefore be of use and robust.

Given the derivation of the signal, spectral representations of surface EEG should directly show changes asserted by the anaesthetic agents. It would appear that this assumption is true and as such there is compelling justification for applying mathematical techniques of increased complexity.

Higher order analyses come with a complexity that even mathematicians find difficult to define. The possibility that the central processing analysis of the market-leading monitor does not provide the information claimed of it by the manufacturers makes these complex approaches less appealing.

Review of literature analysing EEG recorded during sleep identifies several relevant points in the evaluation of EEG as a depth of anaesthesia monitor. Many of the major neurotransmitters are implicated in the circadian cycle, as are many of the anatomical sites known to be affected by anaesthetic agents. However, the electrophysiology of sleep that can be recorded at the scalp does not appear to correlate well with that of any of the anaesthetic agents. Aside from some of the feature anomalies of the EEG recorded during sleep (for example sleep spindles) the fact that the EEG generated during REM sleep confounds many of the signal processing techniques applied to the signal, confirms that these methods do not distinguish wakefulness from unconsciousness. This finding might suggest that the EEG does not hold a direct correlate of consciousness and that development of a 'brain function monitor' may be a more appropriate goal than a depth of anaesthesia monitor. It is certainly a concern that despite many years of research, a fully automated sleep monitor has not been successfully developed. However, it is again an issue of prevalence in the field of sleep monitoring that neuroanatomical links to the characteristics of the recorded surface electrophysiology are largely absent in the literature. The same is true of the mathematical derivation of the algorithms used and so it remains a possibility that the techniques used in the analysis of sleep are as much a problem as the complexity of the goal.

Although the method is not without contention, the monitoring of auditory evoked potentials currently appears to show the most promise for the application of EEG monitoring to the problem of depth of anaesthesia monitoring. The apparent evoked potential characteristic observed during nitrous oxide delivery makes auditory evoked responses a promising method as spontaneous EEG is largely unaffected by this agent. The characteristic features observed when using the technique also appear to be well founded in neurophysiological and electrophysiological theory. Advanced approaches to the extraction of the feature benefit the concept as the time lag inherent in standard analyses may impact on reliability, especially as the delay compounds the problem that when the method indicates the return of consciousness, awareness may already have returned.

It is not uncommon to find monitors that include features such as auditory evoked potential measurement in addition to spontaneous EEG analysis. Auditory evoked response, heart-rate variability or EMG analysis adjuncts are provided on several current EEG products marketed as depth of anaesthesia monitors. Appreciation of the real-time patient context is required

with all of these techniques perhaps making adoption of the products less appealing. However, the inclusion of more than one analysis adjunct could reduce the amount of variables that negatively impact on these measures in a combined analysis.

The study of functional anatomy and neurotransmitter pathways will continue to develop the quality of interpretations of the EEG. Positron emission topography and functional magnetic resonance imaging are already contributing a wealth of pertinent information in this regard.

One of the problems associated with EEG recording has been the preparation required to make good electrode contacts. The cost of proprietary electrodes designed to minimise such preparation is discussed in the literature as a barrier to routine use of some monitors. Since the 1960s the concept of using a physiological signal to control anaesthetic agent delivery has been explored. The disruption to homeostatic control asserted by most anaesthetic agents makes 'un-manned' anaesthesia administration unlikely but the cost of operating theatre human resources is a current issue in the UK health service. This has led to a trial initiative to train Operating Department Practitioners to become Physician Assistants (Anaesthesia) who, in operation, would be overseen by a duty qualified anaesthetist. If current depth of anaesthesia monitors were proven to be reliable, this potential cost reduction could be made with confidence and may provide funding for the use of high cost, application specific electrodes.

Referring to the summary of the work presented by Griffiths and colleagues (1991) discussed in chapter 1, it can be seen that the evidence that formed the foundations of this project is ambiguous. The anaesthetic procedure used lasted some 25 minutes and yet the graphs shown in figure 1.2 only display spectral representations of four-second epochs at four undefined points over this period. There is no evidence provided to show the variance observed over the period of known patient states, nor is there indication that the same four seconds, for example at 4, 8, 12 and 16 minutes, were used in each of the 8 patient recordings. Proper due diligence carried out prior to the inception of the project would have identified that the statistical profile of the metric was incomplete.

The primary objective of the project on which this thesis is based was the development of an EEG monitoring device based around the patented mathematical method. The review of the literature presented in this thesis was carried out after the development. Although understanding of the various fields applicable to the subject of this thesis remains incomplete, research continues and with it our understanding evolves. The need to critically review the fields perpetuates. Ideally of course, if the time were to be had again, the research would have been carried out prior to the development work. The review identifies a number of areas

that should be evaluated in order that the use of EEG in depth of anaesthesia can be assessed.

9.3 Future Work

If further research were to be considered, it would be useful to begin with an approach appropriate to the physiological derivation of the signal. The review in this study indicates that the surface EEG signal might better be termed a 'cortical function monitor' in the context of this application. The term 'depth of anaesthesia monitor' has been shown to be inappropriate, whilst the term 'brain function monitor' implies that the signal represents both cortical and subcortical activity. Whilst this is to some extent true, the term cortical function monitor more clearly indicates that the subcortical activity that is represented in the signal is an indirect representation contributed only through the functionality of the cortex.

It is not clear whether such features would present themselves, but it would appear that if a monitor is to be accepted within the anaesthetist community, physiological links to the characteristics of the signal would prove a distinct advantage in marketing any subsequent product development. For example, it is apparent that whilst Hjorth's parameters are of sound mathematical foundation, the limited physiological interpretation possible of these measures prevented their general adoption.

The manifestation of conscious experience appears to be related to subcortical temporal control of neuronal firing. Studies suggest that a thalamic footprint of this control might be found around the 40Hz region of the EEG signal spectrum. With a high frequency sampling rate it would be possible to derive a spectral sub-bandwidth analysis with high resolution. Use of a wavelet analysis would improve upon the spectral estimation method used in this project as the multi-resolution approach would not only assist in the identification of such a characteristic but would also lend itself to a sub-bandwidth power measurement with lower variance than that seen with use of the method discussed in this study. Changes in the spatial features of a 40Hz characteristic should also be investigated. For example, expectation of useful changes in the phasic relationships observed in the 40Hz region between channels would appear to be well-founded in the literature.

If the raw data were filtered to give a band-pass bandwidth of 10Hz about 40Hz, time domain statistical analyses (for example variance, skewness and kurtosis) could be applied along with entropy and non-linear techniques in order that a characteristic of the physiological phenomenon might be found. It would also seem worthwhile assessing the statistical

characteristics of all of the above analyses over several epochs. For example, the mean and variance of time domain kurtosis measurements may further contribute to the clarity of a subsequent measure or multivariate index.

A similar approach could be applied to assess whether a feature of use is available in the 6-9Hz bandwidth, as this has been identified as representative of hippocampal temporal control of neural communication. In addition, a further set of analyses could be applied in high frequency bandwidths up to 1000Hz such that the potential for a feature of cognition-related cortical activity can be assessed.

Despite doubt as to how much can be interpreted of burst suppression EEG with respect to the application, the phenomenon remains a useful flag of overexposure to anaesthetics and should therefore be included. Various approaches have been used to indicate burst suppression but the simplest of time domain measures is favoured here. Monitoring for large decreases in sample amplitude can be continuously carried out on the raw data.

A scheme would then be required on which to integrate the parameters shown to be of use. Some studies have taken the most promising parameters and applied either fuzzy (sliding scale), or crisp (binary) rules to their integration into a multivariate algorithm. Although the parameters would more conveniently be identified using software-based signal processing research, if useful algorithms identified can be recreated in electronic hardware, then the advantages of stability, and integrity of the final output makes a hardware design a preferred approach to a product development. The use of hardware analyses will affect how each can be integrated into a single output but a blend of analogue and digital techniques may prove advantageous and appropriate.

With either a hardware, software or blended design, the straight forward approach to integration of multiple parameters into a overall processing strategy would be that which is used in the assessment of anaesthetic depth using the clinical signs i.e. where all measures are included with equal weighting to form a single dimensionless index. Thus if one measure is known to fail during nitrous oxide anaesthesia, other measures will still provide an indication of the changes. In practice equal weighting may not be appropriate, but it is worth considering as a design goal as understanding of the derived index would be simpler to communicate.

If characteristics of the EEG cannot be related to the physiology of anaesthetic action, it might be assumed that inter-patient variability will confound any structured analysis method. An alternative approach would link the MAC and TCI measures to an adaptive algorithm that

searches for patient specific time, frequency and higher order domain EEG changes concomitant with calculated effector-site concentrations of the agents in use. Reversal of signal changes identified during anaesthetic onset may be expected to indicate return of consciousness.

Several EEG monitors designed for depth of anaesthesia assessment employ additional analyses to spontaneous EEG monitoring. The inclusion of more than one analysis adjunct could reduce the amount of variables that negatively impact on the combined measure. Of the techniques reviewed, auditory evoked potential (AEP) analysis appears to show much promise. The controversy over whether there is a concomitant relationship between the AEP metric and anaesthetic dose is not necessarily of consequence as long as changes in consciousness are clearly represented. Adding electromyographical data to the analysis enabling facial muscle monitoring would also be useful, as would a heart rate variation monitoring capability. Remaining mindful of the preparation time required before each anaesthetic procedure will ensure the monitor is not disregarded for being too involved or overly complicated to set up.

The analysis of EEG data presented in this thesis shows a good deal of variance even when a patient is in a known state. Although much of the variance has been attributed to incorrect interpretation of the mathematical analysis applied, environmental factors and the patient context will also contribute to this. Ethical approval may not be granted for device development requiring the engineer being present during data collection, but it is possible for a full audio-visual account of the procedure to be made for each data set with real-time commentary by the anaesthetist. In this way, the timing of noxious stimuli, anaesthetic delivery and any other factors that might contribute to the variance observed in the EEG signal, can be considered alongside off-line data analysis and signal processing development.

Artifact rejection is a large topic in the literature of EEG analysis. Sophisticated approaches have been developed but require multiple electrodes to allow signal sources to be spatially separated. Those identified as artifact can then be removed. Whilst such techniques may be of use in some applications, it may not be appropriate here both in terms of the cost of electrodes or the extended preparation time required to use them here. Although crude, the artifact rejection scheme based on time domain signal statistics discussed in this thesis worked reasonably well. Further research would be needed to identify a generalised form, but an approach of this sort would be favoured for reasons of simplicity and mathematical integrity.

It is clear that the field would benefit from some acceptable definitions and metrics that could form a standard by which results could be compared. The difficulty in doing this has been outlined in this study. However, analysis of the performance of a new technique needs a standard by which measurement can be made. The isolated forearm technique appears to be of use here, although it may not stand alone as a solution. Postoperative assessment of each patient should also be conducted to explore the possibility that an experience of intraoperative awareness was explicitly encoded in memory without intraoperative indication from use of the isolated forearm technique.

In addition to the research and development outlined above, various areas of research should be continually reviewed. In addition to ensuring advances in the understanding of the neuropharmacology of the anaesthetic agents are considered, research on the involvement of electrical synpasing in the derivation of the EEG signal and the promise shown in galvanic skin response research would be worth on-going review.

Appendix A

Study Patent

US006748263B2

(12) **United States Patent**
Griffiths et al.

(10) **Patent No.: US 6,748,263 B2**
(45) **Date of Patent: Jun. 8, 2004**

(54) **MONITORING ELECTRICAL ACTIVITY**

(75) Inventors: **Mark James Griffiths**, Clifton upon Teme (GB); **Alan W Preece**, Bristol (GB)

(73) Assignee: **The University of Bristol**, Bristol (GB)

(*) Notice: Subject to any disclaimer, the term of this patent is extended or adjusted under 35 U.S.C. 154(b) by 51 days.

(21) Appl. No.: **10/203,954**

(22) PCT Filed: **Feb. 16, 2001**

(86) PCT No.: **PCT/GB01/00629**

§ 371 (c)(1),
(2), (4) Date: **Oct. 8, 2002**

(87) PCT Pub. No.: **WO01/60252**

PCT Pub. Date: **Aug. 23, 2001**

(65) **Prior Publication Data**

US 2003/0109796 A1 Jun. 12, 2003

(30) **Foreign Application Priority Data**

Feb. 17, 2000 (GB) 0003665

(51) **Int. Cl.**[7] **A61B 5/04**
(52) **U.S. Cl.** **600/544**; 600/300; 600/509; 600/546
(58) **Field of Search** 600/300–301, 600/500–505, 544–546

(56) **References Cited**

U.S. PATENT DOCUMENTS

4,846,190	A		7/1989	John
5,109,863	A	*	5/1992	Semmlow et al. 600/528
5,211,179	A	*	5/1993	Haberl et al. 600/515
5,299,118	A		3/1994	Martens et al.
5,458,117	A		10/1995	Chamoun et al.
5,765,128	A		6/1998	Tsuboi et al.
5,938,594	A	*	8/1999	Poon et al. 600/300
5,940,798	A	*	8/1999	Houde 704/271
6,011,990	A		1/2000	Schultz et al.

* cited by examiner

Primary Examiner—Charles Marmor
Assistant Examiner—Patricia C. Mallari
(74) *Attorney, Agent, or Firm*—Reising, Ethington, Barnes, Kisselle, P.C.

(57) **ABSTRACT**

A method and apparatus for monitoring electrical activity, such as brainwaves, in an animal comprising detecting said activity to produce a corresponding output signal, combining the output signal with a random noise signal to produce a modified signal, and analyzing the modified signal using an autocorrelation technique to detect the relative power density values at a plurality of different frequencies. The random noise signal may be a random number. The autocorrelation technique may involve the Yule-Walker method.

28 Claims, 2 Drawing Sheets

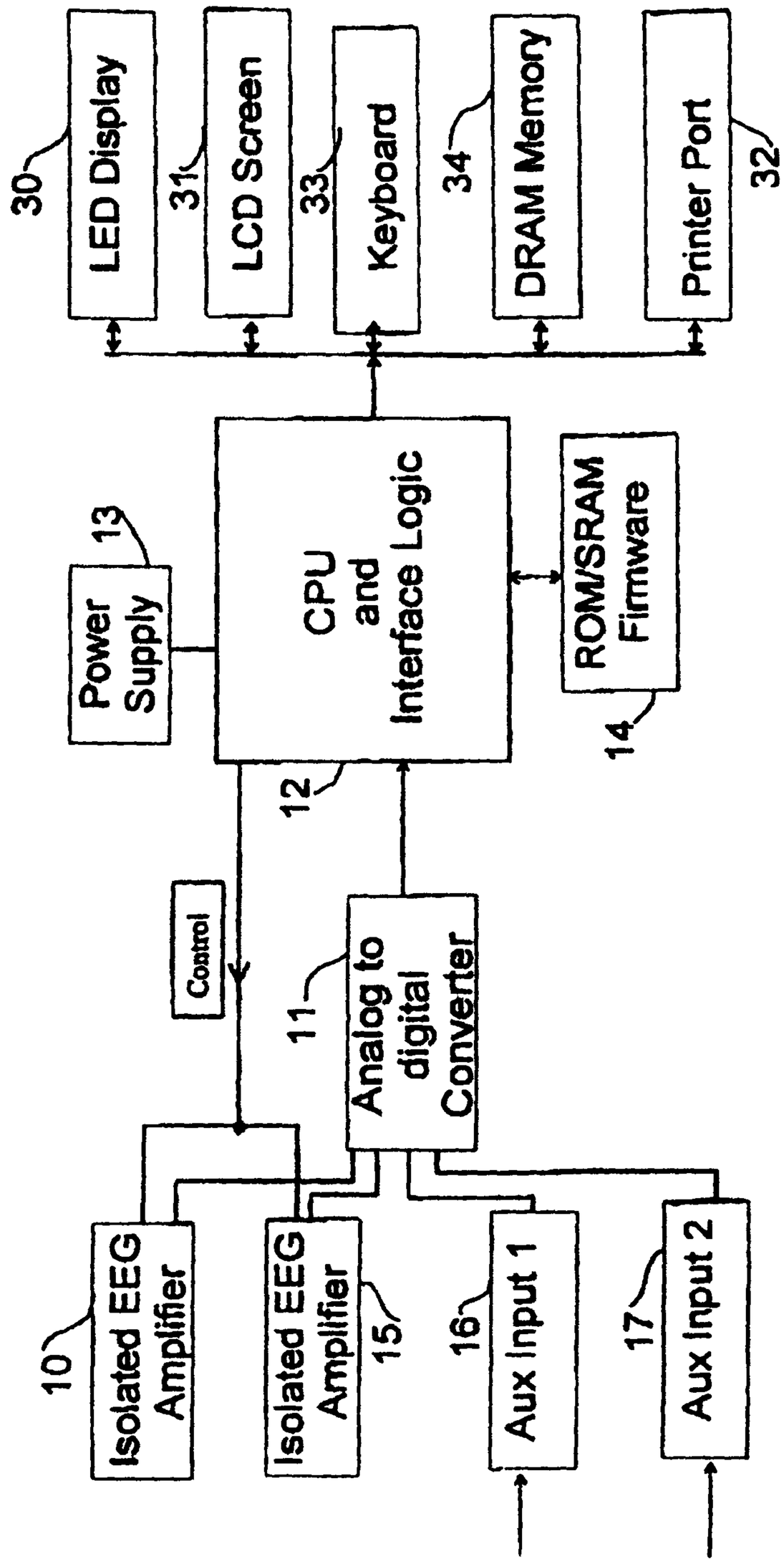
LED Display
30
LCD Screen
31
Keyboard
33
DRAM Memory
34
Printer Port
32
CPU
and
Interface Logic
12
Power
Supply
13
ROM/SRAM
Firmware
14
Control
Analog to
digital
Converter
11
Isolated EEG
Amplifier
10
Isolated EEG
Amplifier
15
Aux Input 1
16
Aux Input 2
17

Fig 1

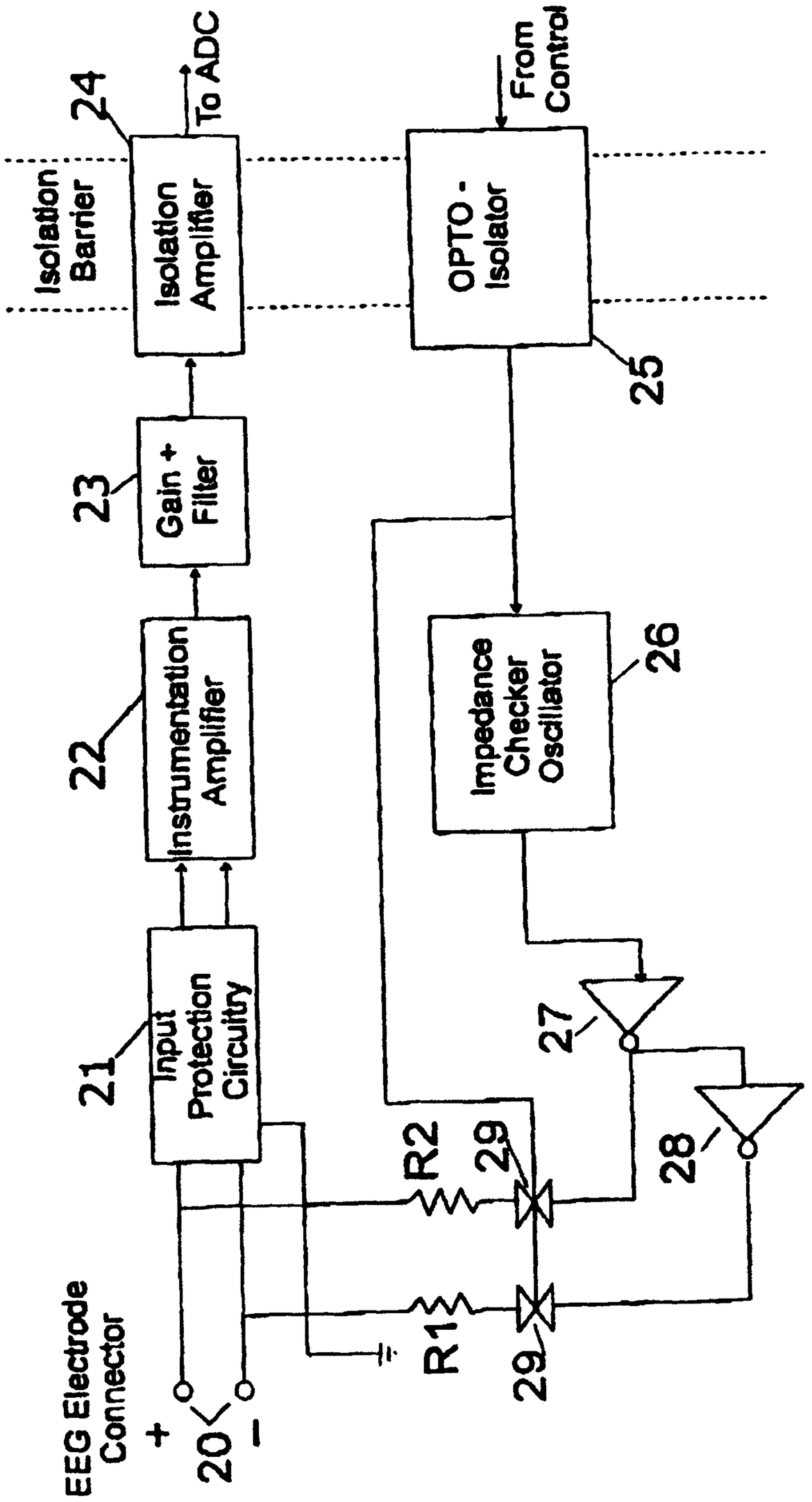
Isolation Barrier
24
Isolation Amplifier
To ADC
From Control
OPTO - Isolator
25
23
Gain + Filter
22
Instrumentation Amplifier
Impedance Checker Oscillator
26
21
Input Protection Circuitry
27
28
R2
29
R1
29
EEG Electrode Connector
+
20
–

Fig 2

US 6,748,263 B2

MONITORING ELECTRICAL ACTIVITY

The present invention relates to a method of monitoring electrical activity in an animal, especially human brain waves, and apparatus for carrying out the method such as an electroencephalograph.

It has been found that when a person is sedated, but not yet anaesthetised, their brain waves contain a frequency component which occurs between 8 and 12 Hz, and is known as the alpha rhythm. As sedation passes to full anaesthesia, the alpha rhythm disappears on termination of anaesthesia as the person returns to a sedated state, it reappears and then tends to disappear again when the person is fully awake.

It has been realised that this effect may be used to detect any undesired transition from anaesthesia to sedation, corresponding to the person beginning to regain consciousness, for example when a surgical operation is taking place. However, the emergence of the alpha rhythm, as anaesthesia passes to sedation, represents a small component in the total brain wave spectrum, and it has not proved possible using known methods to detect the gradual appearance of the alpha rhythm.

In addition, the occurrence of new frequencies lower than the alpha band such as delta, induced by the anaesthetic agent can be used to detect the undesirable presence of true anaesthesia if the intention is to maintain a state of sedation.

Known methods of analysing brain waves via electroencephalographs analyse the brain wave spectra using Fast Fourier Transforms. However, in detecting a weak frequency component, corresponding to the emerging alpha rhythm or low frequency delta rhythm induced by an anaesthetic agent, the use of a Fast Fourier Transform is unsuitable. There are two reasons for this. Firstly, noise in the brain wave signal is analysed by the Fast Fourier Transform as corresponding to many weak frequency components. It is thus not easy to distinguish between weak frequency components due to noise, and weak frequency component due to other reasons, such as the emergence of the new frequencies. Secondly, unless the frequency component being detected corresponds to one of the sampling frequencies of the Fast Fourier Transform, the Fast Fourier Transform will tend to split a frequency signal into a range of spurious frequency components.

The result of these two effects is that the Fast Fourier Transform tends to mask weak components. Hence, it is unsuitable for detecting the emergence of the alpha rhythm. By the time that the alpha rhythm for example is sufficiently significant to be detectable by Fast Fourier Transform, the person will have passed from anaesthesia to sedation, so that it is not possible in this way to carry out early detection of that transition.

Therefore, the present invention seeks to provide an apparatus and a method, of analysing brain waves which permits these rhythms to be detected when they are very weak. This then permits an indication of the anaesthesia or sedation level to be determined. However, as will be explained below, the present invention is not limited to detection of alpha and lower rhythms and could be used to detect other components such as epileptic spikes in the brain wave signal.

According to the present invention, electrical activity is detected and produces a corresponding output signal, the output signal is combined with a random noise signal to produce a modified signal, and the modified signal is analysed using an autocorrelation technique to detect the relative power density values at a plurality of different frequencies.

Preferably, the autocorrelation technique involves use of the Yule-Walker algorithm.

The value of one or more power density values at a frequency or frequencies corresponding to a specific rhythm such as the alpha or delta is then compared with the sum of the power density values over a wider range of frequencies. The result of this comparison gives a measure which may be used to detect the emergence of these rhythms. To express this in another way, the relative power density D_f at various frequency f are derived using Equation 1 below, for a multiplicity of frequencies f.

$$D_f = \frac{1}{\left|1 + \sum_{p=1}^{M} y_p \exp(-i \cdot a \cdot f \cdot p)\right|^2} \qquad \text{Equation 1}$$

where y_p is the pth Yule-Walker coefficient, and a is a constant.

Then, the ratio of the sum of one or more values of D_f at or about the frequencies of the particular rhythms are compared with the sum of the values of D_f over a wider range of values, and the changes in that ratio may be used to detect the emergence of these rhythms.

In general, the maximum frequency of the wider range will be at least approximately double that of the maximum frequencies of the rhythms under consideration.

It should be noted that Yule-Walker methods from which the Yule-Walker coefficients referred to in Equation 1 above are obtained, are a known type of frequency analysis method. For a detailed discussion of Yule-Walker methods, reference may be made to the book "Digital Signal Processing" (second edition) by J G Proakis and D G Manolakis published by McMillan publishing company, New York.

The present invention also consists in an electroencephalograph which monitors brain waves using the method discussed above, to indicate the emergence of specific rhythms, and also consists in a method of operation such as an electroencephalograph.

In order to derive the Yule-Walker coefficients referred to above, the present invention further proposes that a series of autocorrelation products be derived from the brain wave signals. These autocorrelation products may then be used directly, to derive the Yule-Walker coefficients, but it is preferable that an averaging technique is applied to them. It would be possible to determine the autocorrelation direct over a relatively long time period, but it is preferable to use a shorter time period and average over those time periods. The advantage of this is that short bursts of noise are then not carried over from one period to the next. Averaging in this way has the disadvantage of slowing detection of trends, and therefore there is the need to compromise between these factors.

In deriving the autocorrelation products, it has been found advantageous to add random linear noise to the brain wave signals. Provided that the amount of random linear noise added is not too great, the reduction in spectral resolution which results is not of practical consequence. However, it has been found that the addition of such random linear noise tends to reduce or prevent the occurrence of occasional rogue results. It is also preferable that any DC components of the brain wave signals be removed, to counteract the effect of drift.

In order to carry out the analysis of the brain waves as discussed above, an electroencephalograph according to the present invention preferably converts the brain wave signals to digital signals, to enable those signals to be analysed by a suitably programmed processor. The analysis of the rela-

tive power density values may then be used to generate a suitable display and/or audible signal, and/or a control signal for other equipment. In fact, it is preferable that the value corresponding to the comparison of relative power densities discussed above is converted to an index value which is a non-linear function of the initial value, to emphasise changes at low values of the specific rhythm.

An embodiment of the present invention to define the occurrence of the alpha rhythm will now be described in detail, by way of example, with reference to the accompanying drawings, in which:

FIG. **1** shows an electroencephalograph being an embodiment of the present invention;

FIG. **2** shows part of the electroencephalograph of FIG. **1**.

Referring first to FIG. **1**, an electroencephalograph amplifier unit **10** generates electrical signals corresponding to the brain waves, and passes those signals to an analogue-to-digital converter **11**. The resulting digital signals are passed to a processor **12**, in which they are processed using a Yule-Walker method, as will be described in more detail later.

The structure of the amplifier unit **10** is shown in more detail in FIG. **2**. Electrodes **20**, for attachment to a person whose brain waves are to be investigated, are connected to an input protection circuitry unit **21** which protects other parts of the electroencephalograph from damage due to high voltage discharge. The input protection circuitry unit **21** may also act to protect the person to whom the electrodes **20** are connected from failures within the electroencephalograph. As can be seen from FIG. **2**, the input protection circuitry unit **21** is also connected to ground, so that it passes differential signals to an amplifier unit **22**. That amplifier unit removes common mode noise, and produces a single signal from the input thereto which is then passed to a gain and filter unit **23**. The gain and filter unit **23** removes high frequency and DC components from the signal, and further amplifies the signal before it is passed to an isolation amplifier unit **24**. That isolation amplifier unit **24** acts as a isolation barrier between the electroencephalograph amplifier **10** and the analogue to digital converter **11**.

As shown in FIG. **1** the processor **12** is powered from a power supply unit **13**, which may contain a mains connection and a battery back-up so that the power is uninterruptable. The program for controlling the processor **12** during operation is stored in a memory unit **14**.

Furthermore, as is also shown in FIG. **1**, the processor **12** may be connected to a second electroencephalograph amplifier unit **15**, by the analogue digital converter **11**. That second electroencephalograph amplifier **15** may have the same structure as shown in FIG. **2**. Two auxiliary inputs **16**, **17** may be provided to allow digitisation of non-isolated inputs from a CAPNOGRAPH or similar equipment.

FIG. **1** also shows that a signal is passed from the processor **12** to the electroencephalograph amplifiers **10**, **15**. This signal is an enabling signal which is passed via an opto-isolator unit **25** (see FIG. **2**) to an impedance checker oscillator **26** of the electroencephalograph amplifier **10**, **15**. The opto-isolator unit **25** thus provides electrical safety isolation between the processor **12** and the electroencephalograph amplifier unit **10**, **15**, in a similar way to the isolation amplifier unit **24**. When the impedance checker oscillator **26** is enabled by the signal from the processor **12**, it outputs a frequency signal of between e.g. 5 and 10 Hz which is passed via two operational amplifiers **27**, **28** to generate two signals which are passed via transmission gates **29** to respective resistors R1, R2. The resulting signal may be used to assess the input impedance of the electrodes **20**.

It can be seen from FIG. **2** that the transmission gates **29** are enabled by the signal from the processor **12**, which is output from the opto-isolator **25**. The processing carried out by the processor **12** will now be described in more detail.

As was mentioned above, the present invention makes use of a Yule-Walker method to derive relative power density values. However, it should be noted that theoretical frequency analysis using such methods normally assume steady state conditions, which do not apply to brain wave signals. In fact, the consistent frequencies of such signals are often strongly amplitude modulated. Irregular waxing and waning occurs for some or all of the frequencies with successive maxima intervals varying within a range of half a second to two seconds. Furthermore, eye movements of the person to whom the electrodes **20** are connected can cause large irregular voltage excursions, and it has also been found that there are other non-periodic components. There may also be low frequency or DC drift. Hence, in applying a Yule-Walker method to brain wave signals, it is preferable that the processor **12** makes use of practical compromises as discussed below.

In the following discussion, various specific values are used to describe the analysis method. However, the present invention is not limited to these specific values.

The processor **12** analyses the signals corresponding to the brain waves in a series of time periods (epochs). The length of time period need not be fixed, and indeed an electroencephalograph according to the present invention may permit the duration of the epochs to be varied. However, an epoch of about 1.5 s duration has been found to be suitable. Assuming that the sampling rate of the processor **12** was e.g. 128 Hz, this would result in 192 sample values. This can be generalised, however, to N sample values per epoch, being:

$a_0, a_1, \ldots a_{n-1}$

It has been found that it is then preferable to add random linear noise to each of these sampled values, it has been found that if this is not done, consistent results cannot be ensured. Occasional rogue results may be detected which are sufficiently different from those of adjacent epochs to cause inaccurate analysis. Although addition of a random value reduces the spectral resolution that can be obtained, it is possible by suitable selection of the random value, to reduce the requisite error without the reduction of spectral resolution being of practical significance. The consequence of not adding noise in the form of random values is that the frequencies of interest can become too small in comparison to the totality of the other frequencies to be detected at times of high input noise or large DC offsets before these can be removed by averaging. Thus, in this embodiment, a modified sampled value a'_k, may be obtained, as follows.

$$a'_k = a_k + \mathrm{abs}\left(\frac{a_{max}}{20000}\right)(500 - \mathrm{random}(1000)) \qquad \text{Equation 2}$$

In equation 2, a_{max} is the numerically greatest sampled value in the epoch, and "random (1000)" is a random positive integer in the range of 0 to 1000. Such a random positive integer may be obtained from a pseudo-random program of the processor **12**.

There may be a DC component imposed on the brain wave signals, and this DC component may include a drift component. To remove this effect, the average value of a'_k over all the n values is subtracted from each value a'_k to derive a further modified value a''_k. This process can be carried out for each epoch, and it should be noted that the addition of the random value discussed above does not introduce a further bias.

Next, a series of autocorrelation products must be derived. The number of autocorrelation products that need to be derived depend on the order of the Yule-Walker method used. Assuming that order is m, m+1 autocorrelation products will be derived. In practice, values of m between 40 and 50 have been found to give satisfactory results. Then, each autocorrelation product x_p is given by equation 3 below:

$$x_p = \frac{1}{n-p}\sum_{k=0}^{n-p-1} a_k^n a_{k+p}^n \qquad \text{Equation 3}$$

In this equation p is the number of the autocorrelation product, varying between 0 and m. The values of x_p are then a measure in the time domain of the periodic components of the brain wave signals.

Although it is then possible to use those autocorrelation products $x_0 \ldots x_m$ to derive Yule-Walker coefficients, it is preferable first to apply an averaging effect across a plurality of epochs. It has been found that computing autocorrelation over short epochs, and then carrying out an averaging operation, is better than calculating the autocorrelation products directly over longer epochs. Short epochs allow for drift correction, and short bursts of noise do not carry over. Thus, averaging reduces the effect of irregularities in the brain wave signals, but slows the detection of trends.

A compromise needs to be found between these factors, and it has been found that maintaining a running average, over 12 s is a satisfactory compromise. If 1.5 s epochs are used, as mentioned above, then averaging is over 8 epochs. Then, a new running average R_p is derived from the previous running average R'_p by equation 4 below.

$$R_p = \frac{7R'_p + x_p}{8} \qquad \text{Equation 4}$$

Since the running averages R_p of the autocorrelation products are dated for each epoch, they are at any time available for analysis of the brain wave signals. In order to carry out that analysis, it is necessary to solve Equation 5 below.

$$\begin{bmatrix} R_0 & R_1 & \cdots & R_{M-1} \\ R_1 & R_0 & \cdots & R_{M-2} \\ \vdots & \vdots & & \vdots \\ R_{M-1} & R_{M-2} & \cdots & R_0 \end{bmatrix} \begin{bmatrix} Y_0 \\ Y_1 \\ \vdots \\ Y_M \end{bmatrix} = -\begin{bmatrix} R_1 \\ R_2 \\ \vdots \\ R_M \end{bmatrix} \qquad \text{Equation 5}$$

In equation 5, y_0 to y_m are the Yule-Walker coefficients.

Although Equation 5 above can be solved in any satisfactory way, it has been found that the Levinson-Durbin solution algorithm may be used, as this enables the equation to be solved rapidly.

If the sampling rate is at 128 points per second, as previously mentioned, the relative power density D_f at a frequency f is then given by Equation 6 below.

$$D_f = \frac{1}{\left|1 + \sum_{p=1}^{M} y_p \exp\left(-i \cdot \frac{2\pi f}{64} \cdot p\right)\right|^2} \qquad \text{Equation 6}$$

It should be noted that since the analysis that is subsequently used in this embodiment makes use of ratios, rather than absolute values, the numerator in the above equation has been set to 1.

It is convenient to evaluate the relative power density values D_f at intervals of e.g. a quarter Hz.

Then, a ratio α_r can be derived from equation 7.

$$a_r = \left\{\sum_{k=12}^{48} D_{(k/4)}\right\} \Big/ \left\{\sum_{k=2}^{96} D_{(k/4)}\right\} \qquad \text{Equation 7}$$

On the right hand side of this equation, the numerator represents the sum of the relative power density values within the 8 to 12 Hz frequency range in which alpha rhythms occur, whilst the denominator is a sum of the relative power density values over a frequency range of 0.5 to 24 Hz. Hence, α_r gives a measure of the power density within the range corresponding to alpha rhythms, relative to a much wider frequency range encompassing the range of frequencies corresponding to the alpha rhythms. Thus, variations in a_r represent variations in the power present in alpha rhythms.

Since the present invention seeks to detect the emergence of a specific rhythms, it is more important to detect change of α_r, from e.g. 0.02 to 0.05 than to detect a change from 0.2 to 0.3. Therefore, in a final step, the processor may derive a value α_i which is a non linear function of α_r according to Equation 8.

$$\alpha_i = exp\{S.\ ln(\alpha_r)\} \qquad \text{Equation 8}$$

In Equation 8, S is a sensitivity factor. If S equals 1, α_i and α_r would be the same. In practice, S equals 0.4 is a suitable value.

Once the processor **12** in FIG. **1** has derived the value α_i as discussed above, that value may be used to control. a display which the operator of the encephalograph may use to detect the emergence of a rhythm. For example as shown in FIG. **1**, a signal may be passed to a LED display **30** which displays the current value of α_i. In addition, or as an alternative, α_i may be presented as a vertical bar on an LCD screen **31**, to give a graphical indication of variations in that value. Information may also be passed via a printer port **32** either directly to a printer, or to a suitable computer for further analysis. FIG. **1** also shows that the processor **12** is connected to a key board **33** which permits the operator to control the electroencephalograph, for example to input parameters such as the duration of each epoch. The processor **12** is also connected to a dram memory **34** which permits some data to be stored whilst the electroencephalograph is powered up.

It should be noted that calculation of a_i requires the solution of Equation 5. Therefore, that equation could be solved every epoch, enabling the displays **30**, **31** to be updated every 1.5 s. In practice, such an updating rate is not essential, and the processing load on the processor may be reduced by solving equation 8 e.g. every 3 epochs, to give an update of the displays **30**, **31** every 4.5 s.

Furthermore. it can be seen from Equation 7 that suitable selection of the ranges of the values k in the numerator and denominator of that equation will enable the power of other frequency components to be investigated. Hence, although the present invention has been developed primarily to detect alpha rhythms occurring in the 8 to 12 Hz frequency range, the present invention may be applied to the analysis of other frequency components.

What is claimed is:

1. A method of monitoring electrical activity in an animal comprising detecting said activity to produce a corresponding output signal, combining the output signal with a random noise signal to produce a modified signal, and analyzing the

modified signal using an autocorrelation technique to detect the relative power density values at a plurality of different frequencies.

2. A method as claimed in claim 1 in which the output signal is sampled at intervals.

3. A method as claimed in claim 2 in which the samples a_k of the output signal are digital samples.

4. A method as claimed in claim 3 in which the random noise signal consists in a random number that is added to each sample a_k.

5. A method as claimed in claim 4 in which successive samples are averaged over an epoch and the average a_k' subtracted from each sample a_k to produce a modified sample a_k''.

6. A method as claimed in claim 4 in which the samples a_k, a_k'' are processed to derive a number of autocorrelation products x_p, using the Yule-Walker method.

7. A method as claimed in claim 6, in which

$$x_p = \frac{1}{n-p}\sum_{k=0}^{n-p-1} a_k'' a_{k+p}''$$

where p is the number of the autocorrelation product between 0 and m.

8. A method as claimed in claim 7 in which the autocorrelation products x_0 to x_m are averaged over successive epochs.

9. A method as claimed in claim 8 in which a running average R_p of the autocorrelation products is derived from the averages of successive epochs.

10. A method as claimed in claim 8 in which the averaged autocorrelation products are analysed according to the Yule-Walker equation to derive Yule-Walker coefficients y_o to y_m.

11. A method as claimed in claim 10 in which the Levinson-Durbin algorithm is used to derive the Yule-Walker coefficients y_0 to y_m from the Yule-Walker equation.

12. A method as claimed in claim 10 in which the Yule-Walker coefficients are used to derive the relative power density D_f at a frequency f of the output signal, where

$$D_f = \frac{1}{\left|1 + \sum_{p=1}^{M} y_p \exp(-i \cdot a \cdot f \cdot p)\right|^2}$$

13. A method as claimed in claim 12 in which the relative power density D_f is derived for multiple frequencies of the output signal, and the relative power density D_f at one frequency or over a first range of frequencies is compared with the power densities D_f over a wider range of frequencies to detect a change in power density at said one frequency or first range of frequencies.

14. A method as claimed in claim 1 applied to the monitoring of brain waves.

15. Apparatus for monitoring electrical activity in an animal comprising a detector to produce an output signal corresponding to the electrical activity, a random noise generator to produce a random noise signal, and a processor to combine the output signal and random noise signal to produce a modified signal and to analyse the modified signal using an autocorrelation technique to detect the elative power density values at a plurality of different frequencies.

16. Apparatus as claimed in claim 15, in which the processor samples the output signal at intervals.

17. Apparatus as claimed in claim 16 in which the processor samples digital samples a_k of the output signal.

18. Apparatus as claimed in claim 17 in which the random noise generator produces a random noise signal in the form of a random number that is added to each sample a_k.

19. Apparatus as claimed in claim 18 in which the processor averages successive samples over an epoch and subtracts the average a_k' from each sample a_k to produce a modified sample a_k''.

20. Apparatus as claimed in claim 18 in which the processor processes samples a_k, a_k'' to derive a number of autocorrelation products x_p using the Yule-Walker method.

21. Apparatus as claimed in claim 20, in which

$$x_p = \frac{1}{n-p}\sum_{k=0}^{n-p-1} a_k'' a_{k+p}''$$

where p is the number of the autocorrelation product between 0 and m.

22. Apparatus as claimed in claim 21 in which the autocorrelation products x_o to X_m are averaged by the processor over successive epochs.

23. Apparatus as claimed in claim 22 in which a running average R_p of the autocorrelation products is derived by the processor from the averages of successive epochs.

24. Apparatus as claimed in claim 22 in which the averaged autocorrelation products are analysed by the processor according to the Yule-Walker equation to derive Yule-Walker coefficients y_o to y_m.

25. Apparatus as claimed in claim 24 in which the processor uses the Levinson-Durbin algorithm to derive the Yule-Walker coefficients y_o to y_m from the Yule-Walker equation.

26. Apparatus as claimed in claim 24 in which the processor uses the Yule-Walker coefficients to derive the relative power density D_f at a frequency f of the output signal, where

$$D_f = \frac{1}{\left|1 + \sum_{p=1}^{M} y_p \exp(-i \cdot a \cdot f \cdot p)\right|^2}$$

and a is a constant and M is the order of the Yule-Walker equation.

27. Apparatus as claimed in claim 26 in which the processor derives the relative power density D_f for multiple frequencies of the output signal, and compares the relative power density D_f at one frequency or over a first range of frequencies with the power densities D_f over a wider range of frequencies to detect a change in power density at said one frequency or first range of frequencies.

28. An electroencephalograph comprising apparatus as claimed in claim 15.

* * * * *

References

Aftanas, L. and Golosheykin, S., 2005. Impact of regular meditation practice on EEG activity at rest and during evoked negative emotions. Int J Neurosci. 115(6): 893-909

Anderson, R. E. and Jakobsson, J. G., 2004. Entropy of EEG during anaesthetic induction: a comparative study with Propofol or nitrous oxide as sole agent. British Journal of Anaesthesia, 92(2): 167-170

Andrade, J., Englert, L., Harper, C. and Edwards, N.D., 2001. Comparing the effects of stimulation and Propofol infusion rate on implicit and explicit memory formation. British Journal Anaes. 86: 189 – 195

Andrade, J. and Deeprose, C., 2007 Unconscious memory formation during anaesthesia. Best Pract Res Clin Anaesthesiol. 21(3): 385-401

Angelerie, F. and Butler, S., 1997. Analysis of the electrical activity of the brain. John Wiley & Sons

Antkowiak, B., 2002. In vitro networks: cortical mechanisms. British Journal Anaesth. 89: 102–11

Antognini, J.F., Carstens, E., Sudo, M. and Sudo, S., 2000. Isoflurane depresses electroencephalographic and medial thalamic responses to noxious stimulation via an indirect spinal action. Anesth Analg. 91: 1282–8

Antognini, J.F. and Carstens, E., 2002. In vivo characterization of clinical anesthesia and its components. British Journal of Anaesth. 89: 156–66

Antognini, J.F., Saadi, J., Wang, X.W., Carstens, E. and Piercy, M., 2007. Propofol action in both spinal cord and brain blunts electro encephalographic responses to noxious stimulation in goats. Sleep. 24: 26–31

Artusio, J.F., 1955. Ether analgesia during major surgery. Journal of the American Medical Association. 157: 33-36

Baddour, K.E., Beaulieu, N.C., 2005. Autoregressive modeling for fading channel simulation. IEEE Trans. Wireless Comms. 4(4)

Badgaiyan, R.D., Schecter, D.L., and Alpert, N.M., 1999. Auditory priming within and across modalities: evidence from positron emission tomography. J Cogn Neuroscience. 11, 337-348

Baghdoyan, H.A., and Lydic, R., 2002. Neurotransmitters and neuromodulators regulating sleep, Sleep and Epilepsy: The Clinical Spectrum. Edited by: Bazil, C., Malow, B., Sammaritano, M., New York, Elsevier Science: 17-4

Bai, D., Pennefather P.S., MacDonald, J.F., and Orser, B.A., 1999. The general anaesthetic Propofol slows deactivation and desensitization of GABA-A receptors. Journal of Neuroscience. 10: 635-646

Bankman, I. and Gath, I., 1987. Feature extraction and clustering of EEG during anaesthesia. Med & Biol. Eng. Computing. 25: 474-477

Barnard, E.A., Skolnick, P., Olsen, R.W., 1998. International union of pharmacology – xv-subtypes of gamma aminobutyric acid (A) receptors – classification on the basis of subunit structure and receptor function. Pharmacology Review. 50, 291-313

Bauerle, K., Greim, C.A., Schroth, M., Geisselbrcht, M., Kobler, A. and Roewer, N., 2004. Prediction of depth of sedation and anaesthesia by the Narcotrend EEG monitor. B J Anesth. 92:841-845

Bein, B., 2006. Entropy. Best Practice & Research Clinical Anaesthesiology. 20(1): 101-109

Bell, S.L., Smithm, D.C., Allen, R. and Lutman, M.E., 2006. The auditory middle latency response, evoked using maximum length sequences and chrips, as an indicator of adequacy of anaesthesia. Anesth Analg. 102:495-8

Bennett, M.V.L., 2000. Seeing is relieving: electrical synapses between visualized neurons. Nat. Neurosci. 3: 7–9

Bennett, M.V.L., 2004. Electrical Coupling and Neuronal Synchronization in the Mammalian Brain. 41(19): 495-511

Berecek, K.H. and Brody, M.J., 1982. Evidence for a neurotransmitter role for epinephrine derived from the adrenal medulla. Am J Physiol Heart Circ Physiol 242: H593-H601

Berger, H., 1929. Uber das elektrenkephalogramm des menschen, 1st report. Arch Psychiat Nervenkr. 87: 527–70

Berns, G.S., Cohen, J.D., and Minutm, M.A., 1997. Brain regions responsive to novelty in the absence of awareness. Science. 276: 1272-1275

Berry, R. and Randall, M., 2002. Sleep Medicine Pearls. Hanley and Belfus. New York

Betz, H., 1991. Glycine receptors: heterogenous and widespread in the mammalian brain. TINS 14: 458-461

Bigelow, H.J., 1846. Insensibility during surgical operations produced by inhalation. Boston Med Surg J. 35: 309-317

Bjorvatn, B., Fagerland, S., Eid T et al., 1997. Sleep/waking effects of a selective 5-HT1A against given systemaitcially as well as perfused in the dorsal raphe nucleus in rats. Brain Res. 770 (1-2):81-8

Blethyn, K., Hughes, S. and Crunelli, V., 2007. Evidence for electrical synapses between neurons of the nucleus reticularis thalami in the adult brain in vitro. Published online by: Cambridge University Press.

Bonin, R.P. and Orser, B.A., 2008. GABA-A receptor subtypes underlying general anesthesia. Pharmacology Biochemistry and Behavior. Published online by: Science Direct.

Braitenburg, V. and Schuz, A., 1991. Anatomy of the Cortex: Statistics and Geometry, New York: Springer-Verlag

Brazier, A.B., and Finesinger, J.E., 1994. Characteristics of the normal electroencephalograph. J Clin Investigation. 23: 319

Bronzino, J.D., Kelly, M.L., Cordova, C.T., Oley, N.H. and Morgane, P.J., 1981. Utilization of Amplitude Histographs to Quantify the EEG Effects of Systemic Administration of Morphine in the Chronically Implanted Rat. IEEE Transactions on Biomedical Engineering. 28(10): 673 – 678

Bruhn, J., Boullon, T.W. and Shafer, S.L., 2000) Bispectral index (BIS) and burst suppression: reveal a part of the BIS algorithm. J Clin Monit Comput. 16: 593-6

Bruhn, J., Lehmann, L.E., Ropcke, H., Bouillon, T.W. and Hoft, A., 2001. Shannon entropy applied to the measurement of the electroencephalographic effects of Desflurane. Anaesthesiololgy. 95: 30-35

Buckner, R.L., Petersen, S.E., Ojemann, J.G., Miezen, F.M., Squire, L.R., and Raichle, M.E., 1995. Functional anatomical studies of explicit and implicit memory retrieval tasks. Journal of Neuroscience. 15: 12-29

Bullock, T.H., Achimowicz, J.Z., Duckrow, R.B., and Spencer, S.S., 1997. Bicoherence of intracranial EEG in sleep, wakefulness and seizures. Electroencephalography and Clinical Neurophysiology. 103(6): 661-678

Campagna, J.A, Miller, K.W. and Forman, S., 2003. Mechanisms of Actions of Inhaled Anesthetics. New Eng J of Med. 348:2110-2124

Carstens, E. and Antognini, J.F., 2005. Anesthetic effects on the thalamus, reticular formation and related systems. Thalamus & Related Systems. 3(1): 1–7

Celentano, J.J. and Wong, R.K., 1994. Muliphasic desensitization of the GABA-A receptor in outside-out patches. Biophysical Journal. 66: 1039-1050

Celio, M.R., 1986. Parvalbumin in most gamma-aminobutyric acid-containing neurons of the rat cerebral cortex. Science. 231: 995–997

Cellucci, C.J., Albano, A.M. and Rapp, P.E., 2003. Comparative study of embedding methods, Phys Rev. E:67

Chalmers, D., 2002. What is a neural correlate of consciousness? In: Metzinger T, ed. Neural correlates of consciousness. 2nd ed. Cambridge: MIT Press/Bradford Books. 17–40

Charles, G., Watson, L.J. and Herder, J., 2006. Correlates of alpha, beta and theta wave production. Journal of Clinical Psychology. 35(2): 364 – 369

Clark, D.L., Rosner, B.S., 1973. Neurophysiologic effects of general anaesthetics. I. the electroencephalogram and sensory evoked responses in man. Anesthesiology. 38:564-582

Collins, G., 1980. Release of endogenous amino acid neurotransmitter candidates from rat olfactory cortex: possible regulatory mechanisms and effects of pentobarbitone. Brain Research. 190: 517-523

Connors, B. and Long, M., 2004. Electrical synapses in the mammalian brain. Annual Review of Neuroscience. 27: 393-418

Cooley, J.W. and Tukey, JW., 1965. An algorithm for the machine calculation of complex Fourier series. Math. Comput. 19: 297–301

Creutzfeldt, O.D., Watanabe, S., Lux, H.D., 1966. Relations between EEG phenomena and potentials of single cortical cells. II. Spontaneous and convulsoid activity. Clin Neurophysiol. 20: 19–37

Crossland, J. and Merrick A.J., 1954. The effect of anaesthesia on the acetylcholine content of brain. Journal of Physiology (London). 125: 56-66

Cullen, D.J., Eger, E.I. II., Steves, W.C., Smith, N., Cromwell, T.H. and Cullen, B.F., 1972. Clinical sings of anesthesia. Anesthesiology. 36: 21-36

Curio, C., 2005. Ultrafast EEG activities. In: Niedemeyer and da Saliva, Eds. 496-504. Lippincott Williams & Wilkins, Philadelphia, 2005

D'Mello, J., and Butani, M., 2002. Capnography. Indian J. Anaesthesia. 46(4):269-278

Daniel, P., Cardinali, S., Pandi-Perumal, P., 2006. Neuroendocrine Correlates of Sleep/wakefulness. Published online by: Springer. 163 – 178

Davies, P.A., Hanna, M.C., Hales, T.C., Kirkness, E.F., 1997. Insensitivity to anaesthetic agents conferred by class of GABA-A receptor subunit. Nature. 385: 820-823

Deans, M.R., Gibson, J.R., Sellitto, C., Connors, B.W. and Paul, D.L., 2001. Synchronous activity of inhibitory networks in neocortex requires electrical synapses containing connexin36. Neuron 31: 477–485

Del Negro, C. and Edeline, J., 2002. Sex and season influence the proportion of thin spike cells in the canary HVc. Neuroreport. 13(16): 2005-2009

Dement, W.C., 1998. The study of human sleep: a historical perspective. Thorax. 53(3): S2-S7

Demetrescu, M.C., 1975. The aperiodic character of the electroencephalogram. Physiologist. 18:189

Dolin, S. and Little, H., 1986. Augmentation by calcium channel antagonists of general anaesthetic potency in mice. British Journal of Pharmacology. 88: 909-914

Donchin, Y., Field, J.M. and Porges, S.W., 1985. Respiratory sinus arrhythmia during recovery from Isoflurane-nitrous oxide anaesthesia. Anesthesia and analgesia, 64: 811-815

Drummond J.C., 2000. Monitoring depth of anesthesia with emphasis on the application of the bispectral index and the middle latency auditory evoked response to the prevention of recall. Anesthesiology. 93: 876–82

Duberman, S.M. and Bendixen, H., 1986. Mortality, morbidity and risk in anaesthesia. In: Lunn JN, ed. Epidemiology in Anaesthesia. London: Edward Arnold. 37–73

Dumermuth, G., Walz, W., Scollo-Lavizzari, G., Kleiner, B., 1972. Spectral Analysis of EEG Activity in Different Sleep Stages in Normal Adults. Eur Neurol. 7:265-296

Duncum, B.M., 1994. The Development of Anaesthesia. London: Royal Society Medical Press. Electroencephalogr. Clin. Neurophysiol.29: 306–310

Dutton, R.C., Smith, W.D., Bennett, H.L., Archer, S. and Smoth, N.T., 1998). Craniofacial electromyogram activation response: another indicator of anaesthetic depth. J Clin Monit Comput 14: 5-17

Düzel, E., Yonelinas, A.P., Mangun, G.R., Heinze, H.J. and Tulving, E., 1997. Event-related brain potential correlates of two states of conscious awareness in memory. Proc Natl Acad Sci USA. 27;94(11):5973-8

Dwyer, R.C., Rampil, I.J., Eger, E.I. II, Bennett, H.L., 1994. The electroencephalogram does not predict depth of Isoflurane anesthesia. Anesthesiology. 81:403-9

Ebersole, J.S., 1997, Defining epileptogenic foci: past, present, future. Journal of Clinical Neurophysiology. 14: 470-483

Ecoffey, C., Viviand, X., Billard, V., Cazalaa, J.B., Molliex, S., Servin, F. and Laxenaire, M.C. 2001. Target controlled infusion (TCI) anaesthesia using Propofol. Assessment of training and practice in the operating room. Annales Francaises d'Anesthesie et de Reanimation. 20(3): 228-245

Edelberg, R., 1961. The relationship between the galvanic skin response, vasoconstriction and tactile sensitivity. J of Experimental Psychology. 62(2): 187-195

Eger, E. I. II, Saidman, I.J. and Brandstater, B., 1965. Minimum alveolar anesthetic concentration: A standard of anesthetic potency. Anesthesiology. 26: 756

Eger, E.I. II, 1974. Anesthetic Uptake and Action. Williams & Wilkins, London

Eger, E. II, Eisenkraft, J. and Weiskopf, R., 2003 The Pharmacology of Inhaled Anesthetics. Edmund Eger. 1

Ellerkmann, R.K., Sohle, M., Alves, T.M., Liemann, V.M., Wenningmann, I. and Ropcke, H., 2006. Spectral entropy and bispectral index as measures of the electroencephalographic effects of Propofol. Anesth Anal. 102: 1056-62

Elliott, R. and Dolan, R.J., 1998. Neural response during preference and memory judgments for subliminally presented stimuli: a functional neuroimaging study. Journal of Neuroscience. 18: 4697-4704

Elul, R., 1969. Gaussian behaviour of the electroencephalogram changes during performance of mental task. Science. 164: 331

Evans, J.M. and Davies, W.L., 1984. Monitoring Anaesthesia. Clinical Anaesthesia. 2: 243-262

Feng, Z., and Chen, H., 2005. Analyze the Dynamic Features of Rat EEG Using Wavelet Entropy. 1(4):833 – 836

Ferree, T.C., Luu, P., Russell, G.S. and Tucker, D.M., 2001. Scalp electrode impedance, infection risk, and EEG data quality. Clin Neuroscience. 112(3): 536-44.

Ferri, R., 2000. The time course of high-frequency bands (15–45 Hz) in all-night spectral analysis of sleep EEG . Clinical Neurophysiology. 111(7): 1258 – 1265

Fitzgibbon, S.P., Pope, K.J., Mackenzie, L., Clark, C.R., Willoughby, J.O., 2004. Cognitive tasks augment gamma EEG power. Clin Neurophysiol. 115(8):1802-9

Fleisher, L.A., 2000. Risk of anesthesia. In: Miller, R.D., Cuchiara, R.F., Miller, E.D., Reeves, J.G., Roizen, M.F., Savarese, J.J., (eds). Anesthesia. Churchill Livingstone. Philadelphia, London, Toronto, Montreal. 795–823

Forster, I. C., 1974. Measurement of the body capacitance and a method of patientisolation in mains environments. Med.Biol. Eng. & Comp. 9. 730

Forrest, F.C., Tooley, M.A., Saunders, P.R., Prys-Roberts, C., 1994. Propofol infusion and the suppression of consciousness: the EEG and dose requirements. British Journal of Anaesthesia. 72: 35-41

Franks, N.P. and Lieb, W.R., 1994. Molecular and cellular mechanisms of general anaesthesia. Nature. 367: 607-614

Gabrieli, J.D., 1998. Cognitive neuroscience of human memory. Ann Rev. Psychology. 49:87-115

Gajraj, R.J., Doi, M., Mantzaridis, H., and Kenny, G.N.C., 1998. Analysis of the EEG bispectrum, auditory evoked potentials and the EEG power spectrum during repeated transitions from consciousness to unconsciousness. British Journal Aanaes. 80: 46-52

Gal'chenko, A.A. and Vorob'ev, V.V., 1999. Analysis of electroencephalograms using a modified amplitude-interval algorithm. Neuroscience and Behavioral Physiology. 29(2): 157-160

Gibbs, F.A., Gibbs, E.L., Lennox, W.G., 1937. Effect on the electroencephalogram of certain drugs which influence nervous activity. Arch Intern Medicine. 60: 154 166

Gilden, D.L., 2001. Cognitive emissions of 1/f noise. Psychol Rev. 108:33–56

Gjerstad, A.C., Storm, H., Hagen, R., Huiki, M., Qvigstad, E., Raeder, J., 2007. Comparison of skin conductance with entropy during intubation, titanic stimulation and emergence from general anaesthesia. Acta Anaesth Scan. 51: 8-15

Gottesmann, C., 2002. GABA mechanisms and sleep. Neuroscience. 111(2) 231-239

Grant, G., 2007. How the 1906 Nobel Prize in Physiology or Medicine was shared between Golgi and Cajal. Brain Research Reviews. 55(2): 490-498

Glass, P.S., Bloom, M., Kearse, L., Rosow, S., Sebel, P. and Manberg, P., 1997. Bispectral analysis measures sedation and memory effects of propofol, midazolam, isoflurane and alfentanil in health volunteers. Anesthesiology. 86: 836-47

Gray, C.M. and Singer, W., 1988. Stimuls-specific neuronal oscillations in orientation columns of cat visual cortex.Neurobiology. 86:1698-1702

Griffith, D., Jones, J.B., 1990. Awareness and memory in anaesthetised patients. British Journal Anaes. 65: 603-7

Griffiths, M.J., Preece, A.W. and Green, J., 1991. Monitoring sedation levels by EEG spectrum analysis. Anesth Prog. 38:227-231

Griffiths, M.J., Grainger, P., Cox, M.V. and Preece, A.W., 2005. Recent advances in EEG monitoring for general anaesthesia, altered states of consciousness and sports performance science. Medical Applications of Signal Processing

Griss, P., Tolvanen-Laakso, H.K., Merilainen, P., and Stemme, G., 2002. Characterization of micromachined spiked biopotential electrodes, IEEE Trans Biomed Eng. 49(6):597-604

Guedel AE., 1937. Inhalational anesthesia. A fundamental guide. Macmillan, New York

Gunawardane, P.O., Murphy, P.A. and Sleigh, J.W., 2002. Bispectral index monitoring during electroconvulsive therapy under Propofol anaesthesia. Brit Journ Anesth. 88: 184-7

Haas, H. and Panula, P., 2003. The role of histamine and the tuberomamillary nucleus in the nervous system. Nature Reviews Neuroscience. 4: 121-130

Hagihira, S., Takashina, M., Mori, T., Mashimo, T., Sleigh, J.W., Barnard, J., Miller, A. and Steyn-Ross, D.A., 2004. Bispectral analysis gives us more information than power spectral-based analysis. British Journal of Anaes. 92(5): 772-773

Harris, R., Mihic, S. J., Dildy-Mayfield, J.E., and Machu, T.K., 1995. Actions of anaesthetics on ligand-gated ion channels: role of receptor subunit composition. FASEB. 9:1454-1462

Healy, T. and Cohen, P.J., 1995. Eds. A Practice of Anaesthesia.

Hebb, D.O., 1949. The Orgnaisaion of Behaviour. Chichester: John Wiley & Sons.

Heinke, W. and Schwarzbauer, C., 2002. In vivo imaging of anaesthetic action in humans: approaches with PET and fMRI. Br J Anaesth. 89: 112–22

Heinrichs, W., 2008. Using the drug editor to realise drug interactions: example Propofol and Remifentanyl. HPSN 2008 conference presentation.

Hemmerling, T., 2004. BIS Sensor Electrodes Can Cause Skin Lesions: Case Report. Anesthesia Analgesia. 98:1820-21

Herregots, L., Rolly, G., Mortier, E., Bogaert, M., and Mergaert, C., 1989. EEG and SEMG monitoring during induction and maintenance of anesthesia with Propofol. International Journal of Clinical Monitoring and Computing. 6(2): 67-73

Hirota, K. and Kushikata, T., 2001. Central noradrenergic neurones and the mechanism of general anaesthesia. Editorial. British Journal of Anaesthesia. 87(6): 811-813

Hjorth, B., 1970. EEG analysis based on time domain properties. Electroencephalogr. Clin. Neurophysiol.29: 306–310

Hoekema, R., Wieneke, G.H., Leijten, F.S.S., van Veelen, C.W.M., Rijen, P.C., Huiskamp, G.J.M., Ansems, J., and van Huffelen, A.C., 2003. Measurement of the conductivity of skull temporarily removed during epilepsy surgery. Brain Topography. 16: 29-38

Holt, M.R.G., 1997. The use of neural networks in the analysis of the anaesthetic electroencephalogram. PhD Thesis. St Hugh's Collge. Oxford

Hudspith, H.J., 1997. Glutamate: a role in normal brain function, anaesthesia, analgesia and CNS injury. British Journal of Anaes. 78(6): 731-747

Hug, C.C.J., 1990. Does opioid "anesthesia" exist? Anesthesiology. 73: 1–4

Huhta, J. C. and Webster, J. G., 1973. 60-Hz interference in electroardiography. IEEE Tr.Biom.Eng., 20: 2, 91.

Imon, H., Ito, L.D. and McCarley, R.W., 1996. Electrical stimulation of the cholinergic laterodorsal tegmental nucleus elicits scopolamine-sensitive excitatory postsynaptic potentials in medial pontine reticular formation neurons. Neuroscience. 74(2): 393-401

Ingvar, D.H., 1987. Evidence for frontal/prefrontal cortical dysfunction in chronic schizophrenia: the phenomenon of "hypofrontality" reconsidered. In Helmchen, H., Henn, F.A., (eds). Biologic perspectives of schizophrenia. Life Sciences Research Report 40. Chichester: John Wiley & Sons. 201-213

Iohom, G., Gardiner, C., Whyte, A., O'Connor, G. and Shorten, G., 2004. Abnormalities of contrast sensitivity and electroretinogram following Sevoflurane anaesthesia European Journal of Anaesthesiology. 21: 646-652

Isaac, P.A. and Roden, M., 1990. Lower oesophageal conteactility and detection of awareness during anaesthesia. Bristish Journal of Anaes. 65(3): 319-324

Iselin-Chavels, I.A., Flaishon, R., Sebel, P.S., Howell, S., Gan, T.J., Sigl et al., 1998. The effect of thr interaction of propofol and alfentanil on recall, loss of consciosuness and the bispectral index. Anaesth Analg 87:949-55

Jäntti, V., Alahuhta, S., Barnard, J. and Sleigh, J.W., 2004. Spectral entropy—what has it to do with anaesthesia, and the EEG? British Journal of Anaesthesia. 93(1):150-152

Jasper, H.H. and Andrews, H.L., 1938. Electroencephalography. III. Normal differentiation of occipital and precentral regions in man. Arch Neurol Psychiatry. 39:96–115

Johansen, J.W., Sebel, P.S., 2000. The Bispectral Index Scale (BIS), A New Monitor of Hypnosis or Depth of Anesthesia. Anesthesiology. 93:1336–1344

John, E.R., Prichep, R. and Leslie, S., 2005. The Anesthetic Cascade: A Theory of How Anesthesia Suppresses Consciousness Anesthesiology. 102(2): 447-471

John, E.R., Prichep, L.S., Kox, W., Valdés-Sosa, P., Bosch-Bayard, J., Aubert, E., Tom, M., di Michele, F. and Gugino, L.D., 2001. Invariant reversible QEEG effects of anesthetics. Conscious Cogn. 10: 165–183

Joliot, M., Ribary, U. and Llinas, R., 1994. Human oscillatory brain activity near 40 Hz coexists with cognitive temporal binding. Proc Natl Acad Sci USA. 91: 11748–51

Jones, J.G., 1994. Perception and memory during general anaesthesia. British Journal of Anaesthesia. 73: 31-37

Jouvet, M., 1965. Paradoxical sleep: A study of its nature and mechanisms. Prog Brain Res. 18:20-57

Jurd, R, Arras, M, Lambert, S., Zeller, S., Drexler, B., Siegwart, R.M., Crestani, D., Zaugg, M, Vogt, M., Ledermann, B., Antkowiak, B, and Rudolph, U., 2004. Mechanism of action of the general anaesthetics propofol and etomidate. Pharmacology, 72(2): 149-149

Kaneda, T., Ochiai, R., Takeda, J. and Fukushima, K., 1995. Effects of nitrous oxide on electroencephalographic activity during Sevoflurane anesthesia: a zero-crossing analysis. Masui. 44(11): 1498-505

Katz, J., Burkard, F. and Medwetsky, L., 2002. Handbook of Clinical Audiology. Lippincott Williams & Wilkins. 256

Keifer, J.C., Baghdoyan, H.A., Becker, L. and Lydic, R., 1994. Halothane decreases pontine acetylcholine release and increases EEG spindles. Neuroreport. 5(5):577-80

Kelz, M.B., Sun, Y., Chen, J., Meng, Q.C., Moore, J., Veasey, S.C., Dixon, S.,Thornton, M., Funato, H. and Yanagisawa, M., 2008. An essential role for orexins in emergence from general anesthesia. PNAS. 105(4): 1309-1314

Kendall, T.J.G. and Minchin, M.C.W., 1982. The effects of anaesthetics on the uptake and release of amino acid neurotransmitters in thalamic slices. British Journal of Pharmacology. 75: 219-227

Kikuchi, T., Wang, Y., Sato, K. and Okumura, F., 1998. In vivo effects of Propofol on acetylcholine release from the frontal cortex, hippocampus and striatum studied by intracerebral microdialysis in freely moving rats. British Journal of Anaes. 80(5): 644-648

Kim, J., Yao, A., Atherley, R., Carstens, E., Jinks, S.L. and Antognini J.F., 2007. Neurons in the Ventral Spinal Cord Are More Depressed by Isoflurane, Halothane, and Propofol Than Are Neurons in the Dorsal Spinal Cord. Anesth. Analg. 105, 1020-1026

Kirnö, K., Kunimoto, M., Lundin, S., Elam, M. and Wallin, B.G., 1991. Can Galvanic Skin Response Be Used as a Quantitative Estimate of Sympathetic Nerve Activity in Regional Anesthesia? Anesth Analg. 73:138-142

Kin, D.W., Ki, H.Y. and White, P.F., 2001. The effect of noise on the bispectral index during propofol sedation. Anesth Analg. 93:1170-3

Klostermann, F., Gobbele, R., Buchner, H. and Curio, G., 2002. Intrathalamic non-propagating generators of high-frequency (1000 Hz) somatosensory evoked potential (SEP) bursts recorded subcortically in man. Clin Neurophysiol. 113 (7): 1001-5

Kodama, T. and Honda, Y., 1999. Acetylcholine and glutamate release during sleep-wakefulness in the pedunculopontine tegmental nucleus and norepinephrine changes regulated by nitric oxide. Psychiatry and Clinical Neurosciences. 53(2):109-111

Koumoundouros, E., Silbert, B.S., Fambiatos, A., Davies, M.J., Cronin, D. and Cannata, J., 1989. EEG monitoring using aperiodic analysis during carotid and open heart surgery. Australas Phys Eng Sci Med. 12 (3):149-54

Krasowski, M. D. and Harrison, N. L., 1999. General anaesthetic actions on ligand-gated ion channels. Cell. Mol. Life Sci. 55, 1278–1303

Kreuer, S., Biedler, A., Larsen, R., Schoth, S., Altmann, S. and Wilhelm, W, 2001. The Narcotrend – A new EEG monitor designed to measure the depth of anaesthesia: A comparison with bispectral index monitoring during propofol-remifentanil-anaesthesia. Anaesthetist. 50:921-5

Kreuer, S., Biedler, M.D., Larson, R., Altmann, S. and Wilhelm, W., 2003. Narcotrend monitoring allows faster emergence and a reduction of drug consumption in propofol-remifentanil anesthesia. Anesthesiology. 99:34-41

Kumpf, K., Nahm, W., Kochs, E. and Miltner, W., 1997. Dynamical complexity of EEG predicts movement during anesthesia. Electroencephalography and Clinical Neurophysiology.103(1): 198

Lancel, M., 1999. Role of GABAA receptors in the regulation of sleep: Initial sleep responses to peripherally administered modulators and agonists. Sleep. 22:33-42

Lang, E.J., 2001. Organization of olivocerebellar activity in the absence of excitatory glutamatergic input. J. Neurosci. 21: 1663-1675

Langford, R.M., Thomsen, C.E., 1994. The value to the anaesthetist of monitoring cerebral activity. Methods of Information in Medicine. 33:133-138

Larson, C.L., Davidson, R.J., Abercrombie, H.C., Ward, R.T., Schaeffer, S.M., Jackson, D.C., Holden, J.E. and Perlman, S.B., 1998. Relations between PET-derived measures of thalamic glucose metabolism and EEG alpha power. Psychophysiology. 35: 162-169

Larson, J., Wong, D. and Lynch, G., 1986. Pattered stimulation at the theta frequency is optimal for the induction of hippocampal long-term potentiation. Brain Res. 268: 347-250

Laufs, H., Krakow, K., Sterzer, P., Eger, E., Beyerle, A., Salek-Haddadi, A. and Kleinschmidt, 2003. Electroencephalographic signatures of attentional and cognitive default modes in spontaneous brain activity fluctuations at rest. Proc Natl Acad Sci USA. 100(19): 11053–11058

Laureys, S., 2005. The neural correlate of (un)awareness: lessons from the vegetative state. Trends Cogn Sci. 9:556–9

Leake, C. D., 1925. Valerius Cordus and the Discovery of Ether. Isis. 7: 14-24

Ledowski, T., Paech, M.J., Storm, H., Jones, R. and Schug, S.A., 2006. Skin conductance monitoring compaired with bispectral index monitoring to assess emergence from general anaesthesia using Sevoflurane and remifentanil. Brisih Journ Anaes. 92(2): 187-9

Lees, G. and Coyne, L., 2004. The orexins: a novel family of sleep regulating neuropeptides. Current Anaesthesia & Critical Care. 15(1): 75-77

Leopold, D.A. and Logothetis, N.K., 1996. Activity changes in early visual cortex reflect monkeys' percepts during binocular rivalry. Nature. 379: 549-553

Levinson, B.W., 1965. States of awareness during general anaesthesia.. British Journal of Anaesthesia. 37: 544-546

Li, X. and Pearce, R.A., 2000. Effects of Halothane on GABA-A receptor kinetics: evidence for slowed agonist unbinding. Journal of Neuroscience. 20, 899-907

Llinas. R. and Ribary, U., 2001. Consciousness and the Brain: The thalammocortical dialogue in health and disease. Annals of the New York Academy of Science. 929:166-175

Logothetis, N., Schall, J., 1989. Neuronal correlates of subjective visual perception. Science. 245:761–3

Lunn, J.N. and Mushin, W.W., 1982. Mortality associated with anaesthesia. Anaesthesia. 37: 856

Lydic, R. and Baghdoyan, H. A., 2005. Sleep, Anesthesiology, and the Neurobiology of Arousal State Control. Anesthesiology. 103(6): 1268-1295

Mancilla, J. G., Lewis, T. J., Pinto, D. J., Rinzel, J. and Connors, B. W., 2007. Synchronization of Electrically Coupled Pairs of Inhibitory Interneurons in Neocortex. J. Neurosci. 27(8): 2058 – 2073

Mashour, G. A., 2004. Consciousness unbound: toward a paradigm of general anesthesia. Anesthesiology. 100: 428-33

Mashour, G. A., 2005. Cognitive unbinding in sleep and anesthesia. Science. 310: 1768–9

Massimini, M., Ferrarelli, F. and Huber, R., 2005. Breakdown of cortical effective connectivity during sleep. Science. 309:2228–32

McCarley, R.W. and Hobson, J.A., 1975. Neuronal excitability modulation over the sleep cycle: A structural and mathematical model. Science. 189:58-60

McIntosh, A.R., Rajah, M.N. and Lobaugh, N.J., 1999. Interactions of prefrontal cortex in relation to awareness in sensory learning. Science. 284: 1531-1533

McKay, I.D., Voss, L.J., Sleigh, J.W., Barnard, J.P. and Johannsen, E.K., 2006. Pharmacokintec-pharmacodynamic modeling the hypnotic effect of sevoflurane using the spectral entropy of the electroencephalogram. Aesth Analg 102:91-7

Merriam, E. B., Netoff, T. I. and Banks, M. I., 2005. Bistable Network Behavior of Layer I Interneurons in Auditory Cortex. J. Neurosci. 25(26): 6175 – 6186

Messerschmit, D. Autocorrelation matrix eigenvalues and the power spectrum. University of California at Berkeley. Technical report no. UCB/EECS-2006-90

Meyer, H., 1899. Zur Theorie der Alkoholnarkose. Arch Exp Pathol Pharmakol. 42: 109–37

Millar, A.G. and Atwood, H.L., 2004. Crustacean Phasic and Tonic Motor Neurons. Integrative and Comparative Biology. 44(1):4-13

Minchin, M.C.W., 1981. The effects of anaesthetics on the uptake and release of y-aminobutyric acid and D-aspartate in rat brain slices. British Journal of Pharmacology. 73: 681-690

Montia, J.M., and Montib, D., 2007. The involvement of dopamine in the modulation of sleep and waking. Sleep Medicine Reviews. 11(2): 113-133

Morris, N.P., Harris, S.J. and Henderson, Z., 1999. Parvalbumin-immunoreactive, fast-spiking neurons in the medial septum/diagonal band complex of the rat: intracellular recordings in vitro. Neuroscience. 92(2): 589-600

Morris, R.G.M., Anderson, E., Lynch, G.S. and Baudry, M., 1986. Selective Impairment of Learning and Blockade of Long Term Potentiation by an NMDA Receptor Antagonist AP5. Nature. 319: 774-776

Mozurri, G. and Magoun, H.W., 1949. Brainstem reticular formation and activation of the EEG. Electroencephalogram Clinical Neurophysiology. 1: 455-473

Mukaida, K., Shichino, T., Koyanagi, S., Himukashi, S. and Fukuda, K., 2007. Activity of the Serotonergic System During Isoflurane Anesthesia. Anesth Analg. 104:836-839

Muzed, A., Ktonas, P., Gruber, G. and Kecklund, G., 2004. General recommendations for development of new sensors, D1.1.3 Sensation project (EU FP6 507231).

Myers, A.C., 2000. Anatomical characteristics of tonic and phasic postganglionic neurons in guinea pig bronchial parasympathetic ganglia. The Journal of Comparative Neurology. Volume 419(4): 439 – 450

Myles, P.S., Leslie, K., McNeil, J., Forbes, A. and Chan, M.T.V., 2004. For the B-Aware trial group. Bispectral index monitoring to prevent awareness during anaesthesia: the B-Aware randomised controlled trial. Lancet. 363: 1757–1763

Newton, D.E.F., Thornton, C., Creagh-Barry, P., Dore, C.J., 1989. Early cortical suditory evoked responses in anaesthesia: Comparisons of the effects of nitrous oxide and Isoflurane. Bristish Journal of Anaes. 62: 61-65

Nicoll, R.A., and Madison, D.V., 1982. General anesthetics hyperpolarize neurons in the vertebrate central nervous system. Science. 217:1055-7

Niedermayer, E. and da Silva, F., 1993. Electroencephalography: basic principles, clinical application and related fields. Baltimore: Williams and Wilkins. 131-152

Niedermayer, E. and da Silva, F., 1993b. Electroencephalophraphy: Basic Principles, clinical applications and related fields: Lippincott Williams & Wilkins. 489-499

Niemi-Murola, L. and Paloheimo, M., 2005. Feasibility of electromyography (sEMG) in measuring muscular activity during spinal anaesthesia in patients undergoing knee arthroplasty. Acta Anaesthesiologica Scandinavica 49:4, 558–562

Ningler, M., Stockmanns, G., Schneider, G., Dressler, O. and Kochs, E., 2004. Rough Set-Based Classification of EEG-Signals to Detect Intraoperative Awareness: Comparison of Fuzzy and Crisp Discretization of Real Value Attributes. RSCTC.3066: 825-834

Nolte, J., 2002. The Human Brain: An Introduction to Its Functional Anatomy. Mosby. 263-290

Nunez, P.L. and Srinivasan, R., 2006. Electric Fields of the Brain: The neurophysics of EEG. Oxford University Press. 432-480

Ouyang, M., Hellman, K., Abel, T. and Thomas, S.A., 2004. Adrenergic signaling plays a critical role in the maintenance of waking and in the regulation of REM sleep. J Neurophysiol. 92:2071-82

Overton, C.E., 1991. Studies of Narcosis (English translation of Studien uber die Narkose. 1901), R.L. Lipnick, Ed. Chapman Hall, London

Pardey, J., Roberts, S. and Tarassenko, L., 1996. A review of parametric modeling techniques for EEG analysis. Med. Eng. Phys. 18(1):2-11

Pearce, R.A., 1996. Volatile anaesthetic enhancement of paired-pulse depression investigated in the rat hippocampus in vitro. Journal Physiology. 492(Pt 3): 823–840.

Petrovic, P., Magnus, K., Hanssonb, P. and Ingvara, M, 2004. Brainstem involvement in the initial response to pain. NeuroImage. 22(2): 995-1005

Peyron, C., Tighe, D.K., van den Pol, A.N., de Lecea, L., Heller, H.C., Sutcliffe, J.G. and Kilduff, T.S., 1998. Neurons containing hypocretin (orexin) project to multiple neuronal systems. J Neurosci. 18: 9996-10015

Pinault, D., 2004. The thalamic reticular nucleus: structure, function and concept. Brain Research Reviews. 46(1): 1-31

Plourde, G. and Picton, T.W., 1990. Human auditory steady state response during general anaesthesia. Anesth. Analg. 71:460-8

Pomfrett, L.J.D., Sneyd, J.R., Beech, M. and Healy, T.E.J., 1991. Variation in respiratory sinus arrhythmia may reflect levels of anaesthesia. Br J Anaesthesia. 67: 6216

Pomfrett, C.J.D., Barrie, J.R., and Healy, T.E.J., 1993. Respiratory sinus arrhythmia: an index of light anaesthesia. British Journal of Anaesthesia, 71:212-217

Porkka-Heiskanen, T., Strecker, R.E., Thakkar, M., Bjorkum, A.A., Greene, R.W. and McCarley, R.W., 1997. Adenosine: A mediator of the sleep-inducing effects of prolonged wakefulness. Science. 276:1265-8

Pöschel, B., Draguhn, A. and Heinemann, U., 2002. Glutamate-induced gamma oscillations in the dentate gyrus of rat hippocampal slices. Brain Research. 938(1-2): 22-28

Potashner, S.J., Lake, N., Langlois, E.A., Ploffe, L. and Lecavalier, D., 1980. Pentobarbital: differential effects on amino acid transmitter release. In: Fink, B.R., ed. Molecular Mechanisms of Anesthesia (Progress in Anesthesiology Vol. 2). New York: Raven Press. 469-72

Press, Wh., Tuekolsky, S.A., Vetterling, W.T. and Flannery, B.P., 1992. Numerical recipes - The art and science of computing. Second edition. Cambridge University Press.

Proakis, J.G. and Manolakis, D.G., 1996. Digital Signal Processing: principles, algorithms, and applications. Prentice Hall. New Jersey. 600-960

Prys-Roberts, C., 1987. Anaesthesia: A Practical or Impractical Construct? British Journal of Anaesthesia. 59(11):1341-1345

Puma, C. and Bizot, J.C., 1999. Hippocampal theta rhythm in anesthetized rats: role of AMPA glutamate receptors. Computational Neuroscience Neuroreport. 10(11): 2297-2300

Rampil, I.J. and Laster, M.J., 1992. No correlation between quantitative electroencephalographic measurements and movement response to noxious stimuli during Isoflurane anesthesia in rats. Anesthesiology. 77: 920-5

Rampil, I.J., Mason, P. and Singh, H., 1993. Anesthetic potency (MAC) is independent of forebrain structure in rats. Anesthesiology. 78: 707-12

Rampil, I.J., 1994. Anesthetic potency is not altered after hypothermic spinal cord transection in rats. Anesthesiology. 80: 606-10
Rampil, I.J., 1998. A primer for EEG signal processing in anesthesia. Anesthesiology. 89(4): 980-1002

Rampil, I.J., 2003. Consciousness, awareness, and the clinician. Canadian Journal of Anesthesia 50: R3

Ranck, J.B., 1963. Specific impedance of rabbit cerebral cortex. Experimental Neurology 7: 114-152

Rapp, B., 2001. The Handbook of Cognitive Neuropsychology: What Deficits Reveal about the Human Mind. 481

Rechtschaffen, A. and Kales, A. (eds), 1968. A Manual of Standardized Terminology, Techniques and Scoring System for Sleep Stages of Human Subject. National Institute of Health Publication, Washington, USA

Rees, G., Kreiman, G. and Koch, C., 2002. Neural correlates of consciousness in humans. Nat Rev Neurosci. 3: 261–70

Rehburg, B., Xiao, Y.H. and Duch, D.S., 1996. Central nervous system sodium channels are significantly suppressed at clinical concentrations of volatile anaesthetics. Anaesthesiaology. 27A(84): 1223-1233

Rehberg, B., Ryll, C., Hadzidiakos, D. and Baars ,J., 2007. Use of a target-controlled infusion system for propofol does not improve subjective assessment of anaesthetic depth by inexperienced anaesthesiologists. Eur J Anaesthesiol. 24: 920–926.

Rémond , A., 1973. Handbook of Electroencephalography and Clinical Neurophysiology. Elsevier, Netherlands. 5: 33 – 53

Renna, M., Lang, E.M. and Lockwood, G.G., 2000. The effect of Sevoflurane on implicit memory: a double-blind, randomised study. Anaesthesia. 55(7): 634-640

Richards, C.D., 1972. On the mechanism of barbiturate anaesthesia. Journal of Physiology. 227: 749-767

Richards, C.D., 1973. On the mechanism of Halothane anaesthesia.Journal of Physiology. 233: 439-456

Richards, C.D. and White, A.E., 1975. The actions of volatile anaesthetics on synaptic transmission in the dentate gyrus. J Physiol. 252(1): 241-257

Richards, C.D. and Smaje, J.C., 1976. Anaesthetics depress the sensitivity of cortical neurones to 1-glutamate. British Journal of Pharmacology. 58: 347-357

Richards, C.D. and Strupinski, K., 1986. An analysis of the action of pentobarbitone on the excitatory postsynaptic potentials and membrane properties of neurones in the guinea-pig olfactory cortex. British Journal of Pharmacology. 89: 321-325

Riker, R.R., Fraser, G.L. and Wilkins, M.L., 2003. Comparing the bispectral index and suppression ratio with burst suppression of the electroencephalogram during pentobarbital infusions in adult intensive care patients. Pharmacotherapy. 23(9): 1087-93

Robinson, S., Smith, D.M., Mizumori†, S.J.Y. and Palmiter, R.D., 2004. Firing properties of dopamine neurons in freely moving dopamine-deficient mice: Effects of dopamine receptor activation and anesthesia. PNAS. 101(36): 13329–13334

Rodriguez, E., George, N., Lachaux, J.P., Martinerie, J., Renault, B., Varela, F.J., 1999. Perception's shadow: Long-distance synchronization of human brain activity. Nature. 397: 430-3

Roughan, J.V. and Laming, P.R., 1998. Large slow potential shifts occur during Halothane anaesthesia in gerbils. J Comp Physiol. 182: 839–848

Roustan, J.P., Valette, S., Aubas, P., Rondouin, G and Capdevila, X., 2005. Can electroencephalographic analysis be used to determine sedation levels in critically ill patients? Anesth Analg. 101:1141-51

Ruiz-Gimeno, P., Soro, M., Pérez-Solaz, A., Carrau, M., Belda, F., Jover, J. and Aguilar, G., 2005. Comparison of the Eeg-Based Snap TM Index and the Bispectral (BisTM) Index During Sevoflurane - Nitrous Oxide Anaesthesia. The Journal of Clinical Monitoring and Computing. 19(6): 383-389

Russell, I.F., 1979. Auditory perception under anaesthesia. Anaesthesia. 34: 211

Russell, I.F., 1986. Comparison of wakefulness with two anaesthetic regimens, total i.v. balanced anaesthesia. British Journal of Anaesthesia. 58: 965-968

Russel I. F., 1993. Midazolam-alfentanil: An Anaesthetic? An investigation using the isolated forearm technique. British Journal Anaes. 70: 42-46

Russell, I.F. and Wang, M., 1997. Absence of memory for intraoperative information during adequate general anaesthesia. British Journal of Anaesthesia. 78: 3-9

Russell, I.F. and Wang, M., 2001. Absence of memory for intra-operative information during surgery with total intravenous anaesthesia. British Journal Anaes. 86: 196 – 202

Russell, I.F., 2006. The Narcotrend 'depth of anaesthesia' monitor cannot reliably detect consciousness during general anaesthesia: an investigation using the isolated forearm technique. BJA. 96(3):346-52

Russell., I.F., 2008. Personal communication.

Sakuma, Y., Ueda, Y. and Kiode, M., 1989. R-R interval variation and autonomic nervous function under general anesthesia. Masui. 34: 223-227

Sallanon, M., Buda, C., Janin, M., and Jouvet, M., 1985. Implication of Serotonin in Sleep Mechanisms: Induction, Facilitation? Sleep: Neurotransmitter and Neuromodulator. 135-140

Sansom, C.C., 2000. Histamine control of sleep, learning and memory. Drug Discovery Today. 5(3): 94-95

Santamaria, J. and Chiappa, K.H., 1987. The EEG of drowsiness in normal adults. J. Clin. Neurophysiol. 4:327-382

Särkelä, M., Mustola, S., Seppänen, T., Koskinen, M., Lepola, P., Suominen, K., Juvonen, T., Tolvanen-Laakso, H. and Jäntti, V., 2002. Automatic Analysis and Monitoring of Burst Suppression in Anesthesia. Journal of Clinical Monitoring and Computing. 17(2)

Sarter, M., Bruno, J.P. and Berntson, G., 2006. Reticular Activating System. Encyclopedia of Cognitive Science. John Wiley & Sons, Ltd.

Saul, L.J., Davis, H. and Davis, P.A., 1937. Correlations between EEG and psycholofical organization of the individual. Trans Amer Neural Ass. 63: 167

Sayers, B.McA. and Beagley, W.R., 1974. Objective evaluation of auditory evokedEEG responses. Nature. 247: 481-3

Schwarz, G., Voit-Augustin, H., Litscher, G. and Baumgartner, A., 2004. Specific Problems in Interpretation of Absolute Values of Spectral Edge Frequency (SEF) in comparison to Bispectral Index (BIS) for Assessing Depth of Anesthesia. The Internet Journal of Neuromonitoring. 3(2)

Schwender, D., Daunderer, M., Kunze-Kronawitter, H., Klasing, S., Pöppel, E. and Peter, K., 1997. Awareness during general anaesthesia--incidence, clinical relevance and monitoring. Acta Anaesthesiol Scand Suppl. 111: 313-4

Schwilden, H. and Jeleazcov, C., 2002. Does the EEG During Isoflurane/Alfentanil Anesthesia Differ from Linear Random Data? Journal of Clinical Monitoring and Computing. 17(7-8)

Schwilden, H., Kochs, E., Daunderer, M., Jeleazcov, B., Scheller, G., Schneider, J., Schüttler, D., Schwender, G., and Pöppel, E., 2005. Concurrent recording of AEP, SSEP and EEG parameters during anaesthesia: a factor analysis. British Journal of Anaesthesia. 95(2): 197-206

Schwilden, H., 2006. Concepts of EEG processing: from power spectrum to bispectrum, fractals, entropies and all that. Best Practice & Research Clinical Anaesthesiology. 20(1): 31-48

Sebel, P.S., Maynard, D. E., Major, E. and Frank, M., 1983. The Cerebral Function Analysing Monitor (CFAM) A new microprocessor-based device for the on-line anaylsis of the EEG and evoked potentials. Br. J. Anaesth. 55: 1265

Sebel, P.S., Flynn, P.J., Ingram, D.A., Rutherford, C.F. and Rogers, H., 1986. Evoked potentials during isolflurane anaesthesia. Bristish Journal of Anaes. 58: 580-585

Sebel, P.S., Bowdle, T.A., Ghoneim, M.M., Rampil, I.J., Padilla, R.E., Gan, T.J. and Domino, K.B., 2004. The incidence of awareness during anesthesia: a multicenter United States study. Anesth Analg. 99: 833-9

Sem-Jacobsen, C.W., 1956. Depth electrographic studies of the activity in the human brain and the effect of some drugs (including Mescalin, L.S.D.25 and chlorpromazine).EEG Clin. Neurophysiol. 8:717

Shaw, J.C., 2003. The Brain's Alpha Rhythms and the Mind. Elsevier Health Sciences. 55-72

Sice, P.A.J., Depth of Anesthesia. Update in Anaesthesia. 19: 1

Sing, H.C., Kautz, M.A., Thorne, D.R., Hall, S.W., Redmond, D.P., Johnson, D.E., Warren, Kimberly, B., Joshua, R. and Michael B., 2005. High-Frequency EEG as Measure of Cognitive Function Capacity: A Preliminary Report. Aviation, Space, and Environmental Medicine. 76(1): 114-135

Sleigh, J.W., Andrzejowski, J., Steyn-Ross, A. and Steyn-Ross, M., 1999. The Bispectral Index: A Measure of Depth of Sleep? Anesth Analg. 88: 659 –61

Sleigh, J.W., Steyn-Ross, D.A., Steyn-Ross, M.L., Williams, M.L. and Smith, P., 2001. Comparison of changes in electroencephalographic measures during induction of general anaesthesia: influence of the gamma frequency band and electromyogram signal. Br J Anaes. 86: 50-8

Sleigh, J.W., Steyn-Ross, D.A., Steyn-Ross, M.L., Grant, C. and Ludbrook G., 2004. Cortical entropy changes with general anaesthesia: theory and experiment. Physiol. Meas. 25: 921-93

Snow, J., 1847. On the Inhalation of the Vapour of Ether in Surgical Operations. London: John Churchill

Somjen, G.G., 1963. Effects of thiopental on spinal presynaptic terminals. Journal of Pharmacology and Experimental Therapeutics. 140: 396-402

Sou, J.H., Chan, M.H. and Chen, H.H., 2006. Ketamine, but not Propofol, anaesthesia is regulated by metabotropic glutamate 5 receptors. British Journal of Anaes. 96(5): 597-601

Spackman, T.N., Faust, R.J., Cucchiara, R.F. and Sharbrough, F.W., 1987. A comparison of aperiodic analysis of the EEG with standard EEG and cerebral blood flow for detection of ischemia. Anesthesiology. 66(2):229-31

Speckmann, E.J. and Elger, C.E., 1999. Introduction to the Neurophysiological Basis of the EEG and DC Potentials. In: E. Niedermeyer and F. Lopes da Silva, Editors, Electroencephalography: basic principles, clinical applications, and related fields. Williams and Wilkins, Baltimore. 15-27

Steriade,M., 2004. Acetylcholine systems and rhythmic activities during the waking--sleep cycle. Prog Brain Res. 145:179-96

Steyn-Ross, A., and Steyn-Ross, M., 1999. The Bispectral Index: A Measure of Depth of Sleep? Anesth Analg. 88:659 –61

Šušmáková, K., 2004. Human Sleep and Sleep EEG. Measurement science review. 4(2)

Suzuki, M., Edmonds, H.I., Tsueda, K., Malkani, A.L. and Roberts, C.S., 1998. Effect of Ketamine on bispectral index and levels of sedation. Clin Monit Comput.14: 373

Tesche, C.D., Karhu, J., and Tissari, S.O., 1996. Non-invasive detection of neuronal population activity in human hippocampus. Brain. Res. Cogn. Brain Rev. 4: 39-47

Tesche, C.D., and Karhu, J., 2000. Theta oscillations index hippocampal activiation during working memoery task. Proc. Natl. Anad. Sci. USA. 97: 919-924

Thornton, C. and Newton., D.E.F., 1989. The auditory evoked response: a measure of depth of anesthesia. Balliere's Clinical Anaesthesiology. 5: 559-585

Thornton. C., 1991. Evoked potentials in anaesthesia. European Journal of Anesthesiaology, 8:89-107

Tonner, P.H. and Bein, B., 2006. Classic electroencephalographic parameters: median frequency, spectral edge frequency etc. Best Prac Res Clin Anaesthesiology. 20: 147-59

Tooley, M.A., Stapleton, C.L., Greenslade, G.L. and Prys-Roberts, C., 2004. Mid-latency auditory evoked response during Propofol and alfentanil anaesthesia. British Journal of Anaesthesia. 92(1): 25-32

Tooley, M.A., Greenslade, G.L. and Prys-Roberts, C., 1996. Concentration-related effects of Propofol on the auditory evoked response. British Journal of Anaes. 77: 720-726

Tranel, D., Damasio, H. and Damasio, A.H., 1997. A neural basis for the retrieval of conceptual knowledge. Neuropsychologia. 35(10): 1319-1327

Urban, B.W., Frenkel, C., Duch, D.S. and Kauff, A.B., 1991. Molecular models of anesthetic action on sodium channels, including those from human brain. Annals of the New York Academy of Sciences. 625: 327-343

Urban, B.W. and Bleckwenn, M., 2002. Concepts and correlations relevant to general anaesthesia. British Journal of Anaesthesia. 89(1): 3-16

Veselis, R.A., Reinsel, R.A., Feschenko, V.A. and Wronski, M., 1997. The comparative amnestic effects of midazolam, Propofol, thiopental, and fentanyl at equisedative concentrations. Anesthesiology. 87:749-64

Veselis, R.A., Reinsel, R.A., Beattie, B.J., Mawlawi, O.R., Feschenko, V.A., DiResta, G.R., Larson, S.M., Blasberg, R.G., 1997b. Midazolam changes cerebral bloodflow in discrete brain regions: An H2(15)O positron emission tomography study. Anesthesiology. 87: 1106-17

Veselis, R.A., Reinsel, R.A., Tsakanikas, D., Gutzler, M., Feschenko, V.A. and Dnistrian, A.M., 2000. Conscious sedation with Propofol: Preliminary observations using positron emission tomographic imaging, Memory and Awareness in Anesthesia IV. Edited by Jordan C, Vaughan DJA, Newton DEF. London, Imperial College Press. 232-47

Veselis, R.A., Reinsel, R.A., Distrian, A.M., Feschenko, V.A. and Beattie, B.J., 2000b. Asymmetric dose-related effects of midazolam on regional cerebral blood flow, Memory and Awareness in Anaesthesia IV: Proceedings of the Fourth International Symposium on Memory and Awareness in Anaesthesia. Eds Jordan, C., Vaughan, D.J.A. and Newton, D.E.F., London, Imperial College Press. 287-303

Vickers, M.D.A., 1987. Detecting consciousness by clinical means. In Rosen M and Lunn NJ (eds) Consciousness, Awareness and Pain in General Anaesthesia. London. Butterworths.12-17

Viviand, X. and Léone, M., 2001. Induction and maintenance of intravenous anaesthesia using target-controlled infusion systems. Best Practice & Research Clinical Anaesthesiology.15(1): 19-33

Walter, W.G. and Dovey, J.V., 1946. Electroencephalography in case of sub-cortical tumour. J Neurol Neurosurg Psychiatry. 7: 57–65

Watt, R.C., Hameroff, S.R., 1987. Phase Space Analysis of Human EEG during General Anesthesia. Annals of the New York Academy of Sciences 504(1): 286–288

Wauquier, A. and de Ryck, M., van den Broeck, W., van Loon, J., Melis, W. and Janssen, P., 1988. Relationships between quantitative EEG measures and pharmacodynamics of alfentanil in dogs. Electroencephalogr Clin Neurophysiol. 69(6): 550-60

Weakly, J.N., 1969. Effect of barbiturates on quantal synaptic transmission in spinal motorneurones. Journal of Physiology. 204: 63-77

Webster, J.G., 1998. Medical Instrumentation: Application and Design. J. Wiley & Sons. 156-175

Welsh, J.P., Lang, E.J., Sugihara, I. and Llinás, R., 1995. Dynamic organization of motor control within the olivocerebellar system. Nature 374: 453-457

White, D.D. Anaesthesia: a privation of the senses. In: Rosen, M. and Lunn, J.N. (eds), 1987. Consciousness, Awareness and Pain in General Anaesthesia. Butterworths, London

Whittington, R.A. and Virág, L., 2006. Anesthetic pharmacology: Isoflurane Decreases Extracellular Serotonin in the Mouse Hippocampus. Anesth Analg.103:92-98

Willmann, K., Springman, S., Rusy, D. and Daily, E., 2002. A Preliminary Evaluation of a New Derived EEG Index Monitor in Anesthetized Patients. Journal of Clinical Monitoring and Computing. 17(6): 345-350

Woolf, N.J., 1991. Cholinergeric systems in mammalian brain and spinal cord. Prog. Neurobiol. 37: 475-524

Wu, X.S., Sun, J.Y. and Evers, A.S., 2004. Isoflurane inhibits transmitter release and the presynaptic action potential, Anesthesiology. 100(3): 663–670

Yamakura, T. and Harris, R.A., 2000. Effects of gaseous anesthetics nitous oxide and xenon on ligand-gated ion channels. Compairosn with isoflurane and ethanol. Anesthesiology. 93. 1095-1101

Yule, G.U., 1927. On a method of investigating periodicities in disturbed series with special reference to Wolfer's sun-spot numbers. Philos. Trans. R. Society. 276-298

Zhang, X.S., Roy, R.J. and Jensen, E.W., 2001. EEG complexity as a measure of depth of anesthesia for patients. IEEE Trans Biomed Eng. 48(12): 1424-33

Zhu, W.J. and Vicini, S., 1997. Neurosteroid prolongs GABA-A channel deactivation by altering kinetics of desensitizing states. Journal of Neuroscience. 17, 4022-4031